UNIVERSITÉ DE GRENOBLE

# THÈSE

Pour obtenir le grade de

## DOCTEUR DE L'UNIVERSITÉ DE GRENOBLE

Spécialité : **Sciences du Médicament**

Arrêté ministériel : 30 Septembre 2012


Présentée par

**Zhenyu ZHU**

Thèse dirigée par **« Eric PEYRIN »** et **« Corinne RAVELET»**

Préparée au sein du **Département de Pharmacochimie Moléculaire (DPM) UMR5063**
Dans **l'École Doctorale Chimie et Sciences du Vivant**


# Développement de nouveaux outils analytiques à base d'acides nucléiques aptamères pour la détection de petites molécules

Thèse soutenue publiquement le **5, Octobre, 2012**,
devant le jury composé de :

**Mr P. LABBE**
Professeur Université Grenoble I**,** président du jury
**Mr P. PROGNON**
Professeur Université Paris Sud, rapporteur
**Mr J.-L. MARTY**
Professeur Université de Perpignan, rapporteur
**Mr V. NOEL**
Maitre de conférences Université Paris Diderot, examinateur
**Mrs C. RAVELET**
Maitre de conférences Université Grenoble I, co-directeur de thèse
**Mr E. PEYRIN**
Professeur Université Grenoble I, directeur de thèse

*Université Joseph Fourier / Université Pierre Mendès France /*
*Université Stendhal / Université de Savoie / Grenoble INP*

# Acknowledgements

First of all, I would like to express unlimited thanks to my research advisor, **Professor Eric PEYRIN** for his guidance and encouragement. His expertise in guiding students has significantly inspired my curiosity and creativity in scientific research. His wonderful personality has and will continue to influence and shape my behavior throughout my life. His enthusiasm for science and his intellectual honesty and discipline have set up a role model for my professional career.

I would like to thank **Dr. Corinne RAVELET**. It was her that helped and clarified my research directions. As my second advisors, her insights and solid knowledge have helped me a lot during my research. I would also like to thank **Dr. Sandrine PERRIER and Dr. Valérie GUIEU.** They have always given time to guiding and reviewing my research and results, even though they had their own busy work schedule. They have created an effective working atmosphere and helped me a lot in different ways.

I would like to thank **Emmanuelle FIORE** for her assistance in the operation of instruments in the lab. I am especially thankful to **Mustapha ZAHAR** for his help and advice when I first arrived in France.

Thanks to **Pascale BATTISTONI** and **Angèle NICOLE** for handling different documents for me. Thanks to **Magali POURTIER** for providing me necessary information for a graduate student.

I have had a wonderful time in D.P.M., barbecue, ski, football game and la journée du D.P.M., all of these have become part of my precious memories. I would like to thank the past and present group members for their generous help throughout my graduate studies. I wish everything goes well for all the people.

Last but not least, I want to thank my parents and family members for their love, support and encouragement. I also want to express my special thanks to my girlfriend, **Xiaofei ZHANG**, for her love, patience, and everything she has done for me.

# List of Abbrevations

| | |
|---|---|
| ACN | acetonitrile |
| AFP | α-fetoprotein |
| AMP | adenosine 5'-monophosphate |
| ANS | 1-anilino-8-naphthalene sulfonate |
| ATP | adenosine triphosphate |
| AuNP | gold nanoparticle |
| BC | brin complémentaire |
| BHHT | 4, 4'-Bis (1,1,1,2,2,3,3-heptafluoro-4,6-dioxohexan-6-yl)-o-terphenyl |
| BSA | bovine serum albumin |
| CE | capillary electrophoresis |
| CGE | capillary gel electrophoresis |
| CIEF | capillary isoelectric focusing |
| CMACS | continuous-flow magnetic activated chip-based separation |
| CMC | critical micelle concentration |
| CS | complementary strand |
| CTAC | cetyltrimethylammonium chloride |
| CTP | cytidine triphosphate |
| CZE | capillary zone electrophoresis |
| DHFR | dihydrofolate reductase protein |
| DIS | dimerization initiation site |
| DNA | deoxyribonucleic acid |

| | |
|---|---|
| dsDNA | double-stranded DNA |
| ECL | electrogenerated chemiluminescence |
| EGFR | epidermal growth factor receptor |
| EIS | electrochemical impedance spectroscopy |
| ELISA | enzyme-linked immunosorbent assay |
| EOF | electroosmotic flow |
| FA | fluorescence anisotropy |
| FAD | flavin adenine dinucleotide |
| FIS | faradic impedance spectroscopy |
| FMN | flavin mononucleotide |
| FP | fluorescence polarization |
| FPAA | fluorescence polarization aptamer assay |
| FPIA | fluorescence polarization immunoassay |
| FRET | fluorescence resonance energy transfer |
| GDH | glucose dehydrogenase |
| GTP | guanosine triphosphate |
| HIV | human immunodeficiency virus |
| HTS | high-throughput screening |
| I.D. | internal diameter |
| ILITC | isoluminol isothiocyanate |
| ISE | ion-selective electrodes |
| LBA | lysozyme binding aptamer |

| | |
|---|---|
| LIF | laser-induced fluorescence |
| LOD | limit of detection |
| LYS | lysozyme |
| MB | methylene blue |
| MBA | molecular beacon aptamers |
| MECAS | microfluidic electrochemical aptamer-based sensor |
| MEKC | micellar electrokinetic chromatography |
| MRE | molecular recognition element |
| NADH | nicotinamide adenine dinucleotide (reduced) |
| NECEEM | nonequilibrium capillary electrophoresis of an equilibrium mixture |
| O.D. | outer diameter |
| OHP | Helmholtz plane |
| OTA | ochratoxin A |
| pcDNA | partial complementary single strand DNA |
| PCR | polymerase chain reaction |
| PDGF | platelet-derived growth factor |
| PEG | polyethylene glycol |
| PMSA | prostate-specific membrane antigen |
| PtNP | platinum nanoparticle |
| PVA | polyvinyl alcohol |
| QCM | quartz crystal microbalance |
| QD | quantum dot |

| | |
|---|---|
| RCA | rolling circle amplification |
| RNA | ribonucleic acid |
| RT-RCR | reverse transcription-polymerase chain reaction |
| SARS | severe acute respiratory syndrome |
| SAW | surface acoustic wave device |
| SDS | sodium dodecyl sulfate |
| SELEX | systematic evolution of ligands by exponential enrichment |
| SERS | surface-enhanced Raman scattering |
| SPR | surface plasmon resonance |
| SSB | single-stranded DNA binding protein |
| ssDNA | single-stranded DNA |
| SWNTs | single-walled carbon nanotubes |
| TAMRA | carboxytetramethylrhodamine |
| TAR | transactivation responsive element |
| TBA | thrombin binding aptamer |
| TOAB | tetraoctylammonium bromide |
| TR | texas red |
| TREAS | target-responsive electrochemical aptamer switch |
| UTP | uridine triphosphate |
| UV | ultraviolet |
| VEGF | vascular endothelial growth factor |

# Table of Contents

**Chapter II: Experiments and Reslutls**

# Introduction Générale

Les acides nucléiques aptamères sont des oligonucléotides en série ADN ou ARN qui ont été sélectionnés pour leur capacité à reconnaitre une (des) cible(s) pre-déterminée(s) par la méthode *in vitro* nommée SELEX (pour **S**ystematic **E**volution of **L**igands by **EX**ponential enrichment). De par leurs caractéristiques, les acides nucéliques aptamères peuvent être considérés comme des « anticorps chimiques » et, par conséquent, ont été et sont encore très largement employés comme outils potentiels en thérapeutique et diagnostic.

La majeure partie des outils analytiques à base d'aptamères rapportés à ce jour est dédiée à la détection de cibles protéiques. En règle générale, les performances analytiques des aptacapteurs à protéines sont supérieures à celles des aptacapteurs pour petites espèces chimiques. Les constantes de dissociation observées pour les complexes aptamère-protéine sont communément plus faibles que celles obtenues pour les complexes aptamère-petite molécule et les systèmes de transduction sont habituellement de mise en œuvre plus aisée.

L'objectif de ce travail était d'établir de nouvelles approches analytiques à base d'aptamères pour la détection de petites espèces chimiques (adénosine, tyrosinamide et argininamide en tant que composés modèles).

Trois types de méthodologies ont été explorés dans ce travail, basés sur des approches par électrophorèse capillaire (EC), par colorimétrie et par polarisation/anisotropie de fluorescence. Ce manuscrit se subdivise en trois chapitres comme suit :

Le chapitre I correspond à une analyse bibliographique qui regroupe deux parties. La première décrit les caractéristiques générales des aptamères et les méthodes de

sélection par le processus SELEX (et dérivés). La seconde partie introduit les différentes stratégies adoptées pour le développement de méthodes de dosage à base d'aptamères. Les approches de transduction sont également abordées.

Le chapitre II décrit l'ensemble de la partie expérimentale, les résultats et la discussion sous forme de publications. Après une introduction sur l'objectif général du travail, les trois parties sont abordées relativement à la méthodologie générale employée.

Le premier objectif du travail était de développer une nouvelle méthode de détection de petites molécules par EC couplée à une détection par fluorescence induite par laser (FIL) en utilisant, comme sondes, des oligonucléotides marqués par un fluorophore. Ce travail a fait l'objet d'une publication dans ***Analytical Chemistry, 2010, 82, 4613-4620.*** La stratégie d'analyse était fondée sur le concept de « structure-switching » de l'aptamère. Celui-ci repose sur la formation d'un duplex entre l'aptamère et un brin complémentaire (BC) de celui-ci. En présence de la cible, la formation du complexe aptamère-cible entraine la libération du brin complémentaire qui peut-être corrélée à la concentration de la cible dans le milieu de réaction. Deux configurations ont été décrites. La première, dédiée à la détection d'un seul composé, utilise un aptamère marqué par un groupement cholesteryl (Chol-Apt) en tant qu'élément de reconnaissance et un BC marqué par la fluorescéine (BC*) en tant que sonde. En conditions de chromatographie électrocinétique micellaire (en présence de micelles neutres dans le capillaire), la fraction libre de BC* a été efficacement séparée de sa fraction liée à l'aptamère. En présence de cible, la forme hybridée est déstabilisée, entrainant une diminution de l'intensité du pic du duplex et une augmentation de celle du pic du BC*. Le second format, spécifiquement développé pour une détection de plusieurs cibles dans un même capillaire, a utilisé des aptamères de taille différente marqués par la fluorescéine à une extrémité et un groupement cholesteryl à l'autre. La séparation électrophorétique des aptamères, sous forme libre et hybridée, a été démontrée, permettant de suivre les variations de

l'intensité des différents pics en fonction de la concentration des cibles ajoutées dans le milieu. Bien que cette approche permette une analyse « multiplexée » (adénosine et tyrosinamide en seule analyse dans un même capillaire), elle souffre d'un certain nombre d'inconvénients. Elle nécessite l'emploi d'un matériel sophistiqué et couteux et le temps d'analyse s'avère être relativement long.

Afin de remédier à ces problèmes, la deuxième étude s'est focalisée sur le développement d'un aptacapteur colorimétrique simple, rapide et peu coûteux, qui utilise le concept général de protection enzymatique de l'aptamère et les nanoparticules d'or en tant que système de transduction. Ce travail a fait l'objet d'une publication dans ***Analytica Chimica Acta, 2011, 706, 349-353.*** En absence de cible, l'aptamère est hydrolysé par la phosphodiestérase I en mononucléotides et petits fragments d'ADN. De par leur taille réduite, ceux-ci peuvent s'adsorber à la surface des nanoparticules d'or (non modifiées), entrainant leur stabilisation électrostatique et leur capacité à rester dispersées dans des conditions de force ionique importante (couleur rouge). A contrario, la présence de la cible dans le milieu induit un changement de conformation/structure de l'aptamère qui protège, au moins en partie, l'aptamère de l'attaque enzymatique. Dans ces conditions, l'oligonucléotide, de longueur plus importante, n'est plus capable de s'adsorber efficacement sur les nanoparticules d'or qui s'agrègent à force ionique élevée, avec changement de couleur (violet-bleu). La détection de la cible a été effectuée en suivant les rapports d'absorbance à 650 et 520 nm de la solution colloïdale. Cette méthodologie a été appliquée, suivant le même protocole, à la détection de deux cibles différentes (tyrosinamide et adenosine). L'inconvénient majeur de cette approche est lié au fait qu'elle est très difficilement applicable à l'analyse de composés en milieux réels complexes.

Dans ce contexte, nous nous sommes orientés vers la mise en œuvre d'aptacapteurs employant un système de transduction par polarisation/anisotropie de fluorescence, une technologie qui est très fréquemment utilisée pour le dosage d'espèces bioactives

dans des matrices biologiques. Ce travail a fait l'objet de deux publications dans ***Analytica Chimica Acta, 2011, 707, 191-196*** et dans ***Analytical Chemistry, 2012, sous presse.*** La première étude, fondée sur la stratégie « structure-switching » préalablement utilisée en électrophorèse capillaire, a consisté en l'évaluation des paramètres critiques impliqués dans la performance de l'aptacapteur. Dans cette configuration, BC est marqué par un fluorophore (BC*). En absence de cible, le duplex formé limite la rotation du fluorophore et entraine une anisotropie de fluorescence élevée. Lorsque le complexe aptamère-cible se forme, BC* est libéré du duplex avec, comme conséquence, une diminution du signal. Les effets de la composition et du pH du milieu réactionnel, de la température, de la stœchiométrie, de la nature du fluorophore et de la longueur du brin complémentaire sur la sensibilité de la méthode ont été appréhendés, permettant de définir les conditions optimales pour la détection de la cible tyrosinamide. L'un des problèmes de la méthode par « structure-switching » est lié à la faible variation du signal d'anisotropie de fluorescence obtenu (0,04). Pour pallier à cet inconvénient, une nouvelle approche a été proposée. Elle est basée sur l'utilisation de la protéine SSB (pour **S**ingle-**S**tranded **B**inding protein) en tant qu'outil amplification du signal. L'aptamère est marqué par un fluorophore. En absence de cible, la protéine SSB fixe la sonde aptamérique de telle sorte qu'une très forte augmentation de taille est obtenue, induisant une intense variation du signal d'anisotropie de fluorescence. En présence de cible, la formation du complexe aptamère-cible est responsable du déplacement de l'oligonucléotide de son complexe formé avec la protéine. Ce phénomène se traduit par une diminution drastique du signal (0,120 pour l'adénosine). Cette méthode a été utilisée avec succès dans le cas d'une autre cible (argininamide) et d'un autre strategie de biocapteur. Enfin, des expériences en conditions de sérum humain dilué semblent indiquer que cette approche pourrait être utilisée en milieux complexes.

Enfin, le chapitre III correspond à la conclusion générale de cette étude accompagnée d'une discussion sur les perspectives envisagées.

# Chapter I
# Literature Review

# I.1 Aptamers and SELEX

## I.1.1 Introduction

Molecular recognition plays a very important role in the nature. There are different kinds of biomolecular pairs in biological systems, including antibodies and antigens [1], hormones and hormone receptors [2], DNA promoters and transcription factors [3], enzymes and substrates [4], etc. Most of these biomolecular pairs present high binding affinity and specificity and their interactions are widely investigated. They are of great interest for different biological and biomedical applications, one of which being biosensing. A variety of biosensors have been developed since the design of the first enzyme-based biosensor over 40 years ago [5]. However, challenges exist when using these kinds of natural biomolecular systems under the experimental conditions. For example, many biomolecules (e.g., enzymes and antibodies) have unstable functional structures. When they are placed in an environment that is different from their ideal conditions they can be easily denatured and lose their initial biological function. Therefore, these molecular pairs have limited analytical applications in many situations. Clearly, it is of particular interest and importance to explore synthetic ligands which not only have high binding affinity and specificity towards target molecules, but also have special features such as tolerance to rigorous chemical and biological environments. Aptamers were developed to respond to these requirements, the following chapter concisely describes aptamers and the related SELEX technique.

## I.1.2 Selection of aptamers

Aptamers are oligonucleic acid or peptide molecules that bind to a specific target molecule. Ever since the concept of aptamer was first proposed by Ellington [6] and Gold [7] and the technology of Systematic Evolution of Ligands by EXponential

enrichment (SELEX) was developed for isolation of nucleic acid aptamers in 1991 [8], more and more different aptamers have been reported, which could specifically bind to various target ligands. Aptamers are also termed “chemical antibodies” because of their artificial in vitro selection process based on Systematic Evolution of Ligands by EXponential enrichment (SELEX). Unlike the preparation of antibodies, which depends on induction of an animal immune system, the SELEX process enables the preparation of aptamers for non-immunogenic and toxic targets which is otherwise impossible to obtain by the immune system [9]. Moreover, it is also possible to produce aptamers to specific regions of targets, which is sometimes difficult for antibodies, since the animal-immune system inherently contains epitopes on target molecules. Until now, aptamers have been selected toward a broad range of targets, including ions (e.g., $K^+$, $Zn^{2+}$ and $Ni^{2+}$), small organic molecules (e.g., amino acids, nucleosides/nucleotides, drugs, vitamins, organic dyes and toxins), peptides and proteins (e.g., thrombin, growth factors and HIV-associated peptides) and even whole cells or microorganisms (e.g., bacteria, viruses) [10-19]. Significantly, the availability of such a large pool of aptamers makes it possible to explore novel bioassay tools covering various areas including diagnostics, anti-bioterrorism, and environmental and food analysis [20].

### I.1.2.1 General Scheme of SELEX

Figure 1-1 shows a typical SELEX process. The process begins with the generation of a random library that contains up to $10^{13}$ – $10^{15}$ single-stranded DNA or RNA oligonucleotides. The oligonucleotides are synthesized by a combinatorial chemical synthesis technique. These oligonucleotides are comprised of N random nucleotides in the middle of their sequences, flanked by a primer-binding region at each end. During the selection of aptamers, target molecules are incubated with the library to enable molecular recognition between the target molecules and the oligonucleotides. Theoretically, the aptamers will tightly bind to the target molecules while the other

oligonucleotides will stay in solution. Because the aptamer-target complexes and the free oligonucleotides in the binding solution should exhibit different physical properties, they can be separated with a partitioning method or tool. After separation, the sequences bound to the target molecules will be amplified by polymerase chain reaction (PCR) to generate a new library for further selection. This process is usually repeated for 8-12 cycles.

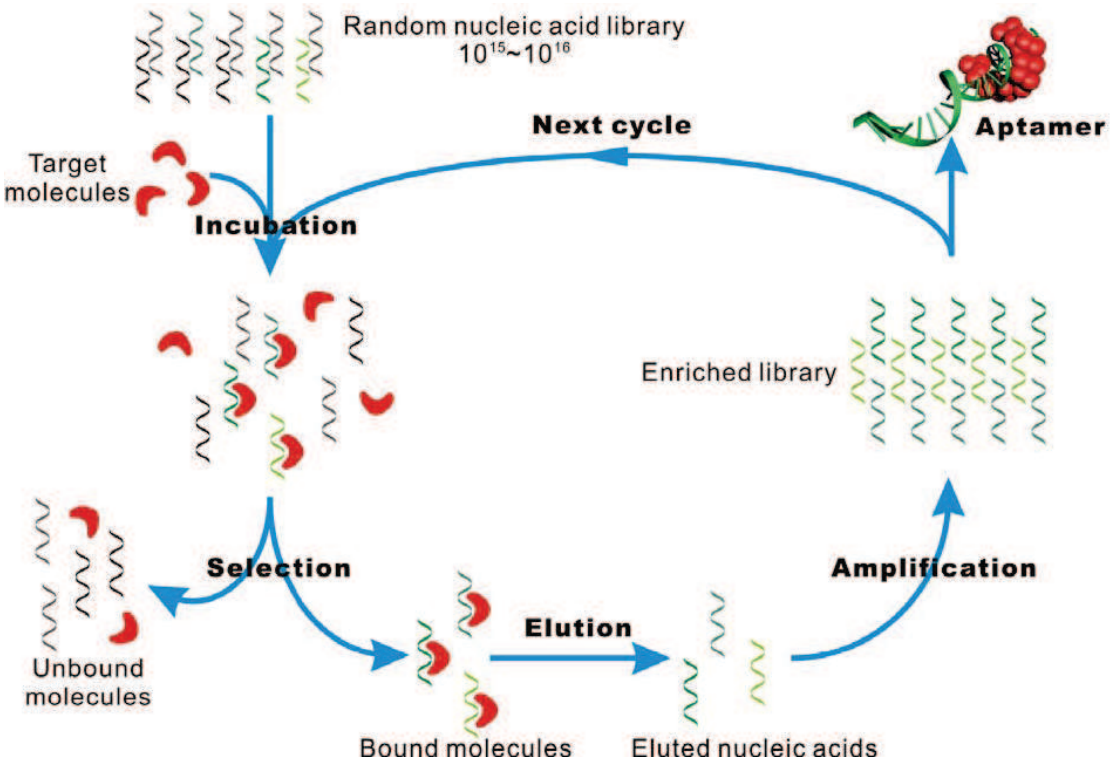


**Figure 1-1:** Scheme for the Systematic Evolution of Ligands by EXponential (SELEX) enrichment process [21]. A random nucleic acid library is incubated with a target molecule, and unbound molecules are separated from bound molecules. Bound nucleic acids are eluted, amplified by PCR and serve as an enriched library for the next cycle. For each target, 8–12 consecutive cycles are performed and the final enriched library is cloned and sequenced.

### I.1.2.2 Different Methods of SELEX

The most critical step of SELEX is the separation of bound oligonucleotides from the unbound ones. Nitrocellulose filtration is the most commonly used technique [6, 7]. As aptamer-related research grew at an increasing pace within the past few years, numerous separation techniques have been used to improve aptamer selection, including affinity surfaces (e.g., affinity magnetic beads [22], titer plates [23], and affinity chromatography [24, 25]), gel mobility shift [26], immunoprecipitation [27], density-gradient centrifugation [28], and tailored SELEX [29]. These techniques are promising to improve aptamer selection. In addition to the development of separation techniques for improving the separation efficiency, other SELEX techniques such as photo-SELEX [30], evolution mimicking algorithm-based SELEX [31], and molecular beacon-based SELEX [32] have been developed to improve the selectivity of the aptamer. To further advance the breadth of aptamer selection, cell-SELEX [33] and tissue-SELEX [34] have recently been studied. These methods have the potential to identify aptamers that can recognize cancer cells or tumor tissues for cancer therapy and diagnosis. However, the aptamer selection process is iterative. It can be very time-consuming, requiring several months or longer to complete. To overcome this problem, automated SELEX [35, 36] and microarray-based SELEX [37] have been developed. These new methods are promising to improve the speed of aptamer-based research.

The Krylov group [38] has developed nonequilibrium capillary electrophoresis of an equilibrium mixture (NECEEM) approach, which can screen aptamers with much fewer rounds of selection and can also determine accurate binding parameters. They further utilized NECEEM in the repetitive partitioning step to improve the affinity of a DNA library by more than 4 orders of magnitude [39, 40]. Recently, the same group used the NECEEM method to screen aptamers against a target protein from a cell lysate without any prior purification of the target protein and subsequently utilized the developed aptamers for protein isolation from the same cell lysate [41]. This

technique was demonstrated to be useful for the selection of aptamers for certain proteins that do not have intrinsic DNA-binding characteristics [42].

CE-based separation methods have greatly accelerated the selection efficiencies due to the fast separation ability based on the differences of electrophoretic mobility between protein-aptamer complexes and free oligonucleotides. However, the approach is limited to mainly proteins, because small species typically do not allow the detectable electrophoretic mobility shift. Magnetic bead-based selection methods, where molecular targets are first immobilized on a magnetic bead surface, show wider applications to any kind of molecules or species. However, the efficiency of magnetic selection techniques is significantly lower than CE. The Soh group, thus, developed a platform that combines magnetic bead-assisted SELEX with microfluidics technology (M-SELEX) to take advantage of robust and efficient features of both separation approaches [43]. This procedure improves the aptamer selection by enabling highly stringent selection conditions through the use of very small amounts of target molecules. The separation of the magnetic bead is based on the magnetic field gradients generated by ferromagnetic patterns imbedded in the microfluidic channel. The M-SELEX could provide a highly efficient, low-cost, and automated system with high-throughput capabilities. In a follow-up work, the Soh group further improved the M-SELEX method using a disposable microfluidic chip to rapidly generate aptamers with high affinity and specificity [44]. In the experiments, picomolar amounts of target molecule bound to beads were recovered with high efficiency. The procedure was performed for both the positive selection toward streptavidin and negative selection against bovine serum albumin (BSA), which greatly increased the selection specificity.

A particularly interesting aptamer selection approach was introduced by Mi *et al.* [34] who questioned whether the in vitro SELEX procedure is effective enough for subsequent in vivo target detection, principally because the environments during selection and application are not identical. To address this potential issue, an in vivo aptamer selection approach was created using intrahepatic colorectal tumor-bearing mice (Figure 1-2). During their procedure, the tumor-bearing mice were injected with

a random library of RNA sequences. After harvesting the tumors, RNA sequences were extracted and amplified with RT-RCR. The resulting RNA pool was again reintroduced into mouse tumors. After this repeated procedure, the resulting RNA molecules demonstrated increasing affinity towards the colorectal tumor protein extract compared to normal tissue cells. The generated aptamers were confirmed to have exceptional in vivo selectivity towards the targeted cancerous mouse tissue.

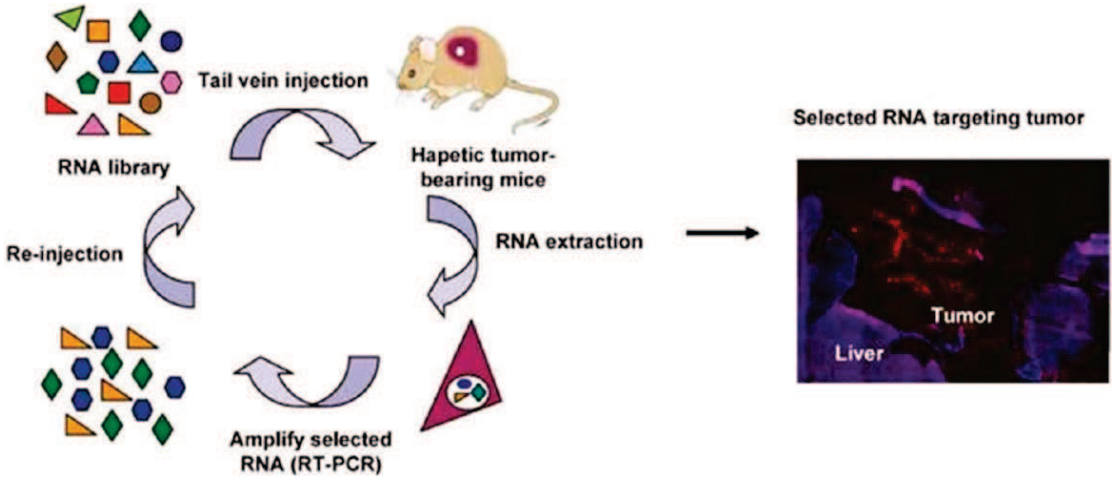


**Figure 1-2:** In vivo selection of aptamers [34]. Tumor-bearing mice are intravenously injected with a random library of RNA sequences. After harvesting the tumors and extracting and amplifying the bound RNA molecules, the reinjection procedure is repeated several more times, resulting in increasing specificity of the bound aptamers. The selected RNA aptamers can finally be used for in vivo tumor imaging.

Besides common molecules such as small organics, peptides, and proteins, whole intact cells or viruses have been increasingly used as targets for the selection of aptamers, since the prior precise knowledge of target molecules is not required [45-48]. The resulting aptamers can be used for cancer cell detection, although the knowledge of exact targeted molecules on the surface of the cells may not be totally clear. Cell-SELEX has become one of the most widely used methods for screening cells. A number of aptamers targeting different cancer cells have since been

developed. Most recently, Li *et al.* [49] reported a slide-based SELEX strategy for in situ selection of tissue samples. They demonstrated the effectiveness of their approach by generating an aptamer with high affinity toward infiltrating ductal carcinoma tissues. Similarly, another aptamer system was developed by Wan *et al.* [50] to capture and enrich EGFR-expressing glioblastoma cells. The cancer is known for its ability to infiltrate human brain regions, and the inability to detect glyoblastoma renders it surgically incurable. The fluorophore-labeled aptamer probe was immobilized on the glass slides and then applied to successfully capture targeted cancer cells with high efficiency and selectivity. Overall, new developments and improvements in the aptamer selection process have made the generation of aptamers a more straightforward and routine practice, leading to greater impact of aptamers and their broader applications in biochemical and medicinal fields.

## I.1.3 Aptamer characteristics

### I.1.3.1 The length of Aptamers

The aptamers identified by the selection procedure (i.e., full-length aptamers) are usually 80 – 100 nucleotides (nt) long. However, not all of the nucleotides in a full-length aptamer play a critical role in the binding to its target. A full-length aptamer usually has three functional regions. The region that plays the role of contacting the target is approximately 10 – 15 nt long [51]. Another region contains nucleotides that do not directly contact the target but play an important role in supporting the interactions between the contacting nucleotides and the target. The nucleotides that either bind to the target or facilitate aptamer binding are the essential nucleotides required for a functional aptamer. In general, the number of essential nucleotides is approximately 25 – 40 nt [52]. The third region comprises the nucleotides that do not bind to the target nor support the binding of the contacting

nucleotides to the target. They are regarded as nonessential nucleotides. It is always desirable to truncate the aptamer to eliminate the nonessential nucleotides after the upstream aptamer-selection process (i.e., downstream truncation) for several reasons. Firstly, in some cases, elimination of nonessential nucleotides can increase the binding functionality of the aptamer [53] presumably because of reduced steric hindrance. Secondly, the smaller aptamers can provide more freedom and space for constructing novel nanostructures with smaller, more desirable dimensions, which is required to develop tiny, more sensitive biosensing devices [54]. Thirdly, although the chemical synthesis of an oligonucleotide is a well-established technique, the synthesis of aptamers longer than 60 nt is still more expensive and difficult to perform.

### I.1.3.2 Structural Features of Aptamers

A distinguishing feature of aptamers is their ability to form pronounced secondary structure. This structure is the result of a combination of hydrogen bonding, electrostatic and van der Waals interactions, Watson-Crick and non-canonical base pairing, and stacking of aromatic rings [55, 56]. It has been shown in many cases that unpaired sites in the oligonucleotide structure are most important for the specific interaction with targets, whereas sites with stable secondary structure are necessary to maintain the proper spatial arrangement of the recognition elements [57, 58]. This is confirmed by the fact that many aptamer sites are non-structured in the free state (like loops in hairpins) and acquire a stable conformation only after binding to the target [58-60].

Usually one or two structural motifs comprise the basis of an aptamer. Most frequent are the following structural elements (Figure 1-3).

1. Hairpins of different structures. It is one of the most widespread secondary structure motifs occurring both in RNA and DNA aptamers.

2. Pseudoknots. The pseudoknot structure is formed as a result of complementary interactions of the sequence located to the right or to the left of a hairpin with the

sequence of the hairpin loop. Pseudoknots are most characteristic of RNA aptamers, but they occur in DNA sequences as well [57, 61, 62].

3. Four-stranded structures (quadruplexes). As a rule, the quadruplex cross section is formed by four guanine nucleotides (G-quartet). Each guanine base in the G-quartet forms hydrogen bonds with two adjacent bases. Usually in a quadruplex there are 2 or 3 G-quartets stacked in succession. Such structures exhibit very high stability compared to simpler structural motifs. The quadruplex is additionally stabilized in the presence of $K^+$ ions coordinated between planes of two neighboring G-quartets [63]. The G-quartet structures appeared to be typical of DNA aptamers, although in some cases they were also found in RNA ligands [64-70]. It is supposed that in all cases the structural motif of the G-quartet is the architectural basis of the aptamer, whereas nucleotides in variable loops between quadruplex strands are involved in protein recognition.

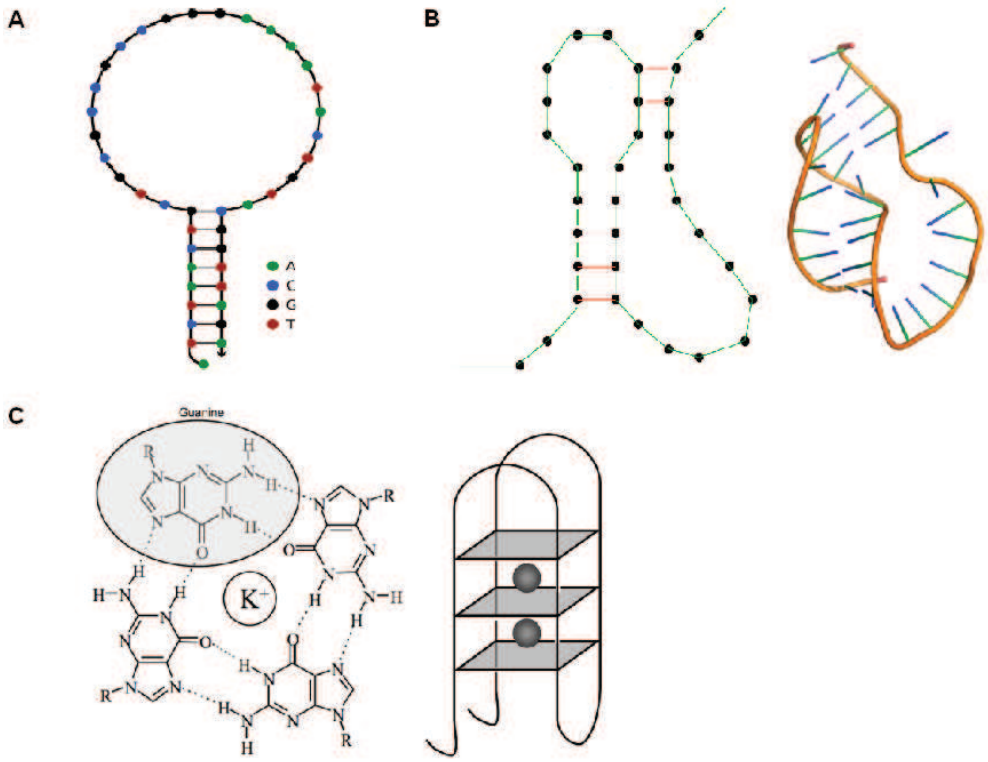


**Figure 1-3:** Scheme for 3 basic structure of aptamer [58-60]: A. hairpin; B. pseudoknots; C. quadruplexes

### I.1.3.3 Aptamer-Target Molecular Recognition

In many ways, aptamers can be considered as nucleic acid-type antibodies with properties comparable with or even superior to conventional antibodies. The binding of an aptamer to its target is very specific. Interactions occurring between aptamers and their molecular targets are usually so specific that even tiny variations in the target molecule may disrupt aptamer binding (e.g., aptamers for theophylline and L-arginine can discriminate closely related chemical structures by factors as high as 4 orders of magnitude [71, 72]). In addition to this high selectivity, aptamers bind to their targets with high affinity, particularly with macromolecules (e.g., proteins), which often possess remarkable dissociation constants ($K_d$) ranging from picomolar to nanomolar [71]. For small molecules, $K_d$ range commonly from nanomolar to millimolar [73] (Table 1).

Aptamers were first described in 1990 by two separate groups targeting either an organic dye [6] or a DNA polymerase [7]. Since the inception of the technology, aptamers have been selected for a vast range of targets including metal ions, small organic molecules, nucleotides and derivatives, cofactors, nucleic acids, amino acids, carbohydrates, antibiotics, peptides, proteins, whole cells, viruses and virus infected cells and bacteria (Table 1).

**Table 1:** Aptamer selected in vitro for different targets

| Target | Type | $K_d$ | References |
|---|---|---|---|
| ***Ions*** | | | |
| $Zn^{2+}$ | RNA | 1.2 mM | [74] |
| $Ni^{2+}$ | RNA | 0.8-29 µM | [75] |
| ***Nucleotides*** | | | |
| ATP / adenosine | RNA | 0.7-50 µM | [73] |
| | DNA | 6 µM | [76] |
| ATP | RNA | 4.8-11 µM | [77] |
| ***Cofactors*** | | | |
| Riboflavine | RNA | 1-5 µM | [78] |
| NAD | RNA | 2.5 µM | [78] |
| Biotin | RNA | 5.7 µM | [79, 80] |
| FAD and FMN | RNA | 0.5-50 µM | [81] |
| ***Amino acids*** | | | |
| L-arginine | RNA | 1 mM | [82] |
| | RNA | 56 µM | [83] |
| | RNA | 330 nM | [72] |
| | DNA | 2.5 mM | [84] |
| L-citrulline | RNA | 62-68 µM | [83] |
| L-histidine | RNA | 8-54 µM | [85] |
| L-isoleucine | RNA | 200-500 µM | [86] |
| L-valine | RNA | 12 mM | [87] |
| L-tyrosine | RNA | 35-743 µM | [88] |
| L-tyrosinamide | DNA | 45-80 µM | [89] |
| D-tryptophan | RNA | 18 µM | [90] |

**Table 1:** Aptamer selected in vitro for different targets (continued)

| *Target* | Type | $K_d$ | References |
|---|---|---|---|
| ***Antibiotics*** | | | |
| Tobramycine | RNA | 2 -3 nM | [91] |
| Lividomycine | RNA | ≤ 300 nM | [92] |
| Kanamycine A | RNA | ≤ 300 nM | [93] |
| Kanamycine B | RNA | 180 nM | [94] |
| Neomycin B | RNA | 100 nM | [95] |
| ***Carbohydrates*** | | | |
| Cellobiose | DNA | 1-100 µM | [96] |
| ***Lipids*** | | | |
| Cholic acids | DNA | 6.4-67.5 µM | [97, 98] |
| ***Peptides*** | | | |
| Substance P | RNA | 190 nM | [24] |
| | RNA | 40 nM | [99] |
| Vasopressine | DNA | 1.2 µM | [100] |
| | RNA | 1 nM | [101] |
| Neuropeptide Y | DNA | 0.3-1 µM | [102] |
| ***Proteins*** | | | |
| **Antibodies** | | | |
| Anti-NES Ab | RNA | 0.1 µM | [103, 104] |
| MAb G6-9 | RNA | 2 nM | [105] |
| Ig E | RNA | 30 nM | [106] |
| | DNA | 10 nM | [106] |

**Table 1:** Aptamer selected in vitro for different targets (continued)

| Target | Type | $K_d$ | References |
|---|---|---|---|
| **Cell surface proteins** | | | |
| β2 integrin LFA-1 | RNA | 0.5-1 μM | [107] |
| L-selectin | DNA | 1.8-5.5 nM | [108] |
| **Enzymes** | | | |
| Reverse transcriptase of HIV-1 | DNA | 5 nM | [61] |
| | RNA | 1 nM | [62] |
| ***Complex targets*** | | | |
| Ribosome | RNA | 4-5 nM | [57] |
| Leukemia cells | DNA | 0.8-229 nM | [33] |

### I.1.3.4 Advantages of Aptamers Compared to Antibodies

Compared with conventional recognition elements like monoclonal antibodies, aptamers present similar or even better characteristics [21, 109, 110]:

- Aptamers possess extremely high affinity and specificity for related ligands as well as for some ligands which could not be recognized by antibodies, such as ions, non-immunogenic and toxic targets, indicating that employing aptamers as recognition components may significantly expand the applications of the corresponding biosensors.
- Once selected, aptamers could be massively synthesized by chemical process, which is more convenient than the production of antibodies which require the

induction of animal immune system. As a result, the cost for fabrication of aptamer-based biosensors could be largely cut down.

- Aptamer can be easily modified by different functional groups at critical, precise locations in order to increase stability or allow signaling using electrochemical probes, fluorophores and quenchers.
- Aptamers are more stable at elevated temperatures, and thermal denaturation of aptamers is reversible, while, as proteins, antibodies are more thermally sensitive, and denaturation of antibodies is usually irreversible. Thus use of aptamers offers a wide range of assay conditions.
- The binding of aptamers with their targets usually relies on specific conformations, such as G-quaduplex, hairpin etc... The conformational variations trigged by the formation of aptamer-ligand complexes offer a great possibility and feasibility for the construction of aptamer-based biosensors.
- Owing to their oligonucleotidic nature, they could interact with other DNA or RNA molecules, such as DNAzymes, allowing designing versatile oligonucleotide machines for either biosensing or clinical applications.
- Nucleic acid aptamers can hybridize with their complementary sequences, which can be used to create antidotes or structure-switching biosensing platform.
- Aptamers can function both inside and outside cells whereas antibodies usually only work outside cells to target secretory proteins or cell surface receptors.
- For therapy, aptamers have shown no intrinsic toxicity and immunogenicity but antibodies, even humanized, could induce immunogenicity.

Due to the above advantages, aptamers are considered as promising alternatives to antibodies in bioassay related fields and have been applied in bio-molecule detection, cell collection and detection [111, 112], imaging [33], or other clinical treatments [109]. The applications of aptamers remain very dynamic, with increasing explorations in the field of biosensing, diagnosis, and therapeutics (some aptamer-based applications are illustrated in Figure 1-4).

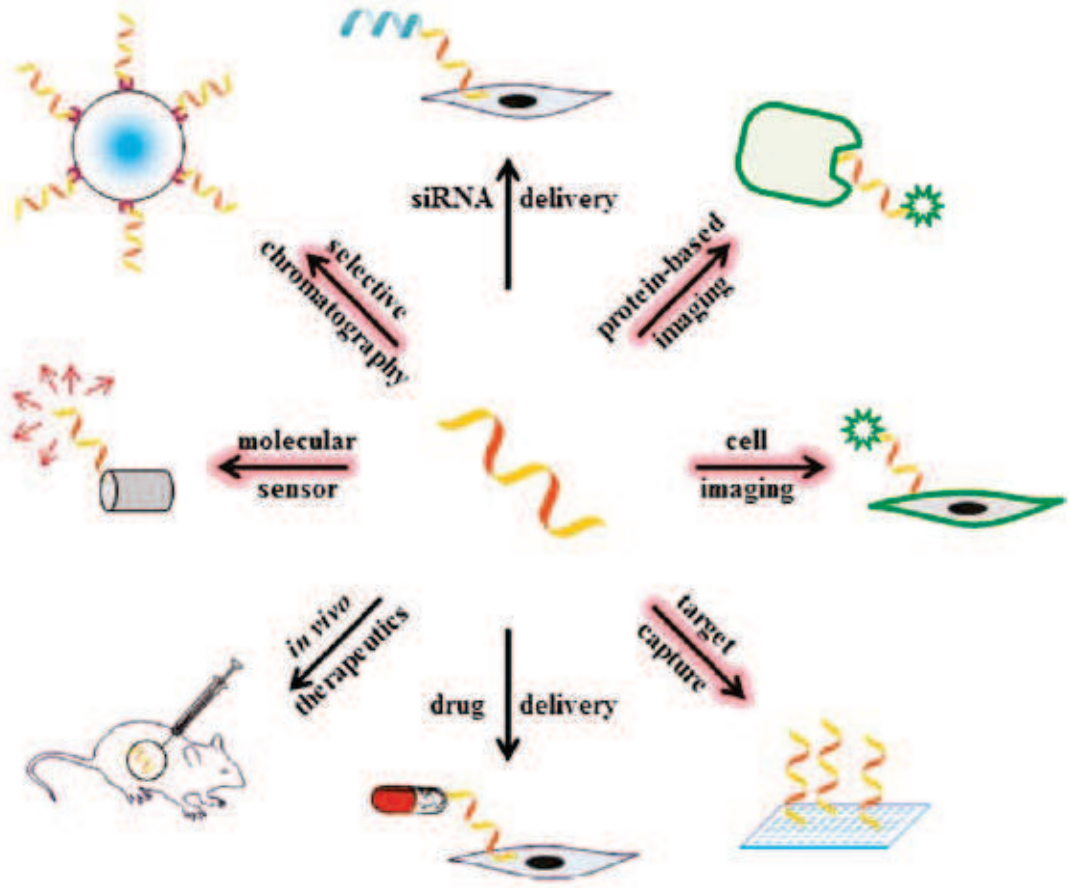


**Figure 1-4:** Widespread use of aptamers for various analytical and biological applications. Bioanalytical applications of aptamers are highlighted in red [113].

### I.1.3.5 Aptamer Modifications

Although aptamers have significantly broadened the utility of nucleic acids as molecular recognition elements (MREs), standard unmodified DNA and RNA aptamers do not have inherent properties with which a convenient method can be adopted to report an aptamer–target interaction. Therefore, to take full advantages of aptamers as bioassay probes, it is necessary and important to find ways to link the excellent molecular recognition capability of aptamers to a signal production process which is simple (without the need of a complicated modification to an aptamer for signal generation), universal (no matter what characteristics an aptamer and its target

exhibit), and convenient to use (with minimal sample operating during the signal generating process). Phosphoramidite chemistry enables easy functionalization of the oligonucleotide sequence at the 3' or 5' end, or in the middle of the sequence. Functional groups, such as biotin, amino, thio, carboxyl, sulfhydryl and a wide range of fluorophores, can all be incorporated during the chemical synthesis of oligonucleotides [114-117]. The modifications can be introduced either during SELEX or after SELEX or both.

The pharmacokinetics of aptamers is determined by their various properties including nuclease-resistance, uptake and distribution in tissues and circulation half-life in the blood of organisms. Modifications of aptamers can help to improve their pharmacokinetics for therapy and in vivo diagnosis.

Modifications such as 2'-$NH_2$, 2'-F, 2'-$OCH_3$ and 4'-SH were introduced to increase the nuclease resistance of aptamers. The half lives of natural RNAs in human serum are from seconds to hours but those of modified aptamers are days (e.g. >> 96 hr for the 2'-$OCH_3$-VEGF aptamer). In addition to nuclease resistance, these modifications also increase the affinities of aptamers by increasing their thermostability and chemical diversity [118, 119]. In one study, post-SELEX modification of an NF-κB aptamer in stem I and in loop region increased the aptamer's thermostability (Tm from 34.8 ℃ to 45.7 ℃). At the same time, the nuclease resistance of the aptamer was increased by three-fold [115]. Capping at the 5' and 3'-termini can also increase resistance of aptamers to exonucleases. The degradation of aptamers in human blood is largely due to exonucleases from 3'-termini to 5'-termini. A commonly used 3'-capping of aptamers is an inverted thymidine (3'-idT), which creates an additional 5'-end without a 3'-end. The 3'-capping with 3'-idT can greatly increase aptamer stability in an organism's blood. The half-life of a platelet-derived growth factor (PDGF) DNA aptamer modified with 2'-F, 2'-$OCH_3$ and 3'-capping by 3'-idT was increased from 0.6 h to 8 h in 85% rat serum [120].

Nuclease-resistance is only one part of the aptamer pharmacokinetics. Uptake and distribution in tissues and circulation half-lives of aptamers are other important

aspects of aptamer pharmacokinetics. Aptamers are relatively small (10-15 kDa, 30-45 nt) and can be easily cleared from human blood through the kidney and liver. To increase the circulation half lives of aptamers, tagging aptamers at the termini is often used. The most commonly used tag is polyethylene glycol (PEG). Pegylation usually has little effect on the affinities of aptamers but it can dramatically increase the circulation half lives of aptamers, thus enhancing in vivo aptamer activity. In addition, pegylation can affect the tissue distribution of aptamers. Tagging with lipids may also increase the circulation half lives of aptamers and tagging with cell-penetrating peptides may help tissue uptake of aptamers.

Some multifunctional aptamers have been developed. A thrombin aptamer, a L-selectin aptamer and a DNA element conjugated to biotin or fluorescence were linked together through duplex linkers or three way junctions. The resulting multivalent aptamers had multiple functions including anticoagulation activity and application as biosensors [121, 122]. Another bifunctional aptamer could sense either AMP or cocaine. The AMP and cocaine aptamer was linked into one piece, which was hydridized to another piece of DNA. Either AMP or cocaine could compete with the hybridized sequence and release it to give colorimetric or electric signal for detection [123]. Another bivalent aptamer was also reported to bind simultaneously to the HIV transactivation responsive element (TAR) and the dimerization initiation site (DIS) in the 5' untranslated region. The two aptamers were linked through a PEG linker. The resulting bifunctional aptamer showed about 10 times higher affinity for HIV RNA 5'-untranslated region compared with those of individual aptamers. The enhanced affinity was due to a slower dissociation rate [124].

# I.2 Aptamers-based Bioanalytical Assays

## I.2.1 Introduction

Aptamers are strong and powerful tools as molecular recognition elements for analytical applications. Researchers have made considerable efforts in recent years to take advantage of the unique features of aptamers to design appropriate strategies to effectively and efficiently use aptamers for biological agent recognition, identification, characterization and quantification.

Generally, a biosensor is a device that comprises two or more of the following parts: recognition component, linker, localization component, signal receptor, signal amplification component and signal transducer, etc. Among them, at least two parts are unavoidable: one is the recognition part, which could specifically recognize and identify target, and the other is the signal transduction part, which could transform the analyte signal into some detectable signal. Recognition components, typically enzymes, antibodies or nucleic acids, directly determine the stability, selectivity, sensitivity, as well as application prospects of biosensors.

In addition to the inherent advantages of biosensors, aptamer-based biosensors offer the advantage of reusability over antibodies. Furthermore, their smaller size and versatility allow efficient immobilization at high density, which is essential in multiplexing miniaturized systems (e.g., bioarrays or biochips). In this chapter, aptamer-based biosensors were classified into three basic modes: target-induced conformation change mode, complementary strand displacement mode, sandwich or sandwich-like mode. Based on these three basic strategies, aptamer-based affinity separation and purification and various detection methods for aptamer-based assays were also discussed.

## I.2.2 Basic Strategies for Aptamer-Based Assays

### I.2.2.1 Target-induced conformation change mode (Direct mode)

In this mode, the targets directly bind to their aptamers, coupled with the corresponding conformational change of aptamers to specific patterns instead of random structures, and this event subsequently leads to the "changes" of detectable properties. These kinds of "changes" include the quantity, position or status of the signal moieties (which are covalently bound to the end of aptamers or adsorbed on the aptamers via electrostatic force, stacking, hydrogen bond, etc.), the size or weight of aptamers, along with the formation of aptamer-target complexes and other properties of aptamers, such as the ability to stabilize gold nanoparticles (AuNPs). Each of the "changes" described above could lead to an alteration of signal which implies a potential opportunity for the design of direct aptamer-based biosensors.

#### I.2.2.1.1 Electrochemical detection

The analytical applications of aptamers are rapidly moving towards electrochemical strategies, not only because electrochemical techniques have high sensitivity but also because the instrumentation is simple, low cost, and can be readily miniaturized. Various electrochemical detection methods have now been utilized with aptamers based on the direct mode, such as the aptamer beacon [125, 126] and target-responsive electrochemical aptamer switch (TREAS) [127]. Upon the binding of the targets to the aptamers immobilized on the surface of electrodes, aptamers change from random flexible conformations into three-dimensional structures such as G-quaduplex. Such conformational changes would alter the relative positions of signal moieties which are covalently linked to the end of aptamers towards the electrodes, leading to the changes of electrochemical signal. Based on such mode, several electrochemical aptamer-based biosensors have been designed. A redox

probe-labeled, signal-off electrochemical biosensor was first developed in 2005 for thrombin detection [128]. Before the binding of thrombin, the electrochemical active redox moiety, methylene blue (MB) which was covalently labeled at the end of aptamer, could transfer electron with the electrode surface due to the flexible conformation of the aptamer. However, once thrombin was captured by the aptamer and the G-quaduplex structure was formed, the MB moiety was kept away from the electrode surface, resulting in the electrochemical signal-off (Figure 1-5). The main disadvantage of such design is negative signal.

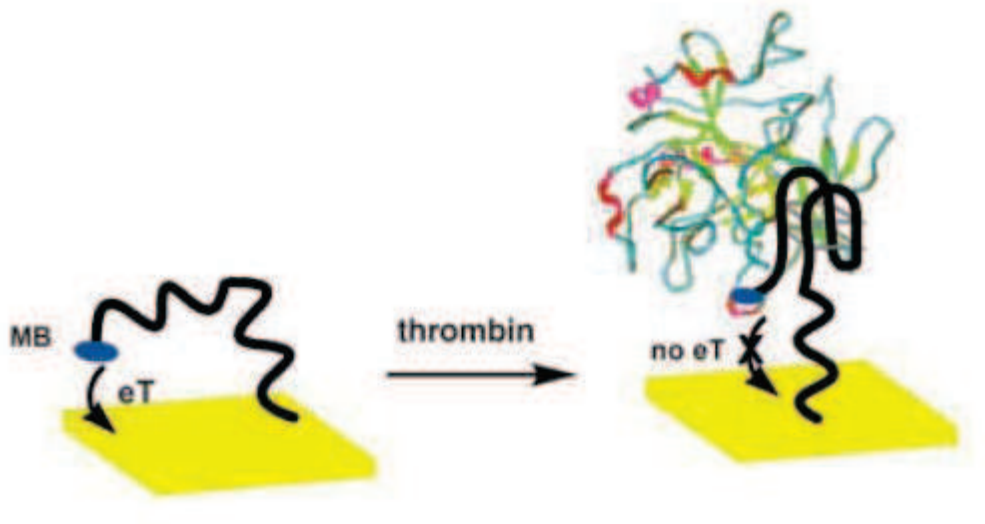


**Figure 1-5:** Design of a signal-off electrochemical aptamer biosensor for thrombin detection [128]. After binding to thrombin, the aptamer probe self-assembles into a G-quadruplex structure and keeps MB away from electron-transfer (eT) communication with the electrode, leading to a negative signal.

To circumvent this problem, several signal-on electrochemical biosensors were developed. In a typical work in 2006, thrombin-binding aptamer immobilized on polycrystalline gold electrode was covalently attached with ferrocene (Fc) at the other end [125]. The electrode surface was further blocked by 2-mercaptoethanol. No signal was obtained before the binding of thrombin, because the flexible unfolded aptamer led to the large electron-tunneling distance between Fc moiety and the electrode. In the presence of thrombin, the formation of a thrombin-aptamers complex made the

G-quadruplex aptamer configuration rigid and resulted in the turning of the ferrocene units towards the electrode (Figure 1-6). This led to electron-transfer between the electro-active ferrocene units and the electrode, and produced a positive signal. However, the flexibility of aptamers immobilized on electrode surface could bring high background signals and influence the reproducibility of biosensors.

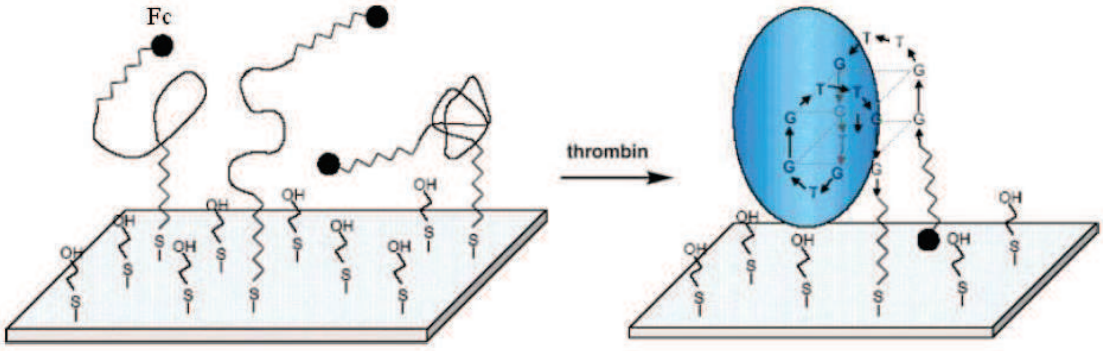


**Figure 1-6:** Design of a signal-on electrochemical aptamer biosensor for thrombin detection [125]. The formation of a thrombin-aptamers complex makes the G-quadruplex configuration rigid and results in the orientation of the ferrocene units towards the electrode, leading to easy electron transfer between the electro-active ferrocene unit and the electrode, producing a positive signal.

Detection in the femtomolar range was achieved with aptamer capture of a protein target followed by electrochemical impedance spectroscopy (EIS) [129] and chemical amplification (10 fM) [130]. However, most of these detection methods were limited to DNA aptamers, and the first example of a RNA aptamer–based electrochemical sensor has been reported by Ferapontova *et al.* in 2008 [131]. For these direct electrochemical aptamer-based sensors, their electroactive reporters such as methylene blue (MB) [132], ferrocene [133], ferrocene-bearing polymers [134], ruthenium complexes [135], and $Fe(CN)_6^{4-/3-}$ [136] were used for signal transduction. These reporters were covalently conjugated to the aptamer itself [132, 133, 137], or indirectly complexed with aptamers [134]. Based on the incorporation of an

electrochemical reporter, detection can be either "signal on" or "signal off," depending on how the redox reporter was shielded from the electrode.

Most of these electrochemical biosensing methods were based on a large conformational change of the aptamer which upon binding of the protein targets, and the preparation of aptamer-modified electrodes could be laborious and timeconsuming. Recently, Limoges *et al.* reported a new electrochemical methodology for monitoring in homogeneous solution the enantiospecific binding of a small chiral analyte to an aptamer [138]. The principle relied on the difference of diffusion rates between the targeted molecule and the aptamer/target complex, and thus on the ability to more easily electrochemically detect the former over the latter in a homogeneous solution (Figure 1-7).

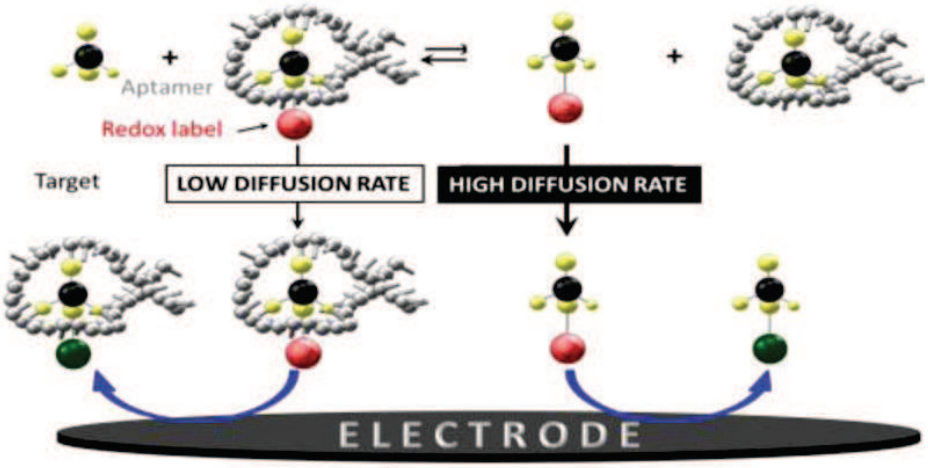


**Figure 1-7:** General principle of the homogeneous electrochemical aptamer-based enantioselective binding assay involving an electrodetectable small target [138].

I.2.2.1.2 Fluorescence/quantum dot detection

Besides electrochemical biosensors, target-induced conformation change mode could be utilized to design optical biosensors. The most important and widely used optical aptamer sensors are based on fluorescently labeled aptamers. Indeed, fluorescence technique is highly compatible with nucleic acid aptamers [139]: firstly,

there are a large number of well-characterized fluorophores and quenchers that can be used to modify nucleic acids during the automated synthesis or using simple post-synthesis chemistries; secondly, fluorophore-dressing of nucleic acids eliminates the need of target-labeling and therefore it can be universally applied to any aptamer–target pair; thirdly, fluorescence offers a very convenient way to report molecular interactions because the detection can be carried out in real time without the need for the separation of target–probe complexes from unbound probes. Furthermore, the availability of many different fluorophores with different excitation and emission wavelengths makes it feasible to conduct multiplexed assays with which several targets within the same sample can be assessed at the same time without cross interference. Since aptamers can be readily modified with fluorescence tags, different approaches have been focused on how to generate fluorescence-labeled aptamers and how to detect fluorescence signal changes in response to aptamer binding to its target [140-150].

As various fluorophores and aptamer modifications have become commercially available, several design strategies have been developed, one of which is based on fluorescence resonance energy transfer (FRET). The simplest format is to label aptamers with a quencher and either one or two fluorophores, enabling both quenching and "light-up" strategies (Figure 1-8). An anti-cocaine DNA aptamer [151] and an anti-PDGF aptamer [152] were destabilized by truncating one of the stems of a three-way junction and labeling the termini with a 5' fluorophore and a 3' quencher. Ligand binding stabilized the engineered stem and brought the quencher and fluorophore in close proximity, resulting in a fluorescence decrease (Figure 1-8a). However, a potential problem with quenching aptamer beacons is that there are a variety of ligands or solvents that may interfere with quenching, leading to a false positive signal. To overcome this problem, beacons can rely upon FRET to signal. For example, in 2002 Tan's group [153] has noted that in the absence of the protein target, an equilibrium existed between the random coil state and the quadruplex states of an anti-thrombin aptamer. By incorporating two fluorophores, coumarin (donor) and fluorescein (acceptor), at the two termini of the aptamer, thrombin binding could be

monitored. In this study, the apparent dissociation constant ($K_d$) and limits of detection for the two-fluorophores aptamer beacon were 4.87 ± 0.55 nM and 429 ± 63 pM, respectively. The FRET beacon gave a ~14-fold signal-enhancement factor (the ratio of acceptor to donor intensity before and after binding). FRET-type aptamer beacons may prove to be particularly useful for real-time analysis of proteins and may be used in living specimens in conjunction with ratiometric imaging. Such beacons have already been used for the detection of angiogenin in serum samples from healthy and lung cancer patients [154]. Aptamers could also be engineered to refold, rather than fold. In one experiment [155], sequence was added to an anti-thrombin DNA aptamer that fixed it in a molecular beacon–like hairpin structure. Upon the addition of thrombin, the conformational equilibrium was shifted from the quenched hairpin to the thrombin-bound quadruplex, resulting in dequenching of the fluorophore and the creation of an optical signal (Figure 1-8b).

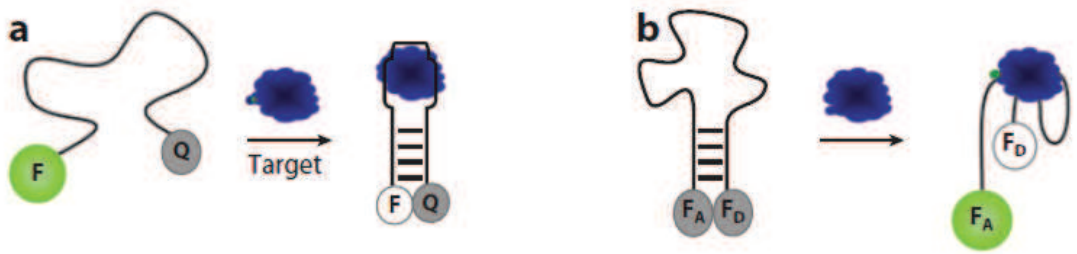


**Figure 1-8:** Schemes for the target-induced conformation change based quenching and "light-up" aptamer beacons. (a) Quenching aptamer beacon: Target binding brought the quencher and fluorophore in close proximity, resulting in a fluorescence decrease [151, 152] (b) "Light-up" aptamer beacon: Upon the addition of thrombin, the conformational equilibrium was shifted from the quenched hairpin to the thrombin-bound quadruplex, resulting in dequenching of the fluorophore and the creation of an optical signal [155].

Another aptamer-fluorescent biosensor for intact cell detection was created by the Jaykus group in 2010 which purified a DNA aptamer with high affinity to pathogenic Campylobacter jejuni cells through the cell-SELEX approach [156]. In another report, a homogeneous label-free quantitation was achieved through measuring fluorescence

decrease of crystal violet via the specific interaction between TBA and thrombin [157]. A highly sensitive aptasensor was also developed by Chang *et al.* in 2010 [141] via the utilization of FRET as the mode of detection on a graphene surface immobilized with thrombin selective aptamer. In the resting state, fluorescence was quenched by the dye-linked aptamer, followed by fluorescence recovery after the introduction of thrombin into the system and complex formation.

Besides the common organic fluorescent dyes, quantum dots (QDs) have also been developed as labels for the sensitive detection [158]. Compared to organic fluorescent dyes [159], QDs are highly photostable and the wavelength of the emitted light can be controlled by changing the size and composition of the materials. Furthermore, QDs have a very broad excitation range with sharp emission, making it possible to excite different QDs with a single wavelength, while still resulting in a variety of emission wavelengths. Dong *et al.* [160] created a platform that combined aptamer-based molecular sensor beacons and a QD-based FRET system in 2010. Aptamer-functionalized quantum dots interact with graphene oxide, thus resulting in fluorescence quenching due to FRET. After the addition of the aptamer-specific target, the binding to the aptamers causes an increase in QD-graphene oxide distance, inhibiting FRET and enabling fluorescence detection. Such an ability to sensitively detect even minor changes in binding could be particularly useful for many applications.

I.2.2.1.3 Chemiluminescence detection

Chemiluminescence detection has been widely applied in various fields, since it does not require external light source like fluorescence to produce light signal and offers simplicity, low cost, and high sensitivity. It is not surprising that chemiluminescence-based aptasensors have recently become a popular field [161, 162]. Taking advantage of this detection approach, a chemiluminescence system was constructed in 2011 on the basis of the lysozyme (LYS) induced fluorescence enhancement of aptamer-grafted single-walled carbon nanotubes (SWNTs) and the $Eu^{3+}$ complex (Figure 1-9) [163]. In the absence of LYS, the SWNTs were wrapped

by the ssDNA, so that they were well dispersed and remained in the supernatant, providing the quenching substrate for the $Eu^{3+}$ chelates. While in the presence of LYS, interaction of the aptamer with LYS made it unable to disperse the SWNTs, after centrifugation to separate the SWNTs, BHHT/$Eu^{3+}$ in solution emitted a strong luminescence.

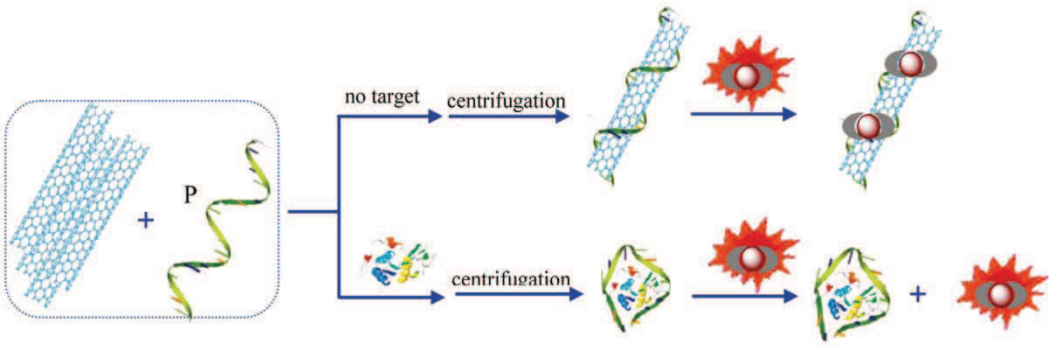


**Figure 1-9:** Schematic representation of luminescent biosensor [163]. In the absence of target, the SWNTs are in complex with the present aptamers, resulting in the quenching of the luminescence signal from the chelated $Eu^{3+}$. After the addition of the target LYS, which binds with the aptamers, the SWNTs aggregate and can be easily removed, resulting in the strong unquenched luminescence signal from the added $Eu^{3+}$.

Similarly, detection of other proteins, like α-fetoprotein (AFP), has been reported with a sensitivity limit of 5 pg /mL, which was much lower than the classical enzyme-linked immunosorbent assay (ELISA). In a report by Ahn *et al.* in 2009 [164] an aptamer nanoarray chip-based chemiluminesce immunosorbent assay was developed for sensitive detection of severe acute respiratory syndrome (SARS) coronavirus nucleocapsid protein. Such a sensitive detection approach could be highly valuable for the virus detection, particularly in the light of SARS disease outbreaks a few years ago.

Chemiluminescence was also used for the detection of ions like $Pb^{2+}$ [165]. In a particularly interesting report in 2010, Li *et al.* [166] used isoluminol isothiocyanate (ILITC) as a chemiluminescent tag on an aptamer, which was then used in a CE-based

method to detect the interacting targets. Such an approach has demonstrated the capability to calculate the dissociation constant ($K_d$) and the number of binding sites.

I.2.2.1.4 Fluorescence polarization (FP) detection

The theory of fluorescence polarization is based on the observation that fluorescent molecules in solution, excited with plane-polarized light, will emit light back into a fixed plane if the molecules remain stationary during the excitation. FP detection works particularly well for binding interactions that lead to significant change in the size of the molecular system that is associated with a reporter fluorophore. Labeling can make use of conventional and readily obtained organic dyes such as fluorescein, Texas Red, and carboxytetramethylrhodamine (TAMRA). There is no need for separation steps to purify complexes from unbound interacting partners, and this offers opportunity to determine parameters such as the dissociation constant by titration. Various classes of binding agents have been identified including aptamers. The molecular size of an aptamer, the availability of functional groups for fluorescence tagging, and the ability to serve as a binding agent or a displacement agent, combine to offer opportunities when considering use of FP to study binding, and to develop diagnostic methods and biosensors.

Numerous aptamer-based FP methods targeting small molecules, peptides and proteins have been developed in the past few years. The aptamer based FP analysis of macromolecules such as proteins is quite simple, and is related to the molecular volume change of the aptamer probe upon macromolecular target complexation. In 1998, Hieftje's group first developed a FP method for the real-time detection of thrombin using aptamer [167]. In a model system, an anti-thrombin DNA aptamer was fluorescently labeled and covalently attached to a glass support. Thrombin in solution was selectively detected by following changes in the evanescent-wave-induced fluorescence anisotropy of the immobilized aptamer. The new biosensor can detect as little as 0.7 amol of thrombin in a 140-pL interrogated volume, had a dynamic range of 3 orders of magnitude, had an inter-sensing-element measurement precision of better than 4% RSD over the range 0-200 nM, and required

less than 10 min for sample analysis. Since then the FP method has been further extended to the detection of other proteins, such as human neutrophil elastase [9], oncoprotein PDGF [168], IgE [169], angiogenin [170], and lysozyme [171].

In contrast, the FP sensing of a small target appears much more complicated as the target binding does not significantly change the size of the labeled functional nucleic acid. The former FP-based analysis of small molecules mainly relied on a competitive format. In 2009, our group has reported a noncompetitive FP technique dedicated to the small molecule sensing [172] (Figure 1-10). This approach was based on the unique induced-fit binding mechanism of nucleic acid aptamers which was exploited to convert the small target binding event into a detectable fluorescence anisotropy signal. An anti-L-tyrosinamide DNA aptamer, labeled by a single fluorescent dye at its extremity, was employed as a model functional nucleic acid probe. The DNA conformational change generated by the L-tyrosinamide binding was able to induce a significant increase in the fluorescence anisotropy signal. The method allowed enantioselective sensing of tyrosinamide and analysis in practical samples. The methodology was also applied to the L-argininamide detection, suggesting the potential generalizability of the direct FP-based strategy. Such aptamer-based assay appeared to be a sensitive analytical system of remarkable simplicity and ease of use. However, this method was confined to certain aptamer system which had a significant conformational change upon target binding.

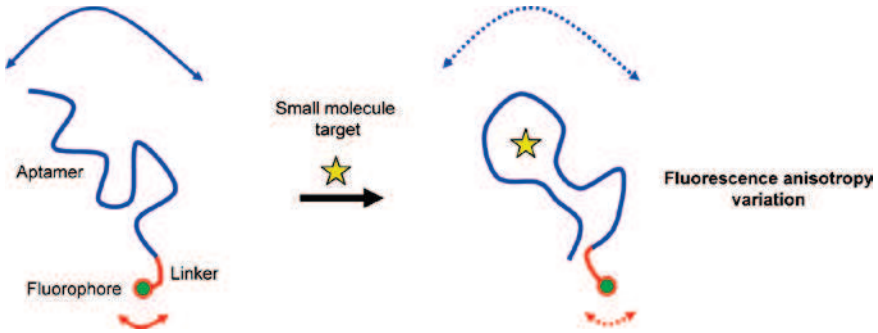


**Figure 1-10:** Schematic representation of the noncompetitive FP strategy for the design of the small molecule aptasensor [172]. Double arrows represent the possible local and global motional contributions to the variation of the fluorescence anisotropy signal.

In order to generalize the direct approach, our group then established a rational FP sensor methodology by engineering instability in the secondary structure of an aptameric recognition element [173]. The anti-adenosine DNA aptamer, labeled by a single fluorescein dye at its 3' extremity, was employed as a model functional nucleic acid probe. The terminal stem of the stem-loop structure was shortened to induce a destabilized/denatured conformation which promoted the local segmental mobility of the dye and then a significant depolarization process. Upon target binding, the structural change of the aptamer induced the formation of a stable stem-loop structure, leading to the reduction of the dye mobility and the increase in the fluorescence anisotropy signal. This reasoned approach was applied to the sensing of adenosine and adenosine monophosphate and their chiral analysis (Figure 1-11).

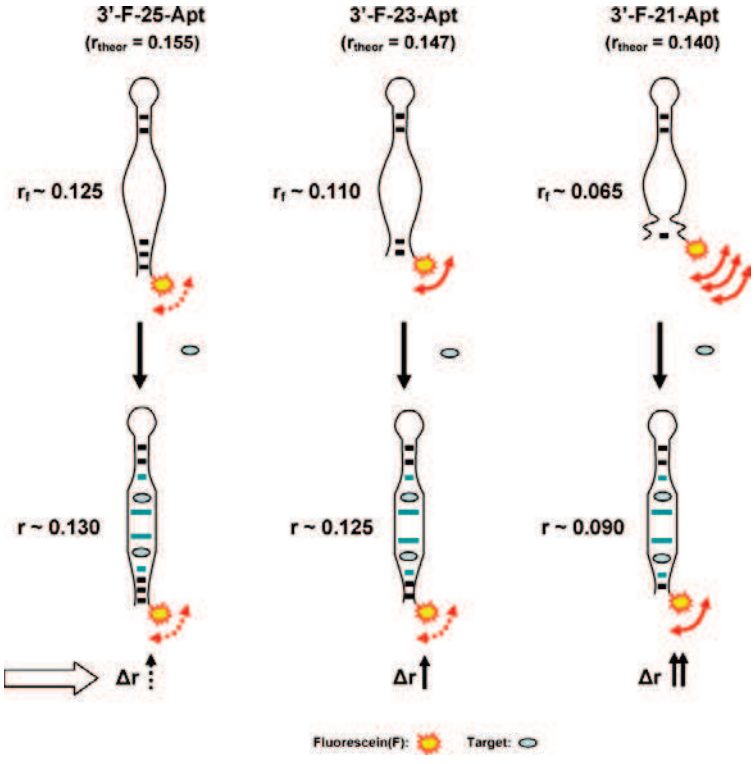


**Figure 1-11:** Proposed representation of the dye local segmental motion contribution (arrow) to the variation of the fluorescence anisotropy signal in relation to the aptamer probe structure. rf is the fluorescence anisotropy in the absence of analyte [173].

As a complement to the direct method, our group reported a FP biosensor based on an aptamer enzymatic cleavage protection strategy in 2011 [174]. The nuclease-mediated size variation of a dye-labeled aptamer induced by the target binding can be effectively monitored through the analysis of the fluorescence anisotropy signal change of the fluorescent probe.

I.2.2.1.5 Mass Sensitive detection

A mass-sensitive biosensor is defined as any device that measures the property that scales proportionally to mass associated with or bound to its sensitive surface assembled with capture probes. Mass sensitive detection has the advantage of recording mass changes on the sensor surface, requiring no additional reagents for the labeling. More importantly, these detection methods can be used for the real-time detection. However, a number of drawbacks are associated with the mass change-based sensing, and therefore, it is normally more applicable for the detection of large analytes like proteins or cells but typically not for small molecules. Frequently used mass-sensitive techniques include surface plasmon resonance (SPR) [175], quartz crystal microbalance (QCM) [176] and surface acoustic wave device (SAW) [177] (Figure 1-12). In an aptamer-based gold nanoparticle (AuNPs) enhanced SPR detection, AuNPs, the SPR signal enhancer, was immobilized via DNA hybridization with the aptamer sequence. Like the target-responsive electrochemical aptamer switch (TREAS) strategy mentioned above, the binding of ATP led to formation of tertiary structure between aptamer and the AuNPs tagged complementary ssDNA, which finally resulted in the decrease of the SPR signal [175].

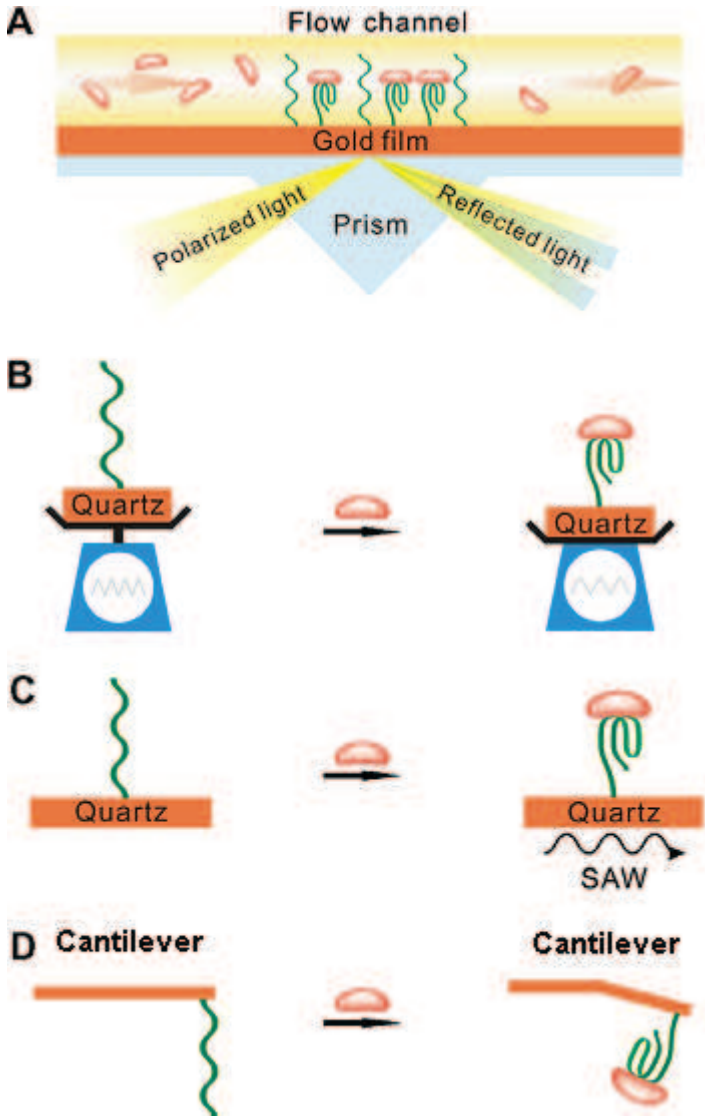


**Figure 1-12:** Mass-sensitive aptasensors. (A) SPR-based aptasensor [175]; (B) QCM-based aptasensor [176]; (C) SAW-based aptasensor [177]; and (D) micromechanical cantilever-based aptasensor [178, 179].

SAW devices work because mass changes on the surface lead to a change in the propagation velocity of acoustic waves, resulting in a reduction in resonance frequency or an alteration of the phase shift between the input and output signals. A special type of SAW sensor, the Lovewave sensor (which uses horizontal waves guided in a layer on the surface of the sensor to reduce energy dissipation of the acoustic wave, thereby increasing surface sensitivity), was combined with aptamers by Schlensog *et al.* [177] for the detection of thrombin and a HIV-1 Rev peptide. The

detection limits for thrombin and HIV-1 Rev peptide were 72 pg $cm^{-2}$ and 77 pg $cm^{-2}$, respectively. Like SAW, QCM employs piezoelectric quartz crystals, but the latter is a simpler and more cost-efficient technique. Aptamers using QCM technique have been used for the detection of thrombin (LOD < 1 nM) (96) and HIV-1 Tat protein (LOD of 0.25 ppm 100 $\mu L^{-1}$ and a dynamic range of 0.25 to 2.5 ppm) [180] by measuring the gravimetric resonance frequency change. Aptazymes may be useful for changing the relative mass present on a QCM. Knudsen *et al.* [181] have adapted the catalytic activity of both ligation and cleavage aptazymes to the detection of a HIV-1 Rev peptide (ligation) or theophylline (cleavage). The catalytic activities of immobilized aptazymes on the sensor surface were observed in real time by monitoring changes in QCM frequency.

A final example of the use of piezoelectric quartz crystals is the construction of microcantilevers that operate in a vibrational mode. Binding is measured by monitoring the differential bending between reference (random DNA) and sensor (aptamer) cantilevers. Taq DNA polymerase [178] and hepatitis C virus [179] were detected using DNA and RNA aptamers with LOD of 15 pM ($K_d$) and 2.1 pM, respectively.

### I.2.2.2 Complementary strand displacement mode (or target-induced structure switching mode)

The most common design strategy reported in the literature is related to the complementary strand displacement approach [137, 182-187]. The fabrication of those aptamer-based biosensors is highly depending on the unique conformations of aptamers (such as G-quaduplex or hairpin conformation) or the specific target-aptamer complex structures. However, in the design of some biosensors, a complementary strand displacement mode, which belongs to a structure-independent strategy, has been proposed [186]. This strategy is related to the unique ability of nucleic acids to form duplex structures with their complementary sequences (CS). In

the absence of target, base pairing between the aptamer and complementary sequences is favored. When the target binds to the aptamer, the hybridization is disrupted, leading to the release of the complementary strand. Therefore, via adequate labeling of the CS and/or the aptamer, the molecular recognition event can be effectively converted into a detectable signal. Because of its great simplicity and its very broad applicability, the duplex-to-complex change concept has been successfully exploited in the design of various aptamer-based assays.

I.2.2.2.1 Electrochemical detection

The electrochemical aptamer sensors based on complementary strand displacement strategy can be further classified into signal-off mode [137, 182, 183], signal-on mode [184, 186] and label-free mode [185, 187], as shown in Figure 1-13. In signal-off mode, the presence of targets can be determined from the signal suppression due to the release of redox-tagged aptamer from the electrode into solution. As an example, signal-off design for ATP and thrombin assay [137], the redox-tag attached aptamers was confined near the electrode surface through the hybridization with their thiolated complementary sequence, which was self-assembled on the gold electrode. In the absence of targets, the redox-tag gave electrochemical signals. When targets were added, the redox-tagged aptamers were released and the electrochemical signals were greatly reduced (Figure 1-13A). Signal-on strategy has also been developed. In the construction of an ATP biosensor [186], the aptamer hybridized with its thiolated complementary sequence which was immobilized on the gold electrode via Au-S bond. As the target ATP was added, the aptamer sequence was released from double strands to form target-aptamer complex. The remained complementary sequence was further hybridized with another Fc-moiety modified ssDNA, resulting in the appearance of electrochemical signal (Figure 1-13B). Furthermore, label-free displacement strategy was also raised. In a faradic impedance spectroscopy (FIS) for lysozyme assay [187], the aptasensor was fabricated by self-assembling the partial complementary single strand DNA (pcDNA)–lysozyme binding aptamer (LBA) duplex on the surface of a gold electrode. To measure lysozyme, the change in

interfacial electron transfer resistance of the aptasensor using a redox couple of $[Fe(CN)_6]^{3-/4-}$ as the probe was monitored. The introduction of target lysozyme induced the displacement of the LBA from the pcDNA–LBA duplex on the electrode into the solution, decreasing the electron transfer resistance of the aptasensor, which was utilized to quantify the concentration of lysozyme (Figure 1-13C).

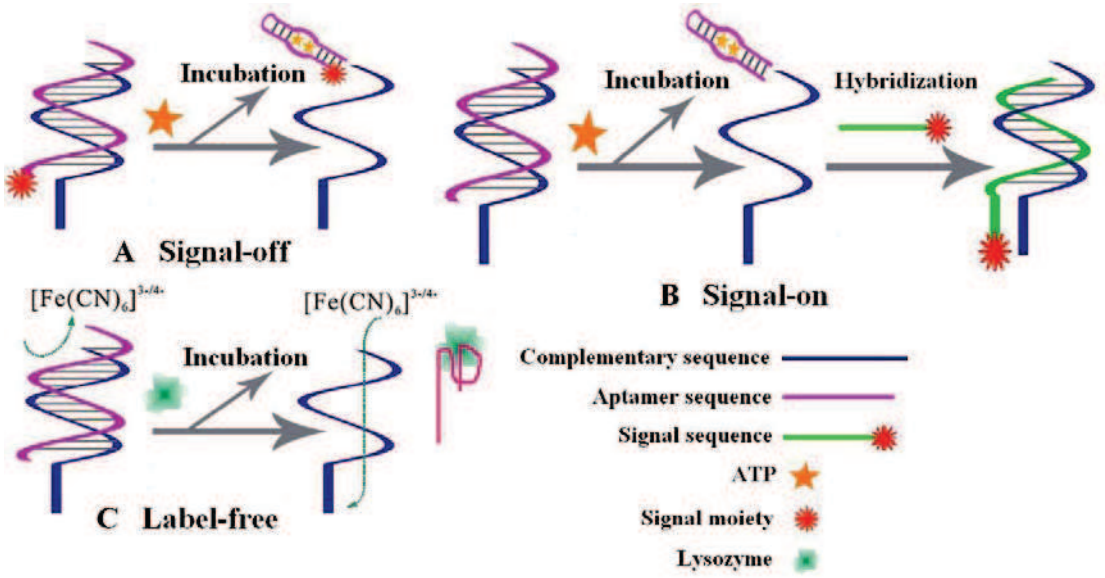


**Figure 1-13:** Schemes for the target-induced complementary strand dissociation/displacement strategies. A. signal off mode [137]; B signal-on mode [186]; C label-free mode [187].

I.2.2.2.2 Fluorescence detection

Besides electrochemical biosensors, the complementary strand displacement mode has also been widely employed in fluorescence detection biosensors. In the Nutiu and Li strategy for the sensing of ATP and thrombin [188] in 2003, a two-stem duplex assembly was designed using fluorophore (F) containing DNA at the 5' end (FDNA) and quencher (Q) containing DNA (QDNA) at the 3' end. The aptamer was linked at the 5' end with a 15-mer sequence complementary to FDNA. QDNA was complementary to the 5' end of the aptamer. The length of QDNA was optimized to meet the requirements of fluorescence quenching and restoration. When all the sequences were in complex, the dabcyl quencher was brought into sufficient proximity to quench the fluorescence signal on FDNA. Upon introduction of the

aptamer target, the aptamer–target complex caused QDNA to dissociate from the complex, thus restoring fluorescence (Figure 1-14a). The displacement mechanism was tested with signals associated with different temperatures as well as the introduction of aptamer targets, such as ATP and non-cognate molecules, such as CTP, UTP and GTP. The engineering strategy was further expanded to a variety of modifications, and all yielded similar results. The generality of this design was further evaluated for protein detection. Here, the 15-mer thrombin aptamer was engineered to generate the required sensor similar to the ones obtained for ATP. By using both ATP and thrombin as targets for these sensors, the versatility of these designs to produce significant signals for real-time detection, irrespective of the binding affinity or size of the aptamer, was demonstrated.

The application of this strategy was further expanded by Yoshida and Yokobayashi in 2007 [189]. They constructed a pair of DNA-based logic gates that could sense the presence of targets to induce a fluorescence signal according to the Boolean logic functions AND and OR. Molecular logic gates based on nucleic acids have many potential advantages. For instance, the straightforward hybridization rules enable convenient interfacing with other molecular computation devices based on DNA and RNA. In addition, both DNA and RNA are known to possess catalytic and molecular recognition abilities which can be used to provide amplification and sensor functions.

Boolean logic gates have been constructed using organic molecules, peptides, proteins, and oligonucleotides. An AND Boolean logic gate was constructed in which there was an output only when all of the inputs were present, whereas an OR logic gate produced a signal when at least one of the inputs was present. The AND Photonic Boolean logic gate was engineered by fusing the adenosine and the thrombin DNA aptamers with 11-mer linkers which have a fluorescein conjugation in the middle (Figure 1-14b (i)). Two short DNA sequences complementary to part of the aptamers and the linkers were conjugated at the 5’ and 3’ ends with quenchers. The binding of these two sequences with the linked aptamers bought the two quenchers in close proximity to the fluorescein, thereby quenching the fluorescence signal. The introduction of either adenosine or thrombin, with the concomitant dissociation of one

of the quencher sequences, did not restore the fluorescence signal since the remaining quencher was strong enough to exert its effect. However, addition of both adenosine and thrombin led to the displacement of both quencher DNA sequences, resulting in enhanced fluorescence signal. A similar construct was designed for the OR logic gate with the following modification. The 11-mer linker lacked the fluorescein conjugation, while one of the short DNA strands was modified with fluorescein at the 5' and the other with quencher at the 3' end (Figure 1-14b (ii)). Here again, the structure of the complex quenched the fluorescence signal. Unlike the AND gate, the addition of either adenosine or thrombin restored the fluorescence signal with the dissociation of either the QDNA or FDNA.

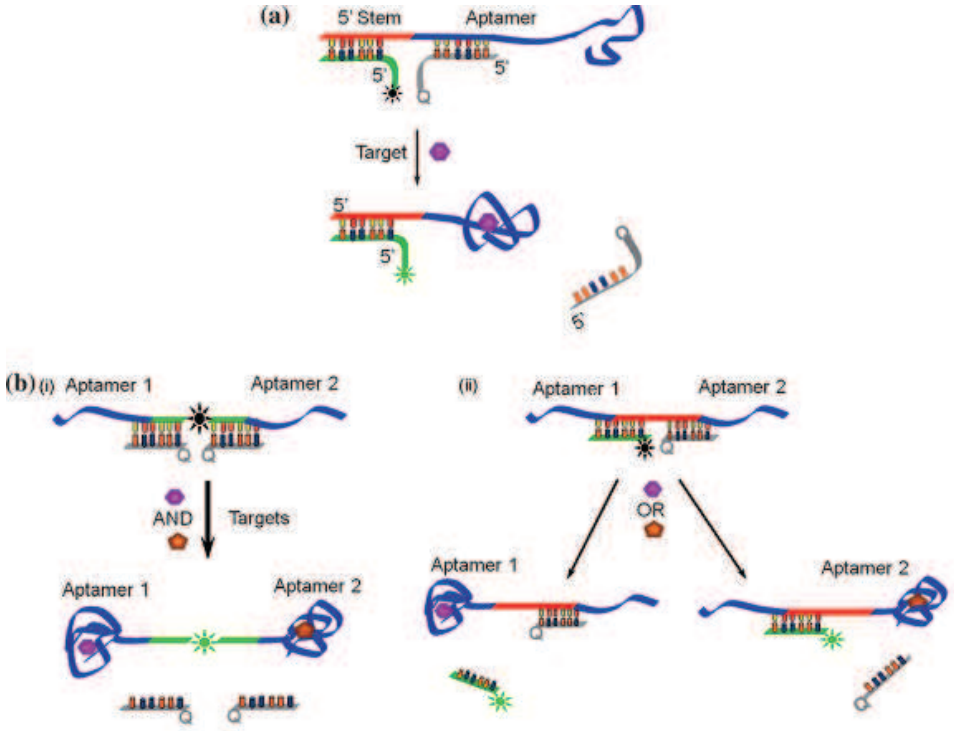


**Figure 1-14:** (a) The aptamer (blue) is linked at the 5' end with 15 mer sequence (orange) complementary to the fluorophore-labeled strand (green) FDNA, while the quencher strand (grey) QDNA, can hybridize with the aptamer. The introduction of the target (purple), results in the release of the QDNA from the complex, and the fluorescence signal is restored [188]. (b) Schemes for the DNA logic gates. The AND logic gate (i) is activated only when both targets (purple and brown) of the two aptamers bind, causing the release of the quencher sequences from the fluorophore. An OR logic gate (ii) can be activated with just one of the aptamer targets [189].

I.2.2.2.3 Colorimetric detection

Colorimetric assays are another popular optical detection technique. In recent years, gold nanoparticles (AuNPs) have been widely used in optical biosensor design, due to their unique characteristic spectroscopic changes during target-induced aggregation or dispersion. Researchers discovered that adsorption of single-stranded DNA (ssDNA) on AuNPs can effectively stabilize the colloid against salt-induced aggregation while the double-stranded DNA (dsDNA) has no such function [190-192]. Then colorimetric aptamer-based biosensors were developed based on this principle in 2007 [193]. When the target ATP was absent, the aptamer hybridized with its complementary sequence to form a rigid duplex, which could not prevent AuNPs from aggregating as salt was added into the system. However, as ATP was present, the duplex structure would switch to ATP-aptamer complex coupled with the release of its complementary sequence, which could stabilize AuNPs and showed high resistance to salt-induced aggregation (Figure 1-15). The changes of solution color caused by AuNPs aggregation could be easily observed by naked eyes. And the corresponding changes in UV-visible spectra could be used to in a quantitative assay for ATP. Similarly, another research indicated that the AuNPs modified by target-binding folded aptamer showed higher stability towards salt-induced aggregation than the AuNPs modified with unbinding aptamer. A colorimetric biosensor was developed for the assay of ATP or $K^+$, according to this target-induced structure switching of the aptamer modified on the surface of AuNPs [194].

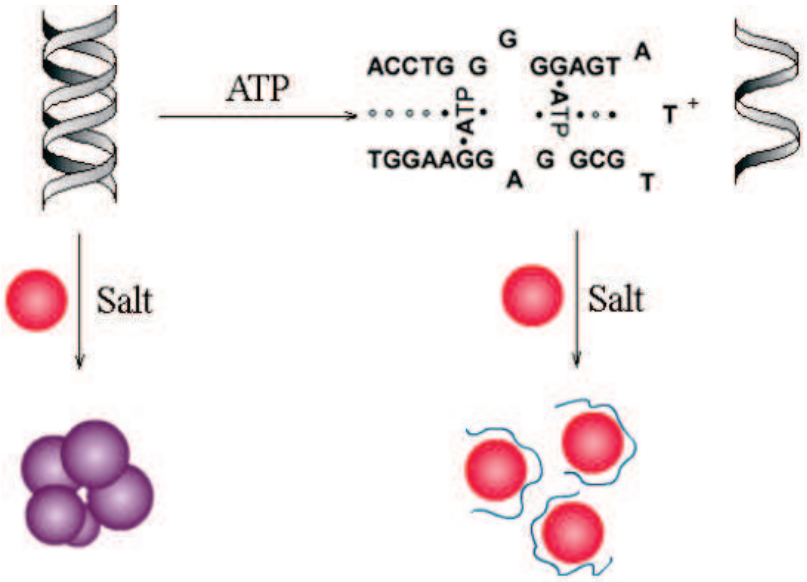


**Figure 1-15:** Scheme for the target-induced structure switching and salt-induced AuNPs aggregation [193]. When the target ATP was absent, the duplex structure could not prevent AuNPs (circles) from aggregating as salt was added into the system. However, as ATP was present, the duplex structure would switch to ATP-aptamer complex coupled with the release of its complementary sequence, which could stabilize AuNPs and show high resistance to salt-induced aggregation.

Thiolated aptamer probes can readily self-assemble at the surface of AuNPs via the well-established Au–S chemistry. These AuNP–aptamer conjugates possess a heavily loaded DNA monolayer (e.g. over 200 probes on a 13 nm AuNP [195]), with aptamer molecules protruding into the solution. Such nanoprobes were extremely stable in solutions of high ionic strength since DNA polyelectrolytes bring high-density negative charges to the surface. These interesting findings formed the basis of biomolecular detection by using AuNPs–aptamer conjugates [196-198].

Lu and coworkers developed a series of methods to detect small molecules based on target-induced conformational change in aptamers and disassembly of AuNP aggregates [199-202]. In their design, AuNP aggregates were prepared by employing a DNA strand containing an aptamer sequence and complementary sequences that crosslinked AuNPs. In the presence of the specific target, the target–aptamer binding displaced the complementary sequences, which altered the crosslinking state and disassembled the AuNPs aggregates. In their experiments, they could detect target

molecules (e.g. adenosine and cocaine) from the purple-to-red colour change within 1 min (Figure 1-16A). Importantly, this strategy can be easily extended to the detection of a variety of targets including DNA, protein, small molecules and ions.

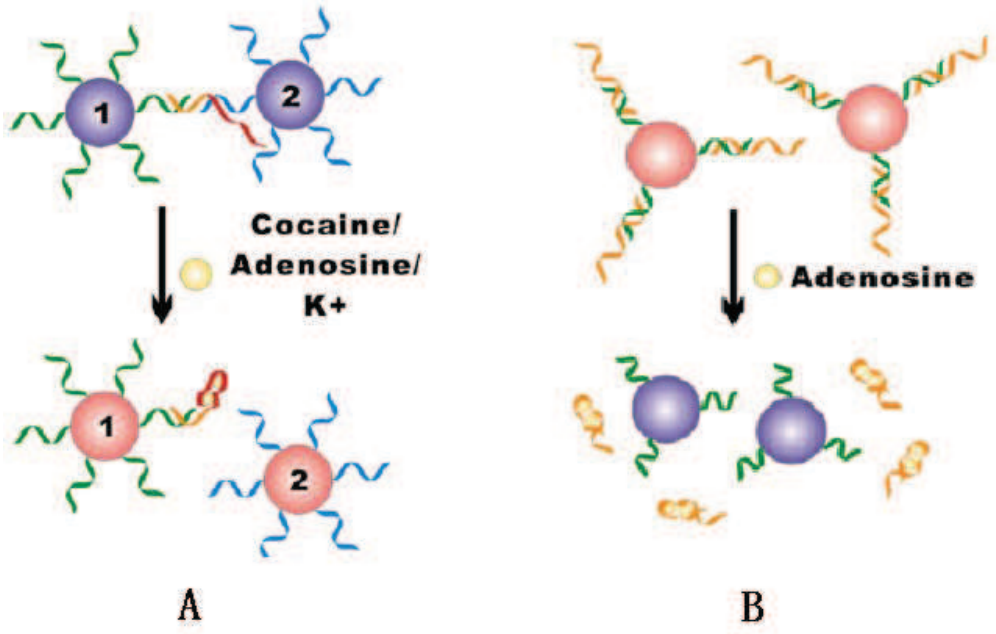


**Figure 1-16:** Colorimetric detection based on AuNPs/Aptamer conjugate crosslinking nanoprobes (A) The AuNPs aggregates containing aptamer linkers were used to detect target with specific binding with aptamer and disassembled the purple aggregates [199]. Colorimetric detection based on AuNPs/Aptamer conjugate non-crosslinking nanoprobes. (B) The aptamer–target binding leads to disassociation from AuNPs surface, and a red-to-purple colour change [203].

The non-crosslinking aggregation mechanism by controlling the DNA structure and conformation on the AuNPs' surface has been proposed as an alternative way to perform DNA-based sensing. It is well known that DNA strands loaded at the surface of AuNPs stabilize AuNPs against high salt concentrations due to the heavy negative charge of the DNA polymers [204-206]. However, it was found that the conformational change in tethered DNA might significantly alter the stability of AuNPs–DNA conjugates against salt induced aggregation. This non-crosslinking

system has its own merits. It is a rapid process and is usually much simpler than the crosslinking system. Moreover, the accessibility of binding sites is usually higher than those encapsulated within aggregates. As a result, the non-crosslinking system has been extensively employed to detect analytes such as small molecules, proteases and their inhibitors.

In 2008, Zhao *et al.* proposed a displacement-based adenosine-sensing assay in which the addition of adenosine caused displacement of DNA aptamers from the AuNP surface, which resulted in the aggregation of AuNPs in salt solution [203] (Figure 1-16B). Such a structure-switching of DNA aptamers and the salt-induced AuNP aggregation formed the basis of a rapid colorimetric assay for adenosine. By using this method, the detection process could be completed in 1 min with sensitivity comparable to fluorescent assays.

Another interesting colorimetric detection approach recently introduced relies on the DNA base-pair recognition on agent-caging hydrogels [207, 208]. Zhu *et al*. reported a colorimetric agent-caging hydrogel as a novel visual detection platform that relies on DNA base-pair recognition and aptamer–target interactions for simple and rapid target detection with the naked eye in 2010 [207] (Figure 1-17). Two pieces of DNA, strand A and strand B, were grafted onto linear polyacrylamide polymers to form polymer strands A and B (PS-A and PS-B), respectively. The sequences of DNA strands A and B were complementary to an adjacent area of a DNA aptamer sequence. When mixed in equal amounts, the polymers grafted with strand A and strand B were in transparent liquid form. The addition of aptamer linker-Apt initiated hybridization of strand A and strand B with the aptamer sequence, thus cross-linking the linear polyacrylamide polymers. As the hybridization proceeded, the cross-linking ratio of polyacrylamide increased, which resulted in the increase of viscosity of the polymer solution. The polymer would finally transform into a gel. Upon introduction of a target, the aptamer would bind with it, and the gel would be dissolved as a result of reducing the crosslinking density by competitive target–aptamer binding. If an enzyme was added prior to the addition of the aptamer, the enzyme would be trapped inside the 3D network of the hydrogel (represented as pink symbols in Figure 1-17).

When target molecules were introduced to dissolve the gel, the enzyme was released and can take part in its catalytic role for signal amplification. A cascade of events was thus set in motion, whereby target binding triggered an enzymatic reaction, which, in turn, changeed the substrate color, thus allowing visual detection. As this aptamer-based cross-linked hydrogel colorimetric platform can be targeted to any ligand for which there was a corresponding aptamer, many visual detection applications became possible in a wide variety of fields.

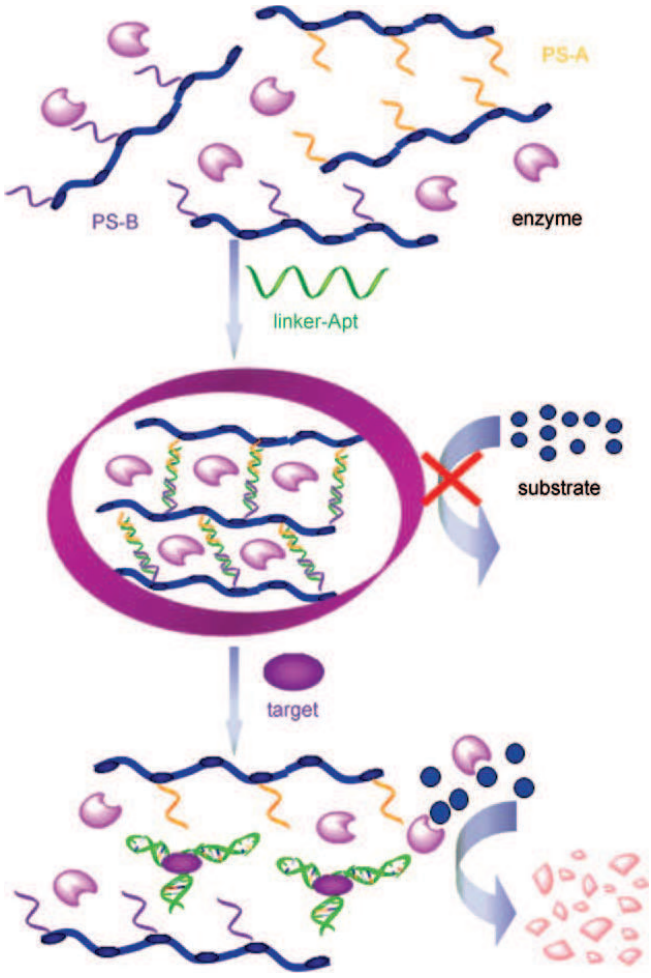


**Figure 1-17:** Working principle of DNA cross-linked hydrogel for signal amplification and visual detection [207]. Addition of the aptamer linker (green) causes the formation of the gel structure as a result of the linking of polymer strands A and B (PS-A and PS-B). In the presence of the aptamer target (purple), however, the gel will be dissolved as a result of reducing the crosslinking density by competitive target–aptamer binding, as a consequence, the trapped enzyme is released and can take part in its catalytic role for signal amplification.

I.2.2.2.4 Chemiluminescence detection

The chemiluminescence detection methods based on the complementary strand displacement mode have also been developed, especially for small molecules like adenosine and cocaine [209-212]. Zhu *et al.* reported a highly sensitive and selective electrochemiluminescent (ECL) biosensor for the determination of adenosine in 2011 [212]. The decrease of ECL intensity has a direct relationship with the logarithm of adenosine concentration in the range of $1.0\times10^{-10}$ to $5.0\times10^{-6}$ $M^{-1}$. The detection limit of the proposed method was $3.0\times10^{-11}$ $M^{-1}$. The developed biosensor also demonstrated very good reusability, as after being reused for 30 times, its ECL signal still kept 91% of its original state.

I.2.2.2.5 Fluorescence polarization (FP) detection

As described above, one of the important requirements for a workable FP probe is that the molecule being measured should induce a significant change in molecular mass before and after recognition. The complementary strand displacement mode, thus, offers great potential for the development of FP strategy for the small molecular detection. In 2008, Penner *et al.* reported one example of FP displacement assay for ochratoxin A (OTA) [213] based on the increase in the fluorescence anisotropy of aptamer when bound by a fluorescently labeled oligonucleotide.

Recently, Yang *et al.* developed a molecular mass amplifying strategy to construct FP aptamer probes for small molecule analysis in complex biological samples [214]. The design of a mass amplifying probe (MAP) is shown in Figure 1-18. Overall, the probe was designed in such a way that only when the target molecule bound to the probe did it activate its binding ability to an anisotropy amplifier (a high molecular mass molecule such as protein), thus significantly increasing the molecular mass and FP value of the complex. Specifically, the aptamer probe consisted of a targeting aptamer domain (blue ribbon in Figure 1-18) against the target molecule and molecular mass amplifying aptamer domain (purple ribbon) for binding with the amplifier protein. The probe was initially deactivated by a short blocking strand (cyan ribbon) which was partially complementary to both target aptamer and amplifier

protein aptamer so that the molecular mass amplifying aptamer domain would not bind to the amplifier protein (Scheme 18a), unless the probe has been activated by the small molecule target (Scheme 18b). In this way, they prepared two probes that constituted a target (ATP and cocaine respectively) aptamer, a thrombin (as the mass amplifier) aptamer, and a fluorophore. Both probes worked well against their corresponding small molecule targets, and the detection limits for ATP and cocaine were 0.5 μM and 0.8 μM, respectively. More importantly, because FP was less affected by environmental interferences, ATP in cell media and cocaine in urine were directly detected without any tedious sample pretreatment. Liang *et al.* have developed an amplified fluorescence polarization aptasensor that relied on aptamer structure-switching triggered nanoparticles (NPs) enhancement for biomolecules detection [215]. This new type of assay exhibited higher detection sensitivity over traditional homogeneous aptasensors by two orders of magnitude and high specificity for target molecules.

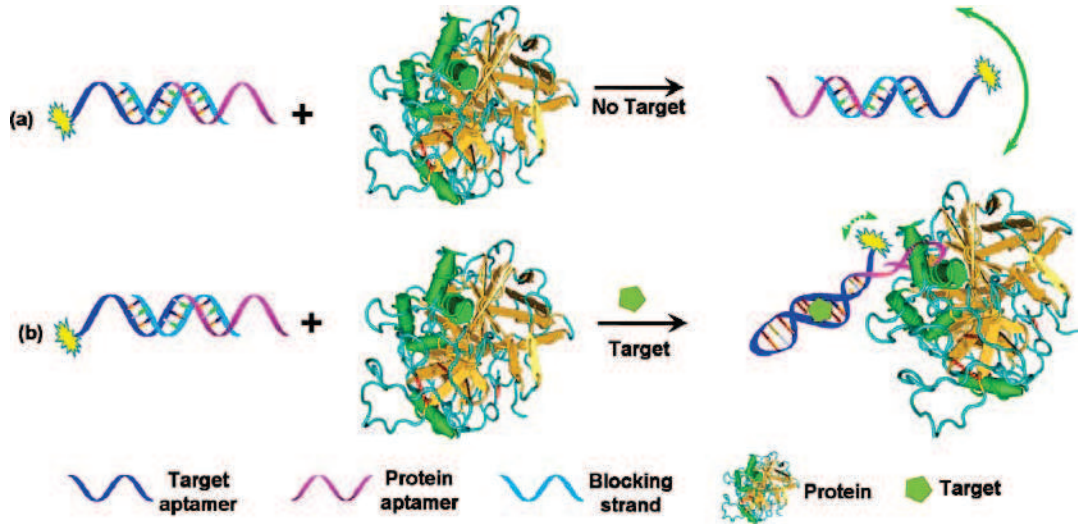


**Figure 1-18:** Working Principle of mass amplifying probe for small molecules FP detection [214].

### I.2.2.3 Sandwich or sandwich-like mode

As named, the sandwich mode devices consist of at least three parts, “a piece of meat” inserted within “two pieces of bread”. Some protein targets, such as PDGF and thrombin, have dual binding sites, which enable them to bind two recognition molecules and form sandwich-like complexes. Since these proteins could specifically bind either aptamers or antibodies, the sandwich structures have three basic formats: aptamer-protein-aptamer, aptamer-protein-antibody and antibody-protein-antibody. The first two formats have been widely used in design of aptamer-based biosensors.

#### I.2.2.3.1 Electrochemical detection

In order to obtain high specificity and sensitivity, sandwich or sandwich-like mode is often employed in aptamer-based electrochemical bioassays. Usually, the biocatalytic properties of enzymes are used to detect and to amplify the analysis of targets with their aptamers. For example, glucose dehydrogenase (GDH) was employed as a biocatalytic label for the amplified amperometric detection of thrombin [216]. Thrombin was linked to a 15-mer thiolated aptamer linked to an Au electrode, and the GDH-avidin conjugate was linked to the surface by its association to the biotinylated 29-mer aptamer bound to the thrombin. The bioelectrocatalyzed oxidation of glucose in diffusional mediator enabled the amperometric detection of the thrombin.

In an improved approach in 2006 [217], aptamer-functionalized platinum nanoparticles (PtNPs) were employed as catalytic labels instead of enzymes (Figure 1-19A). The PtNPs catalyzed the electrochemical reduction of $H_2O_2$ and amplified detection of thrombin with an LOD of 1 nM. This assay format is very similar to the biocatalytic sandwich-type analysis using GDH but improved the LOD by a factor of 80-fold. Besides acting as catalysts, NPs (e.g., AuNPs) have also been employed as carriers for ultrasensitive electrochemical detection of proteins [218]. In this format, AuNPs were functionalized with anti-thrombin aptamers containing a poly-adenine

(poly-A) sequence. They bound to the thrombin captured by immobilized anti-thrombin antibody (Figure 1-19B). The adenine nucleobases were released by acid or nuclease degradation and were directly detected using a pyrolytic graphite electrode. Because one NP carried a large number of aptamers, the thrombin-binding process was substantially amplified, which led to a low LOD of 2.8 pM.

In another sandwich-type electrochemical bioassay, instead of using carriers, the aptamers were designed to allow rolling circle amplification (RCA) [219]. As a result, the aptamer-primer sequence mediated an in-situ RCA reaction that generated hundreds of copies of the circular DNA template, leading to significant enhancement in the detection sensitivity (Figure 1-19C). This assay strategy produced a wide detection range of four orders of magnitude and an LOD as low as 10 fM. Moreover, the novel aptamer-primer design circumvented time-consuming preparation of the antibody-DNA conjugate in conventional immuno-RCA assays.

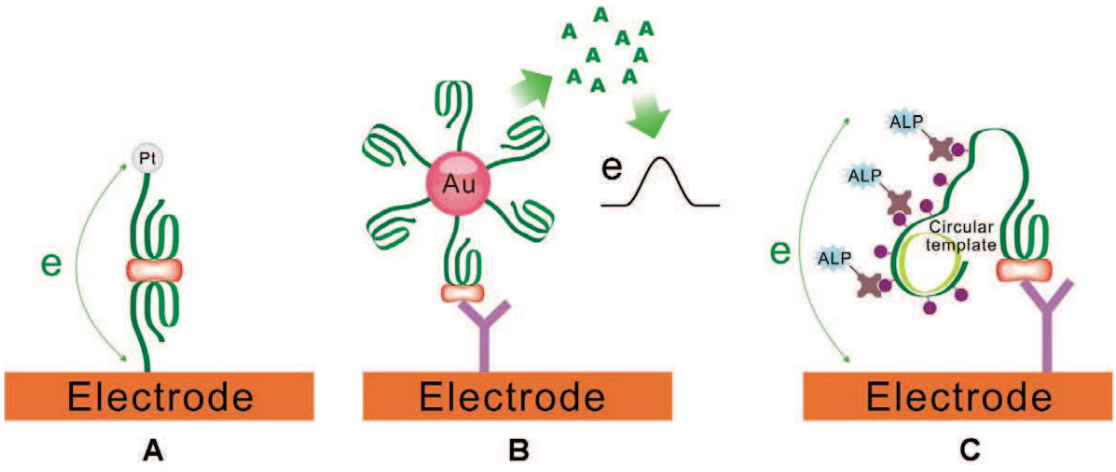


**Figure 1-19:** ''Sandwich''-type aptamer-based electrochemical sensors with signal amplification. (A) Aptamer-functionalized PtNPs were employed as catalytic labels to catalyze the electrochemical reduction of $H_2O_2$ and enabled the amplified detection of targets [217]; (B) AuNPs functionalized with aptamers containing poly-A were used as reporting probes. The adenine nucleobases released from them were directly detected to produce amplified signals [218]; and (C) acting as the reporter, the aptamer-primer sequence mediated an in-situ RCA reaction, leading to significant enhancement in detection sensitivity [219].

I.2.2.3.2 Optical detection

Functionalized AuNPs with aptamers have also been used for the amplified optical detection of proteins in the sandwich configuration [220]. The anti-thrombin aptamer was covalently attached to a maleimide-functionalized siloxane monolayer, and thrombin was bound to the interface. The same aptamer-functionalized AuNPs were then associated to the second thrombin binding site. The resulting AuNP interface was then enlarged in growth solution containing $HAuCl_4$ and reducing agents (Figure 1-20A). The enlargement of AuNPs significantly improved the colorimetric detection sensitivity, which could detect as few as 2 nM thrombin. More recently, Li *et al.* reported a similar approach that employed silver amplification [221] (Figure 1-20B). Their assay simultaneously employed an AuNP-aptamer and a biotin-aptamer that bound to the PDGF, with an extremely low LOD of 83 aM.

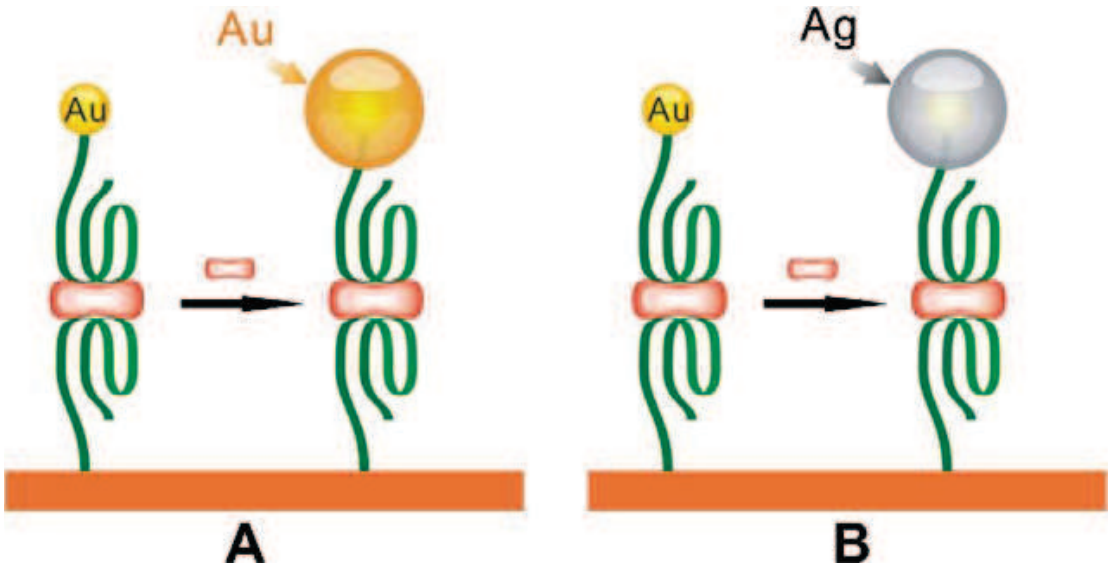


**Figure 1-20:** The ‘‘sandwich’’ type aptamer-based colorimetric bioassays with gold (A) [220] and silver (B) [221] amplification systems.

## I.2.3 Aptamer-Based Affinity Separation and Purification

### I.2.3.1 Chromatography

Aptamers have also been employed in various chromatography techniques, such as liquid chromatography [222] and electrochromatograpy [223]. The advantages of aptamers applied in this field are obvious: wide targets enlarge the range of analytes that can be used; easy synthesis reduces the cost; selected as functional oligonucleotides decreases the adsorption (compared with antibodies); and high affinity guarantees a high selectivity and separation effect. Based on these advantages, processes such as molecular recognition [224, 225], quantitative detection [226], analogy separation [227], and even chiral selection [228-230] have been undertaken using aptamer-based chromatography analysis. Chromatography techniques are also used to assist the SELEX procedure and exhibit increasing potential in this field.

Generally, two strategies have been described for the aptamer immobilization on the chromatographic surface. The first immobilization approach involves the non-covalent binding of the aptamer on a functionalized matrix. The second approach is related to the covalent immobilization of the oligonucleotide on the chromatographic surface. In most cases, the aptamer immobilization has been achieved using the well-known non-covalent biotin–streptavidin bridge. This type of ligand immobilization is frequently chosen because the procedure appears to be easy and rapid to perform. Furthermore, the biotin–streptavidin bridge is known to maintain efficiently the receptor (aptamer) binding ability. Immobilization of aptamer was commonly attained, by mixing streptavidin chromatographic support with the aptamer solution during some hours at 4°C or ambient temperature. About 15–20 nmol of aptamer for 100 μL of separation media are commonly bound using this strategy [227, 229, 231]. Despite the simplicity and the rapidity of this immobilization methodology, such kind of binding procedure presents, in terms of reusability and column lifetime, some major drawbacks for a practical chromatographic use.

Although the streptavidin–biotin link is very strong in solution, the magnitude of the streptavidin–biotin binding constant is greatly reduced when the protein is bound to a surface [232]. In addition, dissociation of the biotin–streptavidin complex can occur at relatively low temperatures, notably in nonionic aqueous solutions or in medium containing a low salt concentration [233]. Furthermore, as classically observed with proteins, the immobilized streptavidin can be also irreversibly denatured under standard reverse phase chromatographic conditions, for example by using a mobile phase containing organic modifiers [234]. Therefore, covalent immobilization strategies have been also described. These involve attachment of the oligonucleotide through the formation of amide or carbamate bonds [235-237]. These approaches allow working under more drastic conditions. For example, it has been demonstrated that the analyte separation can be performed at relatively high temperatures [237] and using strong proportion of organic solvent (methanol, ethanol, acetonitrile, isopropanol) [236, 237], without alteration of binding ability of the immobilized aptamer. In addition, a very good stability over the time can be obtained, even under various conditions of use and storage [237].

A variety of aptamer-based stationary phases have been described for the separation and purification of small molecules and proteins using open tubular capillaries, packed bed columns and monolithic columns [238-240].

I.2.3.1.1 Aptamer-based stationary phases for protein separation

In 1999, Drolet *et al.* reported an aptamer affinity chromatography for the protein purification [222]. A DNA-aptamer specific for human L-selectin was immobilized on a chromatography support to create an affinity column. This column was effectively applied as either the first or second step in the purification of a recombinant human L-selectin–Ig fusion protein from Chinese hamster ovary cell-conditioned medium. The fusion protein was efficiently bound to the column and efficiently eluted by gentle elution schemes. Application of the aptamer column as the initial purification step resulted in a 1500-fold purification with an 83% single step recovery. In 2005, Lee *et al.* developed a bead affinity chromatography system to

purify specific target proteins on a chip [241]. The microbead affinity chromatography system, which is based on photolytic elution, was integrated into a glass-silicon microchip and tested by the biotin-streptavidin model system. In addition, they presented result of the detection of hepatitis C virus (HCV) RNA replicase from a protein mixture using the microsystem packed with the beads immobilized with photo-cleavable RNA aptamer.

Taking advantage of the specific affinity of aptamers and the porous property of the monolith, Le's group developed a capillary chromatography technique for the separation and detection of proteins in 2008 [239]. A biotinylated DNA aptamer targeting cytochrome c was successfully immobilized on a streptavidin-modified polymer monolithic capillary column. The aptamer, having a G-quartet structure, could bind to both cytochrome c and thrombin, enabling the separation of these proteins from each other and from the unretained proteins. Elution of strongly bound proteins was achieved by increasing the ionic strength of the mobile phase. The following proteins were tested using the aptamer affinity monolithic columns: human immunoglobulin G (IgG), hemoglobin, transferrin, human serum albumin, cytochrome c, and thrombin. Determination of cytochrome c and thrombin spiked into dilute serum samples showed no interference from the serum matrix. The benefit of porous properties of the affinity monolithic column was demonstrated by selective capture and preconcentration of thrombin at low ionic strength and subsequent rapid elution at high ionic strength. The combination of the polymer monolithic column and the aptamer affinities made the aptamer-modified monolithic columns useful for protein detection and separation.

I.2.3.1.2 Aptamer-based stationary phases for small molecule separation

The first aptamer affinity chromatography for small molecule separation was reported by Kennedy's group in 2001 [227]. A biotinylated-DNA aptamer that binds adenosine and related compounds in solution was immobilized by reaction with streptavidin, which was covalently attached to porous chromatographic supports. The aptamer medium was packed into fused-silica capillaries (50-150 μm i.d.) to form

affinity chromatography columns. Variation of mobile-phase conditions revealed that ionic strength and $Mg^{2+}$ level had strong effects on retention of analytes while pH and buffer composition had less effect. It was demonstrated that the column could selectively retain and separate cyclic-AMP, $NAD^{+}$, AMP, ADP, ATP, and adenosine, even in complex mixtures such as tissue extracts. Based on this, an aptamer affinity chromatography for rapid assay of adenosine in microdialysis samples collected in vivo was also developed in 2003 [242]. The aptamer stationary phase was the same as the previous one, but the mobile phase is modified to allow selective retention of adenosine. The adenosine assay, which required no sample preparation, was used on microdialysis samples collected from the somatosensory cortex of chloral hydrate anesthetized rats. Total analysis times were shortened enough that dialysate samples could be injected every 5 min.

The enantioselective properties of DNA or RNA aptamers selected against a target enantiomer were adopted to create a new class of target-specific chiral stationary phases (CSPs). The first example of aptamer-based CSP specifically designed against the racemate to resolve has been described by our group in 2003 using a DNA oligonucleotide as selective ligand. The enantiomers of arginine-vasopressin have been separated using an immobilized 55-base DNA aptamer known to bind stereospecifically the (all-D)-isomer of the oligopeptide [228]. The immobilization was achieved using the biotin-streptavidin interaction, as previously described by Kennedy and co-workers [227]. The influence of various parameters (such as column temperature, eluent pH and salt concentration) on the enantiomer retention has been investigated in order to provide information about the binding mechanism and then to define the experimental conditions of the aptamer column. Very important apparent enantioselectivity was observed, the non-target enantiomer being roughly not retained by the column. More, it has been shown by thermodynamic analysis that both dehydration at the binding interface, charge-charge interactions and adaptive conformational transitions contributed to the specific (all-D)-peptide aptamer complex formation. Furthermore, it was established that the aptamer column was stable during an extended period of time. In a further work in 2004, such an approach has been

extended to the chiral resolution of small molecules of biological interest [231]. The DNA aptamers used have been selected against the D-adenosine and L-tyrosinamide enantiomers. An apparent enantioseparation factor of around 3.5 (at 20°C) was observed for the anti-D-adenosine aptamer CSP while a very high enantioselectivity was obtained with the immobilized anti-L-tyrosinamide aptamer. This allowed obtaining baseline resolution even at a relative high column temperature. The anti-D-adenosine aptameric stationary phase can be used for two months without loss of selectivity while some performance degradation was observed for the anti-L-tyrosinamide column over this period. As an important complement, a CSP based on the L-RNA aptamer was also developed by our group in 2005 [229]. It was shown that this approach was a very simple and powerful strategy to develop a highly stable stationary phase due to the intrinsic insensitivity of L-RNA to the RNase degradation. And this method was extended to resolution of the enantiomers of tyrosine and other analogues (11 enantiomeric pairs) [230].

In addition to the separation of simple targets, Tan's group reported the selective capture of cancer cells from a flowing suspension on a simple square capillary by immobilizing aptamers in the capillary [243]. More than 90% capture efficiency can be obtained through this device. The method was extended to aptamer-based differential mobility cytometry for highly efficient enrichment of rare cells [244].

### I.2.3.2 Capillary electrophoresis (CE)

For the capillary electrophoresis analysis, two areas of great importance are the separation of species and the characterization of affinity interactions. For the quantification of analytes, ligands may interact with the analyte before and/or during electrophoresis [245]. The analysis of preincubated target-ligand mixtures is the approach especially useful for quantitative measurements of analytes that form with high-affinity complex with the ligand. Such CE assays are based on separating the analyte-ligand complexes from the free analyte and free ligand by capillary

electrophoresis. Both competitive and non-competitive (direct) assays can be used [245]. In the competitive assay, the analyte is labeled and competes with the unlabeled solute in the sample for binding to a limited amount of the corresponding ligand. A CE separation of the mixture produces two distinct peaks corresponding to the free labeled analyte and the labeled analyte bound to the ligand, allowing the quantification of the target. In the direct assay, the ligand is labeled and added at a constant concentration to the sample for binding the target. Detection and quantification of the complex peak or free ligand peak is related to the amount of the analyte in solution.

Various interacting systems have been studied by capillary electrophoresis using proteins, antibodies or DNAs as specific ligands. The CE assays based on the formation of antigen-antibody complexes are the most frequently formats reported. In principle, direct assays possess several advantages over competitive assays including larger dynamic range, detection limits that are less dependent upon binding constant between the analyte and the ligand and ability to distinguish among cross-reactive species [226]. However, antibodies present some drawbacks for application in such noncompetitive approach. They are electrophoretically heterogeneous and do not migrate as a single sharp peak. More, the fluorescent label may interfere with binding if it is too close to the binding site. On the other hand, aptamers possess several advantages over antibodies that make them especially valuable in direct affinity capillary electrophoresis. They are simple to fluorescently label, possess predictable electrophoresis properties and relatively low molecular mass which simplify the separation of complex from free aptamer.

I.2.3.2.1 Aptamer-based capillary electrophoresis for protein detection

Affinity probe capillary electrophoresis (APCE) refers to a collection of techniques in which high-affinity binding is used in conjunction with CE separation to determine analytes. Combined with laser-induced fluorescence (LIF) detection, this technique has demonstrated potential for rapid determination of trace levels of analyte in complex mixtures. In 1998, Kennedy *et al.* reported the first application of aptamers

to noncompetitive APCE [226]. A DNA aptamer against IgE was labeled with fluorophore and used as a selective fluorescent tag for determining IgE by capillary electrophoresis with laser-induced fluorescence detection. CE-LIF separations of samples containing fluorescently labeled aptamer and IgE were complete in less than 60 seconds and revealed two zones, one corresponding to free aptamer and the other to aptamer bound to IgE. The free aptamer peak decreased and bound aptamer peak increased in proportion to the amount of IgE in the sample so that IgE could be detected with a linear dynamic range of $10^5$ and a detection limit of 46 pM. The assay was highly selective as aptamer was unaffected by the presence of IgG and IgE did not bind other DNA sequences. IgE was determined in serum samples with similar analytical figures of merit. Similar conditions using a thrombin aptamer allowed detection of thrombin. In a further work, Tan *et al.* reported the investigation of protein-protein interactions using molecular aptamers with affinity capillary electrophoresis (ACE) [246]. This assay has been applied to quantify thrombin-anti-thrombin III interaction and to monitor this reaction in real time. And this assay can be an effective approach for studying protein-protein interactions and for analyzing binding site and binding constant information in protein-protein and protein-DNA interaction studies.

In 2003, Krylov's group proposed a new method that allowed the use of low affinity aptamers as affinity probes in quantitative analyses of proteins [247]. The method was based on nonequilibrium capillary electrophoresis of the equilibrium mixture (NECEEM) of a protein with its fluorescently labeled aptamer. The NECEEM method was applied to the analysis of thrombin using a fluorescein-labeled aptamer under the conditions at which the protein-aptamer complex completely decayed during the separation. They demonstrated that, despite the decay, as few as 4 $\times 10^6$ molecules of the protein could be detected with NECEEM without sacrificing the accuracy. This sensitivity was comparable with that reported by others for the aptamer-based equilibrium method. Thus, the proposed NECEEM-based method allows the use of aptamers for highly sensitive affinity analysis of proteins even when protein-aptamer complexes were unstable.

In a separate study, Girardot *et al.* [248] applied CE to study the interaction between lysozyme and aptamer mediated by both monovalent and divalent cations. They found that the binding between an aptamer and its target was highly dependent on the conformation of the aptamer molecule. The experimental setup allowed them to calculate apparent binding constants for divalent cations. Zhang *et al.* [249] introduced another CE technique based on a tunable aptamer for the separation and detection of platelet derived growth factor (PDGF) isomers and their receptors in diluted serum samples. The aptamer can form a stable complex with the B chain but not with the A chain of PDGF, resulting in the difference in electrophoretic mobilities of PDGF isomers.

Methods of kinetic capillary electrophoresis (KCE) facilitated highly efficient selection of DNA aptamers for protein targets. The inability to detect native proteins at low concentrations in capillary electrophoresis created, however, a significant obstacle for many important protein targets. Krylov *et al* [250] suggested that protein labeling with new Chromeo dyes can help to overcome this obstacle. By labeling a number of proteins with Chromeo P503, the labeling procedure enabled accurate detection of proteins in CE without significantly affecting their electrophoretic mobility or their ability to bind DNA. Protein adsorption to inner capillary walls created a major obstacle in all applications of capillary electrophoresis involving protein samples. Recently, Krylov *et al.* [251] introduced a simple pressure-based method for the qualitative assessment of protein adsorption that can facilitate the direct antiadhesive ranking of several coatings toward a protein of interest.

I.2.3.2.2 Aptamer-based capillary electrophoresis for small molecule detection

Compare to the protein analysis, small molecule detection by aptamer-based CE is more complicated as the electrophoretic mobility of aptamer-target complex and free aptamer is similar. New strategies have been developed to circumvent this problem. For example, some intrinsic properties of the target molecules could be beneficial for the development of a new label-free aptamer-base CE method. Cocaine contains a tertiary amino group and can generate strong electrochemiluminescence (ECL)

emission on a platinum electrode in the presence of tris(2,2'-bipyridyl)ruthenium(II) $[Ru(bpy)_3]^{2+}$. Arginine can be electrochemically oxidized on a copper electrode to generate strong electrochemical (EC) signal; the derived argininamide also possesses a high EC activity. However, when the targets are bound to aptamers, they show no luminescent or electrochemical activity. Based on specific chemical and physical properties of these small target molecules, Deng *et al.* reported a novel label-free method for the investigation of the adaptive recognition of small molecules by nucleic acid aptamers using capillary electrophoresis analysis in 2007 [252, 253].

Aptamer-based capillary electrophoresis was also applied to design a highly enantioselective tool for the trace enantiomer detection. In 2006, our group reported the chiral resolution of arginine using an anti-arginine L-RNA aptamer chiral selector in partial-filling CE [254]. The effects of the capillary temperature, sample load, and aptamer plug length on the enantiomeric separation were assessed. In a further work in 2007, an aptamer-based stereoselective assay was developed using an affinity capillary electrophoresis-based competitive, homogeneous format and an on-capillary mixing approach [255]. Detection of as low as 0.01% of the minor enantiomer in a nonracemic mixture can be achieved, in a short analysis time (<5 min). To improve the assay sensitivity, a "hybrid" strategy was developed by our group in 2008 [256] which based on a pre-incubation/on-capillary mixing format using an enantioselective aptamer as affinity ligand. And in 2009, our group also developed an aptamer-modified micellar electrokinetic chromatography methodology which focused on the specific shift of the aptamer mobility in the presence of a nonionic micellar phase [257]. The general principle is illustrated in Figure 1-21.

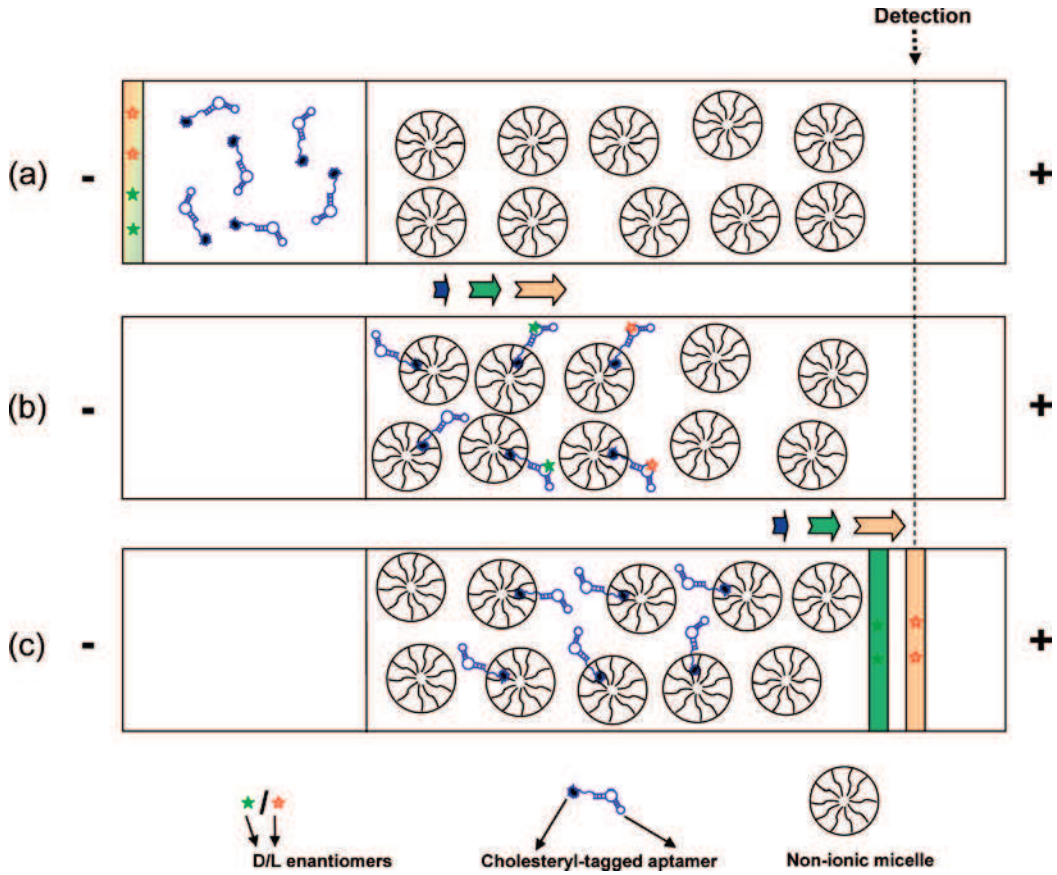


**Figure 1-21:** Principle of the aptamer-modified MEKC mode [257]. (a) A PVA-coated capillary is prefilled with three different plugs, (i) a plug containing a quasi-immobile nonionic micellar phase, (ii) a plug containing the cholesteryl-tagged aptamer, and (iii) a plug containing the AMP sample. (b) When the electric field is applied, the mobility of Chol-Apt is strongly reduced in direct relation to its partitioning into the micellar pseudophase so that the AMP enantiomers pass through the micelle-anchored aptamer zone. (c) The stereoselective interaction between AMP and the micelle-interacting aptamer zone led to the chiral separation. Arrows indicate the migration direction of the interacting species when the electric field is applied, and their respective lengths represent the expected velocity magnitude.

This work reported a new enantioselective aptamer-based CE mode where an aptamer-modified pseudostationary phase was created during the run by an on-capillary mixing approach and served as the active chiral discriminating zone in a partial-filling format. Such an approach allowed extending the use of the CE aptamer to enantioseparation of an anionic target which displayed an electrophoretic mobility identical to that of the selector. The separation window width, selectivity, resolution,

and analysis time can be efficiently modulated by varying some critical electrophoretic factors such as the concentration and the nature of the surfactant, the applied voltage, or the capillary temperature. Moreover, such aptamer-modified MEKC mode could be also find applications in the achiral analysis field for the development of affinity CE assays dedicated to small negatively charged analytes or for the separation of small anionic targets and analogues on the basis of their respective binding affinity for the aptamer ligand.

### I.2.3.3 Microfluidics

For the last few years, increasing efforts have been made to combine aptamers with microfluidics technique. Microfluidics integrates one or several laboratory procedures, such as sample preparation, reaction, separation, detection on a single chip, ranging from millimeters to a few square centimeters in size. The introduction of aptamers on a microchip has been expected to bring several advantages to the field, such as reduced reagent and sample consumption, simplicity, automated processing, faster separation, high throughput, and portability. In 2009, Tan's group [258] immobilized aptamers in a microfluidic channel to capture rare cells to achieve a rapid assay without any pretreatment (Figure 1-22). Their device has demonstrated both outstanding enrichment purity (97%) and over 80% capture efficiency. They were able to further extend the utility of their microfluidic device to simultaneously sort, enrich, and then detect multiple types of cancer cells in a complex sample [259].

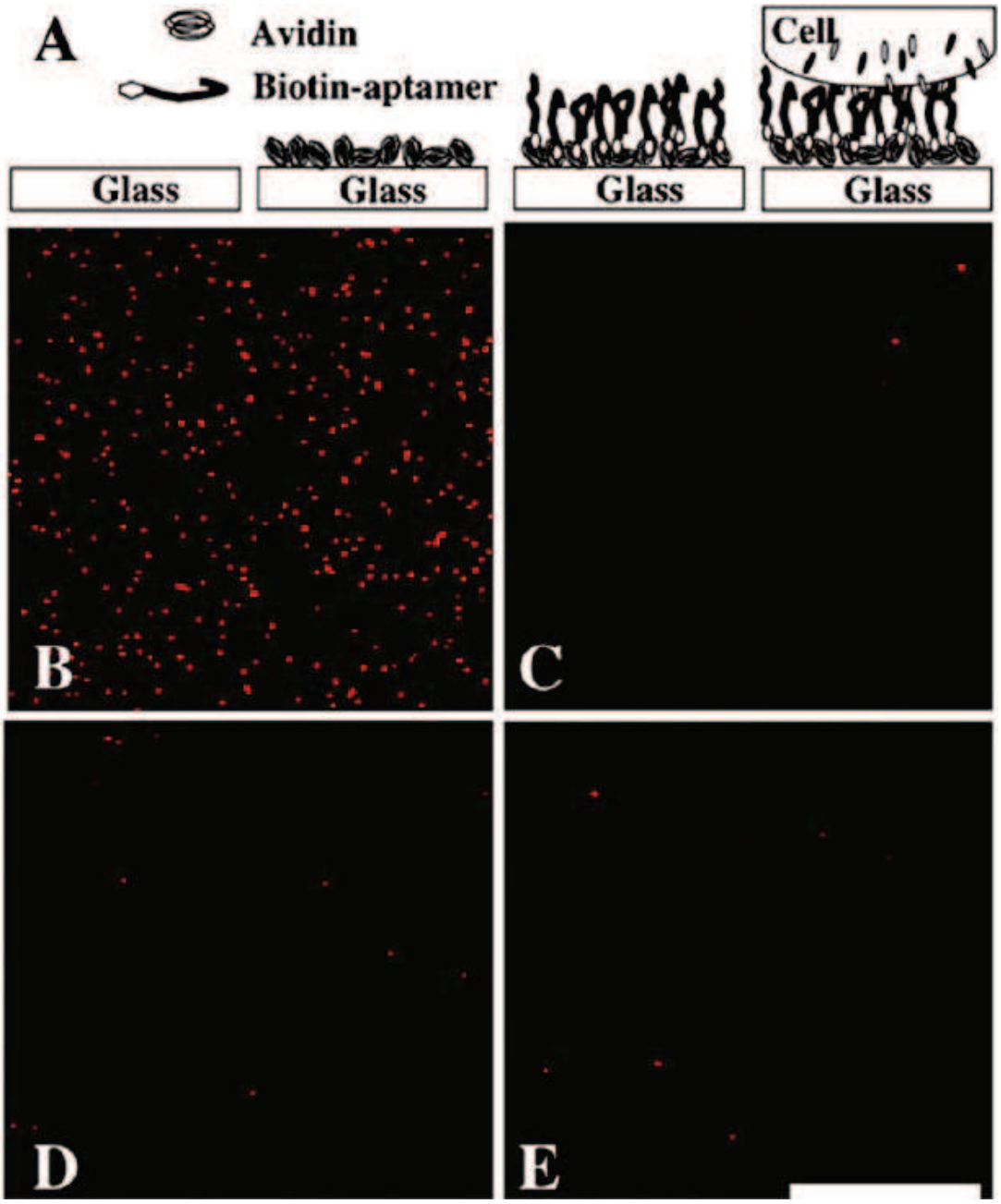


**Figure 1-22:** Aptamer-based capture and enrichment [258]. Immobilized sgc8 aptamer was used to capture its target cells. (A) Schematic representation of the aptamer immobilization and target capture. (B) Specific capture of the target cells using the sgc8 aptamer. (C) Representative capture of the control cells using the sgc8 aptamer. (D) Capture of the target cells using immobilized random DNA sequence. (E) Capture of the control cells using immobilized random DNA sequence.

As another example of the use of aptamer microfluidic devices for bioanalysis, Reif *et al.* [260] have designed a microfluidic device for the simultaneous capture and induction of apoptotic cells in Jurkat cells, providing a tool for the study of the mechanisms and temporal dynamics of apoptosis. The Soper group [261] has also utilized an aptamer-immobilized microfluidic device to selectively capture low abundant cancer cells. In their study, aptamers recognizing prostate-specific membrane antigen (PMSA) were selected and immobilized onto the surface of a microchip and fabricated into a high-throughput microsampling unit. Such combination of sensitive technology and selective aptamer binding resulted in the 90% recovery rate of rare circulating prostate tumor cells from a peripheral blood matrix.

As another interesting development in aptamer-based microfluidics, Soh *et al.* [262] introduced the microfluidic electrochemical aptamer-based sensor (MECAS) chip by integrating target-specific DNA aptamers that can generate an electrochemical signal through conformational changes in response to the analyte binding. The system was applied to achieve continuous, real-time monitoring of cocaine in blood serum at the physiologically relevant concentration and with physiologically relevant time resolution. In another study in 2010, Huang *et al.* [263] have combined flow cytometry with aptamer-functionalized magnetic microparticles for the detection of adenosine in serum.

## I.2.4 Conclusions

Due to their excellent characteristics of high affinity and selectivity, aptamers have been considered as one of the most promising molecular recognition elements in biosensor fabrication. This chapter covered recent research progress in the development of aptamer-based or aptamer related biosensing systems and the aptamer-based biosensors were classified into three basic modes: target-induced conformation change mode, complementary strand displacement mode, sandwich or sandwich-like mode. Based on these three basic strategies, aptamer-based affinity separation and purification and various detection methods for aptamer-based assays were also discussed. Taking into account that such aptasensors emerged only about 10 years ago, it is clear that significant progress has been made in employing nucleic acid aptamers for biosensing applications.

However, several challenges still remain. First, only a small range of targets have already been detected using aptamer-based biosensors, and the total number of nucleic acid aptamers discovered so far is still much less than that of antibodies. It is thus highly desirable to create new, easy and universal methodology for aptamer discovery. Second, up to now, most of the aptamer-based assays are confined to standard samples, only a few of them have been applied in detection of real samples, such as serum or blood, great challenges still remain for the future clinical applications in the sophisticated physiological environment. In addition, in comparison with the conventional bioassay method (such as ELISA), many elegant aptamer-based biosensing systems are still not highly sensitive, which implies that plenty of work could be done to make aptamer-based biosensors to be well-established bioanalytical tools.

## References


1. Thielges M. C., Zimmermann J., Yu W., Oda M., Romesberg F. E., *Exploring the Energy Landscape of Antibody-Antigen Complexes: Protein Dynamics, Flexibility, and Molecular Recognition,* Biochemistry, **2008**. 47: p. 7237-7247

2. Weigent D. A., Carr D. J., Blalock J. E., *Bidirectional communication between the neuroendocrine and immune systems. Common hormones and hormone receptors,* Annals of the New York Academy of Sciences, **1990**. 579: p. 17–27

3. Burnett E., Christensen J., Tattersall P., *A Consensus DNA Recognition Motif for Two KDWK Transcription Factors Identifies Flexible-length, CpG-methylation Sensitive Cognate Binding Sites in the Majority of Human Promoters,* Journal of Molecular Biology, **2001**. 314: p. 1029–1039

4. Kime L., Jourdan S. S., Mcdowall K. J., *Identifying and characterizing substrates of the RNase E/G family of enzymes,* Methods in Enzymology, **2008**. 447: p. 215-241

5. Updike S. J., Hicks G. P., *Enzyme electrode,* Nature, **1967**. 214: p. 986–988

6. Ellington A. D., Szostak J. W., *In vitro selection of RNA molecules that bind specific ligands,* Nature, **1990**. 346: p. 818–822

7. Tuerk C., Gold L., *Systematic evolution of ligands by exponential enrichment: RNA ligands to bacteriophage T4 DNA polymerase* Science, **1990**. 249: p. 505–510

8. Irvine D., Tuerk C., Gold L., *Selexion: Systematic evolution of ligands by exponential enrichment with integrated optimization by non-linear analysis,* Journal of Molecular Biology, **1991**. 222: p. 739-761

9. Jayasena S. D., *Aptamers: An Emerging Class of Molecules That Rival Antibodies in Diagnostics,* Clinical Chemistry, **1999**. 45: p. 1628-1650

10. Ramos E., Pineiro D., Soto M., Abanades D. R., Martin M. E., Salinas M. E., Gonzalez V. M., *A DNA aptamer population specifically detects Leishmania infantum H2A antigen,* Laboratory Investigation, **2007**. 87: p. 409-416

11. Niu W., Jiang N., Hu Y., *Detection of proteins based on amino acid sequences by multiple aptamers against tripeptides,* Analytical Biochemistry, **2007**. 362: p. 126-135

12. Lee S., Kim Y. S., Jo M., Jin M., Lee D. K., Kim S., *Chip-based detection of hepatitis C virus using RNA aptamers that specifically bind to HCV core antigen,* Biochemical and Biophysical Research Communications, **2007**. 358: p. 47-52

13. Ikanovic M., Rudzinski W. E., Bruno J. G., Allman A., Andrews C. J., *Fluorescence assay based on aptamer-quantum dot binding to Bacillus thuringiensis spores,* Journal of Fluorescence, **2007**. 17: p. 193-199

14. De-Los-Santos-Alvarez N., Lobo-Castanon M. J., Miranda-Ordieres A. J.,Tunon-Blanco P., *Modified-RNA Aptamer-Based Sensor for Competitive Impedimetric Assay of Neomycin B,* Journal of the American Chemical Society, **2007**. 129: p. 3808-3809

15. Senior K., *Aptamers as potential probes for cancer,* Lancet Oncology, **2006**. 7: p. 712

16. Rupcich N., Nutiu R., Li Y., Brennan J. D., *Solid-phase enzyme activity assay utilizing an entrapped fluorescence-signaling DNA aptamer* Angewandte Chemie, International Edition, **2006**. 45: p. 3295-3299

17. Guthrie J. W., Hamula C. L., Zhang H., Le X. C., *Assays for cytokines using aptamers,* Methods, **2006**. 38: p. 324-330

18. Minunni M., Tombelli S., Gullotto A., Luzi E., Mascini M., *Development of biosensors with aptamers as bio-recognition element: the case of HIV-1 Tat protein,* Biosensors & Bioelectronics, **2004**. 20: p. 1149-1156

19. Stojanovic M. N., Landry D. W., *Aptamer-Based Colorimetric Probe for Cocaine,* Journal of the American Chemical Society, **2002**. 124: p. 9678-9679

20. Tombelli S., Minunni M., Mascini M., *Aptamers-based assays for diagnostics, environmental and food analysis,* Biomolecular Engineering, **2007**. 24: p. 191-200

21. Song S., Wang L., Li J., Zhao J., Fan C., *Aptamer-based biosensors,* Trends in Analytical Chemistry, **2008**. 27: p. 108-117

22. Lupold S. E., Hicke B. J., Lin Y., Coffey D. S., *Identification and characterization of nuclease-stabilized RNA molecules that bind human prostate cancer cells via the prostate-specific membrane antigen,* Cancer Research, **2002**. 62: p. 4029–4033

23. Rhodes A., Deakin A., Spaull J., Rees S., *The generation and characterization of antagonist RNA aptamers to human oncostatin M,* Journal of Biological Chemistry, **2000**. 275: p. 28555–28561

24. Nieuwlandt D., Wecker M., Gold L., *In Vitro Selection of RNA Ligands to Substance P,* Biochemistry **1995**. 34: p. 5651–5659

25. Muller J., El-Maarri O., Oldenburg J., Potzsch B., Mayer G., *Monitoring the progression of the in vitro selection of nucleic acid aptamers by denaturing high-performance liquid chromatography,* Analytical and Bioanalytical Chemistry, **2008**. 390: p. 1033 – 1037

26. Smith D., Kirschenheuter G. P., Charlton J., Guidot D. M., Repine J. E., *In vitro selection of RNA-based irreversible inhibitors of human neutrophil elastase* Chemistry & Biology, **1995**. 2: p. 41–750

27. Tsai D. E., Harper D. S., Keene J. D., *U1-snRNP-A protein selects a ten nucleotide consensus sequence from a degenerate RNA pool presented in various structural contexts,* Nucleic Acids Research, **1991**. 19: p.:4931–4936

28. Zhang F., Anderson D., *In Vitro Selection of Bacteriophage φ29 Prohead RNA Aptamers for Prohead Binding,* Journal of Biological Chemistry, **1998**. 273: p. 2947–2953

29. Vater A., Jarosch F., Buchner K., Klussmann S., *Short bioactive Spiegelmers to migraine-associated calcitonin gene-related peptide rapidly identified by a novel approach: Tailored-SELEX,* Nucleic Acids Research, **2003**. 31: p. e130

30. Jensen K. B., Atkinson B. L., Willis M. C., Koch T. H., Gold L., *Using in vitro selection to direct the covalent attachment of human immunodeficiency virus type 1 Rev protein to high-affinity RNA ligands,* Proceedings of the National Academy of Sciences of the USA, **1995**. 92: p. 12220–12224

31. Ikebukuro K., Okumura Y., Sumikura K., Karube I., *A novel method of screening thrombin-inhibiting DNA aptamers using an evolution-mimicking algorithm* Nucleic Acids Research, **2005**. 33: p. e108

32. Rajendran M., Ellington A. D., *Selection of fluorescent aptamer beacons that light up in the presence of zinc,* Analytical and Bioanalytical Chemistry, **2008**. 390: p. 1067–1075

33. Shangguan D., Li Y., Tang Z. W., Tan W. H., *Aptamers evolved from live cells as effective molecular probes for cancer study,* Proceedings of the National Academy of Sciences of the USA, **2006**. 103: p. 11838-11843

34. Mi J., Liu Y. M., Rabbani Z. N., Yang Z. G., Clary B. M., *In vivo selection of tumor-targeting RNA motifs,* Nature Chemical Biology, **2010**. 6: p. 22-24

35. Cox J. C., Ellington A. D., *Automated selection of anti-Protein aptamers,* Bioorganic & Medicinal Chemistry, **2001**. 9: p. 2525–2531

36. Hybarger G., Bynum J., Williams R. F., Chambers J. P., *A microfluidic SELEX prototype,* Analytical and Bioanalytical Chemistry, **2006**. 384: p. 191–198

37. Knight C. G., Platt M., Rowe W., Wedge D. C., Kell D. B., *Array-based evolution of DNA aptamers allows modeling of an explicit sequence-fitness landscape,* Nucleic Acids Research, **2009**. 37: p. e6

38. Berezovski M., Drabovich A., Krylova S. M., Krylov S. N., *Nonequilibrium Capillary Electrophoresis of Equilibrium Mixtures: A Universal Tool for Development of Aptamer* Journal of the American Chemical Society, **2005**. 127: p. 3165–3171

39. Berezovski M. V., Musheev M. U., Drabovich A. P., Jitkova J. V., Krylov S. N., *Non-SELEX Selection of Aptamers,* Journal of the American Chemical Society, **2006**. 128: p. 1410–1411

40. Berezovski M. V., Musheev M. U., Drabovich A. P., Jitkova J. V., Krylov S. N., *Non-SELEX: selection of aptamers without intermediate amplification of candidate oligonucleotides* Nature Protocols, **2006**. 1: p. 1359–1369

41. Javaherian S., Musheev M. U., Kanoatov M., Berezovski M. V., Krylov S. N., *Selection of aptamers for a protein target in cell lysate and their application to protein purification* Nucleic Acids Research, **2009**. 37: p. e62

42. Kanoatov M., Javaherian S., Krylov S. N., *Selection of aptamers for a non-DNA binding protein in the context of cell lysate,* Analytica Chimica Acta, **2010**. 681: p. 92–97

43. Lou X. H., Qian J. R., Xiao Y., Viel L., Soh H. T., *Micromagnetic selection of aptamers in microfluidic channels,* Proceedings of the National Academy of Sciences of the USA, **2009**. 106: p. 2989–2994

44. Qian J. R., Lou X. H., Zhang Y. T., Xiao Y., Soh H. T., *Generation of Highly Specific Aptamers via Micromagnetic Selection* Analytical Chemistry, **2009**. 81: p. 5490–5495

45. Fang X. H., Tan W. H., *Aptamers Generated from Cell-SELEX for Molecular Medicine: A Chemical Biology Approach* Accounts of Chemical Research, **2010**. 43: p. 48-57

46. Chen F., Hu Y. L., Li D. Q., Chen H. D., Zhang X. L., *CS-SELEX generates high-affinity ssDNA aptamers as molecular probes for Hepatitis C virus envelope glycoprotein E2* PLoS One, **2009**. 4

47. Tang Z. W., Parekh P., Turner P., Moyer R. W., Tan W. H., *Generating aptamers for recognition of virus-infected cells,* Clinical Chemistry, **2009**. 55: p. 813–822

48. Zheng J. A., Li Y. B., Li J. X., Su Y. Q., *In vitro selection of oligonucleotide acid aptamers against pathogenic vibrio alginolyticus by SELEX* Key Engineering Materials, **2010**. 439-440: p. 1456–1462

49. Li S. H., Xu H., Ding H. M., Huang Y. P., Cao X. X., Shao N. S., *Identification of an aptamer targeting hnRNP AI by tissue slide-based SELEX,* Journal of Pathology, **2009**. 218: p. 327–336

50. Wan Y., Kim Y. T., Li N., Cho S. K., Bachoo R., Iqbal S. M., *Surface-Immobilized Aptamers for Cancer Cell Isolation and Microscopic Cytology,* Cancer Research, **2010**. 70: p. 9371-9380

51. Gold L., Polisky B., Uhlenbeck O., Yarus M., *Diversity of oligonucleotide functions,* Annual Review of Biochemistry, **1995**. 64: p. 763–797

52. Jayasena S. D., *Aptamers: an emerging class of molecules that rival antibodies in diagnostics,* Clinical Chemistry (Washington DC, United States), **1999**. 45: p. 1628-1650

53. White R. R., Shan S., Rusconi C. P.,Sullenger B. A., *Inhibition of rat corneal angiogenesis by a nuclease-resistant RNA aptamer specific for angiopoietin-2,* Proceedings of the National Academy of Sciences of the USA, **2003**. 100: p. 5028–5033

54. Maehashi K., Katsura T., Kerman K., Tamiya E., *Label-Free Protein Biosensor Based on Aptamer-Modified Carbon Nanotube Field-Effect Transistors,* Analytical Chemistry, **2007**. 79: p. 782–787

55. Luzi E., Minunni M., Mascini M., *New trends in affinity sensing aptamers for ligand binding,* Trends in Analytical Chemistry, **2003**. 22: p. 810-818

56. Stoltenburg R., Reinemann C., Strehlitz B., *SELEX-A (r)evolutionary method to generate high-affinity nucleic acid ligands* Biomolecular Engineering, **2007**. 24: p. 381-403

57. Ringquist S., Jones T., Snyder E. E., Gold L., *High-Affinity RNA Ligands to Escherichia coli Ribosomes and Ribosomal Protein S1: Comparison of Natural and Unnatural Binding Sites,* Biochemistry, **1995**. 34: p. 3640-3648

58. Patel D. J., Suri A. K., Jiang F., Nonin S., *Structure, recognition and adaptive binding in RNA aptamer complexes,* Journal of Molecular Biology, **1997**. 272: p. 645-664

59. Convery M. A., Rowsell S., Stonehouse N. J., Stockley P. G., *Crystal structure of an RNA aptamer-protein complex at 2.8 Å resolution,* Nature Structural Biology, **1998**. 5: p. 133-139

60. Hermann T., Patel D. J., *Adaptive recognition by nucleic acid aptamers,* Science, **2000**. 287: p. 820-825

61. Tuerk C., Macdougal S., Gold L., *RNA pseudoknots that inhibit human immunodeficiency virus type 1 reverse transcriptase,* Proceedings of the National Academy of Sciences of the USA, **1992**. 89: p. 6988-6992

62. Schneider D. J., Feigon J., Hostomsky Z., Gold, L., *High-affinity ssDNA inhibitors of the reverse transcriptase of type 1 human immunodeficiency virus,* Biochemistry, **1995**. 34: p. 9599-9610

63. Jing N., Rando R. F., Pommier Y., Hogan M. E., *Ion Selective Folding of Loop Domains in a Potent Anti-HIV Oligonucleotide,* Biochemistry, **1997**. 36: p. 12498-12505

64. Bock L. C., Griffin L. C., Latham J. A., Vermaas E. H., Toole J. J., *Selection of single-stranded DNA molecules that bind and inhibit human thrombin.,* Nature, **1992**. 355: p. 564-566

65. Kulbachinskiy A., Feklistov A., Krasheninnikov I., Nikiforov V., *Aptamers to Escherichia coli core RNA polymerase that sense its interaction with rifampicin, σ-subunit and GreB,* European Journal of Biochemistry, **2004**. 271: p. 4921-4931

66. Tasset D. M., Kubik M. F., Steiner W., *Oligonucleotide inhibitors of human thrombin that bind distinct epitopes,* Journal of Molecular Biology, **1997**. 272: p. 688-698

67. Shi H., Hoffman B. E., Lis J. T., *A specific RNA hairpin loop structure binds the RNA recognition motifs on the Drosophila SR protein B52,* Molecular and Cellular Biology, **1997**. 17: p. 2649-2657

68. Weiss S., Proske D., Neumann M., Winnacker E. L., *RNA aptamers specifically interact with the prion protein PrP,* Journal of Virology, **1997**. 71: p. 8790-8797

69. Andreola M. L., Pileur F., Calmels C., Litvak S., *DNA aptamers selected against the HIV-1 RNase H display in vitro antiviral activity,* Biochemistry, **2001**. 40: p. 10087-10094

70. Wen J. D., Gray D. M., *The Ff Gene 5 Single-Stranded DNA-Binding Protein Binds to the Transiently Folded Form of an Intramolecular G-Quadruplex,* Biochemistry, **2002**. 41: p. 11438-11448

71. Jenison R. D., Gill S. C., Pardi A., Polisky B., *High-resolution molecular discrimination by RNA,* Science, **1994**. 263: p. 1425-1429

72. Geiger A., Burgstaller B., Von Der Eltz H., Roeder A., Famulok M., *RNA aptamers that bind L-arginine with sub-micromolar dissociation constants and high enantioselectivity,* Nucleic Acids Research, **1996**. 24: p. 1029-1036

73. Sassanfar M., Szostak J. W., *An RNA motif that binds ATP,* Nature, **1993**. 364: p. 550-553

74. Ciesiolka J., Gorski J., Yarus M., *Selection of an RNA domain that binds $Zn^{2+}$,* RNA, **1995**. 1: p. 538-550

75. Hofmann H. P., Limmer S., Hornung V., Sprinzl M., *$Ni^{2+}$-binding RNA motifs with an asymmetric purine-rich internal loop and a G-A base pair,* RNA, **1997**. 3: p. 1289-1300

76. Huizenga D. E., Szostak J. W., *A DNA Aptamer That Binds Adenosine and ATP,* Biochemistry, **1995**. 34: p. 656-665

77. Sazani P. L., Larralde R., Szostak J. W., *A Small Aptamer with Strong and Specific Recognition of the Triphosphate of ATP,* Journal of the American Chemical Society, **2004**. 126: p. 8370-8371

78. Lauhon C. T., Szostak J. W., *RNA aptamers that bind flavin and nicotinamide redox cofactors,* Journal of the American Chemical Society, **1995**. 117: p. 1246-1257

79. Wilson C., Szostak J. W., *In vitro evolution of a self-alkylating ribozyme,* Nature, **1995**. 374: p. 777-782

80. Wilson C., Nix J., Szostak J., *Functional requirements for specific ligand recognition by a biotin-binding RNA pseudoknot,* Biochemistry, **1998**. 37: p. 14410-14419

81. Burgstaller P., Famulok M., *Isolation of RNA aptamer for biologival cofactors by in vitro selection,* Angewandte Chemie, International Edition, **1994**. 33: p. 1084-1087

82. Connell G. J., Illangesekare M., Yarus M., *Three small ribooligonucleotides with specific arginine sites,* Biochemistry, **1993**. 32: p. 5497-5502

83. Famulok M., *Molecular recognition of aminoacids y RNA aptamers: an L-citrulline binding RNA Motif and its evolution into an L-arginine binder,* Journal of the American Chemical Society, **1994**. 116: p. 1698-1706

84. Harada K., Frankel A. D., *Identification of two novel arginine binding DNAs,* EMBO Journal, **1995**. 14: p. 5798-5811

85. Majerfeld I., *RNA Affinity for Molecular L-Histidine; Genetic Code Origins,* Journal of molecular Evolution, **2005**. 61: p. 226-235

86. Majerfeld I., Yarus M., *Isoleucine:RNA sites with associated coding sequences,* RNA, **1998**. 4: p. 471-479

87. Majerfeld I., Yarus M., *An RNA pocket for an aliphatic hydrophobe,* Nature Structural & Molecular Biology, **1994**. 1: p. 287-292

88. Mannironi C., Scerch C., Fruscoloni P., Tocchini-Valentini G. P., *Molecular recognition of amino acids by RNA aptamers: the evolution into an L-tyrosine binder of a dopaminebinding RNA motif,* RNA, **2000**. 6: p. 520-527

89. Vianini, E., Palumbo M., Gatto B., *In vitro selection of DNA aptamers that bind Ltyrosinamide,* Bioorganic & Medicinal Chemistry, **2001**. 9: p. 2543-2548

90. Famulok M., Szostak J. , *Stereospecific Recognition of Tryptophan Agarose by in Vitro Selected RNA,* Journal of the American Chemical Society, **1992**. 114: p. 3990-3991

91. Wang Y., Rando R. R., *Specific binding of aminoglycoside antibiotics to RNA,* Chemistry & Biology, **1995**. 2: p. 281-290

92. Lato S. M., Ellington A. D., *Screening chemical libraries for nucleic-acidbinding drugs by in vitro selection: A test case with lividomycin,* Molecular Diversity, **1996**. 2: p. 103-110

93. Lato S. M., Boles A. R., Ellington A. D., *In vitro selection of RNA lectins: using combinatorial chemistry to interpret ribozyme evolution,* Chemistry & Biology, **1995**. 2: p. 291-303

94. Kwon M., Chun S. M., Jeong S., Yu J., *In vitro selection of RNA against kanamycin B,* Molecular Cell, **2001**. 11: p. 303-311

95. Wallis M. G., Ahsen U. V., Schroeder R., Famulok M., *A novel RNA motif for neomycin recognition,* Chemistry & Biology, **1995**. 2: p. 543-552

96. Yang Q., Goldstein I. J., Mei H.-Y., Engelke D. R., *DNA ligands that bind tightly and selectively to cellobiose,* Proceedings of the National Academy of Sciences of the USA, **1998**. 95: p. 5462-5467

97. Kato T., Takemura T., Yano K., Karube I., *In vitro selection of DNA aptamers which bind to cholic acid,* Biochimica et Biophysica Acta, **2000**. 1493: p. 12-18

98. Kato T., Yano K., Ikebukuro K., Karube I., *Interaction of three-way DNA junctions with steroids,* Nucleic Acids Research, **2000**. 28: p. 1963-1968

99. Eulberg D., Buchner K., Maasch C., Klussmann S., *Development of an automated in vitro selection protocol to obtain RNA-based aptamers: identification of a biostable substance P antagonist,* Nucleic Acids Research, **2005**. 33: p. e45

100. Williams K. P., Liu X.-H., Schumacher T. N. M., Bartel D. P., *Bioactive and nuclease-resistant L-DNA ligand of vasopressin,* Proceedings of the National Academy of Sciences of the USA, **1997**. 94: p. 11285-11290

101. Purschke W. G., Eulberg D., Buchner K., Klussmann S., *An L-RNA based aquaretic agent that inhibits vasopressin in vivo,* Proceedings of the National Academy of Sciences of the USA, **2006**. 103: p. 5173-5178

102. Mendonsa S. D., Bowser M. T. , *In vitro selection of aptamers with affinity for neuropeptide Y using capillary electrophoresis,* Journal of the American Chemical Society, **2005**. 127: p. 9382-9383

103. Hamm J., Fornerod M., *Anti-idiotype RNAs that mimic the leucine-rich nuclear export signal and specifically bind to CRM1/exportin 1,* Chemistry & Biology, **2000**. 7: p. 345-354

104. Hamm J., Huber J., Luhrmann R., *Anti-idiotype RNA selected with an anti-nuclear export signal antibody is actively transported in oocytes and inhibits Rev- and cap-dependent RNA export,* Proceedings of the National Academy of Sciences of the USA, **1997**. 94: p. 12839-12844

105. Kim Y. M., Choi K. H., Jang Y. J., Jeong S., *Specific modulation of the anti-DNA autoantibody-nucleic acids interaction by the high affinity RNA aptamer,* Biochemical and Biophysical Research Communications, **2003**. 300: p. 516-523

106. Wiegand T. W., Williams P. B., Dreskin S. C., Tasset D., *High-affinity oligonucleotide ligands to human IgE inhibit binding to Fc epsilon receptor I,* Journal of Immunology, **1996**. 157: p. 221-230

107. Blind M., Kolanus W., Famulok M., *Cytoplasmic RNA modulators of an inside-out signal-transduction cascade,* Proceedings of the National Academy of Sciences of the United States of America, **1999**. 96: p. 3606-3610

108. Hicke B. J., Watson S. R., Lynott C. K., Parma D., *DNA aptamers block L-selectin function in vivo. Inhibition of human lymphocyte trafficking in SCID mice,* Journal of Clinical Investigation, **1996**. 98: p. 2688-2692

109. Que-Gewirth N. S., Sullenger B. A., *Gene therapy progress and prospects: RNA aptamers.,* Gene Therapy, **2007**. 14: p. 283-291

110. Dollins C. M., Nair S., Sullenger B. A., *Aptamers in immunotherapy,* Human Gene Therapy, **2008**. 19: p. 443-450

111. Herr J. K., Smith J. E., Medley C. D., Shangguan D., Tan W. H., *Aptamer-conjugated nanoparticles for selective collection and detection of cancer cells,* Analytical Chemistry, **2006**. 78: p. 2918-2924

112. Smith J. E., Medley C. D., Tang Z., Shangguan D., Lofton C., Tan W. H. , *Aptamer-conjugated nanoparticles for the collection and detection of multiple cancer cells,* Analytical Chemistry, **2007**. 79: p. 3075-3082

113. Iliuk A. B., Hu L. H., Tao W. A., *Aptamer in Bioanalytical Applications,* Analytical Chemistry, **2011**(83): p. 4443-4452

114. Kusser W., *Chemically modified nucleic acid aptamers for in vitro selections: evolving evolution,* Reviews in Molecular Biotechnology, **2000**. 74: p. 27-38

115. Hoshika S., Minakawa N., Matsuda A., *Synthesis and physical and physiological properties of 4'-thioRNA: application to post-modification of RNA aptamer toward NF-kappaB,* Nucleic Acids Research, **2004**. 32: p. 3815-3825

116. Dougan H., Lyster D. M., Vo C. V., Hobbs J. B. , *Extending the lifetime of anticoagulant oligodeoxynucleotide aptamers in blood,* Nuclear Medicine and Biology, **2000**. 27: p. 289-297

117. Kuwahara M., Hanawa K., Ohsawa K., Sawai H., *Direct PCR amplification of various modified DNAs having amino acids: convenient preparation of DNA libraries with high-potential activities for in vitro selection,* Bioorganic & Medicinal Chemistry, **2006**. 14: p. 2518-2526

118. Pagratis N.C., Bell C., Chang Y. F., Dang C., *Potent 2'-amino-, and 2'-fluoro-2'-deoxyribonucleotide RNA inhibitors of keratinocyte growth factor,* Nature Biotechnology, **1997**. 15: p. 68-73

119. Kubik M. F., Bell C., Fitzwater T., Tasset D. M., *Isolation and characterization of 2'-fluoro-, 2'-amino-, and 2'-fluoro-/amino-modified RNA ligands to human IFN-gamma that inhibit receptor binding,* Journal of Immunology, **1997**. 159: p. 259-267

120. Floege J., Ostendorf T., Janssen U., Janjic N., *Novel approach to specific growth factor inhibition in vivo: antagonism of platelet-derived growth factor in glomerulonephritis by aptamers,* American Journal of Pathology, **1999**. 154: p. 169-179

121. Di Giusto D. A., King G. C., *Construction, stability, and activity of multivalent circular anticoagulant aptamers,* Journal of Biological Chemistry, **2004**. 279: p. 46483-46489

122. Di Giusto D. A., Knox S. M., Lai Y., King G. C., *Multitasking by multivalent circular DNA aptamers,* ChemBioChem, **2006**. 7: p. 535-544

123. Elbaz J., Shlyahovsky B., Li D., Willner I., *Parallel analysis of two analytes in solutions or on surfaces by using a bifunctional aptamer: applications for biosensing and logic gate operations. ,* ChemBioChem, **2008**. 9: p. 232-239

124. Boucard D., Toulme J. J., Di Primo C., *Bimodal loop-loop interactions increase the affinity of RNA aptamers for HIV-1 RNA structures,* Biochemistry, **2006**. 45: p. 1518-1524

125. Radi a-E., Acero S., Josep L., Baldrich E., O'sullivan C. K., *Reagentless, reusable, ultrasensitive electrochemical molecular beacon aptasensor,* Journal of the American Chemical Society, **2006**. 128: p. 117-124

126. Mir M., Jenkins A.T.A., Katakis I., *Ultrasensitive detection based on an aptamer beacon electron transfer chain,* Electrochemistry Communications, **2008**. 10: p. 1533-1536

127. Zuo X., Song S., Zhang J., Pan D., Wang L., Fan C., *A target-responsive electrochemical aptamer switch (TREAS) for reagentless detection of nanomolar ATP,* Journal of the American Chemical Society, **2007**. 129: p. 1042-1043

128. Xiao Y., Lubin A. A., Heeger A. J., Plaxco K. W., *Label-free electronic detection of thrombin in blood serum by using an aptamer-based sensor,* Angewandte Chemie, International Edition, **2005**. 44: p. 5456-5459

129. Xu D. K., Xu D. W., Yu X. B., Liu Z. H., Ma Z. Q., *Label-free electrochemical detection for aptamer-based array electrodes,* Analytical Chemistry, **2005**. 77: p. 5107–5113

130. Xu Y., Yang L., Ye X., He P., Fang Y., *An aptamer-based protein biosensor by detecting the amplified impedance signal,* Electroanalysis, **2006**. 18: p. 1449–1456

131. Ferapontova E. E., Olsen E. M., Gothelf K. V., *An RNA aptamer-based electrochemical biosensor for detection of theophylline in serum,* Journal of the American Chemical Society, **2008**. 130: p. 4256–4258

132. Baker B. R., Lai R. Y., Wood M. S., Doctor E. H., Heeger A. J., Plaxco K. W., *An electronic, aptamer-based small-molecule sensor for the rapid, label-free detection of cocaine in adulterated samples and biological fluids,* Journal of the American Chemical Society, **2006**. 128: p. 3138–3139

133. Radi A. E., O'sullivan C. K., *Aptamer conformational switch as a sensitive electrochemical biosensor for potassium ion recognition,* Chemical Communications (Cambridge, United Kingdom), **2006**: p. 3432–3434

134. Le Floch F., Ho H. A., Leclerc M., *Label-free electrochemical detection of protein based on a ferrocene-bearing cationic polythiophene and aptamer,* Analytical Chemistry, **2006**. 78: p. 4727–4731

135. Wang X. Y., Zhou J. M., Yun W., Xiao S., Fang Y. Z., *Detection of thrombin using electrogenerated chemiluminescence based on Ru(bpy)32+-doped silica nanoparticle aptasensor via target protein-induced strand displacement,* Analytica Chimica Acta, **2007**. 598: p. 242–248

136. Li B., Du Y., Wei H., Dong S., *Reusable, label-free electrochemical aptasensor for sensitive detection of small molecules,* Chemical Communications (Cambridge, United Kingdom), **2007**. 2007: p. 3780–3782

137. Yoshizumi J., Kumamoto S., Nakamura M., Yamana K., *Target-induced strand release (TISR) from aptamer-DNA duplex: A general strategy for electronic detection of biomolecules ranging from a small molecule to a large protein,* Analyst, **2008**. 133: p. 323-325

138. Challier L., Mavré F., Moreau J., Peyrin E., NoëL V., Limoges B., *Simple and Highly Enantioselective Electrochemical Aptamer-Based Binding Assay for Trace Detection of Chiral Compounds,* Analytical Chemistry, **2012**. 84: p. 5414-5420

139. Nutiu R., Li Y. F., *Aptamers with fluorescence-signaling properties,* Methods, **2005**. 37: p. 16-25

140. Liu C. W., Huang C. C., Chang H. T., *Highly Selective DNA-Based Sensor for Lead (II) and Mercury (II) Ions,* Analytical Chemistry, **2009**. 81: p. 2383–2387

141. Chang H. X., Tang L. H., Wang Y., Jiang J. H., Li J. H., *Graphene Fluorescence Resonance Energy Transfer Aptasensor for the Thrombin Detection,* Analytical Chemistry, **2010**. 82: p. 2341–2346

142. Chen S. J., Huang C. C., Chang H. T., *Enrichment and fluorescence enhancement of adenosine using aptamer-gold nanoparticles, PDGF aptamer, and Oligreen,* Talanta, **2010**. 81: p. 493-498

143. Huang J., Zhu Z., Bamrungsap S., Zhu G., You M., He X., Wang K., Tan W., *Competition-Mediated Pyrene-Switching Aptasensor: Probing Lysozyme in Human Serum with a Monomer-Excimer Fluorescence Switch,* Analytical Chemistry, **2010**. 82: p. 10158-10163

144. Ma C., Huang H., Zhao C., *An aptamer-based and pyrene-labeled fluorescent biosensor for homogeneous detection of potassium ions,* Analytical Sciences, **2010**. 26: p. 1261-1264

145. Tuleuova N., Jones C. N., Yan J., Ramanculov E., Yokobayashi Y., Revzin A., *Development of an Aptamer Beacon for Detection of Interferon-γ,* Analytical Chemistry, **2010**. 82: p. 1851–1857

146. Tuleuova N., Revzin A., *Micropatterning of Aptamer Beacons to Create Cytokine-Sensing Surfaces,* Cellular and Molecular Bioengineering, **2010**. 3: p. 337-344

147. Xu J. P., Song Z. G., Fang Y. A., Mei J., Jia L., Qin A. J., Sun J. Z., Ji J. A., Tang B. Z., *Label-free fluorescence detection of mercury(II) and glutathione based on Hg2+-DNA complexes stimulating aggregation-induced emission of a tetraphenylethene derivative,* Analyst, **2010**. 135: p. 3002-3007

148. Zhang L. B., Wei H., Li J., Li T., Li D., Li Y. H., Wang E. K., *A carbon nanotubes based ATP apta-sensing platform and its application in cellular assay.* . Biosensors & Bioelectronics, **2010**. 25: p. 1897-1901

149. Book B., Chen J., Irudayaraj J., *Quantification of receptor targeting aptamer binding characteristics using single-molecule spectroscopy,* Biotechnology and Bioengineering, **2011**. 108: p. 1222-1227

150. Mallikaratchy P. R., Ruggiero A., Gardner J. R., Kuryavyi V., Maguire W. F., Heaney M. L., Mcdevitt M. R., Patel D. J., Scheinberg D. A., *A multivalent DNA aptamer specific for the B-cell receptor on human lymphoma and leukemia,* Nucleic Acids Research, **2011**. 39: p. 2458-2469

151. Stojanovic M. N., De Prada P., Landry D. W., *Aptamer-based folding fluorescent sensor for cocaine,* Journal of the American Chemical Society, **2001**. 123: p. 4928-4931

152. Fang X., Sen A., Vicens M., Tan W., *Synthetic DNA aptamers to detect protein molecular variants in a high-throughput fluorescence quenching assay,* ChemBioChem, **2003**. 4: p. 829-834

153. Li J. J., Fang X., Tan W.H., *Molecular aptamer beacons for real-time protein recognition,* Biochemical and Biophysical Research Communications, **2002**. 292: p. 31-40

154. Li W., Yang X., Wang K., Tan W., Li H., Ma C., *FRET-based aptamer probe for rapid angiogenin detection,* Talanta, **2008**. 75: p. 770-774

155. Hamaguchi N., Ellington Ad., Stanton M., *Aptamer beacons for the direct detection of proteins,* Analytical Biochemistry, **2001**. 294: p. 126-131

156. Dwivedi H. P., Smiley R. D., Jaykus L. A., *Selection and characterization of DNA aptamers with binding selectivity to Campylobacter jejuni using whole-cell SELEX,* Applied Microbiology and Biotechnology, **2010**. 87: p. 2323-2334

157. Jin Y., Bai J. Y., Li H. Y., *Label-free protein recognition using aptamer-based fluorescence assay,* Analyst, **2010**. 135: p. 1731-1735

158. Wagner M. K., Li F., Li J. J., Li X. F., Le X., *Use of quantum dots in the development of assays for cancer biomarkers,* Analytical and Bioanalytical Chemistry, **2010**. 397: p. 3213 – 3224

159. Algar W. R., Tavares A. J., Krull U. J., *Beyond labels: A review of the application of quantum dots as integrated components of assays, bioprobes, and biosensors utilizing optical transduction,* Analytica Chimica Acta, **2010**. 673: p. 1–25

160. Dong H. F., Gao W. C., Yan F., Ji H. X., Ju H. X., *Fluorescence Resonance Energy Transfer between Quantum Dots and Graphene Oxide for Sensing Biomolecules,* Analytical Chemistry, **2010**. 82: p. 5511–5517

161. Li Y., Qi H. L., Gao Q. A., Yang J., Zhang C. X., *Nanomaterial-amplified "signal off/on" electrogenerated chemiluminescence aptasensors for the detection of thrombin,* Biosensors & Bioelectronics, **2010**. 26: p. 754-759

162. Qi Y. Y., Li B. X., *A Sensitive, Label-Free, Aptamer-Based Biosensor Using a Gold Nanoparticle-Initiated Chemiluminescence System,* Chemistry - A European Journal, **2011**. 17: p. 1642–1648

163. Ouyang X., Yu R., Jin J., Li J., Yang R., Tan W., Yuan J., *New Strategy for Label-Free and Time-Resolved Luminescent Assay of Protein: Conjugate Eu3+ Complex and Aptamer-Wrapped Carbon Nanotubes,* Analytical Chemistry, **2011**. 83: p. 782-789

164. Ahn D. G., Jeon I. J., Kim J. D., Song M. S., Han S. R., Oh J. W., *RNA aptamer-based sensitive detection of SARS coronavirus nucleocapsid protein,* Analyst, **2009**. 134: p. 1896–1901

165. Li T., Wang E., Dong S., *Lead (II)-Induced Allosteric G-Quadruplex DNAzyme as a Colorimetric and Chemiluminescence Sensor for Highly*

*Sensitive and Selective Pb2+ Detection,* Analytical Chemistry, **2010**. 82: p. 1515–1520

166. Li H. Y., Deng Q. P., Zhang D. W., Zhou Y. L., Zhang X. X., *Chemiluminescently labeled aptamers as the affinity probe for interaction analysis by capillary electrophoresis,* Electrophoresis, **2010**. 31: p. 2452–2460

167. Potyrailo R. A., Conrad R. C., Ellington A. D., Hieftje G. M., *Adapting Selected Nucleic Acid Ligands (Aptamers) to Biosensors,* Analytical Chemistry, **1998**. 70: p. 3419-3425

168. Fang X. H., Cao Z. H., Beck T., Tan W. H., *Molecular aptamer for real-time oncoprotein platelet-derived growth factor monitoring by fluorescence anisotropy,* Analytical Chemistry, **2001**. 73: p. 5752-5757

169. Gokulrangan G., Unruh J. R., Holub D. F., Wilson G. S., *DNA Aptamer-Based Bioanalysis of IgE by Fluorescence Anisotropy,* Analytical Chemistry, **2005**. 77: p. 1963-1970

170. Li W., Wang K. M., Tan W. H., Ma C. B., Yang X. H., *Aptamer-based analysis of angiogenin by fluorescence anisotropy,* Analyst, **2007**. 132: p. 107-113

171. Zou M. J., Chen Y., Xu X., Huang H. D., Li N., *The homogeneous fluorescence anisotropic sensing of salivary lysozyme using the 6-carboxyfluorescein labeled DNA aptamer,* Biosensors & Bioelectronics, **2012**. 32: p. 148-154

172. Ruta J., Perrier S., Ravelet C., Peyrin E., *Noncompetitive Fluorescence Polarization Aptamer-based Assay for Small Molecule Detection,* Anal. Chem., **2009**. 81: p. 7468-7473

173. Perrier S., Ravelet C., Guieu V., Peyrin E., *Rationally designed aptamer-based fluorescence polarization sensor dedicated to the small target analysis,* Biosensors & Bioelectronics, **2010**. 25: p. 1652-1657

174. Kidd A., Guieu V., Perrier S., Ravelet C., Peyrin E., *Fluorescence polarization biosensor based on an aptamer enzymatic cleavage protection strategy,* **2011**. 401: p. 3229-3234

175. Wang J., Zhou H. S., *Aptamer-based Au nanoparticles-enhanced surface plasmon resonance detection of small molecules,* Analytical Chemistry, **2008**. 80: p. 7174-7178

176. Min K., Cho M., Han S. Y., Shim Y. B., Ku J., Ban C., *A simple and direct electrochemical detection of interferon-using its RNA and DNA aptamers,* Biosensors & Bioelectronics, **2008**. 23: p. 1819-1824

177. Schlensog M., Gronewold T., Tewes M., Famulok M., Quandt E., *A Love-wave biosensor using nucleic acids as ligands,* Sensors and Actuators, B: Chemical, **2004**. 101: p. 308-315

178. Savran C. A., Knudsen S. M., Ellington A. D., Manalis S. R., *Micromechanical detection of proteins using aptamer-based receptor molecules,* Analytical Chemistry, **2004**. 76: p. 3194-3198

179. Hwang K. S., Lee S. M., Eom K., Lee J. H., Lee Y. S., Park J. H., Yoon D. S., Kim T. S., *Nanomechanical microcantilever operated in vibration modes with use of RNA aptamer as receptor molecules for label-free detection of HCV helicase,* Biosensors & Bioelectronics, **2007**. 23: p. 459-465

180. Tombelli S., Minunni M., Luzi E., Mascini M., *Aptamer-based biosensors for the detection of HIV-1 Tat protein,* Bioelectrochemistry, **2005**. 67: p. 135–141

181. Knudsen S. M. , Lee J., Ellington A. D., Savran C. A., *Ribozyme-mediated signal augmentation on a mass-sensitive biosensor,* J. Am. Chem. Soc., **2006**. 128: p. 15936–15937

182. Wu Z. S., Guo M. M., Zhang S. B., Chen C. R., Jiang J. H., Shen G. L., Yu R. Q., *Reusable electrochemical sensing platform for highly sensitive detection of small molecules based on structure-switching signaling aptamers,* Analytical Chemistry, **2007**. 79: p. 2933-2939

183. Feng K., Sun C., Kang Y., Chen J., Yu R. Q., *Label-free electrochemical detection of nanomolar adenosine based on target-induced aptamer displacement,* Electrochemistry Communications, **2008**. 10: p. 531–535

184. Fan H., Chang Z., Xing R., Chen M., Wang Q., He P., Fang Y., *An electrochemical aptasensor for detection of thrombin based on target protein-induced strand displacement,* Electroanalysis, **2008**. 20: p. 2113-2117

185. Lu Y., Li X., Zhang L., Yu P., Su L., Mao L., *Aptamer-based electrochemical sensors with aptamer-complementary DNA oligonucleotides as probe,* Analytical Chemistry, **2008**. 80: p. 1883-1890

186. Han K., Chen L., Lin Z., Li G. X., *Target induced dissociation (TID) strategy for the development of electrochemical aptamer-based biosensor,* Electrochemistry Communications, **2009**. 11: p. 157-160

187. Peng Y., Zhang D., Li, Y., Qi H., Gao Q., *Label-free and sensitive faradic impedance aptasensor for the determination of lysozyme based on target-induced aptamer displacement,* Biosensors & Bioelectronics, **2009**. 25: p. 94-99

188. Nutiul R., Li Y., *Structure-Switching Signaling Aptamers,* Journal of the American Chemical Society, **2003**. 125: p. 4771–4778

189. Yoshida W., Yokobayashi Y., *Photonic Boolean logic gates based on DNA aptamers,* Chemical Communications (Cambridge, United Kingdom), **2007**: p. 195-197

190. Li H., Rothberg L., *Colorimetric detection of DNA sequences based on electrostatic interactions with unmodified gold nanoparticles,* Proceedings of the National Academy of Sciences of the United States of America, **2004**. 101: p. 14036-14039

191. Li H., Rothberg L. J., *Label-Free Colorimetric Detection of specific sequences in genomic DNA amplified by the polymerase chain reaction,* Journal of the American Chemical Society, **2004**. 126: p. 10958-10961

192. Yang C., Wang Y., Marty J. L., Yang X. R., *Aptamer-based colorimetric biosensing of Ochratoxin A using unmodified gold nanoparticles indicator,* Biosensors & Bioelectronics, **2011**. 26: p. 2724-2727

193. Wang J., Wang L., Liu X., Liang Z., Song S., Li W., Li G., Fan C., *A gold nanoparticle-based aptamer target binding readout for ATP assay,* Advanced Materials, **2007**. 19: p. 3943-3946

194. Zhao W., Chiuman W., Lam J. C., Mcmanus S. A., Chen W., Li Y., *DNA aptamer folding on gold nanoparticles: From colloid chemistry to biosensors,* Journal of the American Chemical Society, **2008**. 130: p. 3610-3618

195. Demers L. M., Mirkin C. A., Mucic R. C., Viswanadham G., *A fluorescence-based method for determining the surface coverage and hybridization efficiency of thiol-capped oligonucleotides bound to gold thin films and nanoparticles,* Anal. Chem., **2000**. 72: p. 5535-5541

196. He S., Li D., Zhu C., Fan C., *Design of a gold nanoprobe for rapid and portable mercury detection with the naked eye,* Chem. Commun., **2008**: p. 4885-4887

197. Jin R., Wu G., Li Z., Schatz G., *What controls the melting properties of DNA-linked gold nanoparticle assemblies?,* J. Am. Chem. Soc., **2003**. 125: p. 1643-1654

198. Taton T. A., Lu G., Mirkin C. A., *Two-color labeling of oligonucleotide arrays via size-selective scattering of nanoparticle probes,* J. Am. Chem. Soc., **2001**. 123: p. 5164-5165

199. Liu J., Lu Y., *Fast colorimetric sensing of adenosine and cocaine based on a general sensor design involving aptamers and nanoparticles,* Angew. Chem. Int. Edn Engl., **2006**. 45: p. 90-94

200. Liu J., Lu Y., *Preparation of aptamer-linked gold nanoparticle purple aggregates for colorimetric sensing of analytes,* Nature Protocols, **2006**. 1: p. 246-252

201. Liu J., Mazumdar D., Lu Y., *A simple and sensitive 'dipstick' test in serum based on lateral flow separation of aptamer-linked nanostructures,* Angew. Chem. Int. Edn Engl., **2006**. 45: p. 7955-7959

202. Liu R. R., Liew R. S., Zhou H., Xing B. G., *A simple and specific assay for real-time colorimetric visualization of beta-lactamase activity by using gold nanoparticles,* Angew. Chem. Int. Edn Engl., **2007**. 46: p. 8799-8803

203. Zhao W., Brook M. A., Li Y.F., *Design of gold nanoparticle-based colorimetric biosensing assays,* Chem. Bio. Chem., **2008**. 9: p. 2363-2371

204. Glomm W. R., *Functionalized Gold Nanoparticles for Applications in Bionanotechnology,* J. Dispersion Sci. Technol., **2005**. 26: p. 389-414

205. Liang Z. Q., Zhang J., Wang L. H., Li G. X. , *A centrifugation-based method for preparation of gold nanoparticles and its application in biodetection Int. J. Mol. Sci. 8 526,* Int. J. Mol. Sci., **2007**. 8: p. 526-532

206. Walker H. W., Grant S. B., *Coagulation and stabilization of colloidal particles by adsorbed DNA block copolymers: the role of polymer conformation,* Langmuir **1996**. 12: p. 3151-3156

207. Zhu Z., Wu C. C., Liu H. P., Zou Y., Zhang X. L., Kang H. Z., Yang C. J., Tan W. H., *An Aptamer Cross-Linked Hydrogel as a Colorimetric Platform for Visual Detection,* Angewandte Chemie, International Edition, **2010**. 49: p. 1052–1056

208. Yang H., Liu H., Kang H., Tan W., *Engineering Target-Responsive Hydrogels Based on Aptamer-Target Interactions,* Journal of the American Chemical Society, **2008**. 130: p. 6320–6321

209. Yan X. L., Cao Z. J., Kai M., Lu J. Z., *Label-free aptamer-based chemiluminescence detection of adenosine,* Talanta, **2009**. 79: p. 383–387

210. Zhang S. S., Yan Y. M., Bi S., *Design of Molecular Beacons as Signaling Probes for Adenosine Triphosphate Detection in Cancer Cells Based on Chemiluminescence Resonance Energy Transfer,* Analytical Chemistry, **2009**. 81: p. 8695–8701

211. Yan X. L., Cao Z. J., Lau C. W., Lu J. Z., *DNA aptamer folding on magnetic beads for sequential detection of adenosine and cocaine by substrate-resolved chemiluminescence technology,* Analyst **2010**. 135: p. 2400–2407

212. Zhu X., Zhang Y., Yang W., Liu Q., Lin Z., Qiu B., Chen G., *Highly sensitive electrochemiluminescent biosensor for adenosine based on structure-switching of aptamer,* Analytica Chimica Acta, **2011**. 684: p. 121-125

213. Cruz-Aguado J. A., Penner G., *Fluorescence Polarization Based Displacement Assay for the Determination of Small Molecules with Aptamers,* Analytical Chemistry, **2008**. 80: p. 8853-8855

214. Cui L., Zou Y., Lin N., Zhu Z., Jenkins G., Yang C. J., *Mass Amplifying Probe for Sensitive Fluorescence Anisotropy Detection of Small Molecules in Complex Biological Samples,* Analytical Chemistry, **2012**. 84: p. 5535-5541

215. Huang Y., Zhao S., Chen Z. F., Shi M., Liang H., *Amplified fluorescence polarization aptasensors based on structure-switching-triggered nanoparticles enhancement for bioassays,* Clinical Chemistry, **2012**: p. 7480-7482

216. Ikebukuro K., Kiyohara C., Sode K., *Novel electrochemical sensor system for protein using the aptamers in sandwich manner,* Biosensors & Bioelectronics, **2005**. 20: p. 2168–2172

217. Polsky R., Gill R., Kaganovsky L., Willner I., *Nucleic Acid-Functionalized Pt Nanoparticles: Catalytic Labels for the Amplified Electrochemical Detection of Biomolecules,* Analytical Chemistry, **2006**. 78: p. 2268-2271

218. He P. L., Shen L., Cao Y. H., Li D., *Ultrasensitive Electrochemical Detection of Proteins by Amplification of Aptamer-Nanoparticle Bio Bar Codes,* Analytical Chemistry, **2007**. 79: p. 8024-8029

219. Zhou L., Ou L.J., Chu X., Shen G.L., Yu R.Q., *Aptamer-Based Rolling Circle Amplification: A Platform for Electrochemical Detection of Protein,* Analytical Chemistry, **2007**. 79: p. 7492-7500

220. Pavlov V., Xiao Y., Shlyahovsky B., Willner I., *Aptamer-Functionalized Au Nanoparticles for the Amplified Optical Detection of Thrombin,* Journal of the American Chemical Society, **2004**. 126: p. 11768-11769

221. Li Y. Y., Zhang C., Li B. S., Zhao L. F., Li X. B., Yang, W. J., Xu S.Q., *Ultrasensitive densitometry detection of cytokines with nanoparticle-modified aptamers,* Clinical Chemistry (Washington DC, United States), **2007**. 53: p. 1061-1066

222. Romig T. S., Bell C., Drolet D. W., *Aptamer affinity chromatography: combinatorial chemistry applied to protein purification,* Journal of Chromatography B, **1999**. 731: p. 275-284

223. Connor A. C., Mcgown L. B., *Aptamer stationary phase for protein capture in affinity capillary chromatography,* Journal of Chromatography A, **2006**. 1111: p. 115-119

224. Cho S., Lee S. H., Chung W. J., Kim B. G., *Microbead-based affinity chromatography chip using RNA aptamer modified with photocleavable linker,* Electrophoresis, **2004**. 25: p. 3730-3739

225. Li B. L., Wei H., Dong S. J., *Sensitive detection of protein by an aptamer-based label-free fluorescing molecular switch,* Chemical Communications, **2007**: p. 73-75

226. German I., Buchanan D. D., Kennedy R. T., *Aptamers as Ligands in Affinity Probe Capillary Electrophoresis,* Analytical Chemistry, **1998**. 70: p. 4540-4545

227. Deng Q., German I., Buchanan D., Kennedy R. T., *Retention and Separation of Adenosine and Analogues by Affinity Chromatography with an Aptamer Stationary Phase,* Analytical Chemistry, **2001**. 73: p. 5415-5421

228. Michaud M., Jourdan E., Villet A., Ravel, A., Peyrin E., *A DNA Aptamer as a New Target-Specific Chiral Selector for HPLC,* Journal of the American Chemical Society, **2003**. 125: p. 8672-8679

229. Brumbt A., Ravelet C., Grosset C., Ravel A., Villet A., Peyrin E., *Chiral stationary phase based on a biostable L-RNA aptamer,* Analytical Chemistry, **2005**. 77: p. 1993-1998

230. Ravelet C., Boulkedid R., Ravel A., Grosset C., Villet A., Peyrin E., *A L-RNA aptamer chiral stationary phase for the resolution of target and related compounds,* Journal of Chromatography A, **2005**. 1076: p. 62-70

231. Michaud M., Jourdan E., Ravelet C., Villet A., Peyrin E., *Immobilized DNA Aptamers as Target-Specific Chiral Stationary Phases for Resolution of Nucleoside and Amino Acid Derivative Enantiomers,* Analytical Chemistry, **2004**. 76: p. 1015-1020

232. Fujita K., Silver J., *Surprising lability of biotin-streptavidin bond during transcription of biotinylated DNA bound to paramagnetic streptavidin beads,* Biotechniques, **1993**. 14: p. 608-617

233. Holmberg A., Blomstergren A., Nord O., Lukacs M., Uhlén M., *The biotin-streptavidin interaction can be reversibly broken using water at elevated temperatures,* Electrophoresis, **2005**. 26: p. 501-510

234. Millot M. C., *Separation of drug enantiomers by liquid chromatography and capillary electrophoresis, using immobilized proteins as chiral selectors,* Journal of Chromatography B, **2003**. 797: p. 131-159

235. Kotia R. B., Li L., Mcgown L. B., *Separation of Nontarget Compounds by DNA Aptamers,* Analytical Chemistry, **2000**. 72: p. 827-831

236. Clark S. L., Remcho V. T., *Open tubular liquid chromatographic separations using an aptamer stationary phase,* Journal of Separation Science, **2003**. 26: p. 1451-1454

237. Ruta J., Ravelet C., Désiré J., Décout J. L., Peyrin, E., *Covalently bonded DNA aptamer chiral stationary phase for the chromatographic resolution of adenosine,* Analytical and Bioanalytical Chemistry, **2008**. 390: p. 1051-1057

238. Zhao Q., Li X. F., Shao Y. H., Le X. C., *Aptamer-Based Affinity Chromatographic Assays for Thrombin,* Analytical Chemistry, **2008**. 80: p. 7586-7593

239. Zhao Q., Li X. F., Le X. C., *Aptamer-Modified Monolithic Capillary Chromatography for Protein Separation and Detection,* Analytical Chemistry, **2008**. 80: p. 3915-3920

240. Ravelet C., Grosset C., Peyrin E., *Liquid chromatography, electrochromatography and capillary electrophoresis applications of DNA and RNA aptamers* Journal of Chromatography A, **2006**. 1117: p. 1-10

241. Chung W. J., Kim M. S., Cho S., Lee Y. S., *Microaffinity purification of proteins based on photolytic elution: Toward an efficient microbead affinity chromatography on a chip,* Electrophoresis, **2005**. 26: p. 694-702

242. Deng Q., Watson C. J., Kennedy R. T., *Aptamer affinity chromatography for rapid assay of adenosine in microdialysis samples collected in vivo,* Journal of Chromatography A, **2003**. 1005: p. 123-130

243. Martin J. A., Phillips J. A., Parekh P., Sefah K., Tan W., *Capturing cancer cells using aptamer-immobilized square capillary channels,* Molecular BioSystems, **2011**. 7: p. 1720-1727

244. Liu Y., Bae S. W., Wang K., Hong J. I., Zhu Z., Tan W. H., Pappas D., *The effects of flow type on aptamer capture in differential mobility cytometry cell separations,* Analytica Chimica Acta, **2010**. 673: p. 95-100

245. Heegaard N. H., *Applications of affinity interactions in capillary electrophoresis,* Electrophoresis, **2003**. 24: p. 3879-3891

246. Huang C. C., Cao Z. H., Chang H. T., Tan W. H., *Protein-Protein Interaction Studies Based on Molecular Aptamers by Affinity Capillary Electrophoresis,* Analytical Chemistry, **2004**. 76: p. 6973-6981

247. Berezovski M., Nutiu R., Li Y. F., Krylov S. N., *Affinity Analysis of a Protein-Aptamer Complex Using Nonequilibrium Capillary Electrophoresis of Equilibrium Mixtures,* Analytical Chemistry, **2003**. 75: p. 1382-1386

248. Girardot M., Gareil P., Varenne A., *Interaction study of a lysozyme-binding aptamer with mono- and divalent cations by ACE,* Electrophoresis, **2010**. 31: p. 546–555

249. Zhang H. Q., Li X. F., Le X. C., *Differentiation and detection of PDGF isomers and their receptors by tunable aptamer capillary electrophoresis,* Analytical Chemistry, **2009**. 81: p. 7795–7800

250. De Jong S., Krylov S. N., *Protein Labeling Enhances Aptamer Selection by Methods of Kinetic Capillary Electrophoresis,* Analytical Chemistry, **2011**. 83: p. 6330-6335

251. De Jong S., Krylov S. N., *Pressure-Based Approach for the Analysis of Protein Adsorption in Capillary Electrophoresis,* Analytical Chemistry, **2012**. 84: p. 453-458

252. Li T., Li B. L., Dong S. J., *Adaptive Recognition of Small Molecules by Nucleic Acid Aptamers through a Label-Free Approach,* Chemistry - A European Journal, **2007**. 13: p. 6718-6723

253. Li T., Du Y., Li B. L., Dong S. J., *CE with electrochemical detection for investigation of label-free recognition of amino acid amides by guanine-rich DNA aptamers,* Electrophoresis, **2007**. 28: p. 3122-3128

254. Ruta J., Ravelet C., Grosset C., Peyrin E., *Enantiomeric Separation Using an L-RNA Aptamer as Chiral Additive in Partial-Filling Capillary Electrophoresis,* Analytical Chemistry, **2006**. 78: p. 3032-3039

255. Ruta J., Ravelet C., Baussanne I., Peyrin E., *Aptamer-Based Enantioselective Competitive Binding Assay for the Trace Enantiomer Detection,* Analytical Chemistry, **2007**. 79: p. 4716-4719

256. Ruta J., Ravelet C., Baussanne I., Peyrin E., *Competitive affinity capillary electrophoresis assay based on a "hybrid" pre-incubation/on-capillary mixing format using an enantioselective aptamer as affinity ligand,* Journal of Separation Science, **2008**. 31: p. 2239-2243

257. Ruta J., Ravelet C., Grosset C., Peyrin E., *Aptamer-Modified Micellar Electrokinetic Chromatography for the Enantioseparation of Nucleotides,* Analytical Chemistry, **2009**. 81: p. 1169-1176

258. Phillips J. A., Xu Y., Xia Z., Fan Z. H., Tan W. H., *Enrichment of Cancer Cells Using Aptamers Immobilized on a Microfluidic Channel,* Analytical Chemistry, **2009**. 81: p. 1033–1039

259. Xu Y., Phillips J. A., Yan J. L., Li Q. G., Fan Z. H., Tan,W. H., *Aptamer-Based Microfluidic Device for Enrichment, Sorting, and Detection of Multiple Cancer Cells,* Analytical Chemistry, **2009**. 81: p. 7436–7442

260. Reif R. D., Martinez M. M., Wang, K., Pappas D., *Simultaneous cell capture and induction of apoptosis using an anti-CD95 affinity microdevice,* Analytical and Bioanalytical Chemistry, **2009**. 395: p. 787–795

261. Dharmasiri U., Balamurugan S., Adams A. A., Okagbare P. I., Obubuafo A., Soper S. A., *Highly efficient capture and enumeration of low abundance prostate cancer cells using prostate-specific membrane antigen aptamers*

*immobilized to a polymeric microfluidic device,* Electrophoresis, **2009**. 30: p. 3289–3300

262. Swensen J. S., Xiao Y., Ferguson B. S., Lubin A. A., Lai R. Y., Heeger A. J., Plaxco K. W., Soh H. T., *Continuous, Real-Time Monitoring of Cocaine in Undiluted Blood Serum via a Microfluidic, Electrochemical Aptamer-Based Sensor,* Journal of the American Chemical Society, **2009**. 131: p. 4262–4266

263. Huang P. J., Liu J. W., *Flow Cytometry-Assisted Detection of Adenosine in Serum with an Immobilized Aptamer Sensor,* Analytical Chemistry, **2010**. 82: p. 4020–4026

# Chapter II
# Experiments and Results

## II.1 Objective of the work

Although aptamers have been extensively used in many analytical applications as reviewed in chapter I, there are still plenty of potentials to explore for aptamer-based assays. One major challenge is that most of the assays are confined to macromolecules such as proteins since the binding event leads to a significant structure change which can be easily converted into a detectable signal. Aptamer-based small molecule detections are not widely investigated. Furthermore, compare to the conventional bioassay method (such as ELISA), many aptamer-based biosensing systems are still not highly sensitive, which limits the application of aptamers in sophisticated physiological environment. In such circumstances, to explore rapid, sensitive and signal amplification strategy for small biomolecule analysis would be highly valuable.

The objective of the present work is to establish novel methodologies of aptamer-based assay for the small biomolecule detection, using model targets such as adenosine, tyrosinamide and argininamide. According to the different experimental methods, three major works will be described in this chapter: aptamer-based capillary electrophoresis, gold nanoparticle colorimetric and fluorescence polarization assays.

- Our group has already reported aptamer-based CE assay dedicated to small molecule. However, the method is confined to a single analyte detection [257]. In order to develop a multiplexed format, a novel structure-switching aptamer-based micellar electrokinetic chromatography (MEKC) methodology has been designed.
- Taking advantages of specific DNA discriminating feature of AuNP, various aptamer-based gold nanoparticle colorimetric assays have been already developed. In order to increase both simplicity and general applicability, a label-free, homogeneous aptamer-based sensor strategy for the facile colorimetric detection of small target molecules has been described.
- Fluorescence polarization/fluorescence anisotropy (FP/FA) is a versatile and powerful technique that has been widely used to study biomolecular binding interactions. However, FP aptamer-based small molecule detection remains a challenge as their molecular masses are relatively too small to produce observable FA value changes. To circumvent this problem, a complementary strands (CS) displacement strategy and a single-stranded DNA binding protein (SSB)-assisted strategy have been developed.

## II.2 Multiplexed detection of small molecules by aptamer-based capillary electrophoresis

### II.2.1 Introduction

#### II.2.1.1 General description of capillary electrophoresis

Separation of components in analytical chemistry is of great importance in qualitative and quantitative analysis. Due to attractive analytical features such as low sample and reagent consumption, short analysis time, high separation performances, ease of automation, and the possibility of probing molecular interactions under physiological conditions, the capillary electrophoresis (CE) constitutes one of the most powerful separation techniques. CE has been widely used in several major fields, such as food analysis [264], pharmaceutical and biomedical analysis [265], clinical and forensic analysis [266], environmental samples [267], and biotechnology [268]. The present focus of CE has been on method development and applications of CE to a large variety of analytical problems.

Capillary electrophoresis comprises a family of techniques that have dramatically different operative and separative characteristics. The techniques are:

Capillary zone electrophoresis (CZE) is the simplest and most common mode of CE. In CZE, analytes are free to move under an applied voltage depending on their individual structure and the interactions with the uniform buffer.

Capillary gel electrophoresis (CGE) is useful for separations of nucleic acids, proteins and carbohydrates, because CGE is based on differences in solute size as analytes migrate through the pores of the gel-filled column.

Capillary isoelectric focusing (CIEF) is used for the separation of amphoteric analytes. The principle of CIEF is based on the electrophoretic mobility changes of analytes at a pH gradient in a capillary.

Micellar electrokinetic chromatography (MEKC) has the capability of separating both charged and neutral compounds based on the partitioning of analytes into micelles. It is a significant extension of the CE method

### II.2.1.2 Instrumentation

The system for capillary electrophoresis experiments mainly consists of four parts: capillary, high-voltage power supply, sample injection system and detection devices. A voltage is applied to two separation-buffer vials across the capillary through platinum electrodes. Sample solution is introduced into one end of the capillary under a pressure or electric field. The high-voltage power supply and the detector are controlled by a computer. Data are recorded and processed with software. In commercially available CE systems, a cooling system is often integrated to thermostat the capillary during separation.

The core of a CE system is the capillary in which separation is performed. Fused silica is the most commonly-used capillary substrate. Advantages of fused silica include excellent transparency, high thermal conductance and feasible fabrication with various diameters. The internal diameter (I.D.) varies between 10-100 μm and the outer diameter (O.D.) ranges from 190 to 366 μm. The length of capillary is selected as needed, generally from 20-100 cm. Fused silica is fragile. Therefore, a layer of polyimide is coated on the outer surface. This coating provides capillary with flexibility and durability. Polyimide is non-transparent and shows high absorptivity in UV. Therefore, a small part of the polyimide coating is removed by burning for the detection window. Capillaries are generally provided without internal coating and have bare internal walls. The internal walls of a capillary can be modified to adjust electroosmotic flow (EOF) and reduce adsorption of analytes [269]. Therefore, internal walls can be chemically or physically coated with polymers or surfactants. The commonly-used detection methods in CE include UV-VIS absorbance, fluorescence and laser-induced fluorescence (LIF), and electrochemical detection.

### II.2.1.3 Electroosmosis

Electroosmotic flow (or electro-osmotic flow, often abbreviated EOF; synonymous with electroosmosis or electroendosmosis) is the motion of liquid induced by an applied potential across a porous material, capillary tube, membrane, microchannel, or any other fluid conduit. Because electroosmotic velocities are independent of conduit size, as long as the double layer is much smaller than the characteristic length scale of the channel, electroosmotic flow is

most significant in small channels. EOF is an essential component in capillary electrophoresis and it can occur in natural unfiltered water, as well as buffered solutions.

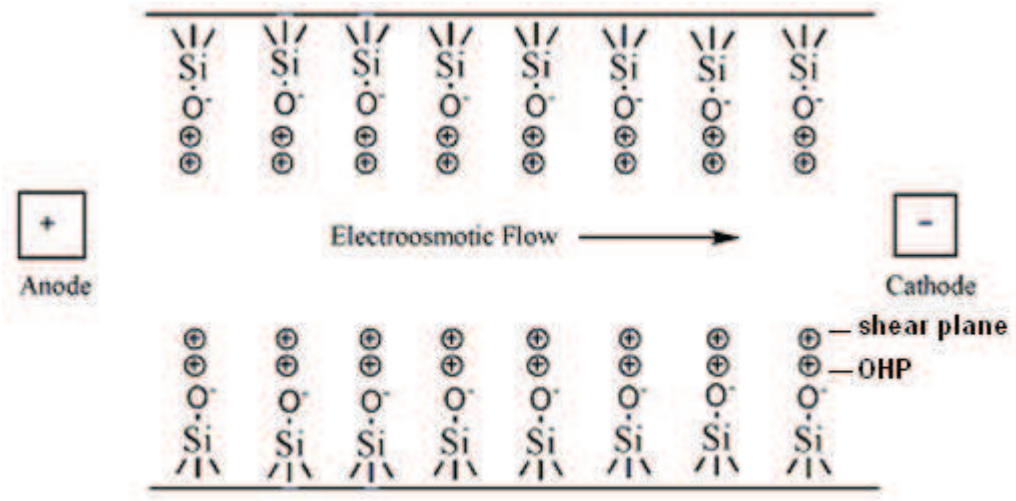


**Figure 2-1:** Schematic diagram of electroosmotic flow (EOF) [62].

The principle of electroosmosis is based on the double-layer formation close to the capillary inner wall as shown in Figure 2-1. For a silica capillary, silanol groups ionize when they are exposed to the buffer solution. The extent of silanol ionization depends notably on the pH of buffer. The higher the pH is, the more extensive the ionization will be. The negatively charged capillary wall attracts a layer of cations from the bulk buffer solution. This layer is essentially static and called the Stern layer. The outer edge of the Stern layer is called the outer Helmholtz plane (OHP). Immediately adjacent to the OHP, a diffuse layer is formed with cations exponentially distributed according to the distance from the capillary wall. There is a layer defined as the shear plane at which hydrodynamic motion becomes possible, and the zeta potential (ζ) is the potential at this shear plane [270, 271]. When a potential is applied across the buffer-filled capillary, cations in the diffuse layer move to the cathode and anions to the anode. The moving ions produce bulk flow due to the water of hydration that is carried with them. The magnitude ($V_{eo}$) of EOF is determined by Equation 1[270].

$$V_{eo} = \frac{\varepsilon \zeta}{\eta} E \qquad (1)$$

where ε is the dielectric constant (permittivity) of the buffer, ζ is the zeta potential, η is the viscosity of the buffer, and E is the applied electric field strength in V/cm. The factor in Equation 1 is defined as electroosmotic mobility ($\mu_{eo}$) as shown in Equation 2.

$$\mu_{eo} = \frac{\varepsilon\zeta}{\eta} \tag{2}$$

The zeta potential ζ is related to the surface charge density (σ, charge per unit surface area) as shown in Equation 3.

$$\zeta = \frac{\delta\sigma}{\varepsilon} \tag{3}$$

where δ is the double-layer thickness. By substituting Equation 3 into Equation 2, the electroosmotic mobility is expressed as in Equation 4.

$$\mu_{eo} = \frac{\delta\sigma}{\eta} \tag{4}$$

The magnitude of electroosmotic mobility is commonly determined using a neutral marker, which is carried by the background buffer and migrates at the mobility of EOF. Mobility is the migration velocity under unit electric field strength. The migration time ($t_o$) of the neutral marker can be determined through electropherograms. The applied voltage (U), the total (L) and the effective (l) lengths of the capillary are known as the running conditions. Therefore, $\mu_{eo}$ can be easily determined according to Equation 5.

$$\mu_{eo} = \frac{V_{eo}}{E} = \frac{lL}{t_0 U} \tag{5}$$

Mobilities are usually expressed in the unit of $cm^2/Vs$. The magnitude of $\mu_{eo}$ typically ranges from $10^{-6}$ to $10^{-4}$ $cm^2/Vs$. Reproducible EOF is highly desirable for identification and quantitation of analytes, because the area of peaks is dependent on the residence time of analytes in the detection window. In addition, uniform EOF produces good precision.

### II.2.1.4 Electrophoretic migration

Electrophoretic migration is a kind of ion movement that is caused by the electric force when exposed to an electric field. The magnitude of the electrophoretic migration is often reported as electrophoretic mobility ($cm^2/Vs$) or electrophoretic velocity (cm/s) in a specific electric field in a buffer (Figure 2-2).

This electrokinetic phenomenon was observed for the first time in 1807 by Reuss (Moscow State University), who noticed that the application of a constant electric field caused clay particles dispersed in water to migrate. It is ultimately caused by the presence of a charged interface between the particle surface and the surrounding fluid.

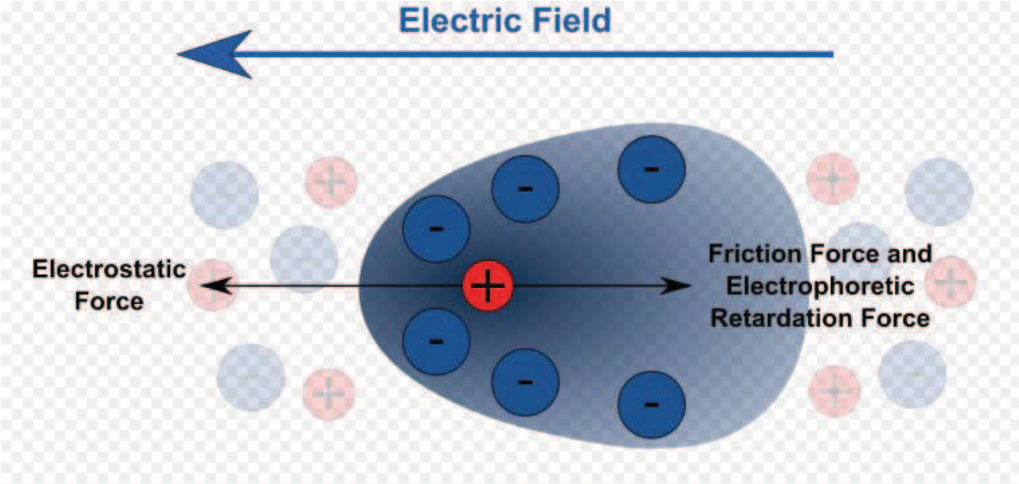


**Figure 2-2:** Scheme of electrophoretic migration [60].

When a compound is dissolved in buffer, it may ionize and exist in several forms at equilibrium. At an infinitely diluted solution, the ionic interactions are negligible. Under an applied voltage across the solution, an electric field is produced across the solution-boundary-defined container, such as a capillary. Ions in the electric field will be accelerated by electric force ($f_e$) and reach a steady migration velocity relative to the solution. The hydrodynamic buffer is viscous and produces a frictional force ($f_d$) which hinders the movement of ions. When the ion is accelerated to a specific magnitude, the frictional force ($f_d$)

will be equal to the magnitude of $f_e$. Under these conditions, the ion migrates at a constant electrophoretic velocity in the homogenous electric field.

The situation about the electrophoretic mobility discussed above is at an ideal condition in which no electrostatic interaction exists at infinite dilution. This situation produces the so-called 'absolute electrophoretic mobility', which is proportional to the equivalent conductance at infinite dilution. In practical applications, analyte ions are surrounded by many counterions present in the buffer solution. These counterions form a so-called ionic atmosphere that causes retardation and relaxation to the ions centered in it. Therefore, the charge ($ze_0$) on the ion needs to be replaced by the smaller effective charge ($q_{eff}$) and the radius (r) by the larger hydrodynamic radius (R) that includes the ionic atmosphere [272].

$$\mu_{ep} = \frac{q_{eff}}{6\pi\eta R} \tag{6}$$

where $\mu_{ep}$ is defined as the effective electrophoretic mobility. Factors affecting the magnitude of $\mu_{ep}$ include temperature, components and ionic strength of the buffer. As can be seen from Equation 6, the electrophoretic mobility of an ion is directly related to the ratio of the charge and its size ($q_{eff}/R$) if the viscosity of the buffer is constant. The magnitude of $\mu_{ep}$ is determined indirectly using $\mu_{eo}$ as expressed in Equation 6 and the apparent mobility of $\mu_a$ , which can be directly obtained by Equation 7,

$$\mu_a = \frac{lL}{Ut_m} \tag{7}$$

where $t_m$ is the migration time of the species of interest. Then, $\mu_{ep}$ can be calculated by Equation 8.

$$\mu_{ep} = \mu_a - \mu_{eo} = \frac{lL}{U}\left(\frac{1}{t_m} - \frac{1}{t_0}\right) \tag{8}$$

If μep > 0, μep is in the same direction of EOF, otherwise it is in the opposite direction of EOF.

### II.2.1.5 Separation and resolution

Separation of analytes in CE is obtained on the basis of the differences in effective electrophoretic mobilities of analytes. As shown in Equation 7, $\mu_{ep}$ is determined by the ratio of $q_{eff}/R$. Therefore, charged analytes are separated with some degree of resolution, while neutral analytes appear as one peak without separation in capillary zone electrophoresis. The efficiency of an electrophoretic system is characterized by the number of theoretical plates ($N$) which is borrowed from chromatography. $N$ can be determined experimentally from an electropherogram with Equation 9.

$$N = 5.54 \cdot (\frac{t_m}{w_{1/2}})^2 \tag{9}$$

where $w_{1/2}$ is the peak width at the half of the peak height.

The resolution ($R_s$) of two peaks shows the extent of the separation and can be calculated according to Equation 10.

$$R_s = \frac{t_2 - t_1}{(w_1 + w_2)/2} \tag{10}$$

where $t_1$ and $t_2$ are migration times, $w_1$ and $w_2$ are peak widths of analytes 1 and 2 on the baseline, respectively.

### II.2.1.6 Micellar electrokinetic chromatography (MEKC)

Micellar electrokinetic chromatography, first developed and introduced by Terabe [273, 274], is suitable for the separation of uncharged as well as charged analytes. It is a significant extension of the CE method.

The principle of MEKC is based on the partitioning of analytes between the micellar and the aqueous phases [274].When the surfactant in aqueous solution is above the critical micelle concentration (CMC), surfactant molecules aggregate to form micelles. Hydrophobic analytes may join the micelles in the core and migrate with micelles under an applied voltage. Anionic surfactants form micelles with negative charges migrating to the anode. Cationic surfactants

form positively charged micelles moving to the cathode. For neutral analytes, the electrophoretic mobility ($\mu_{ep}^{0}$) is determined by Equation 11.

$$\mu_{ep}^{0} = \frac{k'}{k'+1} \cdot \mu_{ep}^{mc} \tag{11}$$

where *k'* is the capacity factor (i.e. retention factor) of the analyte, and $\mu_{ep}^{mc}$ is the electrophoretic mobility of the micelle. Because *k* ' is identical for each analyte, their electrophoretic mobilities are different. Therefore, neutral analytes can be separated from one another. For charged analytes, the electrophoretic mobility ($\mu_{ep}^{i}$) is determined by Equation 12

$$\mu_{ep}^{i} = \frac{k'}{k'+1} \cdot \mu_{ep}^{mc} + \frac{1}{k'+1} \cdot \mu_{ep}^{i} \tag{12}$$

where $\mu_{ep}^{i}$ is the electrophoretic mobility of the charged analyte into the aqueous solution free of surfactant.

The capacity factor of an analyte, the ratio of analytes in the micellar phase to those in the aqueous phase, can be determined using migration times as shown in Equation 13

$$k' = \frac{t_i - t_{eo}}{t_{eo}(1 - t_i / t_{mc})} \tag{13}$$

where $t_t$, $t_{eo}$, $t_{mc}$ are the migration times of the analyte, the EOF marker and the micelle marker, respectively. The EOF marker, such as methanol, should not interact with the micelles. The micelle marker, such as Sudan III, should be completely associated with the micelles. The capacity factor of an analyte increases with the increase of the surfactant concentration in the separation buffer.

Several surfactants can be selected for MEKC according to the physicochemical nature of the analytes. Sodium dodecyl sulfate (SDS), an anionic surfactant, is the most commonly used micellar phase for neutral and cationic analytes [275]. Cetyltrimethylammonium chloride (CTAC), a cationic surfactant, is useful for large molecules and neutral or anionic analytes. Other surfactants, such as non-ionic, zwitterionic, polymer and mixed surfactants, also have been used in different applications [276, 277].

## II.2.2 Experimental Section

The objective of the work is to develop a new methodology for small molecule detection by aptamer-based capillary electrophoresis. Our lab has previously reported four examples of the use of aptamer as additive in the electrolyte background for the small target separation, (see literature review in chapter I). However, all of these methodologies are dedicated to the single cationic or anionic compound analysis during the run. My work was focused on the following two aspects:

- To generalize a rationalized aptamer-based assay for small molecule detection (regardless of the charge of the target in the electrolyte background)
- To establish a predictable methodology for the simultaneous detection of multiple small analytes in a single capillary

In order to achieve these goals, a structure-switching concept was utilized for the design, the complementary sequences of aptamers, instead of aptamers themselves, are employed as tracer to be detected. After incubation with targets, the formed target-aptamer complexes will be liberated into the solution, which leads to the changes of detectable signals. Similar to the previous experiment [257], cholesteryl tag is also labeled to aptamer under MEKC conditions, two assay configurations were designed according to the position where cholesteryl tag was connected: The first one, developed for the single-analyte determination, was based on the use of a cholesteryl-tagged aptamer (Chol-Apt) and its fluorescein-labeled complementary strand (CS*) as the tracer. The second format, especially designed for multianalyte sensing, employed dually cholesteryl- and fluorescein- labeled complementary strands (Chol-CS*) of different lengths and unmodified aptamers (Apt). This method could expand significantly the potential of small biomolecule analysis in terms of simplicity, adaptability, generalizability, and high-throughput analysis capability.

***Article published in Analytical Chemistry, volume 82, 2010, pages 4613-4620***

*Anal. Chem.* **2010,** *82,* 4613–4620

# Multiplexed Detection of Small Analytes by Structure-Switching Aptamer-Based Capillary Electrophoresis

**Zhenyu Zhu,[†] Corinne Ravelet,[†] Sandrine Perrier,[†] Valérie Guieu,[†] Béatrice Roy,[‡] Christian Perigaud,[‡] and Eric Peyrin*,[†]**

*Département de Pharmacochimie Moléculaire, UMR 5063 CNRS, ICMG FR 2607, Université Grenoble I, Campus universitaire, Saint-Martin d'Hères, France, and Institut des Biomolécules Max Mousseron, UMR 5247 CNRS, Université Montpellier 2, Place Eugène Bataillon, Montpellier, France*

**Affinity probe capillary electrophoresis (APCE) assays, combining the separation power of CE with the specificity of interactions occurring between a target and a molecular recognition element (MRE), have become important analytical tools in many application fields. In this report, a rationalized strategy, derived from the structure-switching aptamer concept, is described for the design of a novel APCE mode dedicated to small molecule detection. Two assay configurations were reported. The first one, developed for the single-analyte determination, was based on the use of a cholesteryl-tagged aptamer (Chol-Apt) as the MRE and its fluorescein-labeled complementary strand (CS*) as the tracer (laser-induced fluorescence detection). Under micellar electrokinetic chromatography (MEKC) conditions, free CS* and the hybrid formed with Chol-Apt (duplex*) were efficiently separated (and then quantified) through the specific shift of the electrophoretic mobility of the cholesteryl-tagged species in the presence of a neutral micellar phase. When the target was introduced into the preincubated sample, the hybridized form was destabilized, resulting in a decrease in the duplex* peak area and a concomitant increase in the free CS* peak area. The second format, especially designed for multianalyte sensing, employed dually cholesteryl- and fluorescein-labeled complementary strands (Chol-CS*) of different lengths and unmodified aptamers (Apt). The size-dependent electrophoretic separation of different Chol-CS* forms from each other and from their corresponding duplexes* was also accomplished under MEKC conditions. The simultaneous detection of multiple analytes in a single capillary was performed by monitoring accurately each target-induced duplex-to-complex change. This method could expand significantly the potential of small solute APCE analysis in terms of simplicity, adaptability, generalizability, and high-throughput analysis capability.**

By virtue of its homogeneous format, high resolving capability, short analysis time, advanced instrumentation, minute sample requirements, and sensitivity and selectivity of detection, the laser-induced fluorescence-coupled affinity probe capillary electrophoresis (APCE-LIF) technique, using antibodies and more recently nucleic acid aptamers as specific molecular recognition elements (MREs), constitutes a very interesting alternative to the conventional heterogeneous antibody- or aptamer-based assay methods in a variety of application fields, including clinical, biochemical, and environmental areas.

For the APCE-LIF assays dedicated to protein analysis,[1−11] both competitive and noncompetitive (direct) formats can be used. In the direct assay, the MRE is fluorescently labeled and added at a constant concentration to the sample for binding to the target. After incubation, detection of the complex peak or free MRE peak is related to the amount of the target in solution. In the competitive assay, the protein is labeled and competes with the unlabeled target in the sample for binding to a limited amount of its specific MRE. A CE separation of this preincubated mixture produces two distinct peaks corresponding to the free labeled protein and the labeled protein bound to the MRE, allowing the quantification of the target.

In contrast with the protein analysis, the small molecule detection by the APCE-LIF technique relies, except in rare specific cases,[12] on a competitive format because of the difficulty in separating the target−MRE complex from the free MRE. The typical small target APCE approach then requires the synthesis of a fluorescent analogue of the small analyte (tracer).[13−23] This

* To whom correspondence should be addressed. E-mail: eric.peyrin@ujf-grenoble.fr.

[†] UMR 5063 CNRS, ICMG FR 2607, Université Grenoble 1.

[‡] UMR 5247 CNRS, Université Montpellier 2.

(1) Shimura, K.; Karger, B. L. *Anal. Chem.* **1994**, *66*, 9–15.
(2) Schultz, N. M.; Huang, L.; Kennedy, R. T. *Anal. Chem.* **1995**, *67*, 924–929.
(3) Ou, J. P.; Wang, Q. G.; Cheung, T. M.; Chan, S. T.; Yeung, W. S. *J. Chromatogr., B* **1999**, *727*, 63–71.
(4) Shimura, K.; Hoshino, M.; Kamiya, K.; Katoh, K.; Hisada, S.; Matsumoto, H.; Kasai, K. *Electrophoresis* **2002**, *23*, 909–917.
(5) Giovannoli, C.; Anfossi, L.; Baggiani, C.; Giraudi, G. *J. Chromatogr., A* **2007**, *1155*, 187–192.
(6) German, I.; Buchanan, D. D.; Kennedy, R. T. *Anal. Chem.* **1998**, *70*, 4540–4545.
(7) Huang, C. C.; Cao, Z.; Chang, H. T.; Tan, W. *Anal. Chem.* **2004**, *76*, 6973–6981.
(8) Berezovski, M.; Krylov, S. N. *Anal. Chem.* **2005**, *77*, 1526–1529.
(9) Wang, H.; Lu, M.; Le, X. C. *Anal. Chem.* **2005**, *77*, 4985–4990.
(10) Haes, A. J.; Giordano, B. C.; Collins, G. E. *Anal. Chem.* **2006**, *78*, 3758.
(11) Zhang, H.; Li, X. F.; Le, X. C. *J. Am. Chem. Soc.* **2008**, *130*, 34–35.
(12) Hafner, F. T.; Kautz, R. A.; Iverson, B. L.; Tim, R. C.; Karger, B. L. *Anal. Chem.* **2000**, *72*, 5779–5786.
(13) Chen, F.-T. A.; Evangelista, R. A. *Clin. Chem.* **1994**, *40*, 1819–1822.

10.1021/ac100755q © 2010 American Chemical Society
Published on Web 05/06/2010

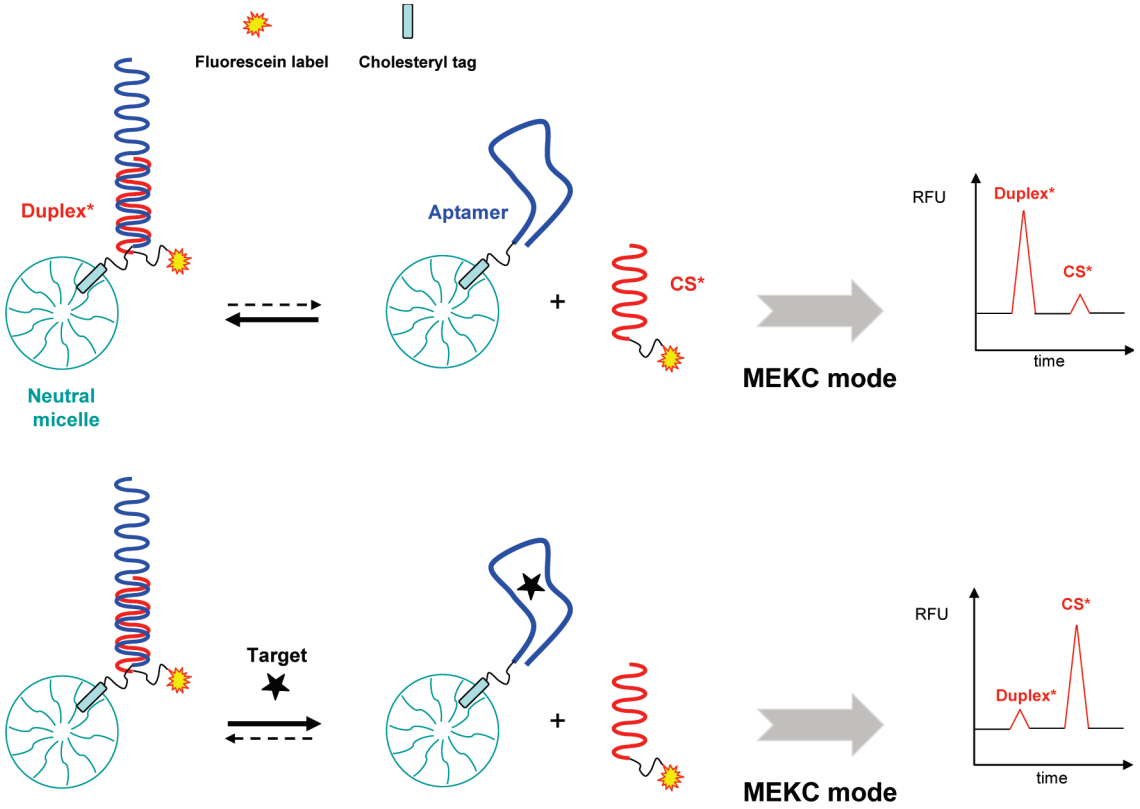


**Figure 1.** Schematic representation of the structure-switching aptamer APCE-LIF assay principle for single-analyte sensing.

constitutes a major limitation of the technique as the labeling step (i) can be laborious and time-consuming,[13,14,21–23] (ii) can produce interfering byproducts,[13,16,21,23] (iii) has to be adapted to each target in relation to its specific reactive groups and its electrophoretic mobility,[13,21] and (iv) can profoundly affect the tracer affinity for the MRE.[19]

In addition, although parallel electrophoretic separations can be accomplished by using capillary array electrophoresis and multiple-LIF detection with different tagging of tracers is possible, the improvement of the APCE high-throughput analysis capability remains a challenging task.[11,19] In this context, previous examples of CE immunoassays have been reported for the simultaneous analysis of multiple drugs in a single capillary.[13,14,16,17] However, the described methodology does not constitute a generalizable approach as it necessitates the careful synthetic design of the multiple tracers to allow the electrophoretic separation of the different labeled analytes from each other and from the antibody−target complexes.[13,16] Furthermore, the solute quantification is solely based on the measurement of the free tracer peak change since the distinctions between the various complexes cannot typically be attained.[13,14,17]

The first objective of this work was to establish a rationalized method for the development of a simpler, faster, and generic APCE-LIF assay dedicated to the identification of small analytes. The general scheme employed a nucleic acid aptamer as the MRE and was based on the structure-switching concept initially described by Li and colleagues.[24,25] This strategy is related to the unique ability of nucleic acids to form duplex structures with their complementary sequences (CS). In the absence of the target, base pairing between the complementary sequences is favored. When the target binds to the aptamer, the hybridization is disrupted, leading to the release of the complementary strand. Therefore, via adequate labeling of the CS and/or the aptamer, the molecular recognition event can be effectively converted into a detectable signal. Because of its great simplicity and its very broad applicability, the duplex-to-complex change concept has been successfully exploited in the design of various fluorescence-, electrochemical-, or nanoparticle-based aptamer assays.[24−29] Herein, the structure-switching aptamer approach was extended to the APCE-LIF analysis. The schematic principle is presented in Figure 1. As the migration of DNA molecules does not change appreciably with

(14) Evangelista, R. A.; Chen, F.-T. A. *J. Chromatogr.* **1994**, *680*, 587–591.
(15) Schmaldzing, D.; Nashabeh, W.; Yao, X. W.; Mhatre, R.; Regnier, F. E.; Afeyan, F. B.; Fuchs, M. *Anal. Chem.* **1995**, *67*, 606–612.
(16) Steinmann, L.; Thormann, W. *Electrophoresis* **1996**, *17*, 1348–1356.
(17) Caslavska, J.; Alleman, D.; Thormann, W. *J. Chromatogr., A* **1999**, *838*, 197–211.
(18) Suzuki, Y.; Arakawa, H.; Maeda, M. *Anal. Sci.* **2003**, *19*, 111–115.
(19) Yeung, W. S. B.; Luo, G. A.; Wang, Q. G.; Ou, J. P. *J. Chromatogr., B* **2003**, *797*, 217–228.
(20) Bromberg, A.; Mathies, R. A. *Anal. Chem.* **2003**, *75*, 1188–1195.
(21) Dunkle, M. N.; Herrmann, J. K.; Colon, H.; Pennington, C.; Colon, L. A. *Microchem. J.* **2006**, *82*, 100–107.
(22) Ruta, J.; Ravelet, C.; Baussanne, I.; Décout, J. L.; Peyrin, E. *Anal. Chem.* **2007**, *79*, 4716–4719.
(23) Zhang, C.; Ma, G.; Fang, G.; Zhang, Y.; Wang, S. J. *J. Agric. Food Chem.* **2008**, *56*, 8832–8837.
(24) Nutiu, R.; Li, Y. *J. Am. Chem. Soc.* **2003**, *125*, 4771–4778.
(25) Nutiu, R.; Li, Y. *Chem.—Eur. J.* **2004**, *10*, 1868–1876.
(26) Xiao, Y.; Piorek, B. D.; Plaxco, K. W.; Heeger, A. J. *J. Am. Chem. Soc.* **2005**, *127*, 17990–17991.
(27) Liu, J.; Lu, Y. *Angew. Chem., Int. Ed.* **2006**, *45*, 90–94.
(28) Wu, Z. S.; Guo, M. M.; Zhang, S. B.; Chen, C. R.; Jiang, J. H.; Shen, G. L.; Yu, R. Q. *Anal. Chem.* **2007**, *79*, 2933–2939.
(29) Wang, M. J.; Wang, L.; Liu, X.; Liang, Z.; Song, S.; Li, W.; Li, G.; Fan, C. *Adv. Mater.* **2007**, *19*, 3943–3946.

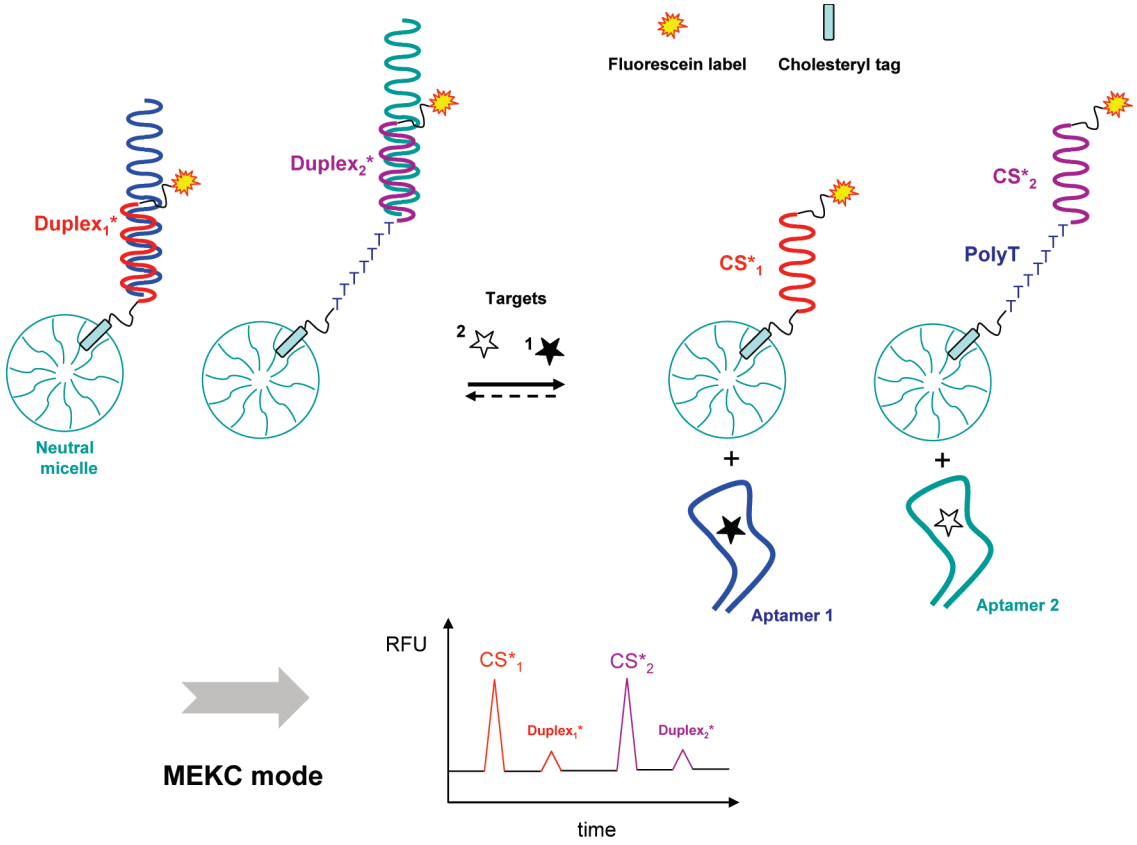


**Figure 2.** Schematic representation of the structure-switching aptamer APCE-LIF assay principle for multiplex sensing.

molecular weight in free solution (except in the presence of metal ions as very recently reported),[30] the free CS and the aptamer (and then the duplex) are assumed to display a similar electrophoretic mobility in capillary zone electrophoresis.[31,32] To overcome this limitation, the CE analysis step of the preincubated mixture was conducted via application of the drag tag strategy. Classically, this approach, known as end-labeled free solution electrophoresis (ELFSE), consists of tagging the nucleic acid fragments with a large, neutral (or nearly neutral) molecule, i.e., the drag tag, to shift their electrophoretic mobility in relation to their length.[33,34] The electrophoretic mobility ($\mu$) of a tagged DNA molecule comprising $N$ monomers is known to vary as follows:[34]

$$\mu = \mu_0\left(\frac{N}{N+\alpha}\right) \qquad (1)$$

where $\mu_0$ is the free solution electrophoretic mobility of the unlabeled DNA and $\alpha$ the hydrodynamic drag dependent on the drag tag employed. Thus, the electrophoretic mobility in the ELFSE increases as the DNA becomes larger. Alternative approaches, based on a similar concept, have been also described.[32,35] Notably, a simpler method, involving the use of neutral surfactant micelles as drag tags, has recently been employed.[35,36] The transient association of hydrophobic group-tagged DNA strands into nonionic micelles, in a micellar electrokinetic chromatography (MEKC) mode, was able to modulate their electrophoretic mobility with an $\alpha$ value similar to that reported for covalently attached drag tags.[35] In this context, the CS of the aptamer was end-labeled with a fluorescein dye (CS*), and the aptamer was end-modified with a lipophilic cholesteryl moiety (Chol-Apt). We, therefore, expected that the duplex* and the CS* species could be separated by MEKC through the specific shift of the mobility of the cholesteryl-tagged species in the presence of the neutral micellar phase.[35−37] This would allow us to monitor the duplex-to-complex change induced by the small target binding to the aptamer (Figure 1).

The second goal of this work was to adapt this strategy to the design of a predictable methodology for the simultaneous detection of multiple small analytes in a single capillary. In such a case, the assay configuration was modified. Cholesteryl-tagged and fluorescein-labeled CS (Chol-CS*) were employed as tracers, whereas unmodified aptamers were used as the MRE (Figure 2). We proposed that the MEKC separation between Chol-CS* and duplex* of multiple aptamers could be rationally attained by modulating the length of Chol-CS*. The introduction of a poly(T) tail of an adequate length at one extremity of a complementary strand was predicted to increase significantly the electrophoretic mobility of both the Chol-CS* and its corresponding duplex* in

(30) Li, T.; Zhang, D.; Luo, W.; Lu, M.; Wang, Z.; Song, Y.; Wang, H. *Anal. Chem.* **2010**, *82*, 487–490.
(31) Pennathur, S.; Baldessari, F.; Santiago, J. G.; Kattah, M. G.; Steinman, J. B.; Utz, P. J. *Anal. Chem.* **2007**, *79*, 8316–8322.
(32) Berezovski, M.; Krylov, S. N. *J. Am. Chem. Soc.* **2003**, *125*, 13451–13454.
(33) Won, J. I.; Meagher, R. J.; Barron, A. E. *Electrophoresis* **2005**, *26*, 2138–2148.
(34) McCormick, L. C.; Slater, G. W. *Electrophoresis* **2006**, *27*, 1693–1701.
(35) Grosser, S. T.; Savard, J. M.; Schneider, J. W. *Anal. Chem.* **2007**, *79*, 9513–9519.
(36) Savard, J. M.; Grosser, S. T.; Schneider, J. *Electrophoresis* **2008**, *29*, 2779–2789.
(37) Ruta, J.; Perrier, S.; Ravelet, C.; Roy, B.; Perigaud, C.; Peyrin, E. *Anal. Chem.* **2009**, *81*, 1169–1176.

**Table 1. Oligonucleotides Utilized in the Structure-Switching Aptamer-Based APCE-LIF Assays[a]**

| | |
|---|---|
| | Single-Analyte Format |
| | AMP Sensing System |
| Chol-Apt-A (32-mer) | 5′-Chol-**AGAGAACCTGGG**GGAGTATTGCGGAGGAAGGT-3′ |
| CS-A* (12-mer) | 5′-**CCCAGGTTCTCT**-F-3′ |
| | Multiplex Format |
| | AMP Sensing System |
| Apt-A (32-mer) | 5′-**AGAGAACCTGGG**GGAGTATTGCGGAGGAAGGT-3′ |
| Chol-CS-A* (12-mer) | 5′-F-**CCCAGGTTCTCT**-Chol-3′ |
| | Tym Sensing System |
| Apt-Ty (38-mer) | 5′-TGGAGCT**TGGATTGATGTG**GTGTGTGAGTGCGGTGCCC-3′ |
| Chol-CS-Ty* (50-mer) | 5′-F-**CACATCAATCCA**-$(T)_{38}$-Chol-3′ |

[a] Abbreviations: Chol, cholesteryl tag; F, fluorescein label. Complementary bases are shown in bold type.

relation to their size (eq 1). This would provide the electrophoretic separation of the different Chol-CS* species from each other and from the associated duplexes* and thus the multiple-target detection via the analysis of each duplex-to-complex change (Figure 2).

In the first step, the feasibility of the structure-switching aptamer-based APCE-LIF mode (Figure 1) was established by employing the adenosine monophosphate (D-AMP) and its corresponding DNA aptamer[38] as a model system. Titration curves with increasing D-AMP concentrations were constructed, and the analytical performances were subsequently analyzed. In the second step, the proof of concept of the approach dedicated to multiplex analysis (Figure 2) was demonstrated for dual-analyte sensing by using two different recognition systems, i.e., D-AMP with the anti-D-AMP DNA aptamer and L-tyrosinamide (L-Tym) with its specific DNA aptamer.[39]

## EXPERIMENTAL METHODS

**Chemicals and Oligonucleotides.** Natural β-D-adenosine (D-A), β-D-adenosine 5′-monophosphate (D-AMP), and β-D-guanosine 5′-monophosphate (D-GMP) nucleotides and L-tyrosinamide (L-Tym) were obtained from Sigma Aldrich (Saint-Quentin, France). β-L-Adenosine 5′-monophosphate (L-AMP) was synthesized, purified, and characterized as previously described by Périgaud and co-workers.[40] Polyoxyethylene(23) lauryl ether (Brij 35), polyoxyethylene(9) dodecyl ether (Thesit), polyoxyethylene(10) octyl phenol ether (Triton X-100), and tris(hydroxymethyl)aminomethane (Tris) were purchased from Sigma Aldrich. HCl, NaCl, and $MgCl_2 \cdot 6H_2O$ were supplied by Prolabo (Paris, France), Chimie-Plus laboratoires (Bruyères de Pouilly, France), and Panreac Quimica (Barcelona, Spain), respectively. Water was obtained from a Purite Still Plus water purification system fitted with a reverse osmosis cartridge. The normal and modified oligonucleotides listed in Table 1 were synthesized and HPLC-purified by Eurogentec (Angers, France). The identity of the oligonucleotides was confirmed by MALDI-TOF mass spectrometry.

**Sample Preparation.** The incubation buffer consisted of a buffered solution [20 mM Tris-HCl (pH 7.50), 50 mM NaCl, and 5 mM $MgCl_2$] containing a neutral surfactant (2.5 or 25 mM in relation to the assay configuration). The analyte stock solutions (D-A, D-AMP, L-AMP, D-GMP, and L-Tym) were dissolved in pure water and stored at 4 °C. The aptamer and complementary strand stock solutions were prepared in pure water and stored at −20 °C. Samples were daily prepared by dilution of the stock solutions in a concentrated incubation buffer with surfactant. The samples were composed of Chol-Apt or Apt and CS* or Chol-CS* oligonucleotides at a final concentration of 250 nM each for D-AMP sensing and 250 and 500 nM, respectively, for L-Tym sensing. For the titration curve, the analyte concentration varied from 0 to 3 mM in the surfactant-containing incubation buffer. The sample solutions were heated at 90 °C for 5 min, left to stand at room temperature for 10 min, and kept at 4 °C for at least 30 min to attain equilibrium of the mixture prior to the CE injection.

**Capillary Electrophoresis Experiments.** An Agilent capillary electrophoresis system (Agilent Technologies, Waldbronn, Germany) equipped with a ZETALIF Discocery laser-induced fluorescence detector (Picometrics, Toulouse, France) adapted for a diode laser source (DPSS Laser Kyma 488 nm, Melles Griot, or SDL-473-030T, Shanghai Dream Lasers Technology) was used throughout. A 50 μm inner diameter (i.d.) and 362 μm outer diameter (o.d.) uncoated fused-silica capillary (total length, 59 cm; effective lengths, 19 cm for the single-analyte format and 40 cm for the multiplex format), with a specific Discocery cell including an ellipsoid lens for the "on-capillary" collection of the emitted light, was employed (Picometrics).[41] Before being used, the capillary was daily treated at 1000 mbar with 1 M NaOH for 10 min and rinsed first with pure water for 15 min and then with running buffer for 30 min. This consisted of 20 mM Tris-HCl (pH 8.75), 65 mM NaCl, and 25 mM neutral surfactant for the single-analyte sensing format or 20 mM Tris-HCl (pH 8.50), 65 mM NaCl, and 2.5 mM neutral surfactant for the multiplex sensing format. To ensure repeatability, the capillary was conditioned at the beginning of the run with 1 M NaOH and pure water for 1 min at 1000 mbar. Prior to injection, the capillary was filled with the surfactant containing running buffer (1000 mbar for 3 min). All experiments were conducted in cationic mode. Samples were injected hydrodynamically at −50 mbar for 8 s into the capillary in triplicate. During the run, the capillary ends were kept in the surfactant containing running buffer. The injected solution volume

(38) Huizenga, D. E.; Szostak, J. W. *Biochemistry* **1995**, *34*, 656.
(39) Vianini, E.; Palumbo, M.; Gatto, B. *Bioorg. Med. Chem.* **2001**, *9*, 2543–2548.
(40) He, J.; Roy, B.; Périgaud, C.; Kashlan, O. B.; Cooperman, B. S. *FEBS J.* **2005**, *272*, 1236.
(41) Rodat, A.; Kalck, F.; Poinsot, V.; Feurer, B.; Couderc, F. *Electrophoresis* **2008**, *29*, 740.

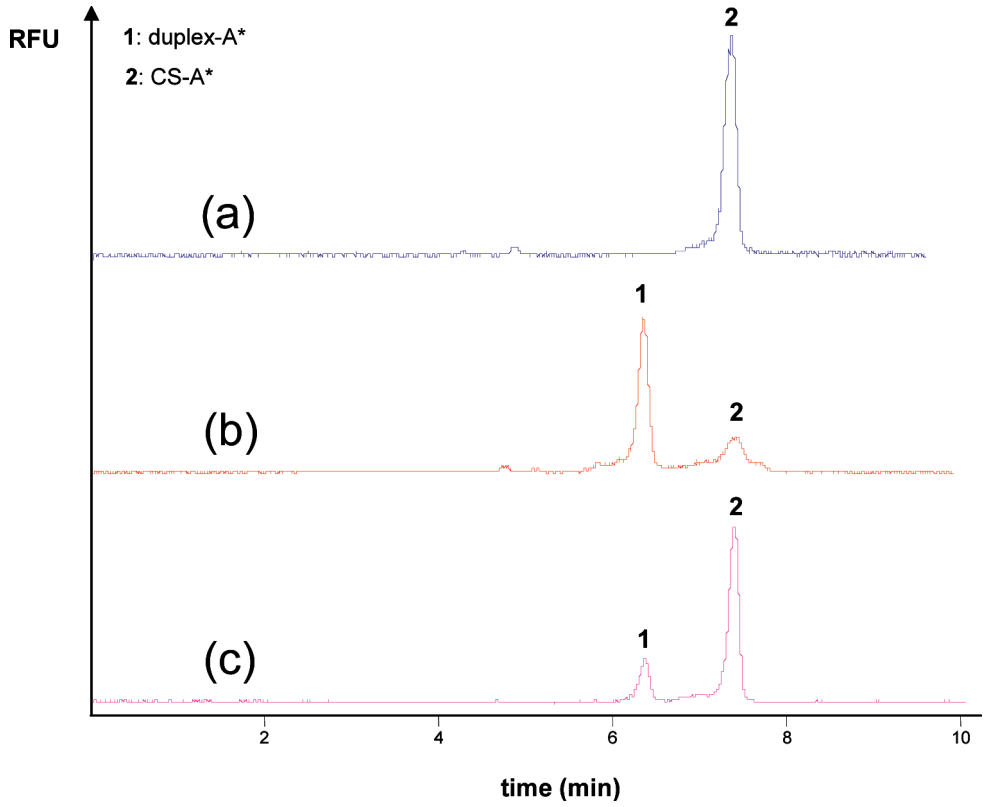


**Figure 3.** Representative electropherograms of the APCE-LIF assay for single-analyte (D-AMP) sensing. Preincubated samples: (a) CS-A* (250 nM), (b) CS-A* (250 nM) and Chol-Apt-A (250 nM), and (c) CS-A* (250 nM), Chol-Apt-A (250 nM), and D-AMP (2 mM). MEKC conditions: running buffer, 20 mM Tris-HCl (pH 8.75), 65 mM NaCl, and 25 mM Brij 35; capillary, 50 $\mu$m i.d.; effective length, 19 cm; uncoated, fused silica capillary with LIF detection; applied voltage, −23 kV; sample injection, −50 mbar for 8 s; capillary temperature, 12 °C.

was determined under the experimental conditions from the time required for CS-A* introduced into the prefilled capillary under a constant pressure of −50 mbar, to reach the detection window. For example, a hydrodynamic injection of 8 s at 25 mM Brij 35 corresponded to ~7 nL which was not affected by the presence of Apt and 3 mM analyte. Moreover, the interday variation of the injected volume was not significant since the relative standard deviation accounted for 3% ($n$ = 8). Between runs, the capillary was cleaned with running buffer solution for 5 min. All solutions were filtered prior to use through 0.20 $\mu$m pore size membranes.

**Calculation Methods.** The titration curves were obtained by plotting the ratio of the area of the peak of the free Chol-CS* ($A_{CS*}$) to the peak areas corresponding to both the duplex* and the Chol-CS* dissociated from the duplex ($A_{duplex*}$)[8] versus the target concentration in the preincubated samples (peak areas corrected by the migration time of each species).

The following modified one-phase exponential association equation was employed to estimate the apparent dissociation constant ($K_d$):[42]

$$Y = (A_{CS*}/A_{duplex*}) - (A_{CS*}/A_{duplex*})_f = [(A_{CS*}/A_{duplex*})_b - (A_{CS*}/A_{duplex*})_f](1 - e^{-kX}) \quad (2)$$

where $(A_{CS*}/A_{duplex*})_f$ is the signal in the absence of target, $(A_{CS*}/A_{duplex*})_b$ the response of the maximally target-associated aptamer, $X$ the concentration of the target molecule, and $k$ a fit parameter.

(42) Perrier, S.; Ravelet, C.; Guieu, V.; Roy, B.; Perigaud, C.; Peyrin, E. *Biosens. Bioelectron.* **2010**, *25*, 1652–1657.

The nonlinear regression of $Y$ versus $X$ plots, where $(A_{CS*}/A_{duplex*})_b$ and $k$ constituted the adjustable parameters, was achieved using Table curve 2D (Systat Software Gmbh, Erkrath, Germany), and the apparent $K_d$ value was determined from the midpoint of the equation, i.e., $-\ln(0.5)/k$.

## RESULTS AND DISCUSSION

**Single-Analyte Sensing Format.** To evaluate the feasibility of the structure-switching aptamer-based APCE-LIF strategy dedicated to single-analyte sensing (Figure 1), we first used the adenosine monophosphate (D-AMP) target and its DNA aptamer[38] as a model system. The sequence of the complementary strand utilized in this study has been previously described for the development of a structure-switching aptamer-based electrochemical sensor.[28]

In initial experiments, the CE-LIF analysis of CS-A* alone and the analysis of a mixture of Chol-Apt-A and CS*-A (in the absence of target) were compared under MEKC conditions (applied voltage, −23 kV; capillary temperature, 12 °C; effective length, 19 cm). A running buffer [20 mM Tris-HCl (pH 8.75) and 65 mM NaCl] containing 25 mM Brij 35 neutral surfactant (critical micelle concentration of ~40−100 $\mu$M)[37] was used. The addition of Chol-Apt-A to CS-A* in the preincubated sample (optimized stoichiometry of 1:1) resulted in a strong reduction in the peak area of the free CS* and the concomitant appearance of a new peak at a lower migration time (compare panels a and b of Figure 3). This latter corresponded to the duplex-A* species that migrated faster than CS-A* as the result of its anchoring into the neutral micelles.[35−37] Such data demonstrate that the MEKC mode was able to separate

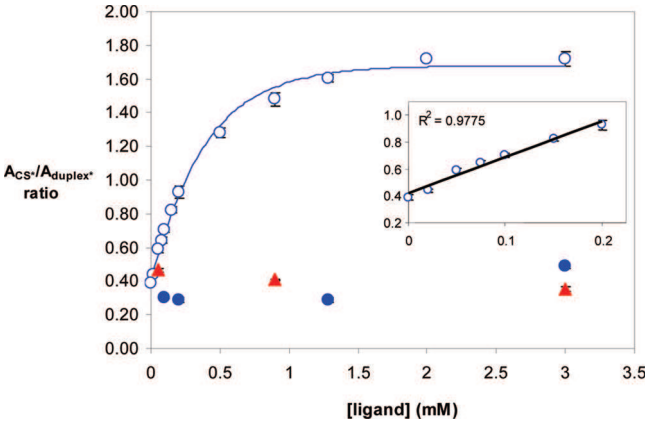


**Figure 4.** Titration curves obtained for D-AMP (○) and L-AMP (●) enantiomers and D-GMP (▲) over a concentration range of 0−3 mM. The solid line was created from eq 2. The inset shows the linear assay response for D-AMP at low concentrations (0−200 $\mu$M) in the sample. CS-A* and Chol-Apt-A concentrations of 250 nM. Error bars represent standard deviations ($n = 3$). The curves were constructed by plotting the ratio of free CS-A* peak area ($A_{CS^*}$) to the peak areas corresponding to duplex-A* and CS-A* dissociated from duplex-A* ($A_{duplex^*}$), corrected by the migration time of each species, vs ligand concentration. MEKC conditions are given in the legend of Figure 3.

the duplex* from the free CS-A*, with an exploitable resolution between the two fluorescent species. The influence of the nature of the neutral surfactant on the MEKC-mediated separation of the CS-A* and duplex-A* components was also considered. A similar resolution between the duplex-A* and CS-A* species was achieved using Thesit or Triton X-100 micelles [25 mM in the same running buffer, with other conditions identical (Figure S1 of the Supporting Information)].

The ability of this approach to monitor the target-induced duplex-to-complex change was evaluated under the MEKC operating conditions reported above. In the absence of target, the $A_{CS^*}/A_{duplex^*}$ ratio was ~0.4 (Figures 3 and 4). From the respective peak areas of the CS-A* and duplex-A* components, we estimated that the fraction of the hybrid form of CS-A* was ~70%. The addition of the D-AMP target at a concentration of 2 mM in the preincubated sample produced a significant increase in the $A_{CS^*}/A_{duplex^*}$ ratio of a factor of ~4 (Figures 3 and 4). This result is consistent with the structure-switching mechanism; the formation of the target−aptamer complex caused the hybridization disruption leading to the release of the free CS-A* component (Figure 1). The signal generation, i.e., the increase in the $A_{CS^*}/A_{duplex^*}$ ratio in the presence of the target, was found to be particularly dependent on the preincubation of the sample with the neutral micellar phase. In fact, when the sample was not preincubated with the micelles, a fraction of the duplex-A* that did not bind to the pseudostationary phase[35−37] comigrated with the free CS-A* and then yielded a lower sensitivity.

The target titration curves were established by plotting the $A_{CS^*}/A_{duplex^*}$ ratio versus the D-AMP concentration (varying from 0 to 3 mM) in the preincubated mixture (Figure 4). The APCE-LIF assay displayed linearity up to 200 $\mu$M, and the detection limit was estimated to be 30 $\mu$M through the statistical analysis of the regression function. The average standard deviation was lower than 4%, demonstrating the reproducibility of the assay. The analysis was also performed successfully with another target of this aptamer, i.e., D-adenosine (D-A).[37] The representative titration curve can be found in the Supporting Information (Figure S2). A similar linear range was obtained with a detection limit of 10 $\mu$M. Such results are comparable with those reported with other homogeneous format-based aptasensors previously designed for the detection of the same targets.[24,42−49] The apparent dissociation constant ($K_d$) for the targets was estimated using eq 2. The $K_d$ values ranged between 100 and 300 $\mu$M for the two analytes, i.e., 270 ± 12 $\mu$M for D-AMP and 126 ± 6 $\mu$M for D-A. The apparent binding affinity appeared to be significantly reduced relative to that retrieved with the original aptamer (by a factor of ~20−30).[38] Such data are in agreement with those reported by Nutiu and Li, who showed that the blockage of the aptamer target-binding site by the complementary strand alters the binding affinity.[24] The target specificity behavior is in accordance with that observed for the unmodified aptamer;[38] i.e., D-AMP displayed a lower apparent affinity than D-A in this system.

The selectivity of the APCE-LIF assay was subsequently evaluated. As shown in Figure 4, the guanosine monophosphate (D-GMP) compound did not induce a significant response over the same concentration range, in accordance with previous results.[38] The development of enantioselective assays constitutes one attractive application of the aptamers in the small molecule sensing field. To date, various aptamer-based chiral analysis approaches have been described.[37,42,45,49−51] To investigate the potentiality of the current methodology to allow the enantioselective sensing of AMP, the binding curves were also constructed with increasing concentrations of the L-enantiomer of this species. L-AMP did not cause any significant response over the tested concentration range (Figure 4). Such a result confirms the strong AMP stereoselective properties recently reported for the anti-AMP aptamer.[37,42] This suggests that the APCE-LIF procedure presented here could provide the detection of an enantiomeric impurity down to approximately 1% in a nonracemic sample.

**Multiplex Sensing Format.** To perform the simultaneous detection of multiple analytes in a single run, we designed a different assay format (Figure 2). In the single-analyte scheme described above, the tracer was not tagged with cholesteryl. Therefore, multiple free CS* forms of different analyte sensing systems could not be differentiated under such conditions as they would display an identical electrophoretic mobility.[31,32] On the other hand, the configuration employing a dually cholesteryl-tagged and fluorescein-labeled complementary strand as the tracer could permit the distinction between multiple pairs of free Chol-CS* and duplex* of different lengths, through the size-dependent shift of their electrophoretic mobility (eq 1). Thus, this option was predicted to allow a more accurate measurement by monitor-

(43) Merino, E. J.; Weeks, K. M. *J. Am. Chem. Soc.* **2005**, *127*, 12766–12767.
(44) Lin, D.; Shlyahovsky, B.; Willner, I. *J. Am. Chem. Soc.* **2007**, *129*, 5804–5805.
(45) Urata, H.; Nomura, K.; Wada, S.; Akagi, M. *Biochem. Biophys. Res. Commun.* **2007**, *360*, 459–463.
(46) Li, N.; Ho, C. M. *J. Am. Chem. Soc.* **2008**, *130*, 2380–2381.
(47) Tang, Z.; Mallikaratchy, P.; Yang, R.; Kim, Y.; Zhu, Z.; Wang, H.; Tan, W. *J. Am. Chem. Soc.* **2008**, *130*, 11268–11269.
(48) Cheng, X. H.; Bing, T.; Liu, X. J.; Shangguan, D. H. *Anal. Chim. Acta* **2009**, *633*, 97–102.
(49) Null, E. L.; Lu, Y. *Analyst* **2010**, *135*, 419–422.
(50) Turney, K.; Drake, T. J.; Smith, J. E.; Tan, W.; Harrison, W. W. *Rapid Commun. Mass Spectrom.* **2004**, *18*, 2367–2374.
(51) Ruta, J.; Perrier, S.; Ravelet, C.; Fize, J.; Peyrin, E. *Anal. Chem.* **2009**, *81*, 7468–7473.

ing the target-induced changes of both the free and bound Chol-CS* peaks. In addition, it was more convenient to modulate the length of the shorter interacting partner (Chol-CS* in the multianalyte design scheme) than that of the larger one (Chol-Apt in the single-analyte design scheme) to enlarge the separation window, i.e., the absolute difference in migration time between the cholesteryl-tagged components and an untagged DNA species.

The ability of such an assay configuration to assess the sensing of a single analyte was first evaluated using the anti-D-AMP aptamer system. To facilitate the size-dependent separation of Chol-CS-A* from duplex-A* and improve the peak spacing, we partly modified the MEKC experimental conditions relative to those employed above. The surfactant concentration was reduced to 2.5 mM,[35] the capillary effective length increased to 40 cm, the running buffer pH set at 8.50, and the applied voltage reduced to −12 kV.[34] Under such conditions, the two species of interest were well-resolved (Figure S3 of the Supporting Information). As predicted by eq 1, Chol-CS-A* displayed a lower migration time than duplex-A* because of its smaller size (12 bases vs 12 + 32 = 44 bases). The hybridized form was found to be less stable than for the precedent configuration ($A_{CS*}/A_{duplex*}$ ratio of ∼0.6). This could result from a lower accessibility of the micelle-anchored Chol-CS-A* or some steric hindrance effects for Apt-A. The introduction of D-AMP (2.5 mM) into the preincubated sample generated the Chol-CS-A* peak increase and the concomitant reduction in the magnitude of the duplex-A* peak (Figure S3). The $A_{CS*}/A_{duplex*}$ ratio increased by a factor of ∼5.5 upon addition of target, higher than the assay response exhibited with the previous format (Figure 4). As the hybrid structure displayed a lower stability, Chol-CS-A* was expected to be dissociated more easily from Apt-A in the presence of D-AMP.[24,25] The apparent dissociation constant, calculated from the titration curve (not shown), was found to be 193 ± 34 $\mu$M. A linear range up to 200 $\mu$M and a detection limit of 15 $\mu$M were obtained. These data demonstrate that the target-induced duplex-to-complex change can be efficiently monitored with the current format. It also appears that the structure-switching aptamer principle can be successfully adapted to diverse APCE-LIF assay configurations.

The proof of principle of the multiplex approach was evaluated for a dual-analyte sensing system by using both the anti-AMP and anti-Tym DNA aptamers as MREs. To date, in contrast with the AMP aptamer, no structure-switching aptamer-based Tym sensor has been reported. Therefore, a fluorescence polarization (FP) approach was performed in initial experiments to determine a suitable cDNA.[52] Details of the FP experiments are presented in the Supporting Information. Two complementary sequences of Apt-Ty were tested for their ability to be displaced from the aptamer by L-Tym binding. One complementary strand of 12-mer was found to respond satisfactorily to the formation of the target−aptamer complex (Figure S4 of the Supporting Information). For the multiassay, Chol-CS-A* was utilized as the D-AMP tracer. The choice of the length of the modulator charge tail, introduced at the 3′-extremity of the L-Tym complementary strand, constituted the following key step. A poly(T) sequence of 38 bases was chosen to design a Chol-CS-Ty* tracer of a (12 + 38) 50-base total length. It was therefore expected that Chol-CS-Ty* could be differentiated from the 44-base duplex-A* species in size (eq 1). This was illustrated in Figure S5 of the Supporting Information. Under the MEKC experimental conditions previously used for the D-AMP analyte, Chol-CS-Ty* appeared to migrate more slowly that duplex-A* because of its larger size (compare Figures S3 and S5). As expected, the injection of the mixture of Chol-CS-Ty* and Apt-Ty (optimized stoichiometry of 2:1) into the capillary resulted in the appearance of a new peak at a higher migration time, which corresponded to the larger duplex-Ty* component (50 + 38 = 88 bases). The introduction of L-Tym into the incubated solution (2.5 mM) was responsible for consistent changes in the peak areas for the two fluorescent species (Figure S5). However, in comparison with D-AMP sensing, a weaker assay response was observed for L-Tym: the $A_{CS*}/A_{duplex*}$ ratio was 2-fold enhanced, varying from ∼0.7 in the absence of target to ∼1.5 with 2.5 mM target. This indicates that, under the experimental conditions described here, L-Tym switched the duplex* into the complex structure with a lower magnitude than D-AMP. The use of a complementary strand that would form a less stable hybrid structure could enhance the L-Tym assay response.[24,25]

Finally, the electropherograms shown in Figure 5 depict the simultaneous dual-analysis approach. Four peaks can be visualized when a mixture containing the Chol-CS-A*, Apt-A, Chol-CS-Ty*, and Apt-Ty components was introduced into the capillary. In accordance with the data reported in Figures S3 and S5, these reflected the specific pairs of Chol-CS* and duplex* for the two targets. The migration order was as follows: Chol-CS-A* (12 bases) < duplex-A* (44 bases) < Chol-CS-Ty* (50 bases) < duplex-Ty* (88 bases). Addition of D-AMP or L-Tym (2.5 mM) to the preincubated solution produced the specific diminution of the corresponding duplex* peak area and the increase in the associated Chol-CS* peak area (data not shown). No change in the response was obtained for the other couple, demonstrating the absence of cross-reactivity between the two sensing systems. When the two targets were simultaneously added to the reaction mixture (2.5 mM each), a variation of the Chol-CS* and duplex* peak area consistent with the duplex-to-complex change mechanism occurred concomitantly for the two pairs (Figure 5). The assay response was identical to that reported above for the separated analysis of each target (Figures S3 and S5), confirming the independent performance of the two assays. Although the proof of principle has been demonstrated for dual-analyte detection, the current method could be extended to the analysis of a larger number of compounds by simply increasing adequately the length of the Chol-CS* tracer for each additional sensing system. If necessary, experiments can be performed using a capillary with a reduced inner diameter at a higher electric field to enhance the analysis speed.

## CONCLUSION

In summary, we have demonstrated that the structure-switching aptamer concept can be successfully exploited in APCE to establish a reasoned, simple, versatile, and generic assay for the identification of small molecules. This greatly extends the potential of this technique and allows the performance of predictable multianalyte detection in a single capillary. In comparison with the typical APCE-LIF small molecule approaches developed to date, this methodology permits elimination of the tedious case-to-case synthesis of the tracer and the time-consuming adjust-

(52) Cruz-Aguado, J. A.; Penner, G. *Anal. Chem.* **2008**, *80*, 8853–8855.

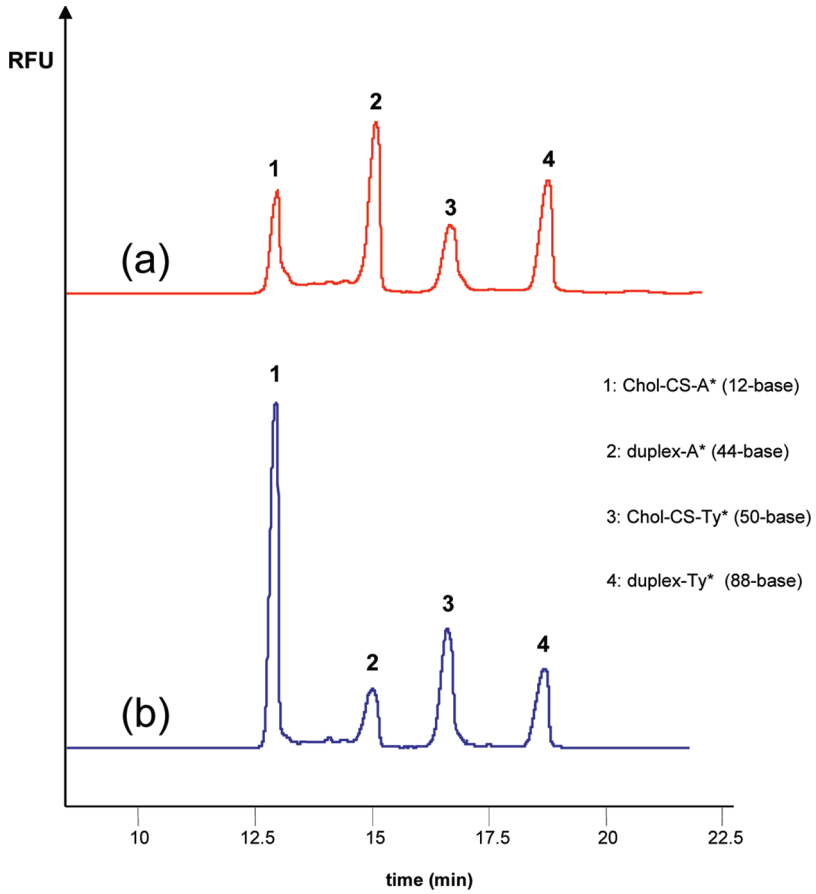


**Figure 5.** Representative electropherograms of the APCE-LIF assay for multianalyte (D-AMP and L-Tym) sensing. Preincubated samples of (a) Chol-CS-A* (250 nM), Apt-A (250 nM), Chol-CS-Ty* (500 nM), and Apt-Ty (250 nM) and (b) the same as panel a with D-AMP and L-Tym (2.5 mM each). MEKC conditions: running buffer, 20 mM Tris-HCl (pH 8.50), 65 mM NaCl, and 2.5 mM Brij 35; capillary, 50 $\mu$m i.d.; effective length, 40 cm; uncoated, fused silica capillary with LIF detection; applied voltage, −12 kV; sample injection, −50 mbar for 8 s; capillary temperature: 12 °C.

ments of both the chemical properties of the reagents and the CE experimental conditions for the optimal separation of the free and bound tracer. Unlike previously described sensors based on the structure-switching aptamer concept,[24−29,49] the method reported here provides accurate monitoring of the changes in both the free CS* and duplex* fractions generated by the target binding to the aptamer. More globally, such an approach offers a significant advantage over the existing aptamer-based sensor platforms which are, except in very few recent reports,[11,53−55] solely dedicated to single-target detection in a single solution.

(53) Hansen, J. A.; Wang, J.; Kawde, A. N.; Xiang, Y.; Gothelf, K. V.; Collins, G. *J. Am. Chem. Soc.* **2006**, *128*, 2228–2229.
(54) Liu, J.; Lee, J. H.; Lu, Y. *Anal. Chem.* **2007**, *79*, 4120–4125.
(55) Zhang, J.; Wang, L.; Zhang, H.; Boey, F.; Song, S.; Fan, C. *Small* **2010**, *10*, 201–204.

## ACKNOWLEDGMENT

We acknowledge the SEST French ANR program (Grant n°2007-013-01) for financial support of this work. Z.Z. was supported by the China Scholarship Council fund from the Ministry of Education of the P. R. China. We thank T. Card for her assistance.

## SUPPORTING INFORMATION AVAILABLE

Figures S1−S5 and additional data as noted in the text. This material is available free of charge via the Internet at http://pubs.acs.org.

Received for review March 24, 2010. Accepted April 26, 2010.

AC100755Q

# Supporting Information

## Multiplexed Detection of Small Analytes by Structure-Switching Aptamer-based Capillary Electrophoresis

**Zhenyu Zhu,**[‡] **Corinne Ravelet,**[‡] **Sandrine Perrier,**[‡] **Valérie Guieu,**[‡] **Béatrice Roy,**[§] **Christian Perigaud,**[§] **Eric Peyrin***[‡]
Département de Pharmacochimie Moléculaire UMR 5063 CNRS, ICMG FR 2607, Université Grenoble I, Campus universitaire, Saint-Martin d'Hères, France
Institut des Biomolécules Max Mousseron UMR 5247 CNRS, Université Montpellier 2, Place Eugène Bataillon, Montpellier, France

* Corresponding author: Email: eric.peyrin@ujf-grenoble.fr

## 1. Supplemental data from the single-analyte format experiments

**Figure S-1** Representative electrophoregrams obtained using different neutral surfactants (25 mM in the running buffer) to separate the CS-A* from the duplex-A* species. Experimental conditions are given in Figure 3 of the manuscript.

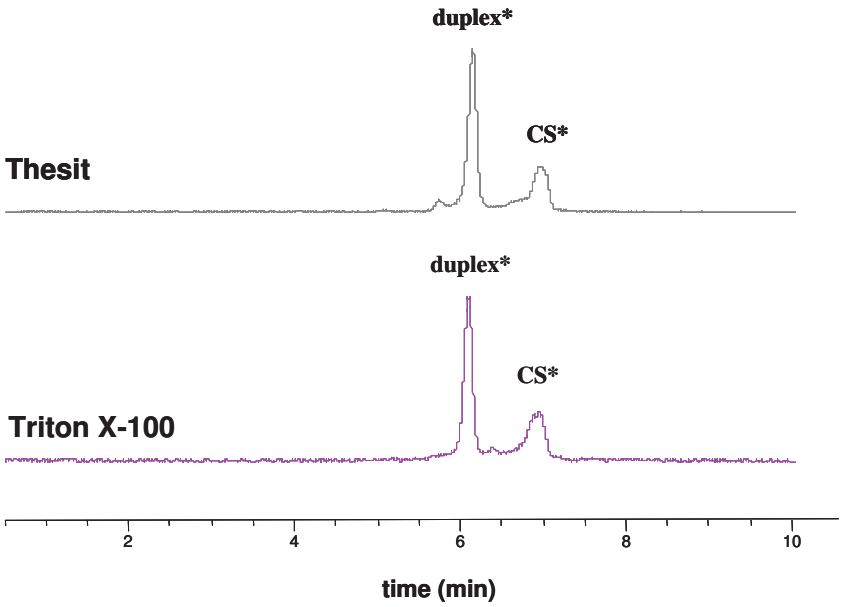


**Figure S-2** Titration curve obtained for D-A over the 0–3 mM concentration range using the single-analyte assay format. Solid line is created from Eq. 2**.** Insert: linear assay response for the target at low concentrations (0-200 μM) in the sample. CS-A* and Chol-Apt-A concentration: 250 nM. Error bars represent SDs (n = 3). The curves were constructed by plotting the ratio of free CS-A* peak area ($A_{CS*}$) to the peak areas corresponding to the duplex-A* and the CS-A* dissociated from the duplex-A ($A_{duplex*}$), corrected by the migration time of each species, versus the ligand concentration. Experimental conditions are given in Figure 3 of the manuscript.

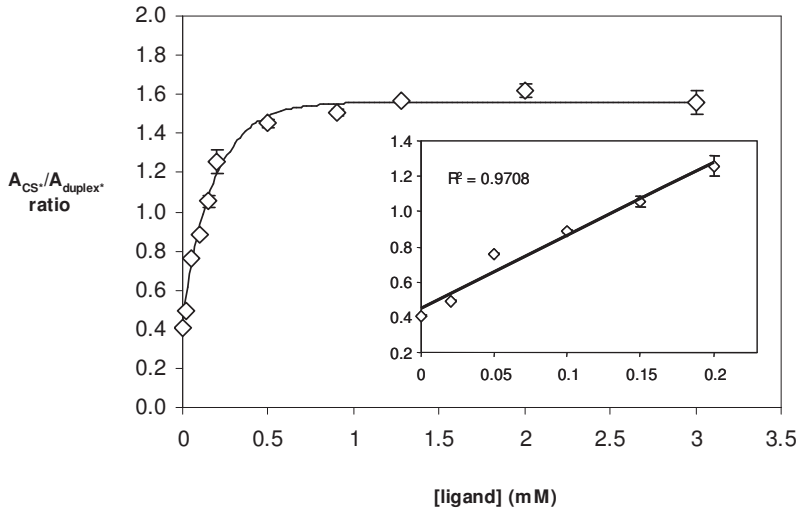

## 2. Supplemental data from the multiplexed format experiments

### 2.1 D-AMP system

**Figure S-3** Representative electropherograms for the D-AMP assay system. Pre-incubated samples: Chol-CS-A* (250 nM), Apt-A (250 nM), D-AMP (2.5 mM). MEKC conditions: running buffer: 20 mM Tris-HCl pH 8.50, 65 mM NaCl, 2.5 mM Brij 35. Capillary: 50-µm-*i.d.*; effective length, 40 cm; uncoated, fused silica capillary with LIF detection. Applied voltage: -12 kV. Sample injection: -50 mbar for 8 s. Capillary temperature: 12°C.

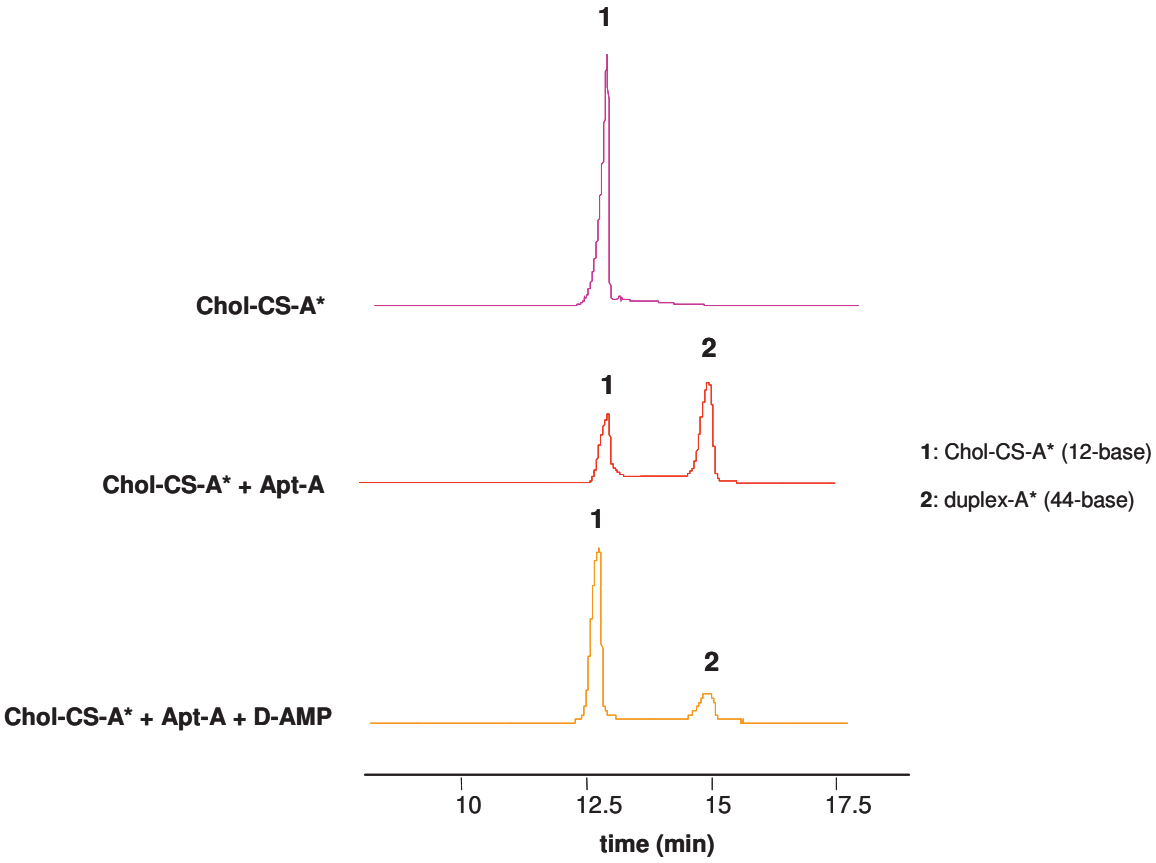


### 2.2 Fluorescence polarization (FP) approach

A FP approach was carried out in order to find an adequate CS of Apt-Ty which could be released upon L-Tym binding to its aptamer. The experiments were based on the monitoring of the fluorescence anisotropy of a fluorescein-labeled CS probe (CS*). As previously described,[1] the formation of the duplex* is assumed to increase the fluorescence anisotropy signal of the probe since the molecular mass of the hybrid is higher than that of the CS* alone. If the target binding to aptamer causes the displacement of the CS* from the aptamer through a structure-switching mechanism, the fluorescence anisotropy of the CS* probe is expected to decrease due to the reduction of its apparent size.[1]

The two following 5'-fluorescein-labeled complementary sequences (CS-1*, 10-mer and CS-2*, 12-mer) of Apt-Ty were synthesized (Eurogentec) and tested (complementary bases are in bold type):

Apt-Ty: 5'-**TGGAGCTTGG**ATTGATGTGGTGTGTGAGTGCGGTGCCC-3'

CS-1*: 3'-**ACCTCGAACC**-F-5'

Apt-Ty: 5'-TGGAGCT**TGGATTGATGTG**GTGTGTGAGTGCGGTGCCC-3'

CS-2*: 3'-**ACCTAACTACAC**-F-5'

Fluorescence anisotropy measurements were taken on a Tecan Infinite F500 microplate reader (Männedorf, Switzerland) using black, 96-well Greiner Bio-One microplates (ref: 675086, Courtaboeuf, France). Excitation was set at 485 ± 20 nm and emission was collected with a 535 ± 25 nm bandpass filter. The binding buffer consisted of 10 mM Tris-HCl, pH 7.5, 25 mM NaCl, 5 mM $MgCl_2$. The different oligonucleotide solutions were prepared in water and stored at -20°C. The working solutions were obtained by adequate dilution of the stock solution in a concentrated binding buffer. The working solutions were heated at 90°C for 5 min and left to stand at room temperature for 30 min. The L-Tym solution was prepared in water. All solutions were filtered prior to use through 0.20 µm membranes. The Apt-Ty and CS* (CS-1* or CS-2*) solutions (final concentration 10 nM each) were mixed into the individual wells at room temperature (final volume = 100 µL). Blank wells of the microplate received 100 µL of the binding buffer. All experiments were done in triplicate. The microplate was placed into the microplate reader for the measurement after further incubation at room temperature for at least 30 min. Anisotropy ($r$) was calculated by the instrument software, as classically reported:

$$r = \frac{I_{vv} - GI_{vh}}{I_{vv} + 2GI_{vh}}$$

where $I_{vv}$ and $I_{vh}$ are the vertically and horizontally polarized components of the emission after excitation by vertically polarized light. The instrumental correction factor $G$ was determined from standard solutions according to the manufacturer's instructions.

As can be seen in Figure S4, the fluorescence anisotropy of both the CS-1* and CS-2* probes increased when Apt-Ty was introduced in the reaction solution. This indicates that these two strands can effectively hybridize with the aptamer. Upon addition of the target (2 mM) in the reaction mixture, the fluorescence anisotropy was strongly reduced for the CS-2* probe while a very slight variation was observed for the CS-1* probe. This indicates that CS-2* was significantly displaced from Apt-Ty by a structure-switching mechanism.[1]

**Figure S-4** Variation of the fluorescence anisotropy for the two CS* probes (10 nM) upon addition of Apt-Ty (10 nM) and Apt-Ty (10 nM) + L-Tym (2 mM) in the reaction mixture.

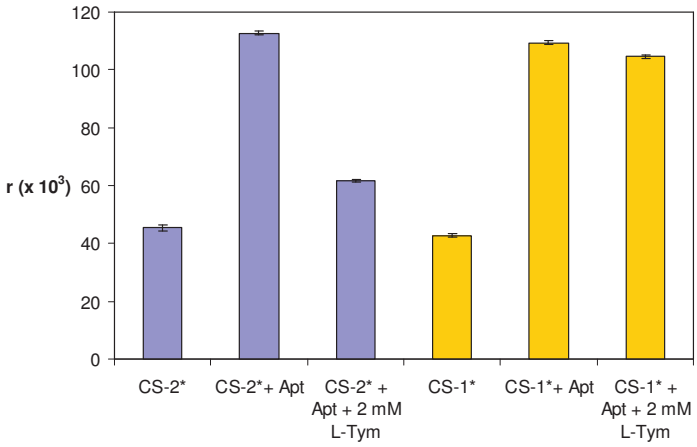


## 2.3 L-Tym system

**Figure S-5** Representative electropherograms for the L-Tym assay system. Pre-incubated samples: Chol-CS-Ty* (500 nM), Apt-Ty (250 nM), L-Tym (2.5 mM). MEKC conditions: running buffer: 20 mM Tris-HCl pH 8.50, 65 mM NaCl, 2.5 mM Brij 35. Capillary: 50-µm-*i.d.*; effective length, 40 cm; uncoated, fused silica capillary with LIF detection. Applied voltage: -12 kV. Sample injection: -50 mbar for 8 s. Capillary temperature: 12°C.

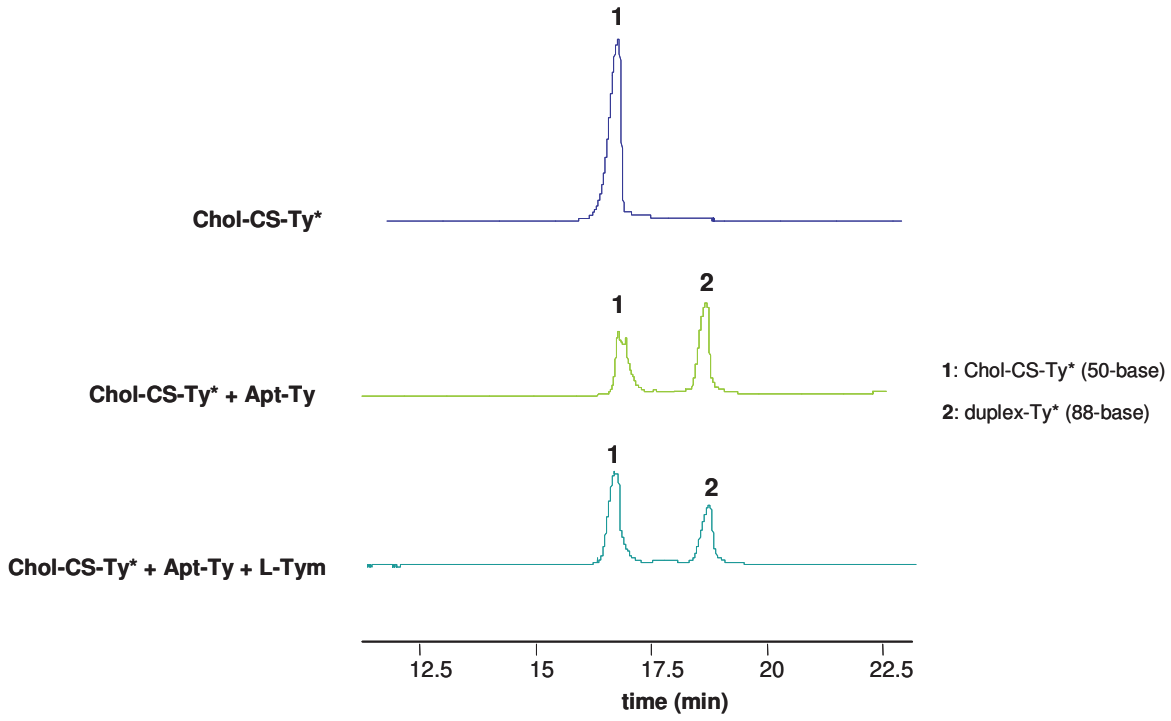


## References

1) Cruz-Aguado, J. A.; Penner, G. *Anal. Chem.* **2008**, *80*, 8853-8855.

## II.2.3 Conclusions

In summary, we have demonstrated that aptamers could be successfully adopted in capillary electrophoresis to establish a reasoned, simple, versatile, and generic assay for the quantification of multiple small molecules. Compared to the typical CE small molecule approaches, this methodology allowed elimination of the tedious case-to-case synthesis of the tracer and the time-consuming adjustments of both the chemical properties of the reagents and the CE experimental conditions for the optimal separation of the free and bound tracers. The method reported provides accurate monitoring of the changes in both the free CS* and duplex* fractions generated by the target binding to the aptamer. In addition, this method made it possible for the small molecule analysis of a larger number of compounds by simply increasing adequately the length of the Chol-CS* tracer for each additional system, which expanded significantly the potential of small molecule analysis.

However, it is also important to point out that some major drawbacks exist. CE analysis is a time consuming approach and requires sophisticated and expensive devices. Thus, it appears of great interest to develop a simpler, quicker and cheaper biosensing platform. In this context, aptamer-based gold nanoparticle colorimetric assay for small molecule detection is described in the following part.

# II.3 Aptamer-based gold nanoparticle colorimetric assay for small molecule detection

## II.3.1 Introduction

### II.3.1.1 General description of gold nanoparticles

Recent developments in nanostructured material synthesis and engineering have made a huge impact on a number of fields including nanoelectronics, photonics, biology, and medicine [278, 279]. Gold nanoparticles exhibit several interesting physical and chemical properties that have made them an integral part of research in nanoscience. Due to the plasmon resonance of gold nanoparticles, they possess strong distance-dependent optical properties. As a result of these properties, many techniques have been developed based on the aggregation of gold nanoparticles to detect ions, genes, and proteins. In addition, gold nanoparticles are also important because of their biofunctionalization and biostability.

Nanotechnology is the broad field of study of the behavior of matter on the nanometer length scale, and tries to understand, control, and manipulate it. Nanoparticles take a very important place in nanotechnology since they serve as the fundamental building blocks of the field. The term nanoparticle refers to an object of size in the range of 1 to 100 nm at least in one of the three dimensions [280]. Nanoparticles can be made of metals, metal oxides, semiconductors, polymers, carbons, organics, or biomolecules. Nanoparticles can also be classified into nanospheres, nanorods, nanotubes, nanowires, nanofibers according to their shapes [280, 281].

Nanoparticles possess unique physical and chemical properties which are significantly different from those of bulk materials [280]. This is the reason why the topic of nanoparticles has attracted attention of so many scientists and researchers and opened up the possibility for numerous applications. The unique properties of nanoparticles can be explained by the high surface area per unit volume, the high proportion of surface atoms and near-surface atoms, and quantum effects that nanoparticles have. In fact, these three characteristics of nanoparticles arise from one feature: the nanometer length scale typical of the object. It is quite clear that the surface area-to-volume ratio and the proportion of surface atoms increase with a decrease in size.

### II.3.1.2 Optical properties of gold nanoparticles

Metallic nanoparticles are of great scientific interest due to their particular optical [282] and electrical [283] properties. These unique physical properties originate from their finite size. Since the size of metal nanoparticles is only a few or tens of nanometers by definition, the movement of their electrons is confined in three-dimensional space. Thus, these systems exhibit discrete energy levels, which are better described by the laws of Quantum Mechanics [281] than by the laws of Classical Physics.

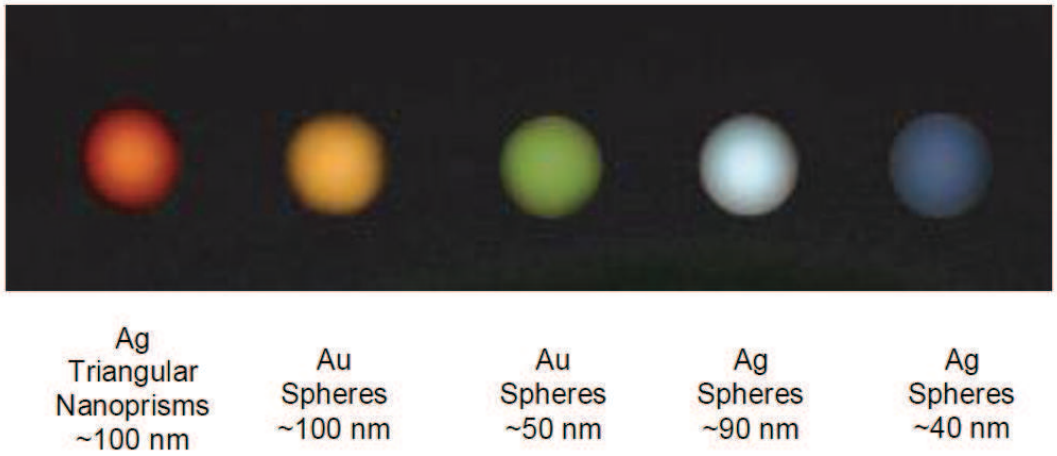


**Figure 2-3:** Rayleigh light-scattering of gold (Au) and silver (Ag) nanoparticles displaying various colors depending on the material, shape, and size [284].

One example of the extraordinary properties of metal nanoparticles is that their color depends on their chemistry, size, and shape. The dependence can be seen in Figure 2-3 where gold and silver nanoparticles of different shapes and sizes display various colors. This is attributed to a phenomenon known as Surface Plasmon Resonance (SPR). SPR is a phenomenon that occurs in selected sizes of semiconductor nanoparticles and metal nanoparticles (e.g., Quantum Dots) [281]. It refers to the oscillation of electrons on the surface of metal nanoparticles caused by the interaction between light and confined electrons of the nanoparticles. The process is schematically represented in Figure 2-4.

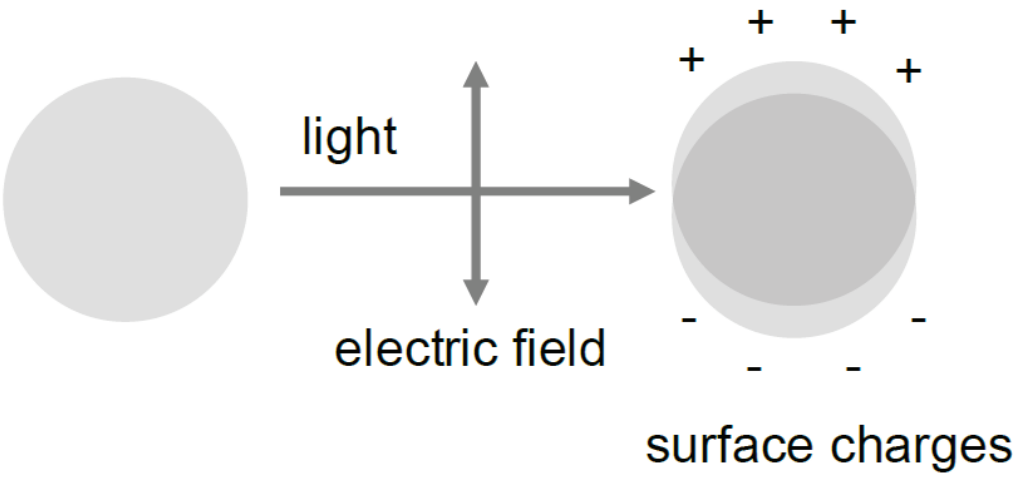


**Figure 2-4:** Schematic illustration of Surface Plasmon Resonance (SPR) - Interaction between light and confined electrons of a metal nanoparticle [281].

When SPR occurs, nanoparticles absorb a specific wavelength from the light that matches the frequency of the oscillation, and display a color. The frequency of the oscillation depends on the chemistry of the material, the size and the shape of the nanoparticle, the surrounding medium, and even on the temperature [285-287]. Consequently metal nanoparticles of different properties display different colors. For aqueous solutions of gold nanoparticles of diameter of 9, 15, 22, 48, and 99 nm, the maximum absorbance has been observed at the wavelengths 517, 520, 521, 533, and 575 nm, respectively. Surface Plasmon Resonance (SPR) has been exploited in biosensor applications [288] and for resolution enhancement of spectroscopic measurements [289].

Recently, significant efforts have been made to use metal nanoparticles in biological applications. A typical example is gold nanoparticles used in drug delivery and biosensors. Gold nanoparticles are known to have excellent biocompatibility and low inherent toxicity. Thus they promise high expectation for possible applications in medical devices. A complex composed of gold and iron oxide nanoparticle can work as a platin delivery agent [290]. Platin is a therapeutic agent for breast cancer. The complex is able to detect a breast cancer cell and release the therapeutic agent in it.

## II.3.1.3 Synthesis and surface functionalization

The scientific synthesis of colloidal gold can be traced back to Michael Faraday's work in 1857, in which the gold hydrosols were prepared by reduction of an aqueous solution of chloroaurate with phosphorus dissolved in carbon disulfide [291]. Later in 1951, Turkevich developed one of the most popular approaches for the synthesis of AuNPs, using citrate reduction of $HAuCl_4$ in water [292]. In this method, citric acid acted as both reducing and stabilizing agent and provided AuNPs with diameters of 20 nm. Further studies by G. Frens enabled control over AuNPs size by varying the feed ratio of gold salt to sodium citrate [293].

After Mulvaney's initial attempt of stabilizing AuNPs with alkanethiols [294], a significant breakthrough in the field of AuNP synthesis was achieved by Brust and Schiffrin in 1994. They reported a two-phase synthetic strategy, (the Brust–Schiffrin method)，utilizing strong thiol–gold interactions to protect AuNPs with thiol ligands (Figure 2-5). In this method, $AuCl_4^-$ is transferred from aqueous phase to toluene using the surfactant tetraoctylammonium bromide (TOAB) and reduced by sodium borohydride ($NaBH_4$) in the presence of dodecanethiol [295]. On addition of $NaBH_4$, a quick color change from orange to deep brown takes place in organic phase. The AuNPs are generated in toluene with controlled diameters in the range 1.5–5 nm. These thiol -protected AuNPs feature superior stability because of the strong thiol–gold interaction and they can be easily handled, characterized, and functionalized. The nanoparticles can be thoroughly dried and then redispersed in organic solvents without any aggregation or decomposition. Various reaction conditions, such as gold/thiol ratio, temperature, and reduction rate, can be used to tune the particle size [296].

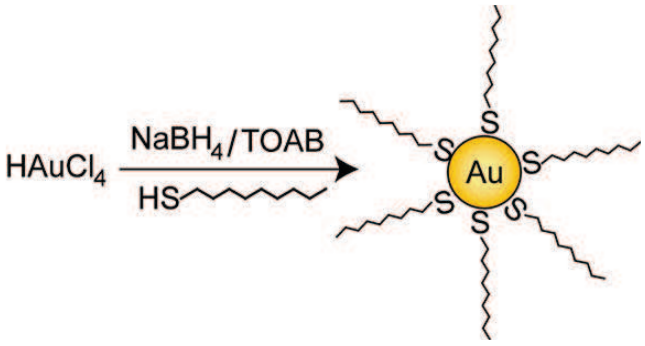


**Figure 2-5：** Brust–Schiffrin method for two-phase synthesis of AuNPs by reduction of gold salts in the presence of external thiol ligands [295].

## II.3.2 Experimental Section

Thiolated aptamer probes can readily self-assemble at the surface of AuNPs via the well-established Au–S chemistry. Such nanoprobes are extremely stable in solutions of high ionic strength since DNA polyelectrolytes bring high-density negative charges to the surface. These interesting findings form the basis of biomolecular detection by using AuNPs–aptamer conjugates [196-198]. However, the reliable and bulk synthesis of such conjugates remains a technical challenge.

More recently, unmodified AuNPs have been employed to probe biomolecular recognition based on interactions between DNA strands and AuNPs. Previous works have demonstrated that unmodified AuNP reporters are able to discriminate between DNA species of different electrostatic properties, i.e. single-stranded versus double-stranded DNA, unfolded versus folded DNA, short versus long single-stranded DNA.

The objective of our work is to utilize the specific DNA discriminating feature of unmodified AuNP to design new aptamer based assay for the small molecule detection. According to the basic binding modes between aptamer and target which was introduced in chapter I, three design strategies could be available: direct mode, displacement mode and sandwich or sandwich-like mode. However, despite the simplicity of the direct mode, such a strategy is not generalizable as it requires a sufficiently large aptamer structural change to generate a detectable signal, while the displacement approach suffers from some drawbacks including the strong alteration of the apparent binding affinity and the careful case-to-case choice of a suitable complementary DNA probe. The sandwich mode necessitates the knowledge of both the aptamer secondary structure and the critical nucleotide positions to select precisely the cut site that does not impede the target binding.

To circumvent this problem, our group designed a label-free, homogeneous aptamer-based sensor strategy for the facile colorimetric detection of small target molecules [297]. The format relied on the target-induced protection of DNA aptamer from the enzymatic digestion and its transduction into a detectable signal through the length-dependent adsorption of single-stranded DNA onto unmodified gold AuNPs. The proof-of-principle of the approach was established by employing the anti-tyrosinamide aptamer as a model functional nucleic acid and further applied to the adenosine detection.

***Article published in Analytica Chimica Acta, volume 706, 2011, pages 349-35***

Analytica Chimica Acta 706 (2011) 349–353

Contents lists available at SciVerse ScienceDirect

Analytica Chimica Acta

journal homepage: www.elsevier.com/locate/aca

# Aptamer enzymatic cleavage protection assay for the gold nanoparticle-based colorimetric sensing of small molecules

Valérie Guieu[a], Corinne Ravelet[a], Sandrine Perrier[a], Zhenyu Zhu[a], Simon Cayez[b], Eric Peyrin[a,*]

[a] Département de Pharmacochimie Moléculaire UMR 5063 CNRS, ICMG FR 2607, Université Grenoble 1, Campus Universitaire, Saint-Martin d'Hères, France
[b] Université de Toulouse, LPCNO, INSA, UMR CNRS 5215, 135 avenue de Rangueil, 31077 Toulouse Cedex 4, France

ARTICLE INFO

*Article history:*
Received 18 July 2011
Received in revised form 27 August 2011
Accepted 31 August 2011
Available online 7 September 2011

*Keywords:*
Aptamer
Unmodified gold nanoparticles
Colorimetric sensing
Enzymatic cleavage protection

ABSTRACT

A label-free, homogeneous aptamer-based sensor strategy was designed for the facile colorimetric detection of small target molecules. The format relied on the target-induced protection of DNA aptamer from the enzymatic digestion and its transduction into a detectable signal through the length-dependent adsorption of single-stranded DNA onto unmodified gold nanoparticles (AuNPs). The proof-of-principle of the approach was established by employing the anti-tyrosinamide aptamer as a model functional nucleic acid. In the absence of target, the aptamer was cleaved by the phosphodiesterase I enzymatic probe, leading to the release of mononucleotides and short DNA fragments. These governed effective electrostatic stabilization of AuNPs so that the nanoparticles remained dispersed and red-colored upon salt addition. Upon tyrosinamide binding, the enzymatic cleavage was impeded, resulting in the protection of the aptamer structure. As this long DNA molecule was unable to electrostatically stabilize AuNPs, the resulting colloidal solution turned blue after salt addition due to the formation of nanoparticle aggregates. The quantitative determination of the target can be achieved by monitoring the ratio of absorbance at 650 and 520 nm of the gold colloidal solution. A limit of detection of ~5 μM and a linear range up to 100 μM were obtained. The sensing platform was further applied, through the same experimental protocol, to the adenosine detection by using its DNA aptamer as recognition tool. This strategy could extend the potentialities, in terms of both simplicity and general applicability, of the aptamer-based sensing approaches.



## 1. Introduction

Gold nanoparticles (AuNPs) are widely used as signal transducers for the development of bioassays in various application fields including diagnostic and biochemical areas [1,2]. AuNPs have become important reporters as the result of their high extinction coefficients and their capability of visual detection, allowing avoiding the use of sophisticated equipments and expensive transduction techniques. The working principle of the AuNP colorimetric probes relies on the color change related to aggregation (red-to-blue) or dispersion of aggregates (blue-to-red) of nanoparticles. Molecular recognition events that lead to changes in aggregation/dispersion states of AuNPs can be thus visually detected by a simple color change of the solution [1,2].

In this context, and owing the impressive advantages of nucleic acid aptamers as molecular recognition tools [3–5], numerous AuNP-based aptamer assays have been described during the last few years for the sensing of a large variety of targets ranging from small species to whole cells [6–15]. The signal generation depends typically on two different systems which are related to interparticle crosslinking or noncrosslinking aggregation phenomena [16]. The first system relies on the formation of interparticle bonds mediated by interacting partners (aptamer and/or DNA probe) immobilized onto the particle surface. This sensing platform suffers from limitations such as the time-consuming functionalization of the nanoparticle surface and the slow interparticle assembly phenomenon. The second system is related to the modification of stabilizing (electrostatic and/or steric) processes, without intervention of interparticle bond formation. In such case, the strategy based on changes of electrostatic stabilization of unmodified AuNPs constitutes a very attractive approach due to its rapidity and its simplicity. Previous works have demonstrated that unmodified AuNP reporters are able to discriminate between DNA species of different electrostatic properties, i.e. single-stranded *versus* double-stranded DNA [17–19], unfolded *versus* folded DNA [20], short *versus* long single-stranded DNA [18,21]. Typically, single-stranded or unfolded DNA sequences can adsorb efficiently to citrate-capped AuNPs *via* facilitated DNA base-Au interactions while double-stranded or folded DNA species bind more weakly to the Au surface due to the limited exposure of their nucleobases.

* Corresponding author. Tel.: +33 04 76 63 53 04; fax: +33 04 76 63 52 98.
*E-mail address:* eric.peyrin@ujf-grenoble.fr (E. Peyrin).

0003-2670/$ – see front matter © 2011 Elsevier B.V. All rights reserved.
doi:10.1016/j.aca.2011.08.047

AuNPs are then electrostatically stabilized by unfolded, single-stranded DNA molecules through the increase in their negative surface charge density, leading to the protection of AuNPs from the colloidal aggregation upon addition of salt [17–19]. On the basis of such DNA discriminating feature, unmodified AuNP-based aptasensors have been reported for the colorimetric determination of diverse analytes including $K^+$, cocaine, adenosine, ATP, ochratoxin A, oxytetracycline or thrombin [20,22–27]. In these cases, three different biosensor strategies involving direct, sandwich-like or displacement mechanisms were designed. The direct strategy implied the target-induced conformational changes of the functional nucleic acid from the unfolded to folded state [20,22,26,27]. Although of valuable simplicity, such a strategy is not generalizable as it requires a sufficiently large aptamer structural change to generate a detectable signal [24]. The sandwich-like strategy was based on the cutting of the aptameric recognition element into two separated single-stranded, unfolded DNA strands which were able to form a folded ternary complex in the presence of target [24,25]. The major limitation of this approach is related to the fact that it necessitates the knowledge of both the aptamer secondary structure and the critical nucleotide positions to select precisely the cut site that does not impede the target binding [24]. In the third strategy, the target binding was responsible for the displacement of an aptamer-binding reporter, i.e. a complementary single-stranded DNA, from its duplex (double-stranded DNA) formed with the functional nucleic acid [23]. Despites its broad applicability, such structure-switching approach suffers from some drawbacks including the strong alteration of the apparent binding affinity [28,29] and the careful case-to-case choice of a suitable complementary DNA probe [30,31]. Therefore, there is a need for the development of an alternative AuNP aptasensor design which would combine the simplicity of the direct strategy with the generalizability of the displacement approach.

Herein, a simple and generic unmodified AuNP-based aptamer assay dedicated to the colorimetric sensing of target molecules was described. The general concept is illustrated in Fig. 1. The sensor design was based on the common ability of nucleic acids to be protected, upon complexation by specific ligands, from enzymatic attacks [32,33]. The ligand binding protects directly (steric hindrance to nucleases) and eventually indirectly (conformational change) the nucleic acid structure from the enzymatic cleavage [32,33]. Due to its universal feature, such type of protection assay has been very widely exploited in several works related to the nucleic acid-related research field [34–37]. Moreover, the target-induced resistance of aptamers against the enzymatic digestion has been previously employed to probe the critical nucleotides implied in the formation of the ligand–nucleic acid complex [38–40] or to develop polymerase chain reaction (PCR)-based protein assays [41,42]. In this work, phosphodiesterase I (PDE I), i.e. a venom exonuclease that successively hydrolyzes 5′-nucleotides from the 3′-hydroxy-termini of both single-stranded and double-stranded DNA, was employed as an enzymatic probe. In the absence of target, the DNA aptamer substrate was predicted to be enzymatically cleaved, leading to the release of mononucleotides/short single-stranded DNA fragments (Fig. 1). Upon binding of specific analyte to the functional DNA, the enzymatic cleavage was expected to be impeded, resulting in the protection of the aptamer structure. Therefore, the target-induced PDE I cleavage protection of the aptamer could be converted into a visual signal through the salt-induced aggregation of unmodified AuNPs (red-to-blue color change) produced by the variation of length of the functional nucleic acid (Fig. 1), i.e. mononucleotides/short single-stranded DNA fragments *versus* long single-stranded DNA [18,21,43,44].

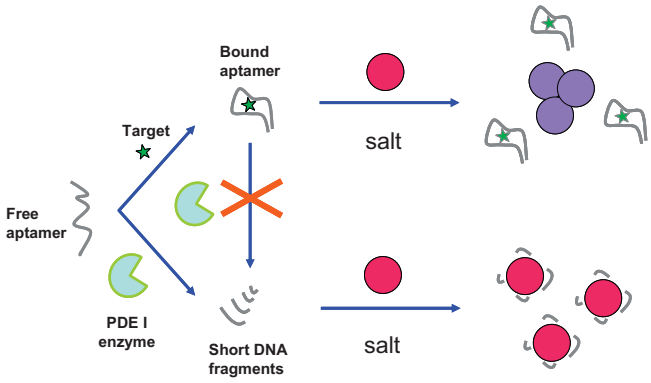


**Fig. 1.** Schematic representation of the enzymatic cleavage protection-based aptamer assay using unmodified gold nanoparticles as colorimetric reporters. PDE I: phosphodiesterase I enzyme.

The proof-of-principle of the unmodified AuNP-based enzymatic protection assay strategy was first evaluated by employing the anti-tyrosinamide (Tym) DNA aptamer [45] (Apt-T) as a model functional nucleic acid. To investigate the potential generality of the approach, the sensing platform was further tested for the adenosine (Ade) detection using its DNA aptamer [46] (Apt-A) as molecular recognition tool.

## 2. Materials and methods

### 2.1. Chemicals

L-Tyrosinamide, L-tyrosine, adenosine, inosine, tris(hydroxymethyl)aminomethane, phosphodiesterase I type IV from Crotalus Atrox (PDE I), $HAuCl_4$ (99%) and trisodium citrate were purchased from Sigma–Aldrich (Saint Quentin, France). NaCl and $MgCl_2$ were purchased from Chimie-Plus laboratories (Bruyère de Pouilly, France) and Panreac Quimica (Barcelona, Spain), respectively. Water was purified on a Purite Still Plus Water system (Thame, UK) fitted with a reverse osmosis cartridge. DNA oligonucleotides were synthesized and purified by Eurogentec. The aptamer and control scrambled sequences used are reported in Table S1 (supplementary content).

### 2.2. Instrumentation

UV–visible spectra of the colloidal solutions were recorded on a Shimadzu UV-1650pc spectrophotometer for wavelengths ranging from 400 to 800 nm in 10 mm quartz suprasil® cuvettes. Microscopy samples were prepared by deposition of a drop of colloidal solution onto a carbon-coated copper grid and observed on a JEOL1011 microscope for bright-field transmission electronic microscopy (TEM) working at 100 kV. The particle size was estimated manually using the ImageJ software.

### 2.3. Preparation of the gold nanoparticles

AuNPs were prepared by citrate reduction as previously reported [47]. Briefly, to 20 mL of boiling $HAuCl_4$ (1 mM in filtered deionized water), 2 mL of trisodium citrate (38.8 mM in water) were added. The solution was maintained boiling under vigorous stirring for 10 min. The color of the suspension changed from pale yellow to dark red. The stirring was then continued until the mixture was cooled to room temperature (RT). The colloidal suspension was finally filtered on PVDF-membrane filters 0.45 μm (Roth) and left aging for 3 days at 4 °C before use.

### 2.4. PDE I cleavage protection-based AuNP assay

A 1 μM aptamer or control scrambled oligonucleotide solution in deionized water was prepared daily from a 100 μM solution of

the corresponding oligonucleotide in a 30 mM $MgCl_2$, 130 mM NaCl, 10 mM Tris, pH 8 buffer which was denatured for 5 min at 80 °C and then cooled to RT during 30 min. The working enzymatic solution of PDE I was prepared daily by a 1/1000 dilution of the stock solution (2 U $mL^{-1}$) in deionized water. The 1 μM oligonucleotide solution (5 μL) was added in an eppendorf to the target (50 μL). The target concentration ranged from 0 to 1 mM for the Tym assay and from 0 to 500 μM for the Ade assay. These mixtures were stored for 30 min at 4 °C. Water (45 μL), PDE I (50 μL, working solution) and AuNPs (100 μL) were then added (final concentration of 0.75 and 3.25 mM for $MgCl_2$ and NaCl, respectively). The enzymatic reaction was performed for 15 min at 25 °C. The digestion was stopped by heating the mixture at 90 °C for 10 min. After 15 min cooling, 250 μL of the 40 mM $MgCl_2$, 20 mM NaCl, 40 mM Tris buffer were finally added to the DNA/AuNPs mixture and the absorption spectrum of the resulting solutions was then recorded. Blank experiments were carried out to test the stability of the AuNPs in the presence of target (up to 1 mM for Tym and Tyr; up to 500 μM for Ade and Ino) or PDE I enzyme (working solution). Control experiments were also performed to evaluate solely the effects of the heating procedure. The titration curves were constructed by plotting the ratio of absorbance at 650 and 520 nm ($A_{650}/A_{520}$) *versus* the ligand concentration ($c$). A high $A_{650}/A_{520}$ value was associated to blue-colored AuNP aggregates while a low $A_{650}/A_{520}$ value corresponded to red-colored dispersed nanoparticles. The sensing platform reproducibility was assessed from triplicate measurements employing AuNP reporters arising from three different batches.

## 3. Results and discussion

To test the feasibility of the proposed AuNP-based enzymatic protection assay strategy (Fig. 1), the anti-tyrosinamide DNA aptamer (Apt-T) and its target (Tym) were firstly chosen as a model molecular recognition system. This is characterized by a dissociation constant in the 1–5 μM range under low ionic strength conditions [48,49]. Previous aptamer-based Tym assays using fluorescence [50], fluorescence polarization [49] and miniaturized separation [51] methods have been successfully reported. Preliminary experiments were carried out in order to (i) investigate the ability of the PDE I enzyme to cleave Apt-T in its free form and (ii) evaluate the potential protection effects that could be induced by the target binding to the DNA aptamer. The PDE I-mediated digestion patterns of Apt-T were analyzed by HPLC (supplementary content for experimental details). Representative chromatograms are presented in Figure S1. The PDE I action was responsible for the complete degradation of free Apt-T. In presence of Tym, the hydrolysis of the DNA aptamer was inhibited, demonstrating that PDE I constituted a particularly well-suited enzymatic probe for the design of the Tym-responsive aptamer protection assay. In the second step, PDE I cleavage protection AuNP-based assay experiments were performed. The features of the prepared AuNPs were initially investigated. As typical dispersed particles, citrate-capped AuNPs (~14 nm, see supplementary content) appeared red in aqueous solution, exhibited a surface plasmon resonance (SPR) absorption band at ~520 nm and was characterized by a low $A_{650}/A_{520}$ ratio of ~0.1 (Figure S2). The addition of an appropriate amount of salts, i.e. 20 mM $MgCl_2$ and 10 mM NaCl in 20 mM Tris buffer, to the colloidal solution produced the characteristic particle aggregation by screening the electrostatic repulsion between AuNPs [17–19] and led to a blue color change associated to a broad, red shifted absorption spectrum (Figure S2). A series of experiments was subsequently conducted through the designed format (Fig. 1) to detect the Tym target. The AuNP solution properties were analyzed in the presence of Apt-T, before and after treatment by PDE I. As shown in Fig. 2, the gold colloid containing the uncleaved Apt-T species changed, after

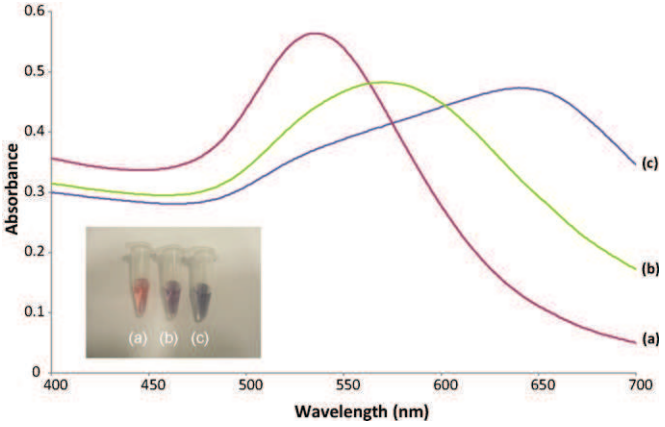


**Fig. 2.** Absorption spectra of the AuNP solution upon salt addition for samples containing (a) Apt-T and PDE I, (b) Apt-T and PDE I after pre-incubation of Apt-T with 1 mM Tym target and (c) Apt-T alone without PDE I treatment. Inset: Representative photographs of the corresponding solutions. See Section 2 for details.

addition of the same amount of salts used above, from red-to-blue with the corresponding absorption broadened and shifted to longer wavelength ($A_{650}/A_{520}$ ~1.3). Such data indicate that the aptamer sequence (38-base length) was unable to prevent the salt-induced aggregation of AuNPs. This is consistent with previous studies that have demonstrated that single-stranded DNA species of length >10 bases adsorbed slowly onto the gold surface [18], leading to a limited electrostatic stabilization effect for the unmodified particles.

On the other hand, the AuNP solution which contained Apt-T submitted to the enzymatic attack retained, under identical salt conditions, the red color and nearly the original band in the absorption spectrum (Fig. 2, $A_{650}/A_{520}$ ~ 0.2). Such a result indicates that the presence of aptamer digestion products arising from the PDE I treatment governed an increase in the colloidal stability. Both mononucleotides [43] and short DNA species [18,21] are known to adsorb quickly and efficiently onto the unmodified AuNPs, providing the protection of the gold colloids against the salt-induced aggregation. When the Apt-T sample was pre-incubated for 30 min at 4 °C with 1 mM Tym target before the PDE I treatment, the resulting AuNP solution turned blue upon salt addition with a red shifted absorption band (Fig. 2, $A_{650}/A_{520}$ ~0.8). As reported above, the Tym binding to Apt-T was able to prevent the PDE I-mediated cleavage of the aptamer structure. Therefore, the long DNA molecule could not stabilize effectively AuNPs [18,21], resulting in the salt-induced aggregation of the nanoparticles (Fig. 1). TEM measurements revealed that AuNPs were mainly dispersed in the absence of target in the sample while they aggregated significantly in the presence of 1 mM of Tym (Figure S3), corroborating the color and absorption spectrum change data described above.

Control experiments were carried out to confirm that the electrostatic stability changes of AuNPs were dependent solely on the enzymatic manipulation of the aptamer structure. In the absence of Apt-T, the addition of Tym or PDE I to the colloidal solution (absence of salt) did not modify the color and absorption spectrum of the citrate-capped nanoparticles (Figure S4). Similarly, the heating procedure employed to stop the enzymatic cleavage process had no effects on the stability of the AuNP solution. Additional control experiment was performed using a scrambled sequence DNA in place of Apt-T. After PDE I treatment and salt addition, the color of the colloidal solution did not change in presence of 0.25–1 mM Tym (Figure S4), indicating that the assay response was specific to the target association with Apt-T.

For the quantitative detection of Tym, the $A_{650}/A_{520}$ ratio was monitored as a function of the target concentration in the sample. The increase in the Tym concentration led to an enhancement

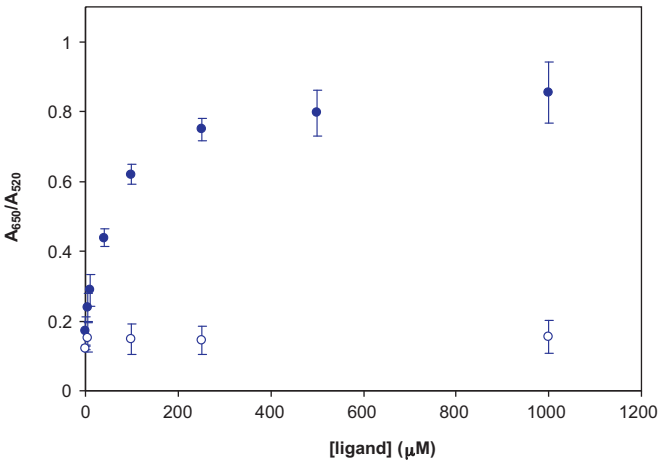


**Fig. 3.** Dose-dependent enzymatic protection assay curves obtained by plotting the $A_{650}/A_{520}$ ratio of the AuNP solution *versus* Tym (filled symbols) and Tyr (open symbols) concentration. See Section 2 for details.

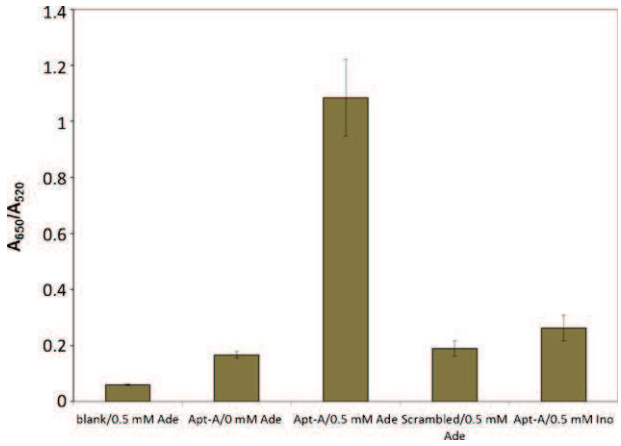


**Fig. 4.** The $A_{650}/A_{520}$ ratio of AuNPs obtained for blank (0.5 mM Ade, no salt addition), assays without (0 mM Ade + Apt-A, PDE I treatment, salt addition) and with adenosine (0.5 mM Ade + Apt-A, PDE I treatment, salt addition), control assay with scrambled oligonucleotide (0.5 mM Ade + control scrambled Apt-A, PDE I treatment, salt addition) and selectivity assay with inosine (0.5 mM Ino + Apt-A, PDE I treatment, salt addition). See Section 2 for details.

of the $A_{650}/A_{520}$ value (Fig. 3), indicating that the binding event can be converted into a suitable colorimetric response related to the magnitude of the salt-induced AuNP aggregation. Although the dissociation constant of the Tym–Apt-T complex is known to be in the micromolar range [48,49], the half-saturation target concentration of the titration curve, i.e. the apparent dissociation constant, appeared relatively high (~60 μM). The protection of the aptamer structure was assumed to depend not only on the binding constant of the target/aptamer complex but also on the enzyme probe. As previously reported [52,53], the cleaving agent may disturb the target–aptamer interaction so that a competitive equilibrium between PDE I and the target can occur, leading to high measured dissociation constant [53]. In addition, a weak sample $Mg^{2+}$ amount was used in the present work to reduce the risk to destabilize AuNPs during the enzymatic digestion process. Previous studies have demonstrated that a low magnesium concentration alters the affinity of the target for the aptamer [48,49]. The limit of detection (LOD) was experimentally estimated to be ~5 μM, comparable or better to the LODs previously obtained with other AuNP-based colorimetric small molecule aptasensors [9,12,13,23–25], and a linear range up to 100 μM was observed. Additional experiments were performed using tyrosine (Tyr) as a non-cognate [45]. No salt-induced red-to-blue color change was observed upon Tyr addition to the sample (Fig. 3), reflecting the selectivity of the present methodology.

The general applicability of the AuNP-based sensor strategy was explored using another small target/aptamer system, i.e. the adenosine (Ade)/anti-Ade DNA aptamer (Apt-A, containing the minimal functional structure of 25 nucleotides) complex that is characterized by a dissociation constant of about 5 μM [46,54]. The PDE I-mediated digestion profiles of free and target-bound Apt-A were also analyzed by HPLC (Figure S5). Apt-A in its free form was found to be efficiently cleaved by PDE I and, upon target binding, resisted, at least partially, to the enzymatic hydrolysis. This result demonstrates the general usefulness of PDE I as cleaving probe for the enzymatic protection assay strategy. The Ade detection was subsequently performed through the exactly same experimental protocol employed above for the Tym determination. The Apt-A/AuNP solutions were submitted to the PDE I treatment, either in the absence or in the presence (500 μM) of the Ade target molecule. After salt addition, a color change from red to blue was observed when the Ade–Apt-A complex was formed while the colloidal solution for the target-free sample retained the red color. Moreover, a significant increase in the $A_{650}/A_{520}$ ratio by a factor of ~6.5 was reported for the sample containing 500 μM of Ade (Fig. 4). Ade (500 μM) was added to the AuNP aqueous solution, in absence of Apt-T and PDE I, to establish blank experiment (no salt addition, Fig. 4). Another control experiment using a scrambled oligonucleotide revealed that the color of the DNA/AuNP solution, after PDE I treatment and salt addition, was unmodified in presence of Ade (Fig. 4). The Ade assay displayed similar linear range (up to 100 μM) and detection limit (~1 μM) than those reported above for the Tym sensing. The LOD is better than those previously reported for colorimetric assays dedicated to the adenosine/AMP detection [55]. As shown in Fig. 4, the aptasensor was able also to discriminate against a structurally related compound, i.e. inosine (Ino), further establishing that the current sensing platform maintained the selective properties of the recognition element.

## 4. Conclusion

In summary, we have described an AuNP-based colorimetric aptamer assay strategy that relies on the protection of the aptamer structure against the PDE I enzymatic cleavage and its colorimetric signal transduction through the ability of gold nanoparticles to discriminate between single-stranded DNA species of variable length. To the best of our knowledge, the present work reports the first small molecule aptasensor based on the target-induced aptamer enzymatic protection principle. The current approach exhibits several attractive features. First, the biosensor functions well even with Apt-A which is known to undergo a limited structural change upon target binding [54,56,57]. Second, the methodology does not necessitate prerequisite aptamer structural information, as exemplified by Apt-T for which (i) the secondary structure is unknown [45] and (ii) none precise knowledge on the target-induced fit mechanism is available [48]. Third, the same assay protocol can be successfully employed with different target–aptamer systems without the requirement of the case-to-case adaptation of the experimental conditions. It is consequently expected that the simple sensing platform reported herein could be applied to a large variety of target-aptamer couples, expanding the potential applications of the AuNP-based aptasensor approaches.

## Acknowledgment

The authors would like to acknowledge the SEST French ANR program (grant no. 2007-013-01) for financial support of this work.

## Appendix A. Supplementary data

Supplementary data associated with this article can be found, in the online version, at doi:10.1016/j.aca.2011.08.047.

## References


[1] N.L. Rosi, C.A. Mirkin, Chem. Rev. 105 (2005) 1547.
[2] P. Baptista, E. Pereira, P. Eaton, G. Doria, A. Miranda, I. Gomes, P. Quaresma, R. Franco, Anal. Bioanal. Chem. 391 (2008) 943.
[3] S.D. Jayasena, Clin. Chem. 45 (1999) 1628.
[4] S.M. Nimjee, C.P. Rusconi, B.A. Sullenger, Annu. Rev. Med. 56 (2005) 555.
[5] S. Tombelli, M. Mascini, Curr. Opin. Mol. Ther. 11 (2009) 179.
[6] J. Liu, Y. Lu, Anal. Chem. 76 (2004) 1627.
[7] C.C. Huang, Y.F. Huang, Z. Cao, W. Tan, H.T. Chang, Anal. Chem. 77 (2005) 5735.
[8] J. Liu, Y. Lu, Nat. Protoc. 1 (2006) 246.
[9] W. Zhao, W. Chiuman, M.A. Brook, Y. Li, ChemBioChem 8 (2007) 727.
[10] J. Liu, Y. Lu, J. Am. Chem. Soc. 129 (2007) 8634.
[11] C.D. Medley, J.E. Smith, Z. Tang, Y. Wu, S. Bamrungsap, W. Tan, Anal. Chem. 80 (2008) 1067.
[12] W. Zhao, W. Chiuman, J.C.F. Lam, S.A. McManus, W. Chen, Y. Cui, R. Pelton, M.A. Brook, Y. Li, J. Am. Chem. Soc. 130 (2008) 3610.
[13] F. Li, J. Zhang, X. Cao, L. Wang, D. Li, S. Song, B. Ye, C. Fan, Analyst 134 (2009) 1355.
[14] Z.-S. Wu, H. Lu, X. Liu, R. Hu, H. Zhou, G. Shen, R.Q. Yu, Anal. Chem. 82 (2010) 3890.
[15] W. Lu, S.R. Arumugam, D. Senapati, A.K. Singh, T. Arbneshi, S.A. Khan, H. Yu, P.C. Ray, ACS Nano 4 (2010) 1739.
[16] W. Zhao, M.A. Brook, Y. Li, ChemBioChem 9 (2008) 2363.
[17] H.X. Li, L.J. Rothberg, Proc. Natl. Acad. Sci. U.S.A. 101 (2004) 14036.
[18] H.X. Li, L.J. Rothberg, J. Am. Chem. Soc. 126 (2004) 10958.
[19] H.X. Li, L.J. Rothberg, Anal. Chem. 76 (2004) 5414.
[20] L. Wang, X. Liu, X. Hu, S. Song, C. Fan, Chem. Commun. (2006) 3780.
[21] Q. Shen, Z. Nie, M. Guo, C.-J. Zhong, B. Lin, W. Li, S. Yao, Chem. Commun. (2009) 929.
[22] H. Wei, B. Li, J. Li, E. Wang, S. Dong, Chem. Commun. (2007) 3735.
[23] J. Wang, L. Wang, X. Liu, Z. Liang, S. Song, W. Li, G. Li, C. Fan, Adv. Mater. 19 (2007) 3943.
[24] J. Zhang, L. Wang, D. Pan, S. Song, F.Y.C. Boey, H. Zhang, C. Fan, Small 8 (2008) 1196.
[25] F. Xia, X. Zuo, R. Yang, Y. Xiao, D. Kang, A. Vallée-Bélisle, X. Gong, J.D. Yuen, B.B.Y. Hsu, A.J. Heeger, K.W. Plaxco, Proc. Natl. Acad. Sci. U.S.A. 107 (2010) 10837.
[26] C. Yang, Y. Wang, J-L. Marty, X. Yang, Biosens. Bioelectron. 26 (2011) 2724.
[27] Y.S. Kim, J.H. Kim, I.A. Kim, S.J. Lee, J. Jurng, M.B. Gu, Biosens. Bioelectron. 26 (2010) 1644–1649.
[28] R. Nutiu, Y. Li, J. Am. Chem. Soc. 125 (2003) 4771.
[29] R. Nutiu, Y. Li, Methods 37 (2005) 16.
[30] J.A. Cruz-Aguado, G. Penner, Anal. Chem. 80 (2008) 8853.
[31] Z. Zhu, C. Ravelet, S. Perrier, V. Guieu, B. Roy, C. Perigaud, E. Peyrin, Anal. Chem. 82 (2010) 4613.
[32] V. Petri, M. Brenowitz, Curr. Opin. Biotechnol. 8 (1997) 36.
[33] A.J. Hampshire, D.A. Rusling, V.J. Broughton-Head, K.R. Fox, Methods 42 (2007) 128.
[34] Y.N. Vashisht Gopal, M.W. Van Dyke, Biochemistry 42 (2003) 6891.
[35] J. Wang, T. Li, X. Guo, Z. Lu, Nucleic Acids Res. 33 (2005) e23.
[36] G.L. Liu, Y. Yin, S. Kunchakarra, B. Mukherjee, D. Gerion, S.D. Jett, D.G. Bear, J.W. Gray, A.P. Alivisatos, L.P. Lee, F.F. Chen, Nat. Nanotechnol. 1 (2006) 47.
[37] C. Chen, C. Zhao, X. Yang, J. Ren, X. Qu, Adv. Mater. 22 (2010) 389.
[38] P. Burgstaller, M. Kochoyan, M. Famulok, Nucleic Acids Res. 23 (1995) 4769.
[39] C. Mannironi, A. Di Nardo, P. Fruscoloni, G.P. Tocchini-Valentini, Biochemistry 36 (1997) 9726.
[40] A.K. Dey, G. Griffiths, S.M. Lea, W. James, RNA 11 (2005) 873.
[41] X.-L. Wang, F. Li, Y.-H. Su, X. Sun, X.-B. Li, H.J. Schluesener, F. Tang, S.-Q. Xu, Anal. Chem. 76 (2004) 5605.
[42] J.S. Lin, K.P. McNatty, Clin. Chem. 55 (2009) 1686.
[43] W. Zhao, W. Chiuman, J.C.F. Lam, M.A. Brook, Y. Li, Chem. Commun. (2007) 3729.
[44] Y. Wang, F. Yang, X. Yang, Nanotechnology 21 (2010) 205502.
[45] E. Vianini, M. Palumbo, B. Gatto, Bioorg. Med. Chem. 9 (2001) 2543.
[46] D.E. Huizenga, J.W. Szostak, Biochemistry 34 (1995) 656.
[47] K.C. Grabar, R.G. Freeman, M.B. Hommer, M.J. Natan, Anal. Chem. 67 (1995) 735.
[48] P.H. Lin, S.L. Yen, M.S. Lin, Y. Chang, S.R. Louis, A. Higuchi, W.Y. Chen, J. Phys. Chem. B 112 (2008) 6665.
[49] J. Ruta, S. Perrier, C. Ravelet, B. Roy, C. Perigaud, E. Peyrin, Anal. Chem. 81 (2009) 7468.
[50] E.J. Merino, K.M. Weeks, J. Am. Chem. Soc. 127 (2005) 12766.
[51] M. Michaud, E. Jourdan, C. Ravelet, A. Villet, A. Ravel, C. Grosset, E. Peyrin, Anal. Chem. 76 (2004) 1015.
[52] B. Ward, R. Rehfuss, J. Goodisman, J.C. Dabrowiak, Biochemistry 27 (1988) 1198.
[53] R. Rehfuss, J. Goodisman, J.C. Dabrowiak, Biochemistry 29 (1990) 777.
[54] S. Perrier, C. Ravelet, V. Guieu, B. Roy, C. Perigaud, E. Peyrin, Biosens. Bioelectron. 25 (2010) 1652.
[55] X. Yan, Z. Cao, M. Kai, J. Lu, Talanta 79 (2009) 383.
[56] A. Nishihira, H. Ozaki, M. Wakabayashi, M. Kuwahara, H. Sawai, Nucleic Acids Symp. Ser. (Oxf.) 48 (2004) 135.
[57] H. Urata, K. Nomura, S. Wada, M. Akagi, Biochem. Biophys. Res. Commun. 360 (2007) 459.

# Supplementary Content

## Aptamer Enzymatic Cleavage Protection Assay for the Gold Nanoparticle-Based Colorimetric Sensing of Small Molecules

**Valérie Guieu,[a] Corinne Ravelet,[a] Sandrine Perrier,[a] Zhenyu Zhu,[a] Simon Cayez,[b] Eric Peyrin[a]***
[a]Département de Pharmacochimie Moléculaire UMR 5063 CNRS, ICMG FR 2607, Université Grenoble I, Campus universitaire, Saint-Martin d'Hères, France
[b]Université de Toulouse, LPCNO, INSA, UMR CNRS 5215, 135 avenue de Rangueil, 31077 Toulouse Cedex 4, France

* Corresponding author: Email: eric.peyrin@ujf-grenoble.fr

### Chromatographic analysis of the PDE I-mediated aptamer digestion pattern

The binding buffer consisted of 50 mM Tris-HCl pH 7.5, 5 mM NaCl and 10 mM $MgCl_2$. The solutions of aptamers, analytes and PDE I were prepared in water and stored at -20 °C. Binding buffer and water were filtered prior to use through 0.45 µm membranes. The stock solutions of aptamers were first diluted to 20 µM in 2x concentrated binding buffer, heated at 80 °C for 5 min and left to stand at room temperature for 30 min. The working aptamer solutions (5 or 10 µM) were obtained by the adequate dilution of the former solution mixed with the analyte and/or the PDE I enzyme (0.18 or 0.9 mU). Enzyme containing samples were incubated at 25 °C for 30 min and the enzymatic reaction was stopped by heating at 90 °C for 10 min. The resulting solutions were centrifugated. Samples were analyzed by reversed-phase HPLC using an Uptisphere-WRP (5 µm, 300 Å, 250 × 4.6 mm) column purchased from Interchim (Montluçon, France). The HPLC system consisted of a LC Shimadzu pump 10AD (Sarreguemines, France), a Rheodyne injection valve model 7125 (Interchim, Montluçon, France) fitted with a 20 µL loop, a Shimadzu SPD-10A UV-visible detector (detection at 254 nm) a Shimadzu SCL-10A system controller with Class-VP software (Shimadzu) and an oven Igloocil (Interchim). The elution of compounds was achieved at a flow rate of 1 mL/min in the gradient mode using acetonitrile (5% for 5 min and from 5 to 25% during 60 min) in 100 mM NaCl and 25 mM sodium phosphate buffer at pH 6.6 (for Apt-T) or 25 mM Tris-HCl buffer at pH 6.4 (for Apt-A), the column being maintained at a temperature of 50 °C.

### Determination of particle size

AuNP size and concentration were characterized using spectral data (Figure S2), as previously described [1]. The particle size of citrate-capped AuNPs and the final molar concentration were found to be ~14 nm and ~2.2 nM, respectively. The particle size was confirmed (14.1 ± 2.0 nm) by transmission electronic microscopy measurements (n = 50).

**Table S1.** Aptamer and control scrambled sequences used in the present work.

| | |
|---|---|
| **Anti-Tym 38-base aptamer (Apt-T)** | 5'-TGG-AGC-TTG-GAT-TGA-TGT-GGT-GTG-TGA-GTG-CGG-TGC-CC-3' |
| **Control scrambled Apt-T** | 5'-CGT-GTT-TGG-GGC-AAT-TTG-GCG-GCA-GTT-GTG-GTA-GGT-CG-3' |
| **Anti-Ade 32-base aptamer (Apt-A)** | 5'-AGA-GAA-CCT-GGG-GGA-GTA-TTG-CGG-AGG-AAG-GT-3' |
| **Control scrambled Apt-A** | 5'-GTG-AAA-GGG-CAA-TGG-CGC-AGT-AGA-GGT-AGG-TG-3' |

**Figure S1.** Chromatograms obtained from the reversed-phase HPLC analysis of samples containing **(a)** Tym and Apt-T, **(b)** Apt-T submitted to the PDE I treatment (30 min) in the absence of Tym and **(c)** Apt-T submitted to the PDE I treatment (30 min) in the presence of Tym. Apt-T and Tym concentrations were 10 µM and 3.5 mM, respectively. PDE I enzyme: 0.9 mU. The sample submitted to the enzymatic treatment in absence of Tym **(b)** was characterized by the disappearance of the aptamer peak and the appearance of four peaks, characterized by lower retention time (4.4, 6.5, 8.6 and 12.1 min), which corresponded to the digestion products. Upon target addition to the medium before the PDE I treatment **(c)**, the Apt-T peak was almost similar to the control peak while the low retention time peaks disappeared, reflecting the ability of Tym to inhibit the PDE I-mediated hydrolysis of the DNA aptamer.

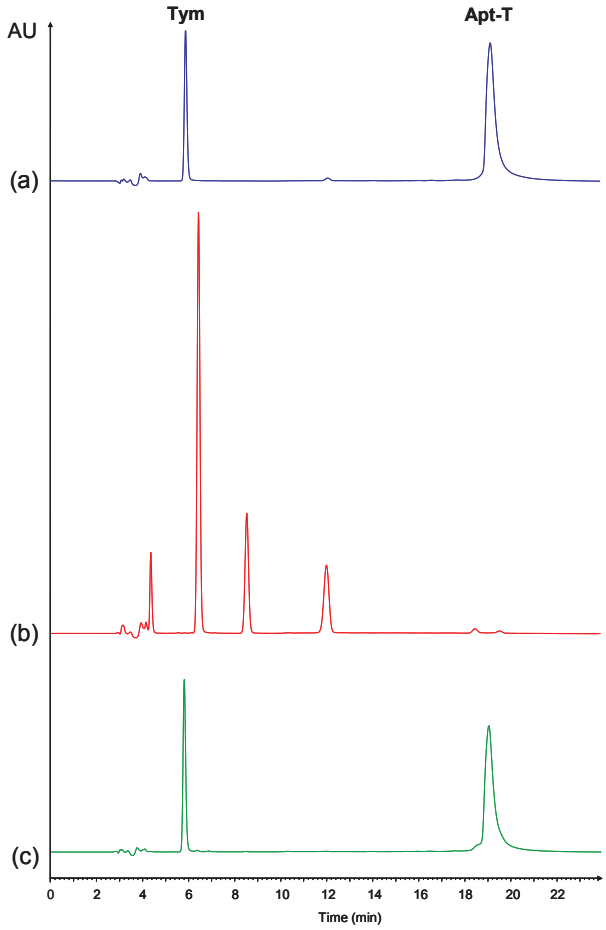


**Figure S2.** Absorption spectra of the prepared citrate-capped AuNP solution (~2.2 nM) before and after salt addition (20 mM $MgCl_2$ and 10 mM NaCl in 20 mM Tris buffer).

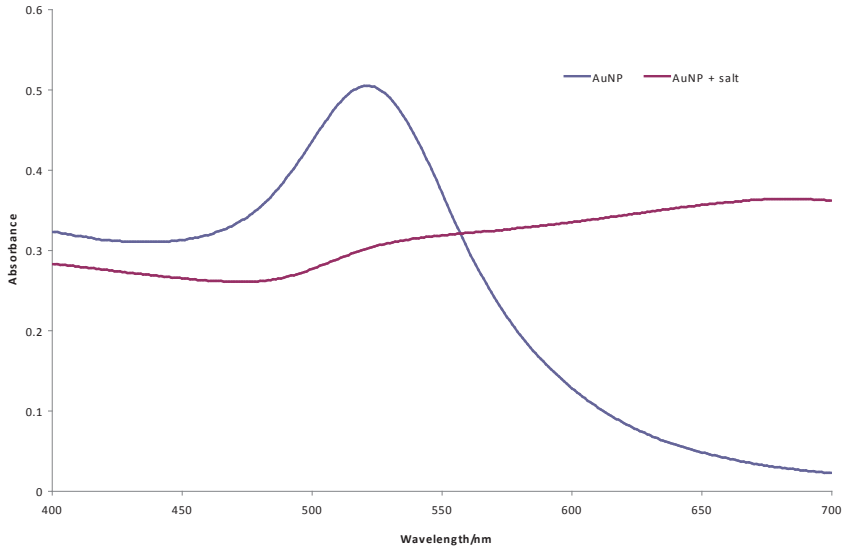


**Figure S3.** TEM images of AuNPs for samples containing **(a)** Apt-T and PDE I and **(b)** Apt-T and PDE I mixture after pre-incubation of Apt-T with 1 mM Tym target.

**(a)**

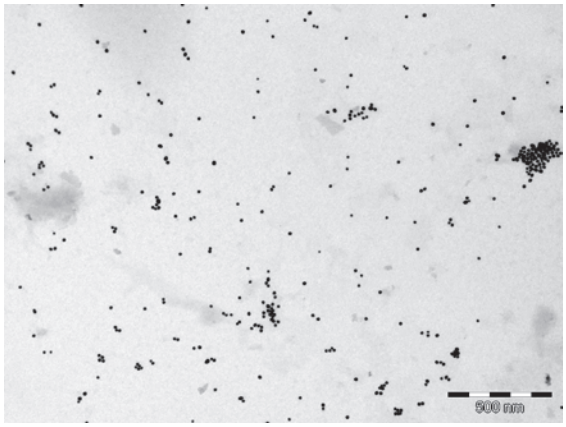


**(b)**

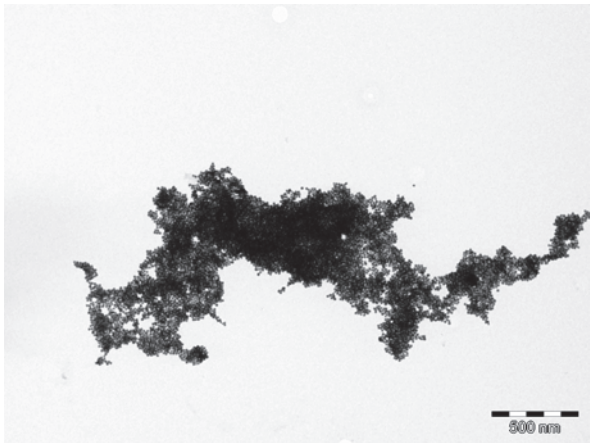


**Figure S4.** The $A_{650}/A_{520}$ ratio of AuNPs obtained for blank Tym (1 mM Tym, with or without salt addition), blank PDE I (PDE I working solution, with or without salt addition)

and control with scrambled oligonucleotide (1 mM Tym + scrambled Apt-T, with or without PDE I treatment, salt addition).

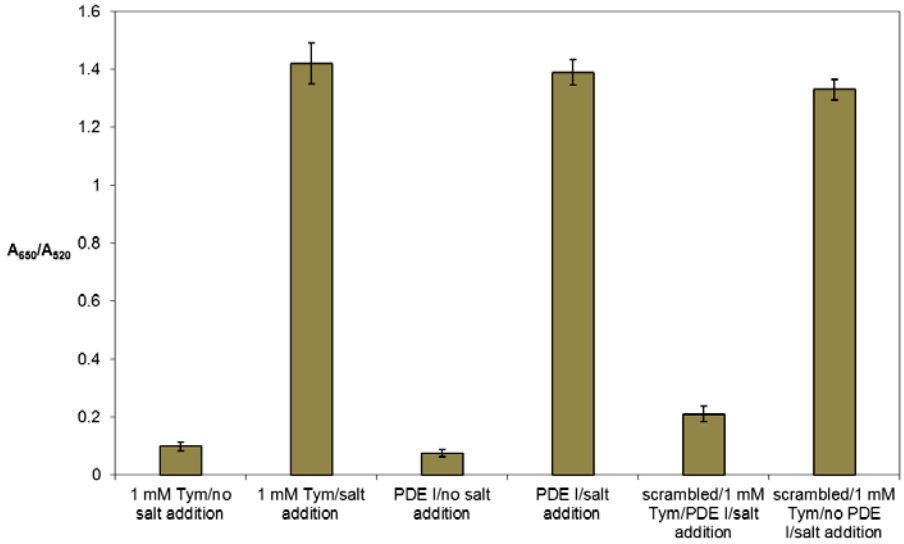


**Figure S5.** Chromatograms obtained from the reversed-phase HPLC analysis of samples containing **(a)** Ade and Apt-A, **(b)** Apt-A submitted to the PDE I treatment (30 min) in the absence of Ade and **(c)** Apt-A submitted to the PDE I treatment (30 min) in the presence of Ade. Apt-A and Ade concentrations were 5 µM and 3.125 mM, respectively. PDE I enzyme: 0.18 mU.

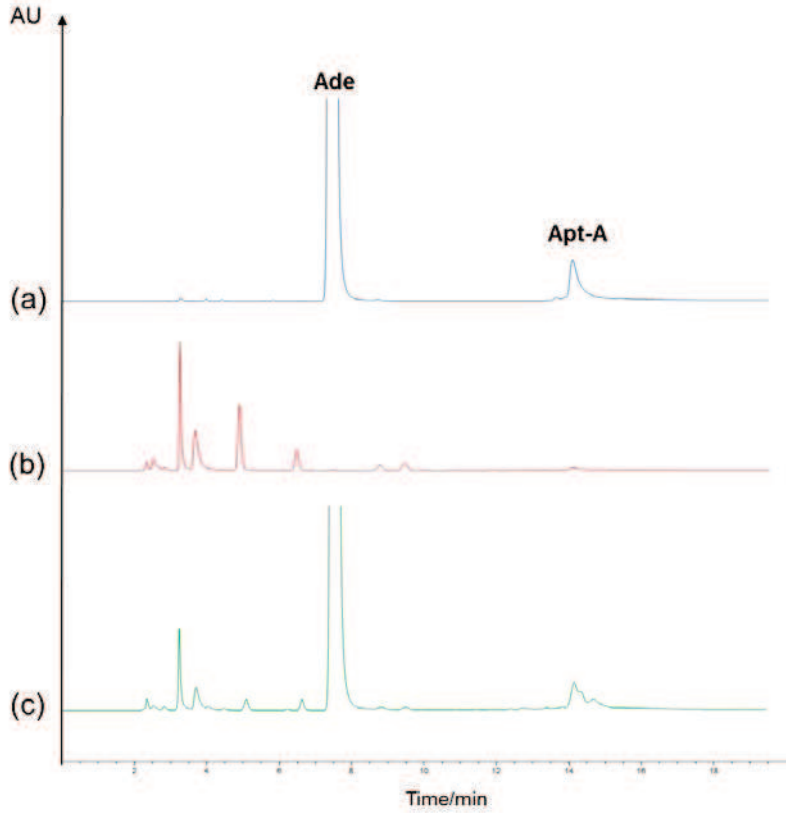


**References**

[1] W. Haiss, N. T. K. Thanh, J. Aveyard, D. G. Fernig, Anal. Chem. 79 (2007) 4215

## II.3.3 Conclusions

Gold nanoparticles have emerged as a promising material for biosensing that provide a useful complement to more traditional sensing techniques. The combination of low toxicity, high surface area, rich surface functionalization chemistry and colloidal stability allow them to be safely integrated into the sensor systems for detection in vitro and in vivo. However, optimization of parameters for the sensing systems is still required to meet the demands of clinical diagnosis for the future development of personalized medicine. In particular, due to the aggregation ability of AuNPs under some high ionic strength, pH conditions, etc., the development of efficient sensors to detect analytes in complex biological fluids such as urine, serum, and blood remains a challenge. Further studies on the optical properties of AuNPs as well as their aggregates, and interactions between AuNPs and different biomolecules may eventually lead to highly useful biosensors in diagnosis, environment monitoring and civil defence.

In order to meet the need of clinical diagnosis for the future development, it is of great interest and important to explore aptamer-based methodologies which could be applied in complicated biological environment. Furthermore, the investigation of aptamer-target binding interactions mechanism including the influence of the aptamer secondary structure has far-reaching significance. A novel rapid, homogeneous, sensitive detection method for the molecule interaction study becomes an urgent need, which makes fluorescence polarization (FP) an excellent candidate for the new aptamer-based assay.

# II.4 Aptamer-based fluorescence polarization assay for small molecule detection

## II.4.1 Introduction

### II.4.1.1 General description of fluorescence polarization (FP)

The investigation of biomolecular binding interactions remains one of the most popular studied topics using techniques that are based on emission of fluorescence. Several technologies have been successfully used including fluorescence resonance energy transfer, fluorescence quenching or fluorescence polarization (FP) methods. During the past few decades, the increase in the number and diversity of fluorescence polarization studies has been astonishing and the method is now extremely widespread in the clinical and biomedical fields. The virtual explosion of polarization studies, which began during the mid-1980s, was due to several factors: FP assays utilize single fluorescent label strategy and avoid the use of radioisotopes and filtration or separation steps. Thus, fewer reagents are generally needed, and the assay protocol is a simple mix-and-read (i.e., homogenous) with the assay reagents being overall inexpensive. Additionally, reagent equilibrium is not disturbed due to lack of separation step, and plates can often be repetitively measured as FP detection does not destroy samples.

Fluorescence polarization/fluorescence anisotropy (FP/FA) is a versatile solution-based technique that has been widely used to study molecular interactions, enzymatic activity and nucleic acid hybridization. After its first theoretical description in 1926 by Perrin [298], the application has evolved from obtaining binding isotherms under carefully controlled settings to the study of small molecule-protein, antigen-antibody and hormone-receptor binding in miniaturized automated settings. It was not until the mid-1990s that FP was adopted in high-throughput screening (HTS) to facilitate the drug discovery process, with its use being extended from direct interaction studies to complex enzymatic assays.

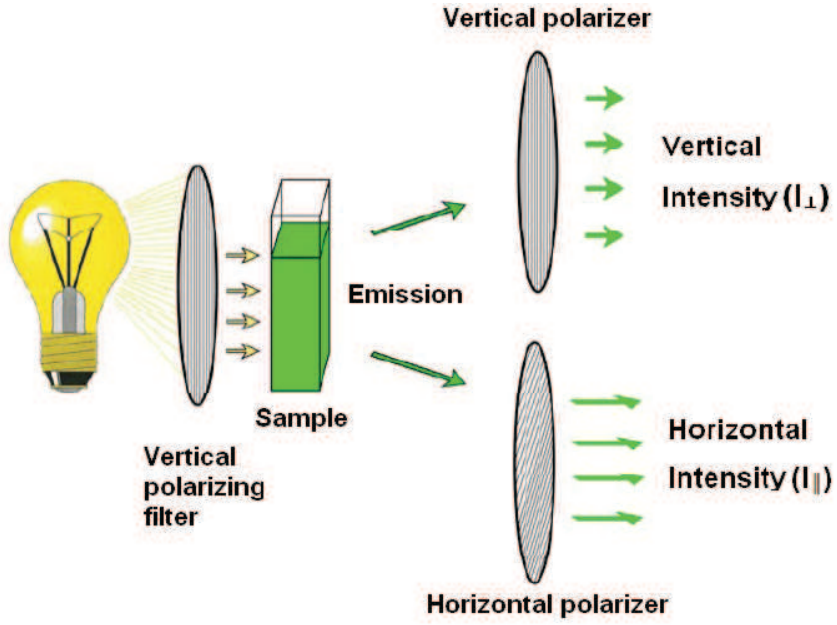


**Figure 2-6:** Basic principle of fluorescence polarization [299]. A fluorophore is excited with light that is linearly polarized by passing through an excitation polarizing filter; the polarized fluorescence is measured through an emission polarizer either parallel or perpendicular to the exciting light's plane of polarization. Two intensity measurements are obtained ($I_{\perp}$ and $I_{\parallel}$) and used for the calculation of FA or FP.

When a fluorophore in solution is exposed to plane-polarized light at its excitation wavelength the resulting emission is depolarized. The depolarization results from the motion of the fluorophore during the processes of excitation and emission. Because of this, the more rapid the motion of the fluorophore the more the emission is depolarized. The fluorescence emission can be segregated, using polarizers, into horizontal and vertical components, shown schematically in Figure 2-6. Quantitatively, FP/FA is defined as the difference of the emission light intensity parallel ($I_{\parallel}$) and perpendicular ($I_{\perp}$) to the excitation light plane normalized by the total fluorescence emission intensity (Equations 14 and 15, FP and FA are used interchangeably [300, 301]).

$$FP = \frac{I_{\parallel} - I_{\perp}}{I_{\parallel} + I_{\perp}} \tag{14}$$

$$FA = \frac{I_{\parallel} - I_{\perp}}{I_{\parallel} + 2I_{\perp}} \tag{15}$$

It can be seen from Equations 14 and 15 that the FP value is independent of fluorophore concentration as it is not dependent on the absolute intensities of the emission light collected at either orientation. On the other hand, the intrinsic fluorescence intensity of a fluorophore may change on binding to its cognate partner, thus resulting in significantly different contributions of the bound versus free forms of the fluorophore to the total fluorescence intensity of the sample, which in turn can complicate the interpretation of FP measurements [302, 303]. As instruments may have unequal sensitivity in detecting light in the perpendicular and the parallel orientations, a grating factor (commonly referred to as G factor) [304]has been introduced to correct for that bias in order to calculate absolute polarization values and for cases where data obtained from different instruments are to be compared [305].

Polarization relates a fluorophore's lifetime (t) (defined as the average time lapse between excitation and emission of the fluorophore) with its rotational relaxation time (μ), the latter being defined as the time it takes for a molecule to rotate through an approximate 68.5° angle after excitation [298] (Equation 16):

$$\mu = 3\eta v/RT \tag{16}$$

where R is the universal gas constant, V is the molar volume of the rotating molecule, T is the absolute temperature and η is the solvent viscosity. It can be seen from Equation 16 that rotational relaxation time is dependent on molar volume provided that temperature and viscosity remain constant. Therefore, as molecular size of the fluorescent species is being altered through dissociation/breakdown or association/binding events, the degree of depolarization of plane polarized light changes accordingly, thereby, directly affecting the FP value.

### II.4.1.2 Fluorophore Rotation and Anisotropy

The utility of fluorescence polarization in the clinical and biomedical sciences ultimately rests on the dependence of the observed polarization on the rotational diffusion rate of molecules. It is easy to imagine that the rotational rate will be slower as the molecule gets larger. For example, the rotational rate of a small molecule, e.g., of molecular weight 300 Da, will be much faster than the rotational rate of a large molecule, e.g., 100,000 Da. During the same fixed time interval, we would thus expect the small molecule to rotate through a larger

angle than the large molecule and, hence, we would expect that the light emitted by the smaller molecule will be more equally distributed in all directions, compared to the case of the larger molecule, whose emission will be oriented more or less in line with the original excitation direction. This scenario is illustrated in Figure 2-7.

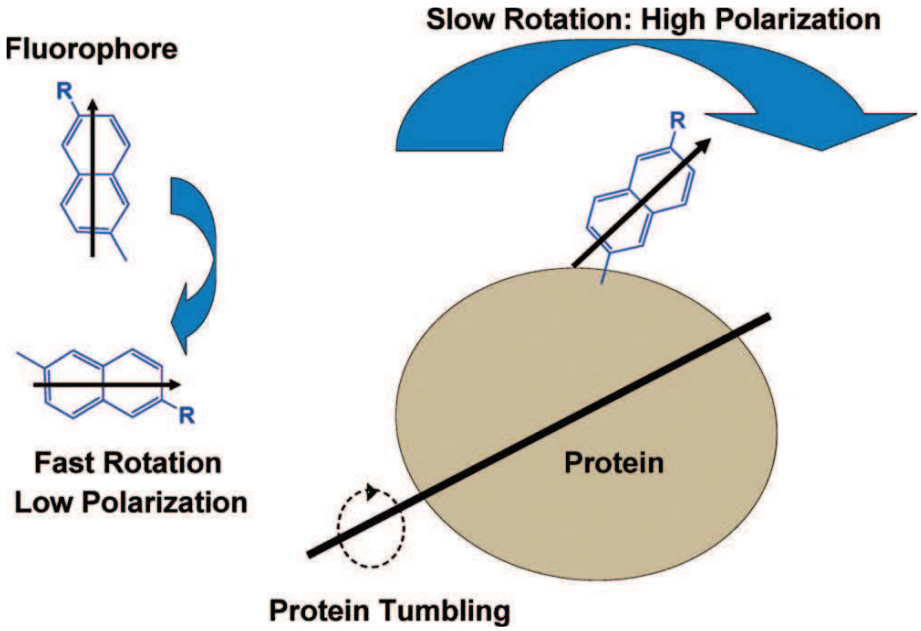


**Figure 2-7:** Illustration of the rotation of a fluorophore free in solution as compared to a fluorophore attached to a protein or macromolecule [306]. As indicated in the figure, the fluorophore free in solution can rotate rapidly (compared to its fluorescence lifetime) and hence gives rise to a low polarization value whereas a fluorophore attached to a protein (either covalently or noncovalently) rotates more slowly (relative to its fluorescence lifetime), due to the larger mass of the macromolecule, and hence gives rise to a high polarization.

In the case of fluorescent probes linked noncovalently to proteins (for example, porphryins, FAD, NADH, ANS, or fluorescent-antigen/antibody complexes), the probe is typically held to the protein matrix by several points of attachment, and hence, its "local" mobility, that is, its ability to rotate independently of the overall "global" motion of the protein, is restricted. In the case of a probe covalently attached to a protein, via a linkage through an amine or sulfhydryl groups, for example, or in the case of tryptophan or tyrosine side chains, considerable "local" motion of the fluorophore can occur. Such local probe mobility will result in a lower polarization than expected from consideration of the probe lifetime and the size of the protein.

### II.4.1.3 Applications

FP is a homogeneous method that allows rapid and quantitative analysis of diverse molecular interactions and enzyme activities. This technique has been widely utilized in clinical and biomedical settings, including the diagnosis of certain diseases and monitoring therapeutic drug levels in body fluids. It has also been applied to the analysis of molecular interactions including protein-protein, protein-DNA and protein-ligand binding events, separately. FP applications can be classified based on target class or molecular interaction.

A FP assay can be configured through direct binding of the protein with its substrate in a design scheme similar to that applied in receptor-ligand binding (Figure 2-8A). In this case, the substrate is fluorescently labeled, and in the assay the FP value increases due to the formation of the larger enzyme-substrate complex [307]. In non-affinity-based methods, the substrate is usually labeled with a fluorophore and possesses a low rotational relaxation; thus, the readout almost always follows a decrease in polarization value as the enzymatic reaction, such as a proteolytic or hydrolysis process, leads to the breakdown of the fluorescently labeled substrate and thus a decrease in its molecular size (Figure 2-8B) [308].

Fluorescence polarization immunoassay (FPIA) is an antibody-based technique that usually follows the competition between unlabeled antigen and labeled antigen for binding to an antibody. On the displacement of the labeled antigen by the unlabeled antigen, the rate of the tumbling motion is increased due to increased amount of free labeled antigen, resulting in a lower polarization (Figure 2-8C). This method requires a substantial degree of substrate phosphorylation [309], and assay sensitivity can be improved by switching to a competitive FPIA format. In competitive FPIA [310], a fluorescently labeled phosphopeptide tracer representing the kinase reaction product is bound to an antibody, corresponding to a high FP value. Displacement of the tracer by increased amount of reaction-generated phosphopeptide product causes higher molecular mobility of the tracer and, consequently, a decrease in FP value (Figure 2-8D).

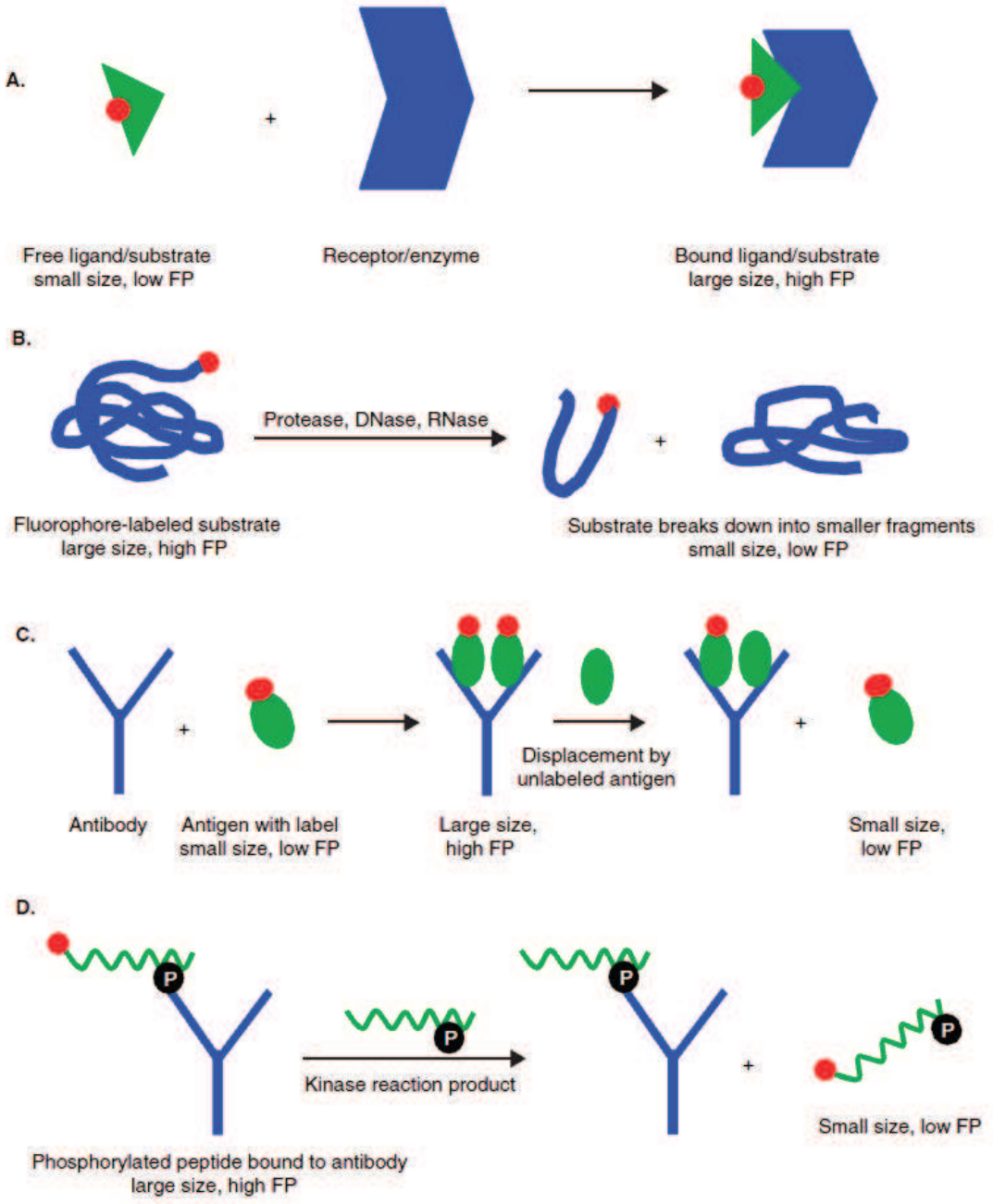


**Figure 2-8:** Schematic illustration of FP principle in relation to: A) Schematic illustration of FP principle in relation to receptor-ligand interaction [307] B) degradative enzymatic reactions (during hydrolysis, breakdown of fluorophore-labeled substrate into smaller molecules produces species with lower FP, which can be used to measure enzymatic activity) [308], C) FPIA (binding of a labeled antigen to its antibody leads to an increase in FP; displacement of labeled antigen by unlabeled antigen reduces the FP value and the degree of FP reduction is correlated with the antigen concentration in unknown samples) [309], D) competitive FPIA for kinase (displacement of a fluorescently labeled phosphopeptide tracer from phosphospecific antibodies by kinase reaction-generated phosphopeptide product (unlabeled) results in a decrease in FP, which can be used to measure kinase activity) [310].

## II.4.2 Experimental Section

### II.4.2.1 Complementary strands (CS) displacement strategy

Despite its simplicity and sensitivity, direct (non-competitive) strategy is not widely applicable as it requires a sufficiently large aptamer conformational/structural change or the rational engineering of the aptameric element to produce detectable fluorescence anisotropy responses. The indirect format, on the other hand, takes advantage of the ability of nucleic acids to form duplex structures with their complementary sequences [311]. The fluorescence anisotropy signal of the duplex is expected to be greater than that of the free fluorescently labeled complementary strand (CS) since the molecular mass of the hybrid is higher than that of the CS probe alone. This indirect approach has advantages over the direct FP strategy. The aptamer does not have to be modified to obtain a significant signal, which does not depend on a large conformational change within the oligonucleotide. More importantly, the methodology displays a broad applicability [213].

A structure-switching aptamer assay based on a fluorescence polarization (FP) signal transduction approach and dedicated to the L-tyrosinamide sensing was described and optimized by our group [312]. A fluorescently labeled complementary strand (CS) of the aptamer central region was used as a probe. The effects of critical parameters such as buffer composition and pH, temperature, aptamer:CS stoichiometry, nature of the dye (Fluorescein (F) or Texas Red (TR)) and length of the CS (15-, 12-, 9- and 6-mer) on the assay analytical performances were evaluated.

***Article published in Analytica Chimica Acta, volume 707, 2011, pages 191-196***

Analytica Chimica Acta 707 (2011) 191–196

Contents lists available at SciVerse ScienceDirect

Analytica Chimica Acta

journal homepage: www.elsevier.com/locate/aca

# Optimization of the structure-switching aptamer-based fluorescence polarization assay for the sensitive tyrosinamide sensing

Zhenyu Zhu, Thomas Schmidt, Maroi Mahrous, Valérie Guieu, Sandrine Perrier, Corinne Ravelet, Eric Peyrin*

*Département de Pharmacochimie Moléculaire UMR 5063 CNRS, ICMG FR 2607, Université Grenoble I, Campus Universitaire, Saint-Martin d'Hères, France*

ARTICLE INFO

*Article history:*
Received 3 February 2011
Received in revised form 31 August 2011
Accepted 14 September 2011
Available online 22 September 2011

*Keywords:*
Aptamer
Fluorescence polarization
Structure switching
Complementary strand

ABSTRACT

In this paper, a structure-switching aptamer assay based on a fluorescence polarization (FP) signal transduction approach and dedicated to the L-tyrosinamide sensing was described and optimized. A fluorescently labelled complementary strand (CS) of the aptamer central region was used as a probe. The effects of critical parameters such as buffer composition and pH, temperature, aptamer:CS stoichiometry, nature of the dye (Fluorescein (F) or Texas Red (TR)) and length of the CS (15-, 12-, 9- and 6-mer) on the assay analytical performances were evaluated. Under optimized experimental conditions (10 mM Tris–HCl, 5 mM $MgCl_2$ and 25 mM NaCl, pH 7.5 temperature of 22 °C and stoichiometry 1:1), the results showed that, for a 12-mer CS, the F dye moderately increased the method sensitivity in comparison to the TR label. The F labelled 9-mer CS, however, did not allow the hybrid formation with the functional nucleic acid, thus emphasizing the importance of the nature of the fluorophore. In contrast, the same 9-mer CS labelled with the TR dye was able to effectively associate with the aptamer and was easily displaced upon target binding as demonstrated by a significant improvement of the sensitivity and a detection limit of 250 nM, comparable to those reported with direct aptasensing methods. The present study demonstrates that not only the CS length but also the nature of the dye played a preponderant role in the performance of the structure-switching aptamer assay, highlighting the importance of interdependently controlling these two factors for an optimal FP-based sensing platform.



## 1. Introduction

Aptamers are artificial oligonucleic acids selected *in vitro* through SELEX (systematic evolution of ligands by exponential enrichment) [1,2]. Aptamers display high affinity and specificity to a wide range of target molecules, including drugs, proteins and other organic or inorganic species. Due to their numerous advantages [1–3], aptamers have become an attractive alternative to antibodies as molecular recognition elements in several biosensor applications. A number of aptamer-based sensors have been designed and optimized [4–6], using fluorescent [7–14], colorimetric [15–19], magnetic [20,21], electrochemical [22–24] or mass sensitive [25–27] transduction systems. Among aptamer-based sensors, fluorescent sensors are particularly interesting, due notably to their high intrinsic sensitivity and the capability for automated, high-throughput and multiplexed analysis.

The simplicity, speed and accuracy of the fluorescence polarization (FP) approach has made it one of the most appealing and thus commonly used techniques for the routine analysis of small molecules in a variety of areas [28]. Aptamers have recently been employed for the quantitative determination of small target molecules by measuring the change in the fluorescence anisotropy signal using two different strategies. The first approach relies on a direct (non-competitive) mechanism [29,30] while the second is based on an indirect structure-switching mechanism [31]. In the direct format, the target binding induces aptamer conformational and/or structural changes that affect precisely labelled sites or regions of the functional nucleic acid. These changes lead to alter local dye motions, which are then monitored by variations in the total fluorescence anisotropy signal [29,30]. Despite its simplicity and sensitivity, such a strategy is not widely applicable as it requires a sufficiently large aptamer conformational/structural change [30] or the rational engineering of the aptameric element to produce detectable fluorescence anisotropy responses [29]. The indirect format, on the other hand, takes advantage of the ability of nucleic acids to form duplex structures with their complementary sequences [10]. The fluorescence anisotropy signal of the duplex is expected to be greater than that of the free fluorescently labelled complementary strand (CS) since the molecular mass of the hybrid is higher than that of the CS probe alone. In this indirect assay, the aptamer is initially hybridized to its strand (CS), forming a duplex. In the absence of the target, base pairing between the

* Corresponding author.
*E-mail address:* eric.peyrin@ujf-grenoble.fr (E. Peyrin).

0003-2670/$ – see front matter © 2011 Elsevier B.V. All rights reserved.
doi:10.1016/j.aca.2011.09.022

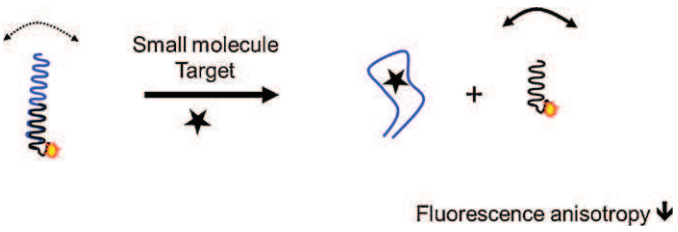


**Fig. 1.** Schematic representation of the indirect FP strategy for the design of the small molecule aptasensor (aptamer in blue, CS in black, target as a star). (For interpretation of the references to color in this figure legend, the reader is referred to the web version of the article.)

complementary sequences is favoured. When the target is introduced, it binds to the aptamer and the aptamer–CS hybridization is disrupted, leading to the displacement of the complementary strand [31] (Fig. 1) and thus resulting in an observable decrease in the fluorescence anisotropy signal. This indirect approach has advantages over the direct FP strategy. The aptamer does not have to be modified to obtain a significant signal, which does not depend on a large conformational change within the oligonucleotide. More importantly, the methodology displays a broad applicability [31].

However, compared to direct assays, this strategy suffers from poor sensitivity that is directly related to the stability of the CS–aptamer duplex [32]. As the target–aptamer association competes with the CS–aptamer interaction (Fig. 1), a stable duplex structure significantly alters the apparent binding affinity of the target for the aptamer, causing performance deterioration of the assay performances [10,11].

Improvement in the assay sensitivity is an important goal of the method development since a majority of biological events occur at very low analyte levels. To date, no study has been performed to identify and analyze the factors involved in the analytical performances of the structure-switching-based FP aptasensor. The study described here used the L-tyrosinamide 38-mer DNA aptamer (Apt-Tym) as model system [9,30]. Under optimized binding conditions, the FP biosensor titration curves with increasing target concentration were generated for both the Fluorescein-tagged and the Texas Red-tagged CS duplexes, and the assay performances were compared.

## 2. Experimental

### 2.1. Chemicals and apparatus

L-Tyrosinamide (L-Tym), L-tyrosine (L-Tyr), and tris(hydroxymethyl)aminomethane were obtained from Sigma Aldrich (Saint-Quentin, France). NaCl and $MgCl_2$ were obtained from Chimie-Plus Laboratoires (Bruyères de Pouilly, France) and Panreac Quimica (Barcelona, Spain), respectively. Water was obtained from a Purite Still Plus water purification system (Thame, UK) fitted with a reverse osmosis cartridge. The normal and modified oligonucleotides listed in Table 1 were synthesized and HPLC-purified by Eurogentec (Angers, France). The identity of the oligonucleotides was confirmed by MALDI-TOF mass spectrometry. Fluorescence anisotropy was measured on a Tecan Infinite F500 microplate reader (Männedorf, Switzerland) using black, 96-well Greiner Bio-One microplates (ref: 675086). Excitation was set at 485 ± 20 nm or 585 ± 20 nm and emission was collected with 535 ± 25 nm or 635 ± 30 nm bandpass filters in relation to the wavelengths associated with the fluorescent dyes.

**Table 1**
Oligonucleotides utilized in the structure-switching aptamer-based fluorescence polarization assays.[a]

| | Polarization homogeneous assay |
|---|---|
| Apt-Tym (38-mer) | 5′-TGGAGCT**TGGATTGATGTG**GTGTGTGAGTGCGGTGCCC-3′ |
| F-CS-15* (15-mer) | 3′-**CGAACCTAACTACAC**-F-5′ |
| F-CS-12* (12-mer) | 3′-**ACCTAACTACAC**-F-5′ |
| F-CS-9* (9-mer) | 3′-**TAACTACAC**-F-5′ |
| Apt-Tym (38-mer) | 5′-TGGAGCT**TGGATTGATGTG**GTGTGTGAGTGCGGTGCCC-3′ |
| TR-CS-12* (12-mer) | 3′-**ACCTAACTACAC**-TR-5′ |
| TR-CS-9* (9-mer) | 3′-**TAACTACAC**-TR-5′ |
| TR-CS-6* (6-mer) | 3′-**CTACAC**-TR-5′ |

[a] F: fluorescein label; TR: Texas red; complementary bases are in bold type.

### 2.2. Sample preparation

Unless otherwise stated, the binding buffer for fluorescence polarization assay (FP) consisted of 10 mM Tris–HCl, pH 7.5, 5 mM $MgCl_2$ and 50 mM NaCl. The aptamer (Apt) and CS stock solutions were prepared in pure water at $10^{-6}$ M and stored at −20 °C. The working CS or CS–aptamer solutions were prepared from the stock solutions by diluting 1.28× with concentrated binding buffer for FP. The working solutions were heated at 90 °C for 5 min and then cooled at 4 °C for 30 min in order to reach equilibrium prior to use. The analyte solutions were prepared in water. For L-Tym titration curve, the analyte concentration varied from 25 μM to 2000 μM (except for the TR-CS 9 mer). All solutions were filtered before use through 0.45 μm membrane filters.

To establish the titration curves, CS, Apt and analyte solutions were mixed into individual wells (final volume = 100 μL) at room temperature (22 °C, unless otherwise notified), resulting in both Apt and CS oligonucleotide final concentrations of 10 nM. Blank wells of the microplate received 100 μL of the binding buffer. All experiments were done in triplicate. The microplate was placed into the microplate reader for the measurement after 15 min of incubation in dark.

### 2.3. Parameter determination

The anisotropy ($r$) was calculated by the instrument software, as classically reported:

$$r = \frac{I_w - GI_{vh}}{I_w + 2GI_{vh}}$$

where $I_{vv}$ and $I_{vh}$ are the vertically and horizontally polarized components of the emission after excitation by vertically polarized light. The instrumental correction factor $G$ was determined from standard solutions according to the manufacturer's instructions.

Fluorescence anisotropy change $\Delta r$ was calculated as follows:

$$\Delta r = r - r_f$$

where $r$ is the anisotropy of the hybrid (dye-labelled CS with aptamer) and $r_f$ is the anisotropy of the free complementary strand. $\Delta r_{max}$ is the maximal fluorescence anisotropy difference, obtained in the absence of target. Relative $\Delta r$ was obtained as follows:

$$\text{relative } \Delta r = \frac{\Delta r \times 100}{\Delta r_{max}}$$

## 3. Results and discussion

It is well established that the sensitivity of a biosensor platform is dependent on both the affinity of the molecular recognition element for the target analyte and the signal transduction technology employed [33]. The stability of the aptamer–CS duplex in the structure-switching aptamer approach to biosensors is known

to have a strong impact on the sensitivity of the method [10,11]. Thus, the key factors in the development of this type of biosensor strategy are the hybridization conditions and the choice of an appropriate CS probe. To note, the core sequence (12-mer) of the complementary strands utilized in this study (Table 1) has been previously described in the development of a structure-switching aptamer assay for a multiplexed detection of small analytes by capillary electrophoresis [34].

### 3.1. Influence of the buffer composition on the FP response

The influence of the salt concentration in the binding buffer on the FP response was firstly studied. For the anti-L-tyrosinamide aptamer, it has been previously shown that the magnesium concentration played an essential role in both the 3D aptamer stabilization and target binding [35]. Thus, in preliminary experiments, different titration curves of the aptamer-based Tym sensor were constructed under four $MgCl_2$ concentrations (NaCl concentration fixed at 50 mM) (Fig. 2a). In the absence of aptamer, the fluorescence anisotropy values of the F-CS-12 with all $MgCl_2$ concentration were equivalent (around $0.043 \pm 0.001$). The addition of the aptamer in the absence of L-Tym resulted in a large increase in fluorescence anisotropy values ($0.083 \pm 0.001$, $0.094 \pm 0.001$, $0.106 \pm 0.001$ and $0.110 \pm 0.001$ for 2.5, 5, 10 and 15 mM of $MgCl_2$, respectively). The presence of a high amount of $MgCl_2$ was favourable to the hybrid species formation. The fluorescence anisotropy change upon target binding was found to be slightly dependent on the $MgCl_2$ concentration. The optimal signal was attained between 2.5 and 10 mM of $MgCl_2$ with the best results for 5 mM. The weaker fluorescence anisotropy change was observed for higher $MgCl_2$ concentration, indicating the preponderant role of $MgCl_2$ concentration in duplex formation.

To determine whether the concentration of NaCl might affect the assay response, a series of aptamer-based indirect sensing measurements were performed under different salt concentrations (Fig. 2b). The $\Delta r$ value was also found to vary with the NaCl concentration. For an $MgCl_2$ concentration set to 5 mM, the response was optimal for the 25 mM NaCl concentration. To note, the hybrid species was formed even in absence of NaCl, showing that the presence of $MgCl_2$ was sufficient to promote the duplex formation. Lowering the salt concentration enhanced the structure-switching aptamer mechanism (Fig. 2b). In contrast, the presence of a high amount of NaCl favoured the hybridization so that displacement by the target, and hence the formation of target–aptamer complex, was hindered under such salt conditions.

The role of the buffer pH on the fluorescence anisotropy variation was also evaluated. No significant change was observed between pH 7 and pH 7.5 and 8 (data not shown). Thus, the buffer pH was set to 7.5 for all experiments of the present study.

### 3.2. Influence of the temperature and stoichiometry on the FP response

As reported by previous FP studies on the target–aptamer interaction [30,36], temperature constitutes a preponderant parameter in the signal response. As the rotational correlation time is inversely related to the temperature, the effect of increasing temperature results in reduced FP changes [36]. Furthermore, the decrease in the temperature typically improves the target binding to aptamer, resulting in enhanced assay sensitivity for direct FP aptamer-based assays [30,36]. To evaluate the effect of temperature on the current displacement assay, mixed duplex-analyte samples were incubated in a cold room (4 °C) or in controlled thermal bath (22 °C or 37 °C) for a 15 min period. The samples were then transferred into the individual wells and the fluorescence anisotropy measurement was immediately performed. The titration curves were constructed as

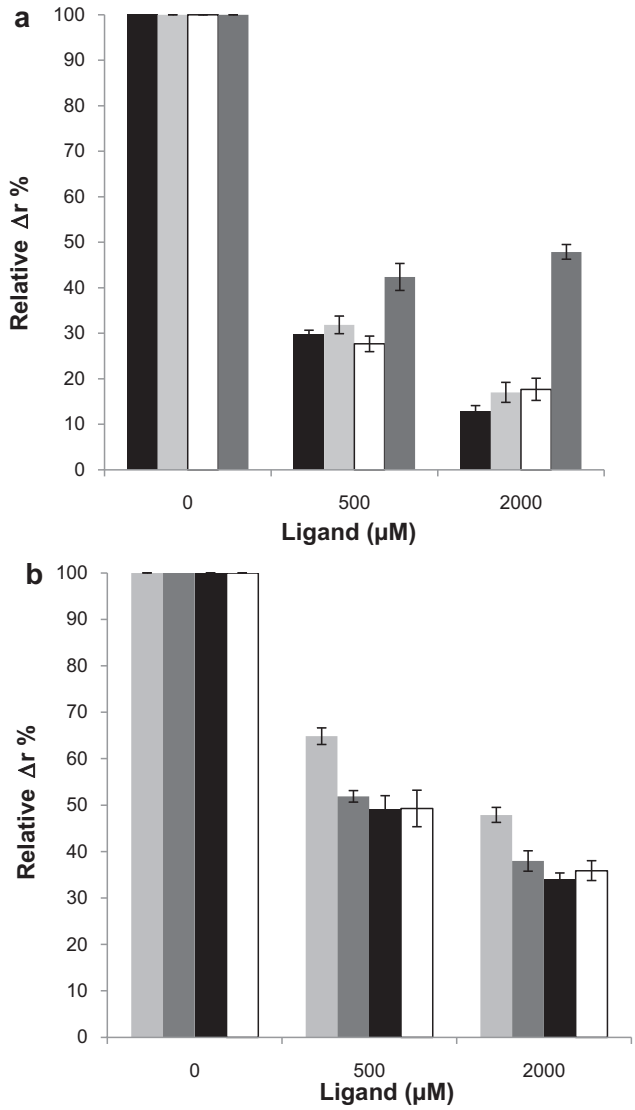


**Fig. 2.** Fluorescence anisotropy change (relative $\Delta r$ %) of F-CS-12 and Apt-Tym with increasing L-Tym (cognate ligand) under (a) 2.5 mM (blanck), 5 mM (black), 10 mM (light grey) and 15 mM (grey dark) $MgCl_2$ concentration (50 mM NaCl). (b) Fluorescence anisotropy change (relative $\Delta r$ %) under 5 mM $MgCl_2$ concentration and various NaCl concentration conditions 0 mM (black), 25 mM (blanck), 50 mM (grey dark), 100 mM (light grey). Probe concentration: 10 nM. Aptamer concentration: 10 nM. Binding buffer conditions: 10 mM Tris–HCl, pH = 7.5. Triplicate experiments.

shown in Fig. 3a. Similar FP responses were observed for 37 °C and 22 °C while a weaker fluorescence anisotropy change was obtained for the 4 °C experiment. It can be suggested that the hybridized form was more stable at lower temperature than higher temperature so that the fast displacement of the CS upon target binding was favoured at 22 or 37 °C. For convenience reasons, 22 °C was chosen as standard temperature for subsequent experiments.

Finally, the influence of the CS:aptamer stoichiometry were investigated to fine-tune the FP response. The oligonucleotide probe concentrations were optimized to 10 nM concentration in a previous study to reach a fluorescence intensity signal-to-noise ratio >10. [30]. In the present work, various aptamer concentrations varying from 5 to 50 nM were tested). A weak fluorescence anisotropy variation was observed for 50 nM aptamer concentration, indicating that a large amount of aptamer was unfavourable to the CS displacement by the free target. When aptamer was in insufficient concentration (5 nM), the sensitivity of the method was

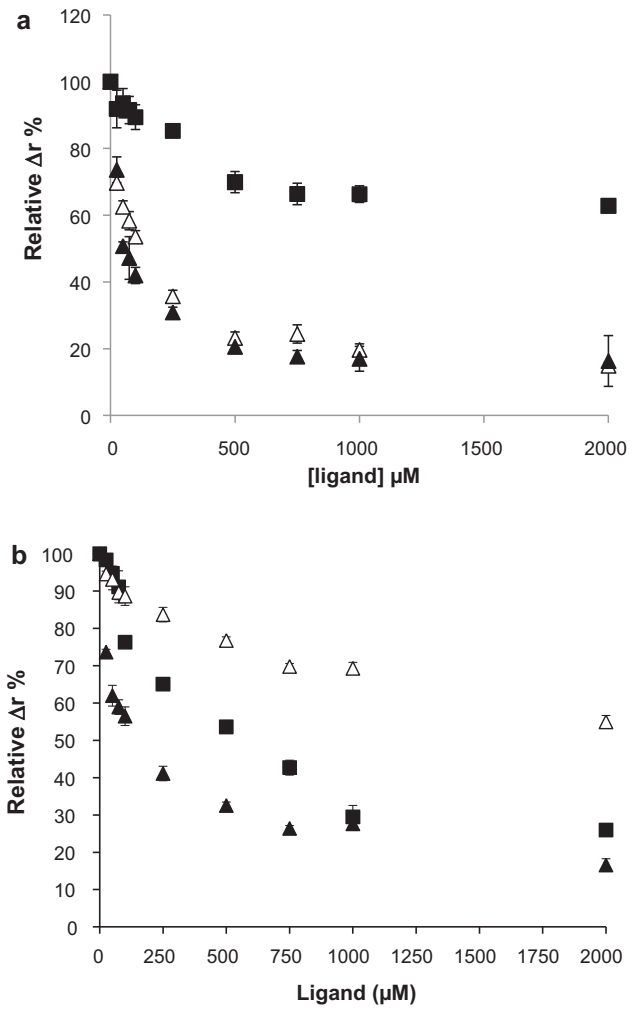


**Fig. 3.** Fluorescence anisotropy change (relative $\Delta r$ %) of F-CS-12 and Apt-Tym with increasing L-Tym (cognate ligand) under (a) different temperature 4 °C (filled square), 22 °C (open triangle) and 37 °C (filled triangle) (aptamer concentration: 10 nM). (b) 5 nM (filled square), 10 nM (filled triangle), 50 nM (open triangle). Probe concentration: 10 nM. Binding buffer conditions: 10 mM Tris–HCl, pH 7.5, 5 mM $MgCl_2$, 25 mM NaCl.

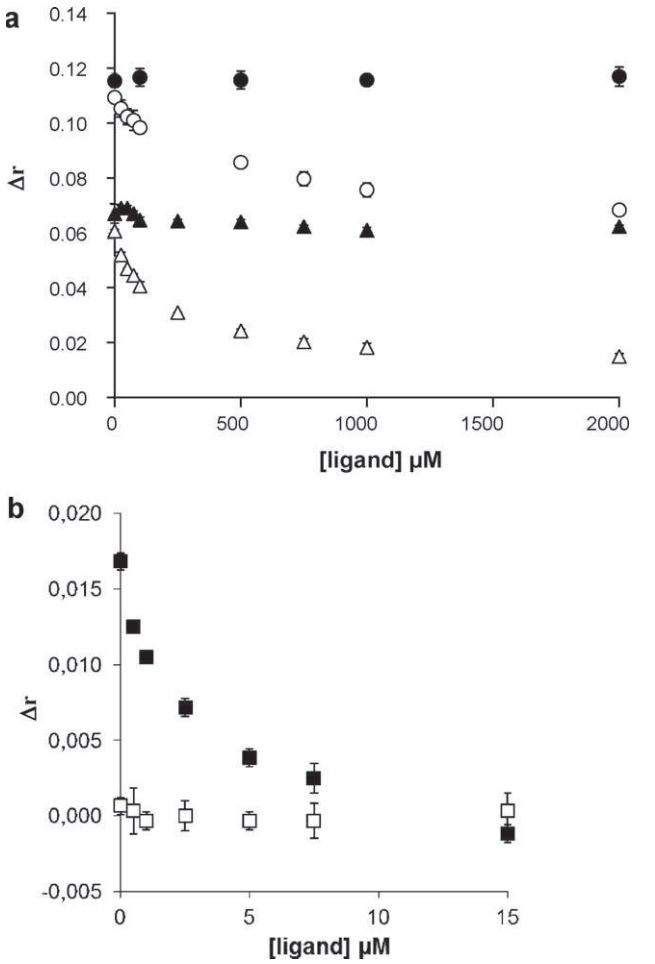


**Fig. 4.** Titration curves of (a) F-CS-15 (filled triangle), F-CS-12 (open triangle), TR-CS-12 (open circle), (b) F-CS-9 (open square), TR-CS-9 (filled square) and Apt-Tym with increasing L-Tym (cognate ligand) and L-Tyr (non-cognate ligand for TR-CS-12 (filled circle)). Triplicate experiments. $\Delta r = r - r_f$ where $r_f$ is the fluorescence anisotropy in absence of analyte. Probe concentration: 10 nM. Aptamer concentration: 10 nM. Binding buffer conditions: 10 mM Tris–HCl, pH 7.5, 5 mM $MgCl_2$, 25 mM NaCl.

affected. The best result was obtained for 1:1 stoichiometry (with 10 nM aptamer concentration).

### 3.3. Influence of the dye nature and CS length on the FP response

Numerous studies have shown that the fluorophore nature significantly influences the sensitivity of the FP assays involving labelled DNA species [30,36]. To evaluate the impact of the dye nature on the structure-switching aptamer based assay, two different dyes, i.e. F and TR, were used. The titration curves with increasing L-Tym concentrations (from 25 to 2000 μM) were established using the tagged complementary strands F-CS and TR-CS under the optimized binding buffer conditions (10 mM Tris–HCl, 5 mM $MgCl_2$ and 25 mM NaCl, temperature of 22 °C see above). In the absence of target, the fluorescence anisotropy values varied from $0.045 \pm 0.001$ for the F-CS-12 probe to $0.091 \pm 0.002$ for the TR-CS-12 probe under the binding buffer conditions. Such behaviour could be attributed to the specific physico-chemical features of the two dyes. FP measurements typically reflected the contributions from (i) the local motional freedom of the fluorescent reporter and (ii) the global rotational diffusion of the entire species [37,38]. The rotation of the anionic F moiety in an end-labelled CS is largely uncoupled from the global motion of the molecule, explaining the low anisotropy value of the F-CS-12 probe. On the other hand, the TR on the TR-CS molecule has been shown to exhibit a higher degree of coupling to the whole macromolecule as the result of its cationic character [39]. Moreover, the predicted fluorescence anisotropy value for the CS was estimated to be 0.094 using the procedure previously described by Gokulrangan et al. [36]. The *r*-value for the TR-CS-12 probe was consistent with this theoretical data while the measured fluorescence anisotropy of F-CS-12 was significantly lower. Upon aptamer addition, an increase in the fluorescence anisotropy was observed for both probes. Fluorescence anisotropy values of $0.105 \pm 0.001$ and $0.200 \pm 0.002$ were obtained for F-CS-12 and TR-CS-12, respectively, consistent with the formation of the duplex structure. The duplex formed with TR-CS-12 displayed a higher $\Delta r_{max}$ value $0.109 \pm 0.001$ than that obtained with the F-CS-12 probe ($0.061 \pm 0.001$). With the two probes, L-Tym could be detected between 25 μM and 100 μM in a linear pattern (Fig. 4a). Detection limits (~6 and ~11 μM for F-CS-12 and TR-CS-12, respectively), based on a statistical analysis by regression function were obtained (Table 2). The use of the F-CS-12 probe was responsible for a greater assay sensitivity (slope = $-1.90 \times 10^{-04} \pm 2.65 \times 10^{-05}$) as compared to the method that used TR-CS-12 (slope = $-1.05 \times 10^{-04} \pm 1.05 \times 10^{-05}$) (Fig. 4a).

**Table 2**
Comparison of the L-tyrosinamide assay sensitivity for different methods.

| Analytical method | Label | Detection limit | Linear dynamic range | Apparent $K_d$ | References |
|---|---|---|---|---|---|
| Structure switching | Fluorophore labeled CS | | | | This work |
| polarization fluorescence | F-CS-12 | 6 μM | 25–100 μM | 160 μM | |
| | TR-CS-12 | 11 μM | 25–100 μM | 260 μM | |
| | TR-CS-9 | 250 nM | 0.5–2.5 μM | 3 μM | |
| Direct polarization | Fluorophorelabeled aptamer | | | | [30] |
| fluorescence | 3′-F-9-Apt-Tym | 200 nM at 25 °C | 20 nM–1.5 μM | 1.7 μM | |
| | | 100 nM at 4 °C | 20–750 nM | 0.7 μM | |
| | 3′-F-15-Apt-Tym | 280 nM at 25 °C | 20 nM–2 μM | 2.2 μM | |
| Direct fluorescent intensity | Fluorescent aptamer adduct | ∼3 μM[a] | 5–100 μM[a] | 40 μM | [9] |

[a] Graphically estimated.

These results correlated well with the values of the apparent dissociation constants ($K_d$), which were estimated from the mid-point of the maximum of the titration curves. $K_d$ values of 160 μM and 260 μM were observed for the F-CS-12-Apt and TR-CS-12-Apt hybrids, respectively (Table 2). The higher assay sensitivity obtained with F-CS-12 could be then explained by the ability of the probe to be more easily displaced from the aptamer by the target binding. The negative charge on the fluorescein was expected to govern the dye-duplex backbone repulsion that could favour the CS release. On the other hand, the duplex involving the TR-CS-12 was assumed to be more stable due favourable electrostatic and van der Waals interactions with DNA [36] such that the L-Tym target molecule could not displace the labelled probe from Apt as efficiently.

To investigate the specificity of the present structure switching aptamer based FP assay, we further examined the aptamer binding reaction with tyrosine. Fig. 4a shows the fluorescence anisotropy changes in response to the addition of various concentrations of L-tyrosine under the same experimental conditions used above. No significant changes were observed upon L-tyrosine addition, demonstrating the specificity of the sensing platform.

It is well established that the length of the CS constitutes one of the main parameters that governs the stability of the duplex [10]. The effect of the CS length on the structure-switching aptamer system was thus subsequently evaluated. For a 15-mer CS, containing the 12-mer core sequence CS-12 used above, the addition of the aptamer in the absence of target resulted in a large increase in fluorescence anisotropy value (0.110). As obviously expected, this indicated that F-CS-15 annealed very efficiently to the aptamer. However, a very slight variation was observed upon target binding due to the too strong duplex stability (Fig. 4a). Ideally, the optimized CS should be capable of hybridizing to the aptamer with low/moderate strength in order to facilitate fast displacement upon target binding. So, a truncated sequence of CS-12 (12-mer) was designed (CS-9, 9-mer) and the assay performances were again evaluated. Both F and TR were used as reporters for CS-9 to evaluate the interdependent role of the two factors. In the absence of the target molecule, no variation in the FP value was observed upon aptamer addition to F-CS-9 (Fig. 4b), indicating that the duplex cannot be effectively formed between F-CS-9 probe and the aptamer. On the other hand, hybridization was effectively observed between the TR-CS-9 probe and Apt. As reported above, such difference observed for the two reporters can be attributed to the different DNA-interacting features of the labels. Due to a lower hybrid fraction formed, experiments involving TR-CS-9 exhibited a lower $\Delta r_{max}$ value ($0.017 \pm 0.001$) (Fig. 4a) than those performed with the TR-CS-12 probe ($0.109 \pm 0.001$) (Fig. 4b). The titration curve obtained with the TR-CS-9 probe was characterized by a steep slope (slope = $-3.52 \times 10^{-03} \pm 8.87 \times 10^{-04}$). This is attributed to the weak stability of the duplex structure, and implies great assay sensitivity. Such sensitivity using TR-CS-9 was much higher than the sensitivity obtained above with the F-CS-12-Apt and TR-CS-12 probes, by a factor of about ∼20 and ∼30, respectively. With TR-CS-9 probe, L-tyrosinamide could be detected in a shorter linear range from 0.5 μM to 2.5 μM and a detection limit of 250 nM was obtained (Table 2), comparable to that of the direct polarization L-tyrosinamide aptamer-based sensor [30] and better than that obtained with direct fluorescent intensity measurement [9]. Moreover, the apparent $K_d$ of the titration curve of TR-CS-9 probe was estimated to be about 3 μM from the mid-point of the titration curve, ∼50 or ∼90 times lower than the ones obtained for the two other probe systems. Of particular interest is the fact that this $K_d$ value was close to the dissociation constant of the original L-Tym-Apt complex determined by direct polarization assay (Table 2) and isothermal titration calorimetry [35], suggesting that the association between the TR-CS-9 probe and the aptamer did not alter too much the binding ability of the target. In order to try to further improve the sensitivity of the FP assay, a 6-mer truncated sequence of TR-CS-9 was subsequently evaluated. In the absence of the target molecule, no variation in the FP value was observed upon aptamer addition to TR-CS-6. This shows that hybridization cannot occur even with the cationic dye as label.

## 4. Conclusion

In summary, the structure-switching aptamer based FP assay has been optimized through the study of the effects of the buffer composition and pH, temperature, aptamer:CS stoichiometry, CS length and label nature on the assay performances. For the same length of a 12-mer CS, the anionic nature of F dye constitutes an advantage in comparison to the cationic TR label. On the other hand, when the CS length was shortened, the use of the TR label for the structure-switching aptasensing method resulted in great sensitivity, with a detection limit comparable to the ones obtained with direct aptamer-based assays. This study demonstrates that the fluorescence anisotropy signal generation is dependent on the fine interconnection between the dye nature and the length of the CS to carefully control (i) the duplex stability and (ii) the relative affinity between the aptamer–CS duplex and aptamer–target complexes.

## Acknowledgments

This work was supported by grants from the "SEST-Micraptox" n° 2007-013-01 ANR program.

The authors are thankful to Dr. Jayna Chan for a critical reading of this manuscript.

## References

[1] A.D. Ellington, J.W. Szostak, Nature 346 (1990) 818.
[2] C. Tuerk, L. Gold, Science 249 (1990) 505.
[3] C.L.A. Hamula, J.W. Guthrie, H. Zhang, X.-F. Li, X.C. Le, TrAC 25 (2006) 681.

[4] S. Jhaveri, M. Rajendran, A.D. Ellington, Nat. Biotechnol. 18 (2000) 1293.
[5] J. Liu, Z. Cao, Y. Lu, Chem. Rev. 109 (2009) 1948.
[6] W. Mok, Y. Li, Sensors 8 (2008) 7050.
[7] B. Juskowiak, Anal. Bioanal. Chem. (2010), doi:10.1007/s00216-010-4304-5.
[8] C.-C. Huang, H.-T. Chang, Chem. Commun. (2008) 1461.
[9] E.J. Merino, K.M. Weeks, J. Am. Chem. Soc. 127 (2005) 12766.
[10] R. Nutiu, Y. Li, J. Am. Chem. Soc. 125 (2003) 4771.
[11] R. Nutiu, Y. Li, Methods 37 (2005) 16.
[12] R. Nutiu, Y. Li, Angew. Chem. Int. Ed. 44 (2005) 5464.
[13] B. Shlyahovsky, D. Li, Y. Weizmann, R. Nowarski, M. Kotler, I. Willner, J. Am. Chem. Soc. 129 (2007) 3814.
[14] Z. Tang, P. Mallikaratchy, R. Yang, Y. Kim, Z. Zhu, H. Wang, W. Tan, J. Am. Chem. Soc. 130 (2008) 11268.
[15] J. Liu, Y. Lu, Angew. Chem. Int. Ed. 45 (2006) 90.
[16] J. Wang, L. Wang, X. Liu, Z. Liang, S. Song, W. Li, G. Li, C. Fan, Adv. Mater. 19 (2007) 3943.
[17] J. Zhang, L. Wang, D. Pan, S. Song, F.Y.C. Boey, H. Zhang, C. Fan, Small 4 (2008) 1196.
[18] W. Zhao, M.A. Brook, Y. Li, ChemBioChem 9 (2008) 2363.
[19] W. Zhao, W. Chiuman, J.C.F. Lam, S.A. McManus, W. Chen, Y. Cui, R. Pelton, M.A. Brook, Y. Li, J. Am. Chem. Soc. 130 (2008) 3610.
[20] M.V. Yigit, D. Mazumdar, H.K. Kim, J.H. Lee, B. Odintsov, Y. Lu, ChemBioChem 8 (2007) 1675.
[21] M.V. Yigit, D. Mazumdar, Y. Lu, Bioconjug. Chem. 19 (2008) 412.
[22] Y. Du, B. Li, F. Wang, S. Dong, Biosens. Bioelectron. 24 (2009) 1979.
[23] X. Zuo, Y. Xiao, K.W. Plaxco, J. Am. Chem. Soc. 131 (2009) 6944.
[24] A. Sassolas, L.J. Blum, B.D. Leca-Bouvier, Electroanalysis 21 (2009) 1237.
[25] M.E. Stewart, C.R. Anderton, L.B. Thompson, J. Maria, S.K. Gray, J.A. Rogers, R.G. Nuzzo, Chem. Rev. 108 (2008) 494.
[26] Z. Wang, Y. Lu, J. Mater. Chem. 19 (2009) 1788.
[27] T.-C. Chiu, C.-C. Huang, Sensors 9 (2009) 10356.
[28] D. Smith, S. Eremin, Anal. Bioanal. Chem. 391 (2008) 1499.
[29] S. Perrier, C. Ravelet, V. Guieu, J. Fize, B. Roy, C. Perigaud, E. Peyrin, Biosens. Bioelectron. 25 (2010) 1652.
[30] J. Ruta, S. Perrier, C. Ravelet, J. Fize, E. Peyrin, Anal. Chem. 81 (2009) 7468.
[31] J.A. Cruz-Aguado, G. Penner, Anal. Chem. 80 (2008) 8853.
[32] F.T. Hafner, R.A. Kautz, B.L. Iverson, R.C. Tim, B.L. Karger, Anal. Chem. 72 (2000) 5779.
[33] T.M. Jackson, R.P. Ekins, J. Immun. Methods 87 (1986) 13.
[34] Z. Zhu, C. Ravelet, S. Perrier, V. Guieu, B. Roy, C. Perigaud, E. Peyrin, Anal. Chem. 82 (2010) 4613.
[35] P.-H. Lin, S.-L. Yen, M.-S. Lin, Y. Chang, S.R. Louis, A. Higuchi, W.-Y. Chen, J. Phys. Chem. B 112 (2008) 6665.
[36] G. Gokulrangan, J.R. Unruh, D.F. Holub, B. Ingram, C.K. Johnson, G.S. Wilson, Anal. Chem. 77 (2005) 1963.
[37] J.R. Lakowicz, Principles of Fluorescence Spectroscopy, Springer, US, 2006, p. 1.
[38] B.J. Lee, M. Barch, E.W. Castner, J. Volker, K.J. Breslauer, Biochemistry 46 (2007) 10756.
[39] J.R. Unruh, G. Gokulrangan, G.H. Lushington, C.K. Johnson, G.S. Wilson, Biophys. J. 88 (2005) 3455.

### II.4.2.2 Single-stranded DNA binding protein (SSB)-assisted strategy

In indirect complementary strands displacement approaches, the FP signal results from the competition between the target and fluorescent complementary strand (CS) for the binding to aptamer. However, the ability of the fluorophore to rotate independently from the global motion of the tracer (classically referred as the "propeller effect") can significantly reduce the FP signal for the bound state [305, 306]. In addition, as typically reported for the FP-based DNA hybridization monitoring [313, 314], the low molecular weight difference between the free CS and the CS-aptamer duplex limits the fluorescence anisotropy variation window in structure switching FP assay.

Single-stranded DNA-binding protein, or SSB, binds to single-stranded regions of DNA to prevent premature annealing, to protect the single-stranded DNA from being digested by nucleases in cells. These unique binding features have been taken into account to develop SSB-based analytical tools for detecting DNA hybridization, single nucleotide polymorphisms and specific DNA-protein interaction. Our group described a new FP aptamer assay strategy which was based on the use of SSB protein from *E. Coli* as a strong FP signal enhancer tool. This approach relied on the unique ability of the SSB protein to bind the nucleic acid aptamer in its free state but not in its target-bound folded one [315], a large global diffusion difference between the target- and SSB-bound aptamer probes was expected due to the high molecular weight of the protein (~76 kDa). Furthermore, in this case, the interfering "propeller effect" could be restricted as the ssDNA strongly coiled around the SSB protein so that close contacts should occur between the aptamer and the protein.

***Article published in the Analytical Chemistry (in press)***

analytical chemistry

Article

pubs.acs.org/ac

# Single-Stranded DNA Binding Protein-Assisted Fluorescence Polarization Aptamer Assay for Detection of Small Molecules

Zhenyu Zhu, Corinne Ravelet, Sandrine Perrier, Valérie Guieu, Emmanuelle Fiore, and Eric Peyrin*

Département de Pharmacochimie Moléculaire UMR 5063, Institut de Chimie Moléculaire de Grenoble FR 2607, CNRS-Université Grenoble I (Joseph Fourier), 38041 Grenoble cedex 9, France

Supporting Information

**ABSTRACT:** Here, we describe a new fluorescence polarization aptamer assay (FPAA) strategy which is based on the use of the single-stranded DNA binding (SSB) protein from *Escherichia coli* as a strong FP signal enhancer tool. This approach relied on the unique ability of the SSB protein to bind the nucleic acid aptamer in its free state but not in its target-bound folded one. Such a feature was exploited by using the antiadenosine (Ade)−DNA aptamer (Apt-A) as a model functional nucleic acid. Two fluorophores (fluorescein and Texas Red) were introduced into different sites of Apt-A to design a dozen fluorescent tracers. In the absence of the Ade target, the binding of the labeled aptamers to SSB governed a very high fluorescence anisotropy increase (in the 0.130−0.200 range) as the consequence of (i) the large global diffusion difference between the free and SSB-bound tracers and (ii) the restricted movement of the dye in the SSB-bound state. When the analyte was introduced into the reaction system, the formation of the folded tertiary structure of the Ade−Apt-A complex triggered the release of the labeled nucleic acids from the protein, leading to a strong decrease in the fluorescence anisotropy. The key factors involved in the fluorescence anisotropy change were considered through the development of a competitive displacement model, and the optimal tracer candidate was selected for the Ade assay under buffer and realistic (diluted human serum) conditions. The SSB-assisted principle was found to operate also with another aptamer system, i.e., the antiargininamide DNA aptamer, and a different biosensing configuration, i.e., the sandwich-like design, suggesting the broad usefulness of the present approach. This sensing platform allowed generation of a fluorescence anisotropy signal for aptamer probes which did not operate under the direct format and greatly improved the assay response relative to that of the most previously reported small target FPAA.

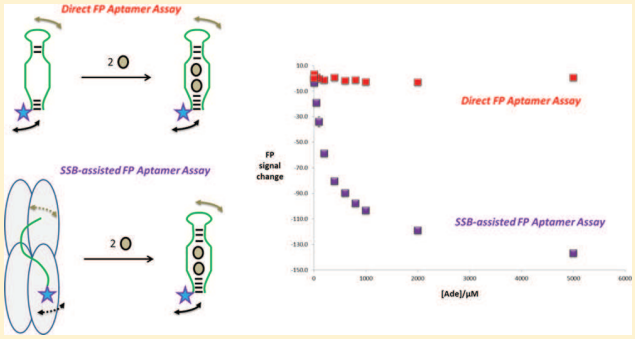


Fluorescence polarization (FP) is one of the most versatile and popular techniques used in clinical chemistry as illustrated by the numerous applications reported in the therapeutic drug monitoring and abused drug and toxic screening. FP is a fast, homogeneous method, is insensitive to the solution color, and is especially suitable for a high-throughput format assay.[1] Despite the large success of FP immunoassay (FPIA), several efforts have been carried out, during the past couple decades, to couple the FP technique to alternative affinity tools. For example, FP molecular imprinted sorbent assay (FPMIA) has also proved to be an efficient approach to detect small analytes such as propranolol or fluoroquinolones.[2,3] However, at the present time, the alternative selective binders most frequently used in FP technology are nucleic acid aptamers for both protein and small analyte sensing through FP aptamer assays (FPAAs).[4−16] Compared to antibodies, aptamers present several attractive features, including smaller size (especially advantageous for the direct FP-based detection of proteins), enhanced stability, chemical synthesis, and ease of incorporating modifications and/or labels at precise locations.

For small molecule sensing, different FPAA methodologies have been established based on either direct or indirect formats.[11−16] However, these strategies typically yield a limited FP signal. This constitutes a serious drawback that significantly affects the analytical performances as well as the applicability of such sensing platforms.[17,18] It is well established that the fluorescence anisotropy of a probe (or tracer) results from its global diffusion (dependent on its overall size) and the fluorophore local motion (dependent on the probe flexibility and dye movement freedom) contributions.[19] In the direct FPAA format, the FP signal depends on the target-induced structural/conformational change of the aptamer tracer that modifies the local dye mobility.[14,15] However, a restricted modification of the aptamer flexibility and/or dye motion for the target-bound aptamer complex can be responsible for a very weak or nil assay response. Thus, the direct approach is not easily generalizable, requiring a sufficiently large induced-fit

**Received:** June 10, 2012
**Accepted:** July 12, 2012

   dx.doi.org/10.1021/ac301552e | *Anal. Chem.* XXXX, XXX, XXX−XXX

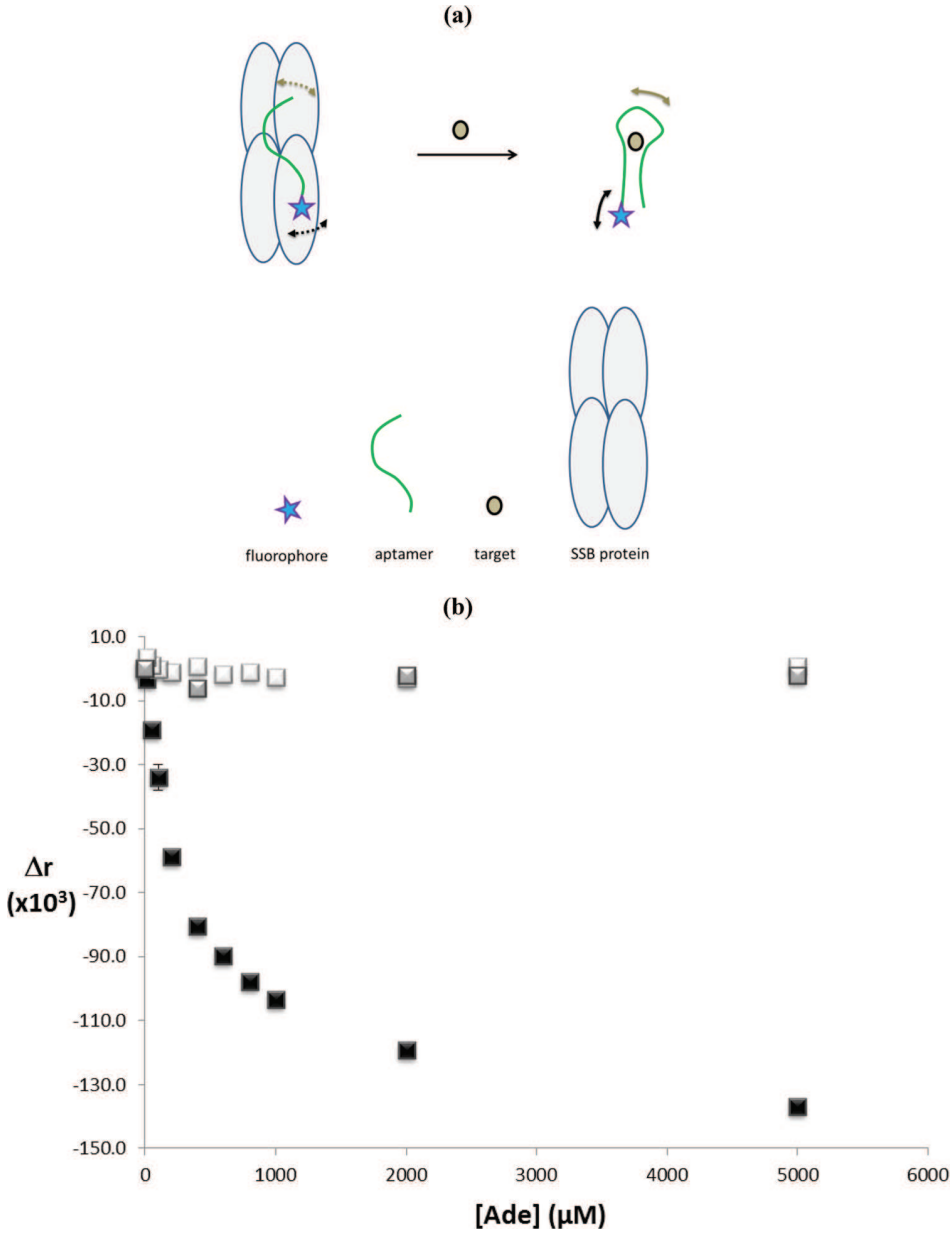


**Figure 1.** (a) Schematic representation of the SSB-assisted FPAA: gray double arrows, global diffusion contribution; black double arrows, local dye mobility contribution. (b) Titration curves of 5′-F-Apt-A with increasing Ade concentration under SSB-assisted (black symbols) and direct (white symbols) FPAA modes. Gray symbols are for SSB-assisted FPAA using the scramble 5′-F-Apt-A. The probe concentration was 10 nM and the SSB concentration 0.33 $\mu$M. Binding buffer conditions: 50 mM Tris−HCl, pH 7.5, 5 mM NaCl, 20 mM $MgCl_2$. $\Delta r = r - r_0$, where $r_0$ is the fluorescence anisotropy in the absence of analyte.

mechanism or the knowledge of the secondary/tertiary structure to engineer the aptameric probe.[15] In indirect FPAA approaches, the FP signal results from the competition between the target and an additional species, i.e., a fluorescent analogue in "conventional" competitive assay,[11] a fluorescent complementary strand (CS) in structure switching assay,[12,13] or an enzyme in aptamer enzymatic cleavage protection assay,[16] for binding to the aptamer. However, the ability of the fluorophore to rotate independently from the global motion of the tracer (classically referred as the "propeller effect") can significantly reduce the FP signal for the bound state.[19,20] In addition, as typically reported for FP-based DNA hybridization monitoring,[17,18] the low molecular weight difference between the free CS and the CS−aptamer duplex limits the fluorescence anisotropy variation window in structure switching FPAA. Due to the partial protection of the complexed DNA substrate against enzymatic attack, the fluorescence anisotropy change can also be of weak magnitude using the aptamer enzymatic cleavage protection strategy.[16] Finally, the synthesis of the fluorescently labeled analogue in conventional competitive FPAA can be laborious, with limited possibilities to functionalize the small molecule target, leading to a poor capability to manipulate both the binding affinity and the fluorescent properties of the tracer. Very recently, two approaches based on a mass amplifying strategy have been proposed to improve the FP assay response.[21,22] However, one method, coupling a targeting aptamer to a molecular mass amplifying aptamer,[21] does not ameliorate the FP signal change relative to that of the


dx.doi.org/10.1021/ac301552e | Anal. Chem. XXXX, XXX, XXX−XXX

previously described FPAA. The other one, dependent on $SiO_2$ nanoparticle-mediated mass enhancement,[22] requires the time-consuming preparation of the DNA−nanoparticle conjugates and a careful design of the aptamer probe.

Single-stranded binding (SSB) proteins are essential proteins for stabilization and access control to ssDNA within cells. One of them, SSB from *Escherichia coli*, is involved in several processes through interaction with enzymes as well as the formation of RecA filaments on DNA. SSB exists as a stable homotetramer, each subunit having an $M_w$ of ∼19 000, that is able to bind tightly to ssDNA but not to duplex DNA or stable folded ssDNA conformations.[23,24] These unique binding features have been taken into account to develop SSB-based analytical tools for detecting DNA hybridization, single nucleotide polymorphisms, and specific DNA−protein interaction through electrochemical, surface plasmon resonance imaging, fluorescent molecular beacon, gold nanoparticle, or capillary electrophoresis approaches.[25−28]

Here, we describe a new FPAA strategy utilizing the *E. coli* SSB protein as a signal enhancer tool. The general concept is illustrated in Figure 1a. In such a method, the fluorescently labeled aptamer is used as an FP probe. The first objective of the present approach was to establish a potentially general methodology by exploiting the ability of the SSB protein to bind the DNA aptamer in its free state but not in its target-bound folded one (Figure 1a). The second objective of the SSB-assisted strategy was to improve the FP signal by acting rationally on both the global and local fluorescence anisotropy contributions. The SSB−DNA complex was assumed to exhibit a much more important molecular size, due to the high molecular weight of the protein (∼76 000), than the free oligonucleotide. Thus, a large global diffusion difference between the target- and SSB-bound aptamer probes was expected, just like in conventional FPAA dedicated to protein analysis.[4−9] Furthermore, ssDNA is known to be strongly coiled around the SSB protein so that close contacts should occur between the aptamer and the protein.[24] This would lead to restricted DNA flexibility and/or hindered label motion in the SSB-bound state and then would limit the interfering propeller effect. Finally, due to the ease of synthesis and modification of oligonucleotides, different kinds of fluorophores can be readily introduced into specific sites of aptamers. This should allow the wide random screening of various labeled aptamers to select the appropriate tracer with convenient signaling features.

To test the feasibility of the SSB-assisted FPAA method and establish the proof-of-principle, the antiadenosine (Ade)−DNA aptamer (Apt-A) was first used as a model functional nucleic acid.[29] A competitive displacement model was developed to describe the mechanistic aspects of the SSB-assisted FPAA and consider the critical factors involved in the FP response. The optimal tracer was selected, and the methodology performances were investigated under buffer and realistic medium conditions, i.e., in diluted human serum. The general applicability of the present strategy was subsequently appreciated using another aptamer system, i.e., the antiargininamide (Rm) aptamer (Apt-R).[30] Finally, to further examine the broad usefulness of the SSB-assisted approach, the possibility of applying the SSB-assisted principle to a split aptamer biosensing platform[31] was also explored.

## EXPERIMENTAL SECTION

**Chemicals and Apparatus.** Adenosine (Ade), argininamide (Rm), inosine (Ino), tris(hydroxymethyl)aminomethane (Tris), and human serum were obtained from Sigma-Aldrich (Saint-Quentin, France). NaCl and $MgCl_2$ were obtained from Chimie-Plus Laboratoires (Bruyères de Pouilly, France) and Panreac Quimica (Barcelona, Spain), respectively. *E. coli* single-stranded DNA binding protein (SSB) was obtained from Tebubio (Le Perray en Yvelines, France). Water was obtained from a Purite Still Plus water purification system (Thame, U.K.) fitted with a reverse osmosis cartridge. All the unlabeled and fluorescein (F) or Texas Red (TR) labeled DNA oligonucleotides were synthesized and HPLC-purified by Eurogentec (Angers, France), and their identity was confirmed by MALDI-TOF mass spectrometry. The sequences of the aptamer, scramble, and split aptamer oligonucleotides studied are listed in Table IS (Supporting Information). Fluorescence anisotropy readings were taken on a Tecan Infinite F500 microplate reader (Männedorf, Switzerland) using black, 96-well Greiner Bio-One microplates (Courtaboeuf, France). Excitation was set at 485 ± 20 or 585 ± 20 nm, and emission was collected with 535 ± 25 or 635 ± 30 nm bandpass filters in relation to the nature of the fluorescent dyes.

**Assay Protocols.** The binding buffer for the Ade assay consisted of 50 mM Tris−HCl, pH 7.5, 5 mM NaCl, and 20 mM $MgCl_2$. The binding buffer conditions for the Rm assay were 10 mM Tris−HCl, pH 7.5, and 100 mM NaCl. The SSB and different aptamer stock solutions were prepared in pure water and stored at −20 °C. The working aptamer solutions were obtained by adequate dilution of the stock solution in 2.5× concentrated binding buffer. Prior to the first use, the working solutions were heated at 80 °C for 5 min and left to stand at room temperature for 30 min. The analyte solutions were prepared in water. All solutions were filtered prior to use through 0.2 μm membranes. To construct the SSB saturation curve, the aptamer (10 nM) and SSB (from 0 to 0.84 μM) solutions were mixed into the individual wells (final volume 100 μL) at room temperature for 30 min. Blank wells of the microplate received 100 μL of the binding buffer. To construct the competition displacement curves, the oligonucleotides were first mixed with SSB for 5 min. The analyte was then added, and the resulting solution was incubated for 30 min at room temperature. These samples were transferred into the individual wells (final volume 100 μL). For the Ade titration curve, the analyte concentration varied from 0 to 2000 μM (unless otherwise stated), and for the Rm titration curve, the analyte concentration varied from 0 to 5000 μM. The microplate was immediately placed into the microplate reader for the measurement. All experiments were done in triplicate. Human serum samples were used to test the Ade assay performances under biological conditions. Samples were diluted in water spiked with the target and filtered through 0.2 μm membranes. Three replicate samples were then analyzed as described above. For sandwich-like assay, the half-pieces of a slightly modified version of Apt-A (St1* and St2; see Table IS, Supporting Information) were mixed (10 nM St1* with an St1*:St2 stoichiometry of 1:8) for a 5 min period at room temperature, in the absence or presence of SSB, using the same binding buffer used above. As St1* and St2 are shorter oligonucleotides (13-mer), the SSB concentration in the reaction mixture was increased relative to that of the full aptamer experiments (St1*:SSB stoichiometry of 1:167) to


dx.doi.org/10.1021/ac301552e | *Anal. Chem.* XXXX, XXX, XXX−XXX

obtain a sufficient fraction of the SSB-bound probe. The target was then introduced into the reaction solution (0−2000 $\mu$M Ade concentration range), and the resulting mixture was incubated for 30 min at room temperature.

The measured fluorescence anisotropy ($r$) was calculated by the instrument software as follows:

$$r = \frac{I_{vv} - GI_{vh}}{I_{vv} + 2GI_{vh}} \quad (1)$$

$I_{vv}$ and $I_{vh}$ are the vertically and horizontally polarized components of the emission after excitation by vertically polarized light. The instrumental correction factor $G$ was determined from standard solutions according to the manufacturer's instructions. The model equations (Supporting Information) were fitted to the fluorescence anisotropy data using the software Table Curve 2D (SPSS Science Software GmbH, Erkrath, Germany).

## RESULTS AND DISCUSSION

**Feasibility of SSB-Assisted FPAA.** The proof-of-principle of the SSB-assisted FPAA was first investigated using the antiadenosine (Ade)−DNA aptamer (Apt-A) couple. This choice was motivated by the fact that the binding and structural properties of Apt-A have been very well studied and characterized in previous works.[32] In the unbound state, Apt-A is constituted of two short stems and a large, unstructured internal bubble, while the target-bound aptamer folds into a stabilized structure through the formation of base mismatches and three-base platforms (Figure 1S, Supporting Information). 5′-End fluorescein-labeled Apt-A (5′-F-Apt-A) was used as an FP probe. In initial experiments, the FP titration curve of 5′-F-Apt-A with increasing SSB concentration was constructed to investigate the ability of SSB to bind DNA aptamer in its free form. Under the binding buffer conditions used, the measured $r$ value of 5-F-Apt-A (10 nM) was ∼0.100, lower than the theoretical one estimated previously (0.155).[15] This difference indicates that the fluorescein label displayed a significant degree of local motional freedom that contributed to the total fluorescence anisotropy. When the SSB protein was added to the medium, the $r$ value of the probe was strongly increased to reach 0.265 for the highest protein concentration (0.84 $\mu$M). This signal enhancement can be typically attributed to the expected increase in the molecular weight of 5′-F-Apt-A upon SSB binding, theoretically from ∼7000 for the free oligonucleotide to ∼84 000 for the complex. It has been previously demonstrated that the association between short oligonucleotides (in the 27−35-mer range) and the SSB protein follows multiple stages.[24] For low protein-to-DNA ratios, two oligonucleotide molecules can interact with each SSB tetramer (considering that one SSB subunit may bind a ∼15-mer-long DNA),[33] while only the 1:1 DNA−SSB complex can be stably formed under excess protein conditions.[24] In addition, the high fluorescence anisotropy value of the SSB−Apt-A complex suggests that the local mobility of the dye (propeller effect) was significantly reduced in the SSB-bound state of the aptameric tracer. A previous work has reported that the fluorescence anisotropy of protein-bound DNA probes ($M_w$ > 100 000) displayed an $r$ value higher than ∼0.240 when the local motional freedom of the fluorophore was hindered by close contacts between the interacting partners.[34] It is well established that SSB binds to DNA by disrupting secondary structures and inducing nucleic acid to wrap around the protein so that close interactions occur between both the nucleic acid backbone and bases and the protein.[23,24] This would govern the strong coupling of the fluorophore with SSB, explaining the very high FP signal increase for the tracer.

The feasibility of the SSB-assisted FPAA approach was subsequently evaluated. The target was added to the mixture containing the DNA−SSB complex (1:33 stoichiometry). The solution was incubated for a 30 min period at room temperature, and the fluorescence anisotropy was then measured. As shown in Figure 1b, the fluorescence anisotropy value decreased very significantly, as exemplified by the FP change ($\Delta r = r - r_0$, where $r_0$ is the fluorescence anisotropy in the absence of analyte) of −0.135 observed in the presence of 5 mM Ade. This result reflects the decrease in the molecular size of the probe upon target binding, confirming that the structured state of the target-bound aptamer allowed the release of the DNA oligonucleotide from the SSB protein. Such an effect is in accordance with previous results from Krauss at al., who have shown that stable folded conformations are unfavorable for the binding to the SSB protein.[23] A control experiment was performed using a 5′-end fluorescein-labeled scramble sequence of Apt-A as the tracer. The $r$ value did not vary significantly when the Ade concentration increased (Figure 1b), indicating that the fluorescence anisotropy change was dependent on the specific target binding to Apt-A.

FPAA experiments were performed under a direct format, i.e., without SSB in the reaction medium, to examine the eventual FP signal change attributable to the target-induced fit mechanism. The titration curve of the probe with increasing target concentration showed that the addition of the target did not change the $r$ value for 5′-F-Apt-A (Figure 1b). These data demonstrate the advantage of the present strategy relative to the direct format one. In accordance with previous studies,[15,32,35,36] the 25-mer Apt-A did not undergo, upon analyte binding, a sufficiently high structural change in the extremity region (Figure 1S, Supporting Information) to trigger a direct assay response. In contrast, the SSB-assisted FPAA allowed generation of a great fluorescence anisotropy signal due to the strong modification of the DNA structure between the protein-induced unfolded state and the target-mediated folded one of the aptameric probe. Such data reveal also that the FP signal variation with increasing Ade concentration was dependent solely on the target-promoted displacement of the probe from the SSB protein.

**Study of the SSB-Assisted FPAA Mechanism.** An important issue to address was how to quantitatively describe the target-induced release of aptamer tracer from the SSB protein to (i) consider the contributions of the key parameters involved in the assay response and (ii) select a good tracer candidate for Ade sensing. The SSB-assisted FPAA mechanism was considered through the development of a competitive displacement model. Model equations (eqs 1S−6S) and simulated competitive displacement curves (Figure 2S) are presented in the Supporting Information.

The insertion of a label on a DNA sequence as well as the nature of the fluorophore may affect the affinity of a nucleic acid for interacting partners[4,37,38] through various mechanisms such as direct contact with the fluorophore, change in accessibility, modification of the nucleic acid conformation, steric hindrance effects, etc. In addition, the photophysical properties of a fluorescent nucleic acid conjugate are highly sensitive to the surrounding environment of the dye[39,40] so that significant changes in the fluorescence parameters typically


dx.doi.org/10.1021/ac301552e | Anal. Chem. XXXX, XXX, XXX−XXX

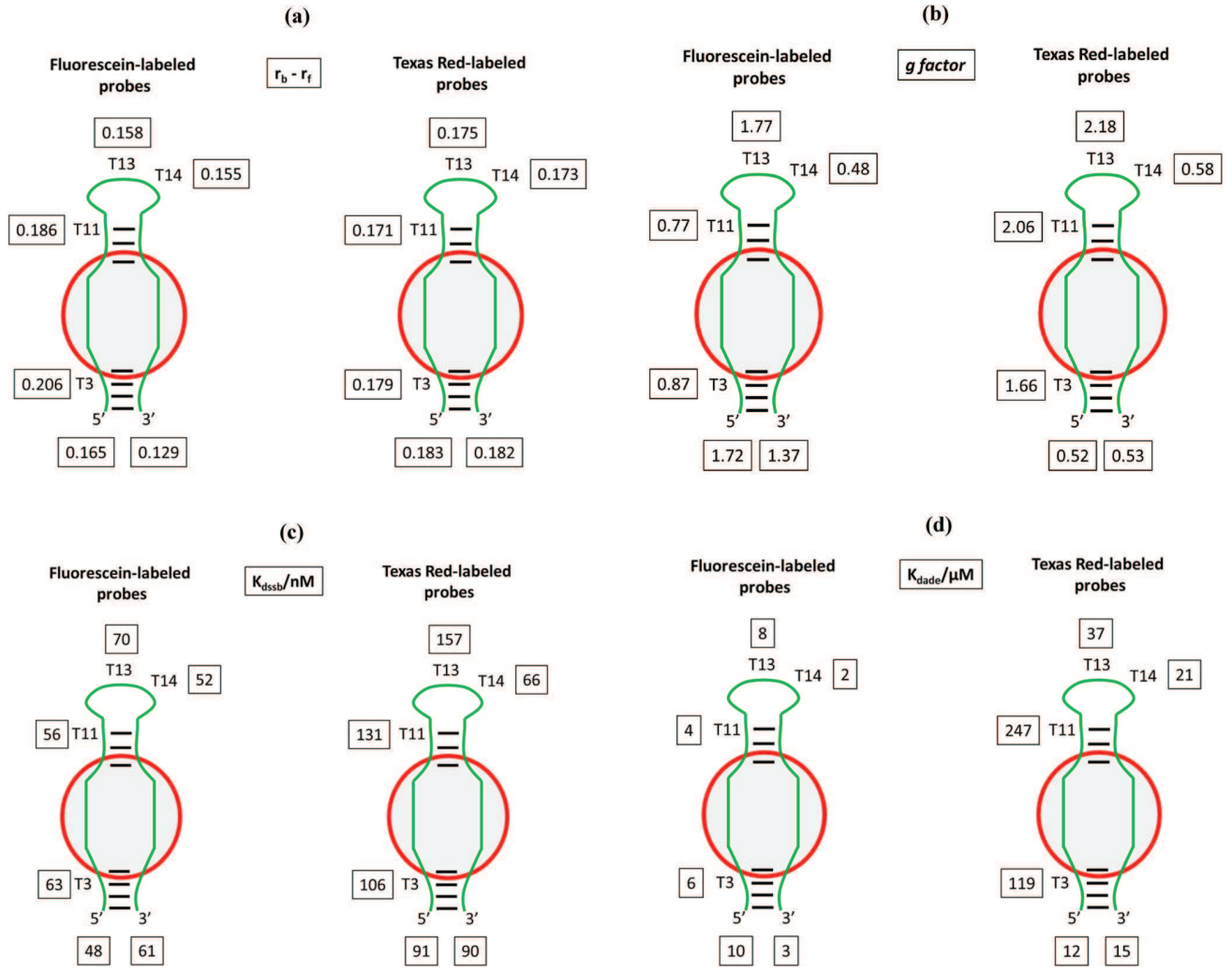


**Figure 2.** Summary of the fluorescent and binding affinity parameters extracted from the analysis of the SSB saturation and competitive displacement curves obtained with the different Apt-A probes tested: (a) $r_b - r_f$ ($r_f$ and $r_b$ are the fluorescence anisotropies for the free and SSB-bound probes, respectively), (b) $g$ factor (ratio of the total emission intensity of the SSB-bound probe to that of the free probe), (c) $K_{dssb}$ ($K_d$ for the SSB−Apt-A complex), (d) $K_{dade}$ ($K_d$ for the Ade−Apt-A complex). All these parameters are presented in relation to the labeling site and fluorophore nature of the probes (the binding pocket is encircled).

occur upon molecular interactions.[37,41] In this context, the Ade-induced FP signal variation achieved with Apt-A labeled with two fluorophores at different sites was explored. A wide set of experimental data obtained from a dozen different tracers were faced to the theoretical model to appreciate the relevance of this approach.

Five other Apt-A probes, terminally or internally labeled on thymidine by fluorescein (3′-end, T3, T11, T13, and T14 locations), were first tested. The SSB titration curves were constructed as reported for the 5′-F-Apt-A tracer (Figure 3S, Supporting Information). The maximal variation range of fluorescence anisotropy ($r_b - r_f$, where $r_f$ and $r_b$ are the respective fluorescence anisotropy for the free and SSB-bound tracers) and the $g$ factor (the ratio of the total emission intensity of the SSB-bound tracer to that of the free tracer) varied with the dye position, from 0.130 to 0.200 and from 0.5 to 1.8, respectively (Figures 2a,b). Binding isotherms displayed a sigmoid shape in all cases, in accordance with previous results obtained for the interaction between short fluorescently labeled ssDNA and SSB.[42] From such binding isotherms, the apparent $K_d$ values for the SSB−Apt-A complexes ($K_{dssb}$) were extracted by the Hill model equation (4S, Supporting Information) fitting (Figure 3S). As can be seen in Figure 2c, $K_{dssb}$ was in the 50−70 nM range (with an average Hill coefficient of 2.25). This is in agreement with the binding data of Webb and co-workers, who reported a $K_d$ value of 43 nM for the dT27−SSB complex.[24]

Ade titration curve experiments were then performed with the different probes for the DNA:SSB stoichiometry of 1:33. As shown in Figure 4S (Supporting Information) for two representative probes (T14- and T13-F-Apta-A), the $r$ value decreased when the target molecule was introduced into the sample. No change in the $r$ and total emission intensity values was observed upon Ade addition in the direct format (without SSB in solution) whatever the probe. In addition, for the most displaced probe (T14-F-Apta-A), the $r$ value returned roughly to its original value in the presence of 2 mM Ade (0.079 versus 0.071). This reveals that the target-bound aptamer probe interacted weakly, if at all, with the SSB protein. The displacement model equation (6S, Supporting Information) was then fitted to the $r$ versus Ade concentration plots. Excellent agreement of the predicted fluorescence anisotropy signal with the experimentally obtained response was achieved


dx.doi.org/10.1021/ac301552e | Anal. Chem. XXXX, XXX, XXX−XXX

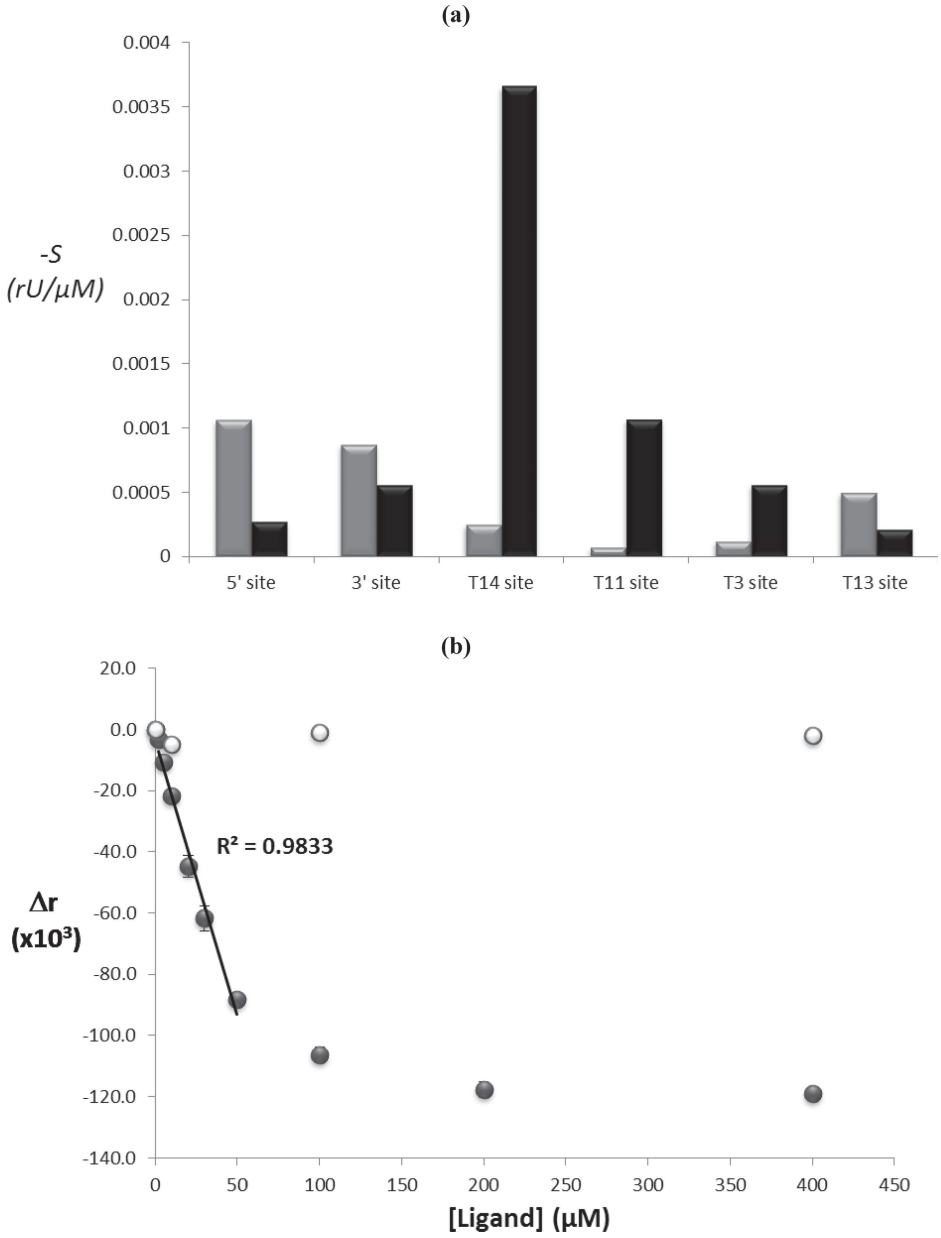


**Figure 3.** (a) First derivative ($S$) of the fitted displacement curves as a function of the labeling site and dye type (black, F-Apt-A; gray, TR-Apt-A) of the probes. (b) Calibration curve for Ade (black symbols) using the most efficient T14-F-Apt-A probe. White symbols represent the data for the noncognate ligand Ino. The probe concentration was 10 nM and the SSB concentration 0.25 $\mu$M. Binding buffer conditions: 50 mM Tris−HCl, pH 7.5, 5 mM NaCl, 20 mM $MgCl_2$. $\Delta r = r - r_0$, where $r_0$ is the fluorescence anisotropy in the absence of analyte.

(Figure 4S). The $K_d$ values for the Ade−Apt-A complex ($K_{dade}$) were estimated from the nonlinear regression fit. To note, these values constitute solely apparent data as the system is known to form a 1:2 stoichiometry complex.[32] $K_{dade}$ was in the 2−10 $\mu$M range with an average value of 5 $\mu$M (Figure 2d). Such data are in very good agreement with the previously reported apparent dissociation constant for this aptamer−target couple observed in solution and under label-free conditions (6 ± 3 $\mu$M),[29] suggesting the suitability of the proposed model. These data also indicate also that the labeling by the fluorescein dye roughly maintained the molecular recognition properties of the aptamer for the attachment sites studied.

To further investigate the pertinence of the model, another set of data was gathered using Apt-A labeled with Texas Red on the same locations. Such a fluorophore was chosen as its electrostatic and photophysical properties differ a lot from those of fluorescein.[39] The six Texas Red-labeled probes were titrated by SSB, and the target-induced displacement curves were constructed. To note, as reported for the fluorescein-labeled tracers, both the $r$ and total emission intensity values did not change significantly upon Ade addition under the direct format. Two representative examples of such curves are presented in Figure 4S (Supporting Information) with data derived from the equation (6S, Supporting Information) fitting procedure. Theoretical data appeared in very good agreement with the experimental ones, confirming the results obtained with the fluorescein-labeled probes. The parameters extracted from experimental results and fitting processes are also reported in Figure 2.


dx.doi.org/10.1021/ac301552e | Anal. Chem. XXXX, XXX, XXX−XXX

Some general trends were brought out from the data collected for the 12 tested probes. The replacement of fluorescein by Texas Red had strong effects on the apparent $K_{dade}$ value (Figure 2d). From an aggregate point of view, the Texas Red-labeled probes displayed a mean value of about 75 $\mu$M, i.e., 15-fold higher than that observed for the fluorescein-labeled probes (5 $\mu$M). Such behavior could be attributed to the fact that, in contrast to the anionic fluorescein, the cationic Texas Red dye is able to interact strongly with the DNA helix through van der Waals and electrostatic interactions.[39,40] This would lead to some critical changes in the active conformation/structure of the aptamer and/or steric hindrance effects at the binding site. For instance, an important loss of affinity was observed for the Texas Red labeling position flanking the central binding pocket of the aptamer, i.e., at the T3 and T11 locations (Figure 2d). Smaller differences were observed for the sites located in the apical loop and at the 3′-end site, while no significant perturbation was reported at the 5′-end position (Figure 2d).

The $K_{dssb}$ values were also affected by the nature of the fluorophore, but to less extent (Figure 2c). The average value was 110 nM for the Texas Red-labeled tracers, i.e., about 2-fold higher than that observed for the fluorescein-labeled probes (60 nM). Previous works have demonstrated that the structure of DNA labeled with the Cy3 cationic fluorophore can be stabilized through stacking interactions between the dye and DNA base pairs.[43] Thus, considering the positions of the fluorophore, it could be expected that interactions between Texas Red and DNA bases would favor short base-paired regions of the aptamer (Figure 1S, Supporting Information) to the detriment of the single-stranded structure, reducing the affinity of SSB for the Texas Red-labeled probe.

Although the mean values of the maximal fluorescence anisotropy change were comparable for the two kinds of tracers (0.167 versus 0.177), the signal variation ranges were almost identical for the Texas Red-labeled probes, whereas they varied more importantly for the fluorescein-labeled probes (Figure 2a). This could result very likely from the well-known coupling of Texas Red to the rotational dynamics of the aptamer, i.e., the lower contribution of the dye local mobility to the total fluorescence anisotropy.[40] Moreover, the higher $r$ values observed using the Texas Red-labeled probes (Figure 4S, Supporting Information) were consistent with a dye motion which was significantly coupled to the rotational mobility of DNA.

Finally, the $g$ factor exhibited similar average values for the F- and TR-Apt-A tracers (1.15 versus 1.25). However, as a result of specific site-dependent changes in the fluorophore local environment from the free to SSB-bound states of tracers, a significant variability was reported in both cases (Figure 2b).

**Performances of the Ade SSB-Assisted FPAA.** Figure 3a shows the first derivative ($S$) of the fitted displacement curves as a function of the labeling site and dye type of the probes studied. Such a parameter corresponds to the sensitivity of the SSB-assisted FPAA, i.e., the fluorescence anisotropy unit (rU) per Ade concentration, attained with the various tracers. As a consequence of the relative contributions of the binding affinity and fluorescent parameters reported above (Figure 2), strong differences in the $S$ values were obtained for both fluorescein- and Texas Red-labeled probes. These ranged from $-0.07 \times 10^{-3}$ to $-1.06 \times 10^{-3}$ rU/$\mu$M for TR-Apta-A and from $-0.21 \times 10^{-3}$ to $-3.65 \times 10^{-3}$ rU/$\mu$M for F-Apta-A, i.e., a variation of the assay sensitivity by a factor of ∼15−17 by modifying solely the attachment position of the dye. The assay sensitivity can be further enhanced by a factor as high as ∼50 when the nature of the fluorophore is also considered (T11-TR-Apt-A versus T14-F-Apt-A).

The performances of the Ade SSB-assisted FPAA were then analyzed using the most efficient T14-F-Apta-A tracer. The DNA:SSB complex stoichiometry was adjusted to 1:25 to increase the assay sensitivity while maintaining a valuable signal variation window. Under buffer conditions, a $\Delta r$ value of −0.120 was found over the 0−400 $\mu$M Ade concentration range (Figure 3b). As a comparison, the fluorescence anisotropy changes reported previously for small target molecule sensing did not exceed 0.065 whatever the format used,[11−16,21] except in a very recent case of nanoparticle-based mass amplifying approach.[22] It is also instructive to highlight that even direct FPAA for protein determination displayed typically lower assay responses, in the 0.050−0.100 range.[4−8,10] The detection limit, based on a signal-to-noise ratio >3, was equal to 1 $\mu$M with a linear range of 2−50 $\mu$M, $R^2$ = 0.9833 (Figure 3b). This limit of detection was better than those commonly obtained with most aptasensing methodologies based on a simple and homogeneous format,[36,44−50] i.e., excluding aptasensors that require a surface immobilization step of aptamer or target or a sophisticated amplification approach (Table IIS, Supporting Information). Moreover, the Ade detection limits attained under direct (using the previously engineered, truncated 21-mer Apt-A probe)[15] and enzymatic cleavage protection[16] FPAA formats were 10 and 5 $\mu$M, respectively. The relative standard deviation ranged from 0.3% to 3.0%, showing the high repeatability of the method. The specificity of the assay was demonstrated using inosine (Ino) as a structurally related compound (Figure 3b).

The ability of the SSB-assisted FPAA to function under realistic conditions, i.e., in diluted human serum, was also examined. The fluorescence anisotropy was found to increase as the dilution factor decreased. For example, the $r_0$ values were equal to 0.203, 0.216, 0.224, and 0.245 for the buffer and 50-, 10-, and 5-fold-diluted human serum conditions, respectively. This behavior could be attributed, at least in part, to the matrix proteins interacting nonspecifically with DNA as well as the viscosity modification of the reaction medium. Nevertheless, as shown in Figure 5S (Supporting Information), the FP signal change was roughly maintained, even in 5-fold-diluted serum, suggesting the practical potential of the sensing methodology.

It is important to note that, in terms of analytical performances, the main drawback of the present FPAA approach was related to the significant stability difference observed between the SSB−aptamer and target−aptamer complexes. Indeed, the value of the overall dissociation constant for the competitive system, i.e., the $K_{dade}/K_{dssb}$ ratio, was found to be about 40 for the T14-F-Apta-A tracer (with a mean value for the F- and TR-Apt-A probes equal to ∼90 and ∼650, respectively). As predicted by the competitive displacement model (Supporting Information), this lowered the sensitivity potentialities of the assay. The use of other SSB proteins, which display features similar to those of *E. coli* SSB but with a weaker binding affinity for ssDNA,[33] could possibly overcome this limitation and further improve the performances of the current aptasensor.

**General Applicability of the SSB-Assisted Strategy.** To subsequently evaluate the general applicability of the SSB-assisted strategy, the current approach was tested for (i)

another target−aptamer couple and (ii) a different aptasensing platform.

First, the antiargininamide (Rm) aptamer (Apt-R)[30] was chosen as an alternative biorecognition element of the SSB-assisted FPAA designed above (Figure 1a). The Apt-R structure is characterized by a stem−loop domain (Figure 6S, Supporting Information). The secondary structure stability of free Apt-R is assumed to be higher than that of unbound Apt-A due to a longer seven-base-pair stem.[51] Apt-R was labeled at the 5′-end by the fluorescein dye. The fluorescence anisotropy of the 5′-F-Apt-R probe was strongly increased when the SSB protein was added to the reaction medium, from 0.080 in the free state to 0.250 at the highest protein concentration tested. Under SSB-assisted FPAA conditions, the fluorescence anisotropy of the aptamer probe decreased from 0.225 (1:33 stoichiometry for DNA:SSB) to 0.110 with increasing Rm concentration, confirming the data reported above for the Ade−Apt-A system (Figure 6S). The direct format of FPAA was also performed. In the absence of SSB, the $r$ value was not significantly modified when the Rm concentration increased (Figure 6S), confirming the usefulness of the present approach. A control experiment with a 5′-end fluorescein-labeled scramble sequence of Apt-R was carried out using the same DNA:SSB stoichiometry. No change in the fluorescence anisotropy was observed, except at high Rm concentration where the signal slightly diminished.

Second, the possibility to expand the SSB-assisted strategy to another sensing design was evaluated by focusing our attention on the sandwich-like platform. Initially introduced by Stojanovic et al.,[31] this mode consisted of the assembly of split aptamer fragments mediated by the target (Figure 7S, Supporting Information). Such a method has been widely utilized to facilitate the transduction of the binding event into a detectable signal using different technologies such as optical or electrochemical techniques.[31,48,52] In initial experiments, the feasibility to develop an FPAA based on the sandwich-like design was explored using Apt-A as a model aptamer. It is of interest to note that such an FP-based assay has not yet been reported in the literature. The 25-mer Apt-A was cut in the apical loop between the T13 and T14 sites, the T13 base was deleted, and one A·T base pair was added at the extremities.[32] A 13-mer DNA strand corresponding to half of such an Apt-A sequence was labeled at the 5′-end by the fluorescein dye (St1*, 10 nM). The addition of the second nonlabeled piece of Apt-A (St2) at a 1:8 stoichiometry (St1*:St2) did not change the fluorescence anisotropy ($r$ = 0.070) due to the lack of association between the two DNA fragments in the absence of Ade. When the target was introduced into the reaction medium, the formation of the ternary complex (St1*−Ade−St2) led to an increase in the FP signal. However, the FP response was low ($\Delta r$ = 0.025 at 2 mM Ade concentration), dependent on the weak change in the molecular size between the free St1* strand and the ternary complex (molecular weight theoretically from 3500 to 7500), associated probably with some propeller effect (Figure 7S). The Ade assay displayed linearity up to 200 $\mu$M with a limit of detection estimated at 15 $\mu$M. To work under SSB-assisted sandwich-like FPAA conditions, the protein was added to the reaction medium (fluorescent DNA:SSB stoichiometry of 1:167) following the same procedure described above (Figure 7S). In the absence of target, single-strand DNA pieces interacted strongly with SSB so that the FP signal increased from 0.070 to 0.195. Upon Ade addition, the structured, ternary complex was formed, leading to the release of the DNA fragments from the protein. Such behavior was associated with a large reduction of the fluorescence anisotropy, as exemplified by the $\Delta r$ value of −0.070 at 2 mM Ade concentration. This led to a wider dynamic linear range up to 600 $\mu$M with a detection limit of 10 $\mu$M (Figure 7S).

In summary, we have described a novel FPAA approach which is able to detect small target molecule binding through an SSB-based competitive displacement strategy. This approach presents several attractive features. First, as a consequence of the strong structural changes between SSB-induced unfolded and target-mediated folded states of the aptameric probe, the present mode allows generation of a response for aptamer probes which do not operate under the direct assay format. Second, a strongly improved FP assay response is reached relative to that obtained with the FPAA previously described due to the combined effects of the SSB protein on the molecular size and the local dye motion of the tracer during the interaction processes. Third, the assay is simple, homogeneous, and potentially applicable to target sensing under biological conditions. Finally, the strategy displays adaptability features as demonstrated by the results obtained through the sandwich-like assay configuration.

## ■ ASSOCIATED CONTENT

### Supporting Information

Tables IS and IIS, competitive displacement model, and Figures 1S−7S as noted in text. This material is available free of charge via the Internet at http://pubs.acs.org.

## ■ AUTHOR INFORMATION

### Corresponding Author

*E-mail: eric.peyrin@ujf-grenoble.fr.

### Notes

The authors declare no competing financial interest.

## ■ ACKNOWLEDGMENTS

This work was supported in part by a grant from the DGA program (09C7001). Z.Z. was supported by the China Scholarship Council fund from the Ministry of Education of the People's Republic of China.

## ■ REFERENCES

(1) Smith, D. S.; Eremin, S. A. *Anal. Bioanal. Chem.* **2008**, *391*, 1499−1507.
(2) Hunt, C. L.; Pasetto, P.; Ansell, R. J.; Haupt, K. *Chem. Commun.* **2006**, 1754−1756.
(3) Ton, X. A.; Acha, V.; Haupt, K.; Tse Sum Bui, B. *Biosens. Bioelectron.* **2012**, *36*, 22−28.
(4) Potyrailo, R. A.; Conrad, R. C.; Ellington, A. D.; Hieftje, G. M. *Anal. Chem.* **1998**, *70*, 3419−3425.
(5) Fang, X.; Cao, Z.; Beck, T.; Tan, W. *Anal. Chem.* **2001**, *73*, 5252−5757.
(6) Gokulrangan, G.; Unruh, J. R.; Holub, D. F.; Ingram, B.; Johnson, C. K.; Wilson, G. S. *Anal. Chem.* **2005**, *77*, 1963−1970.
(7) Li, W.; Wang, K.; Tan, W.; Ma, C.; Yang, X. *Analyst* **2007**, *132*, 107−113.
(8) Wang, M. S.; Black, J. C.; Knowles, M. K.; Reed, S. M. *Anal. Bioanal. Chem.* **2011**, *401*, 1309−1318.
(9) Zou, M.; Chen, Y.; Xu, X.; Huang, H.; Liu, F.; Li, N. *Biosens. Bioelectron.* **2012**, *32*, 148−154.
(10) Zhang, D.; Zhao, Q.; Zhao, B.; Wang, H. *Anal. Chem.* **2012**, *84*, 3070−3074.
(11) Wang, Y.; Killian, J.; Hamasaki, K.; Rando, R. R. *Biochemistry* **1996**, *35*, 12338−12346.

(12) Cruz-Aguado, J. A.; Penner, G. *Anal. Chem.* **2008**, *80*, 8853−8855.
(13) Zhu, Z.; Schmidt, T.; Mahrous, M.; Guieu, V.; Perrier, S.; Ravelet, C.; Peyrin., E. *Anal. Chim. Acta* **2011**, *707*, 191−196.
(14) Ruta, J.; Perrier, S.; Ravelet, C.; Fize, J.; Peyrin, E. *Anal. Chem.* **2009**, *81*, 7468−7473.
(15) Perrier, S.; Ravelet, C.; Guieu, V.; Roy, B.; Perigaud, C.; Peyrin, E. *Biosens. Bioelectron.* **2010**, *25*, 1652−1657.
(16) Kidd, A.; Guieu, V.; Perrier, S.; Ravelet, C.; Peyrin, E. *Anal. Bioanal. Chem.* **2011**, *401*, 3229−3234.
(17) Walker, T. G.; Linn, C. P.; Nadeau, J. G. *Nucleic Acids Res.* **1996**, *24*, 348−353.
(18) Kumke, M. U.; Li, G.; McGown, L, B.; Walker, G. T.; Linn, C. P. *Anal. Chem.* **1995**, *67*, 3945−3951.
(19) Jameson, D. M.; Ross, J. A. *Chem. Rev.* **2010**, *110*, 2685−2708.
(20) Moerke, N. J. *Curr. Protoc. Chem. Biol.* **2009**, *1*, 1−15.
(21) Cui, L.; Zou, Y.; Lin, N.; Zhu, Z.; Jenkins, G.; Yang, C. J. *Anal. Chem.* **2012**, *84*, 5535−5541.
(22) Huang, Y.; Zhao, S.; Chen, Z. F.; Shi, M.; Liang, H. *Chem. Commun.* **2012**, *48*, 7480−7482.
(23) Krauss, G.; Sindermann, H.; Schomburg, U.; Maass, G. *Biochemistry* **1981**, *20*, 5346−5352.
(24) Kunzelmann, S.; Morris, C.; Chavda, A. P.; Eccleston, J. F.; Webb, M. R. *Biochemistry* **2010**, *49*, 843−852.
(25) Kerman, K.; Morita, Y.; Takamura, Y.; Tamiya, E. *Anal. Bioanal. Chem.* **2005**, *381*, 1114−1121.
(26) Tan, Y. N.; Lee, K. H.; Su, X. *Anal. Chem.* **2011**, *83*, 4251−4257.
(27) Tang, D.; Liao, D.; Zhu, Q.; Wang, F.; Jiao, H.; Zhang, Y.; Yu, C. *Chem. Commun.* **2011**, *47*, 5485−5487.
(28) Berezovski, M.; Krylov, S. N. *J. Am. Chem. Soc.* **2003**, *125*, 13451−13454.
(29) Huizenga, D. E.; Szostak, J. W. *Biochemistry* **1995**, *34*, 656−665.
(30) Harada, K.; Frankel, A. D. *EMBO J.* **1995**, *14*, 5798−5811.
(31) Stojanovic, M. N.; de Prada, P.; Landry, D. W. *J. Am. Chem. Soc.* **2000**, *122*, 11547−11548.
(32) Lin, C. H.; Patel, D. J. *Chem. Biol.* **1997**, *4*, 817−832.
(33) Lohman, T. M.; Ferrari, M. E. *Annu. Rev. Biochem.* **1994**, *63*, 527−570.
(34) Wang, H.; Lu, M.; Tang, M. S.; Van Houten, B.; Ross, J. B. A.; Weinfeld, M.; Le, X. C. *Proc. Natl. Acad. Sci. U.S.A.* **2009**, *106*, 12849−12854.
(35) Nishihira, A.; Ozaki, H.; Wakabayashi, M.; Kuwahara, M.; Sawai, H. *Nucleic Acids Symp. Ser.* **2004**, *48*, 135−136.
(36) Urata, H.; Nomura, K.; Wada, S.; Akagi, M. *Biochem. Biophys. Res. Commun.* **2007**, *360*, 459−463.
(37) Jhaveri, S. D.; Kirby, R.; Conrad, R.; Maglott, E. J.; Bowser, M.; Kennedy, R. T.; Glick, G.; Ellington, A. D. *J. Am. Chem. Soc.* **2000**, *122*, 2469−2473.
(38) Zhang, D.; Lu, M.; Wang, H. *J. Am. Chem. Soc.* **2011**, *133*, 9188−9191.
(39) Unruh, J. R.; Gokulrangan, G.; Wilson, G. S; Johnson, C. K. *Photochem. Photobiol.* **2005**, *81*, 682−690.
(40) Unruh, J. R.; Gokulrangan, G.; Lushington, G. H.; Johnson, C. K.; Wilson, G. S. *Biophys. J.* **2005**, *88*, 3455−3465.
(41) Merino, E. J.; Weeks, K. M. *J. Am. Chem. Soc.* **2005**, *127*, 12766−12767.
(42) Wan, Q. H.; Le, X. C. *Anal. Chem.* **2000**, *72*, 5583−5589.
(43) Spiriti, J.; Binder, J. K.; Levitus, M.; van der Vaart, A. *Biophys. J.* **2011**, *100*, 1049−1057.
(44) Cheng, X. H.; Bing, T.; Liu, X. J.; Shangguan, D. H. *Anal. Chim. Acta* **2009**, *633*, 97−102.
(45) Xu, W.; Lu, Y. *Anal. Chem.* **2010**, *82*, 574−578.
(46) Xiang, Y.; Tong, A.; Lu, Y. *J. Am. Chem. Soc.* **2009**, *131*, 15352−15357.
(47) Yoshida, W.; Sode, K.; Ibebukuro, K. *Anal. Chem.* **2006**, *78*, 3296−3303.
(48) Liao, D.; Jiao, H.; Wang, B.; Lin, Q.; Yu, C. *Analyst* **2012**, *137*, 978−982.
(49) Lu, N.; Shao, C.; Deng, Z. *Chem. Commun.* **2008**, 6161−6163.
(50) Nishizawa, S.; Sato, Y.; Xu, Z.; Morita, K.; Li, M.; Teramae, N. *Supramol. Chem.* **2010**, *22*, 467−476.
(51) Bishop, G. R.; Ren, J.; Polander, B. C.; Jeanfreau, B. D.; Trent, J. O.; Chaires, J. B. *Biophys. Chem.* **2007**, *126*, 165−175.
(52) Chen, J.; Zhang, J.; Li, J.; Yang, H. H.; Fu, F.; Chen, G. *Biosens. Bioelectron.* **2010**, *25*, 996−1000.

# SUPPORTING INFORMATION

# Single-Stranded DNA Binding Protein-Assisted Fluorescence Polarization Aptamer Assay for Detection of Small Molecules

*Zhenyu Zhu, Corinne Ravelet, Sandrine Perrier, Valérie Guieu, Emmanuelle Fiore, Eric Peyrin**

*Département de Pharmacochimie Moléculaire UMR 5063, Institut de Chimie Moléculaire de Grenoble FR 2607, CNRS-Université Grenoble I (Joseph Fourier), 38041 Grenoble cedex 9, France.*

- Tables I-IIS
- Theoretical model
- Figures 1-7S

**Table IS.** List of oligonucleotides used.[a]

| Oligonucleotides | Sequences and labeling sites |
|---|---|
| 5'-F-Apt-A | 5'-CCTGGGGGAGTATTGCGGAGGAAGG-3' |
| 3'-F-Apt-A | 5'-CCTGGGGGAGTATTGCGGAGGAAGG-3' |
| T14-F-Apt-A | 5'-CCTGGGGGAGTATTGCGGAGGAAGG-3' |
| T11-F-Apt-A | 5'-CCTGGGGGAGTATTGCGGAGGAAGG-3' |
| T3-F-Apt-A | 5'-CCTGGGGGAGTATTGCGGAGGAAGG-3' |
| T13-F-Apt-A | 5'-CCTGGGGGAGTATTGCGGAGGAAGG-3' |
| 5'-TR-Apt-A | 5'-CCTGGGGGAGTATTGCGGAGGAAGG-3' |
| 3'-TR-Apt-A | 5'-CCTGGGGGAGTATTGCGGAGGAAGG-3' |
| T14-TR-Apt-A | 5'-CCTGGGGGAGTATTGCGGAGGAAGG-3' |
| T11-TR-Apt-A | 5'-CCTGGGGGAGTATTGCGGAGGAAGG-3' |
| T3-TR-Apt-A | 5'-CCTGGGGGAGTATTGCGGAGGAAGG-3' |
| T13-TR-Apt-A | 5'-CCTGGGGGAGTATTGCGGAGGAAGG-3' |
| Scramble 5'-F-Apt-A | 5'-AACGCGGAAGGGGTAGTTGTGGCGG-3' |
| Split 5'-F-Apt-A (St1*) | 5'-ACCTGGGGGAGTA-3' |
| Split Apt-A (St2) | 5'-TGCGGAGGAAGGT-3' |
| 5'-F-Apt-R | 5'-GATCGAAACGTAGCGCCTTCGATC-3' |
| Scramble 5'-F-Apt-R | 5'-CGATGGCCAGGTATCACACATGCT-3' |

[a]Each labeling site is underlined (green for fluorescein and red for Texas Red)

**Table IIS.** Comparison of the Ade detection limits for the existing aptasensors.[a]

| Assay strategy | Limit of detection | Ref |
|---|---|---|
| Fluorescence resonance energy transfer direct assay | 10 μM[b] | 36 |
| Label-free fluorescent direct assay | 10 μM | 44 |
| Label-free fluorescent direct assay | 20 μM | 45 |
| Label-free fluorescent direct assay | 3 μM | 46 |
| Enzymatic activity inhibition assay | 25 μM | 47 |
| Label-free fluorescent sandwich-like assay | 12 μM | 48 |
| G-quadruplex enzyme colorimetric direct assay | 6 μM | 49 |
| Label-free fluorescent direct assay | 2 μM | 50 |
| Direct FPAA | 10 μM | 15 |
| Enzymatic cleavage protection FPAA | 5 μM | 16 |
| SSB-assisted FPAA | 1 μM | This work |

[a]Excluding sensing platforms which involved heterogeneous format or sophisticated amplification approach
[b]Estimated from the Ade titration curve

**Theoretical model.** A competitive displacement model was developed to describe the target-induced FP signal change of the SSB-assisted FPAA. This is derived from the two following binding equilibria that involve the aptamer probe (Apt*), the protein (SSB) and the target (T):

SSB + Apt* ⇄ SSB.Apt* (1S)

T + Apt* ⇄ T.Apt* (2S)

For the binding equilibrium between SSB and aptamer, i. e. Eq (1S), the fraction of the SSB-bound aptamer ($f_b$) is derived from the measured fluorescence anisotropy $r$ as follows:[S1]

$$f_b = \frac{(r - r_f)}{g(r_b - r) + (r - r_f)} \tag{3S}$$

where $r_f$ and $r_b$ represent the anisotropy for the free and SSB-bound aptamer probe, respectively. The $g$ factor is derived from the ratio of the total emission intensity ($I$) of the SSB-bound aptamer probe ($I_b$) to that of the free tracer ($I_f$), i. e. $I_b/I_f$.[S1b] It is introduced into Eq (3S) in order to consider possible change in the fluorescence quantum yield of the probe between the two states.[S1a] Both $r_b$ and $I_b$ values can be estimated from the asymptote of the $r$ and $I$ *versus* SSB concentration curves. As frequently observed for DNA-protein associations,[S2] $f_b$ can be linked to the average dissociation constant of the aptamer-SSB complex ($K_{dssb}$) and the free concentration of SSB ([SSB]) through the Hill binding model:[S3]

$$f_b = \frac{[SSB]^{n_H}}{K_{dssb} + [SSB]^{n_H}} \tag{4S}$$

where $n_H$ corresponds to the Hill coefficient. Under conditions for which the total aptamer probe concentration ($c_{apt}$) is limiting ($c_{apt} \leq K_{dssb}/5$), the total concentration of SSB can closely approximate its free concentration. The presence of target in the reaction system can be accounted by introducing an additional competitive term into Eq (4S) as follows:[S4]

$$f_b = \frac{[SSB]^{n_H}}{K_{dssb}(1 + \frac{[T]}{K_{dtarget}}) + [SSB]^{n_H}} \tag{5S}$$

where $K_{dtarget}$ and [T] are the apparent dissociation constant of the target-aptamer complex and the free target concentration, respectively. Under limiting aptamer probe concentrations, the total concentration of target can be used in place of its free concentration into Eq (5S). In this relation, the interaction between the folded target-bound aptamer and the SSB protein is considered to be sufficiently weak to be neglected. Thus, combining Eqs (3S) and (5S), and assuming that the fluorescence anisotropy and total emission intensity values are similar for the free and target-bound aptamer states, the change of the probe fluorescence anisotropy when the target concentration varies is described by the following expression:

$$r = \frac{[SSB]^{n_H}\left(gr_b - r_f\right) + r_f\left\{K_{dssb}\left(1 + \frac{[T]}{K_{dtarget}}\right) + [SSB]^{n_H}\right\}}{g[SSB]^{n_H} + K_{dssb}\left(1 + \frac{[T]}{K_{dtarget}}\right)} \qquad (6S)$$

Figure 2S (see below) presents theoretical data, at a given SSB concentration, created from Eq (6S) for various $K_{dssb}$, $K_{dtarget}$, ($r_b$-$r_f$) and $g$ factor values (all other parameters being held constant). The increase in $K_{dssb}$ and ($r_b$-$r_f$) values and/or the decrease in $K_{dtarget}$ and $g$ factor values govern an enhancement of the displacement curve slope, i. e. an increase in the assay sensitivity. This is achieved at the expense of the FP signal variation range for the $K_{dssb}$ and $g$ factor effects.

---

**References**


(S1) (a) Jameson, D. M.; Ross, J. A. *Chem. Rev.* **2010**, *110*, 2685-2708. (b) Potty, A. S.; Kourentzi, K.; Fang, H.; Schuck P.; Willson, R. C. *Int. J. Biol. Macromol.* **2011**, *48*, 392-397.

(S2) Weinberg, R. L.; Veprintsev, D. B.; Fersht, A. R. *J. Mol. Biol.* **2004**, *341*, 1145-1159

(S3) Wilson, G. M. *Reviews in Fluorescence*; Springer Science: New York, 2005; Chapter 10.

(S4) Hieb, A. R.; D'Arcy, S.; Kramer, M. A.; White, A. E.; Luger, K. *Nucleic Acids Res.* **2012**, *40*, e33.

**Figure 1S.** Predicted secondary structures for the Apt-A probe and Apt-A-Ade complex (adapted from ref 32).

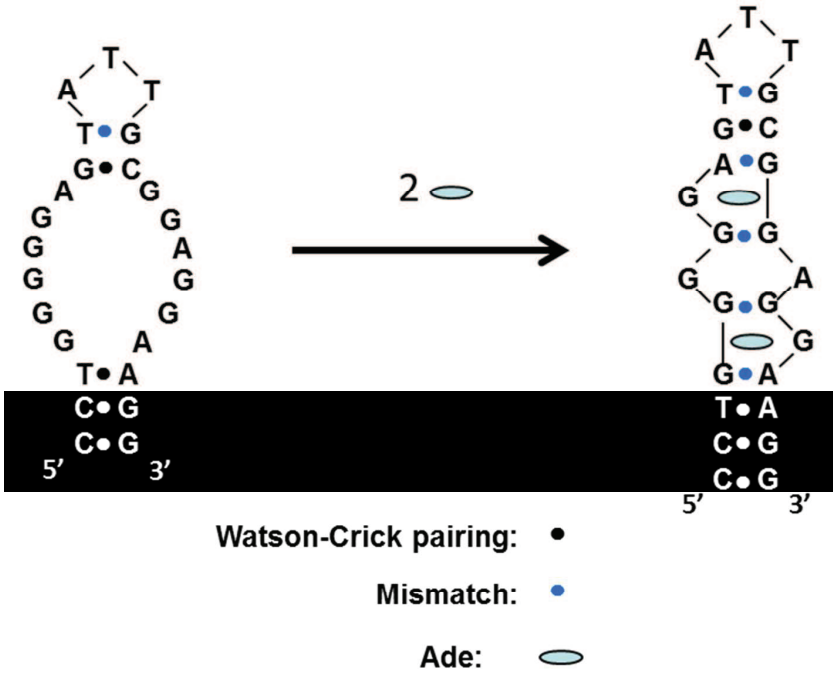

**Figure 2S.** Theoretical data created from Eq (6S) for different values of **(a)** $K_{dssb}$: 50 nM (triangles), 100 nM (diamonds) and 150 nM (squares); fixed parameters: $r_b$ = 0.250, $r_f$ = 0.100, $K_{dtarget}$ = 10 µM, *g* factor = 1. **(b)** $K_{dtarget}$: 40 µM (triangles), 10 µM (diamonds) and 2.5 µM (squares); fixed parameters: $r_b$ = 0.250, $r_f$ = 0.100, $K_{dssb}$ = 50 nM, *g* factor = 1. **(c)** ($r_b$-$r_f$): 0.200 (triangles), 0.150 (diamonds) and 0.100 (squares); fixed parameters: $r_f$ = 0.100, $K_{dssb}$ = 50 nM, $K_{dtarget}$ = 10 µM, *g* factor = 1. **(d)** *g* factor: 2.5 (triangles), 1 (diamonds) and 0.4 (squares); fixed parameters: $r_b$ = 0.250, $r_f$ = 0.100, $K_{dssb}$ = 50 nM, $K_{dtarget}$ = 10 µM. Total SSB concentration and $n_H$ are fixed to 300 nM and 2, respectively.

**(a)**

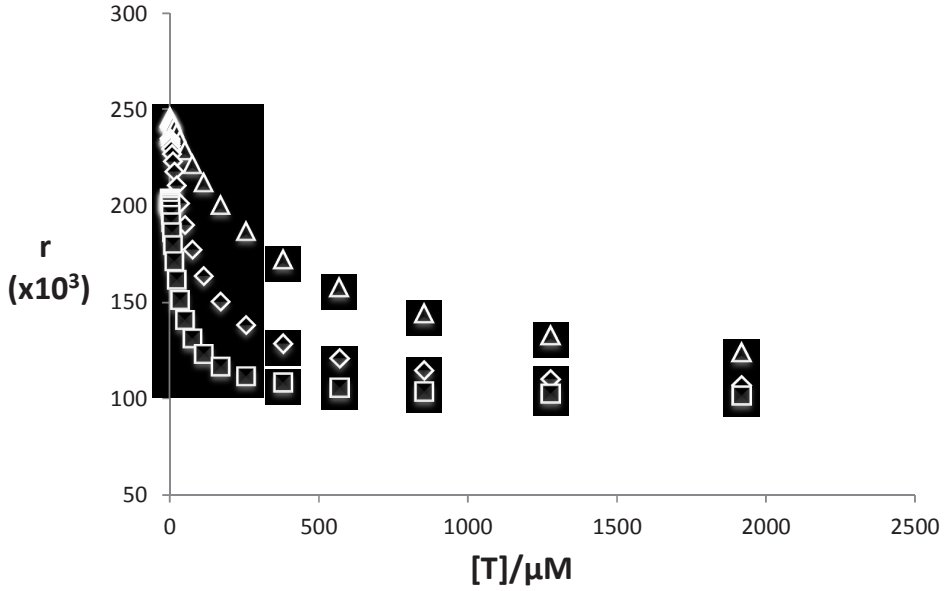


**(b)**

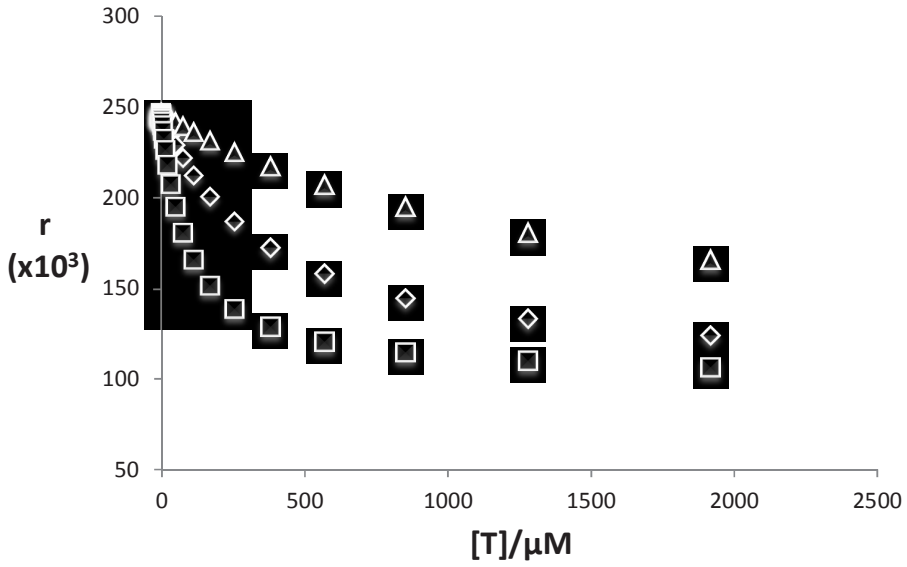

**(Continued)**

**(c)**

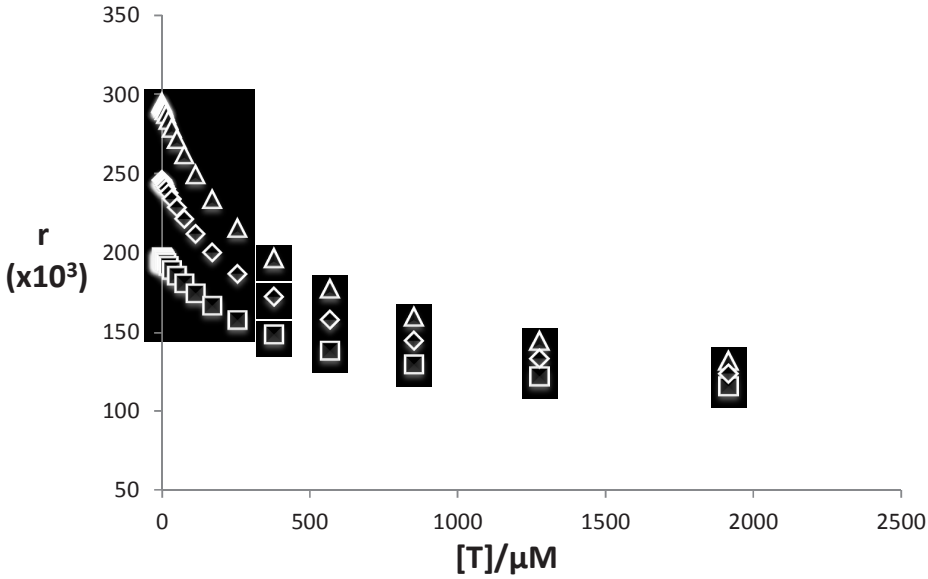


**(d)**

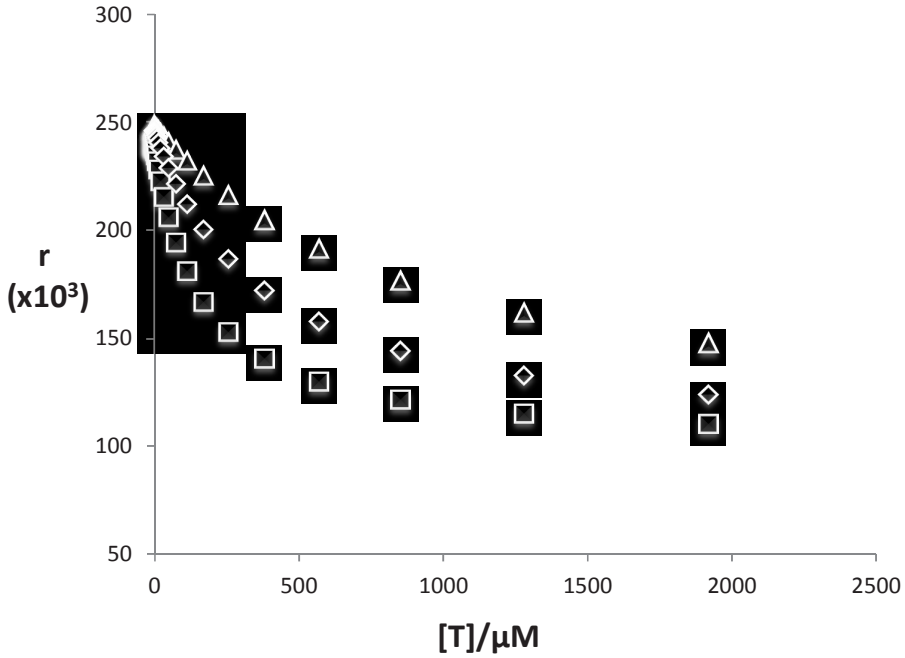

**Figure 3S.** SSB titration curve using the 5'-F-Apt-A probe. The theoretical curve (——) is recreated using equation parameters (see Figure 2 in the manuscript) obtained by fitting Eq (4S) to $f_b$. Probe concentration = 10 nM. Binding buffer conditions: 50 mM Tris-HCl, pH = 7.5, 5 mM NaCl, 20 mM $MgCl_2$.

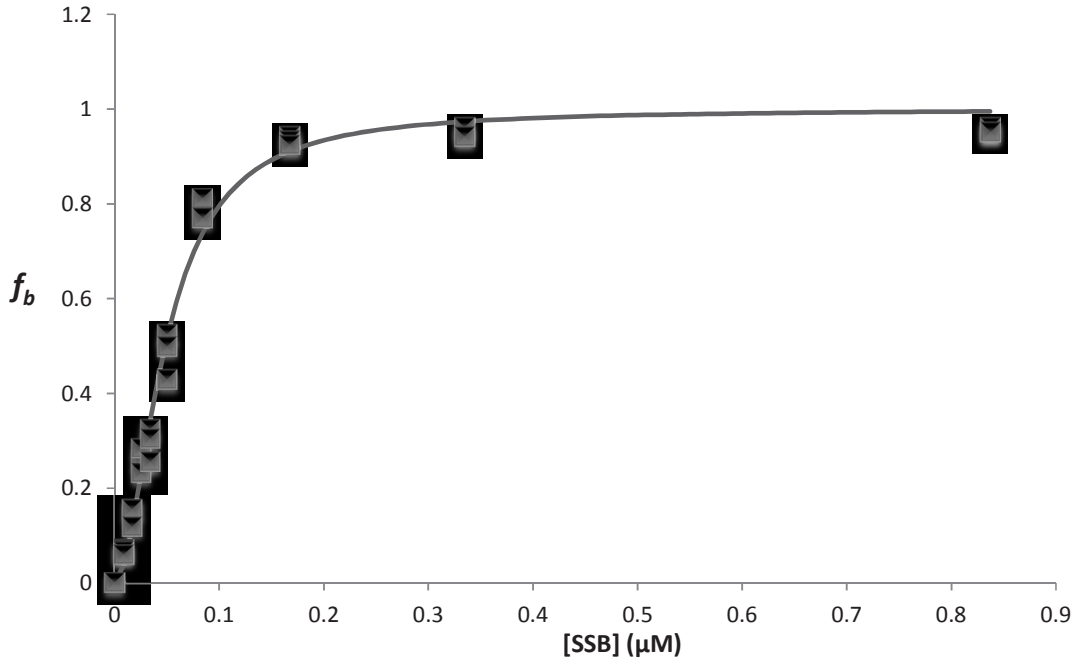

**Figure 4S.** Representative competitive displacement curves using T14-F-Apt-A (black circles), T13-F-Apt-A (white circles), 3'-TR-Apt-A (black squares) and T11-TR-Apt-A (white squares). The theoretical curves (——) are recreated using equation parameters (see Figure 2 in the manuscript) obtained by fitting Eq (6S) to *r*. Probe concentration = 10 nM. SSB concentration = 0.33 μM. Binding buffer conditions: 50 mM Tris-HCl, pH = 7.5, 5 mM NaCl, 20 mM $MgCl_2$.

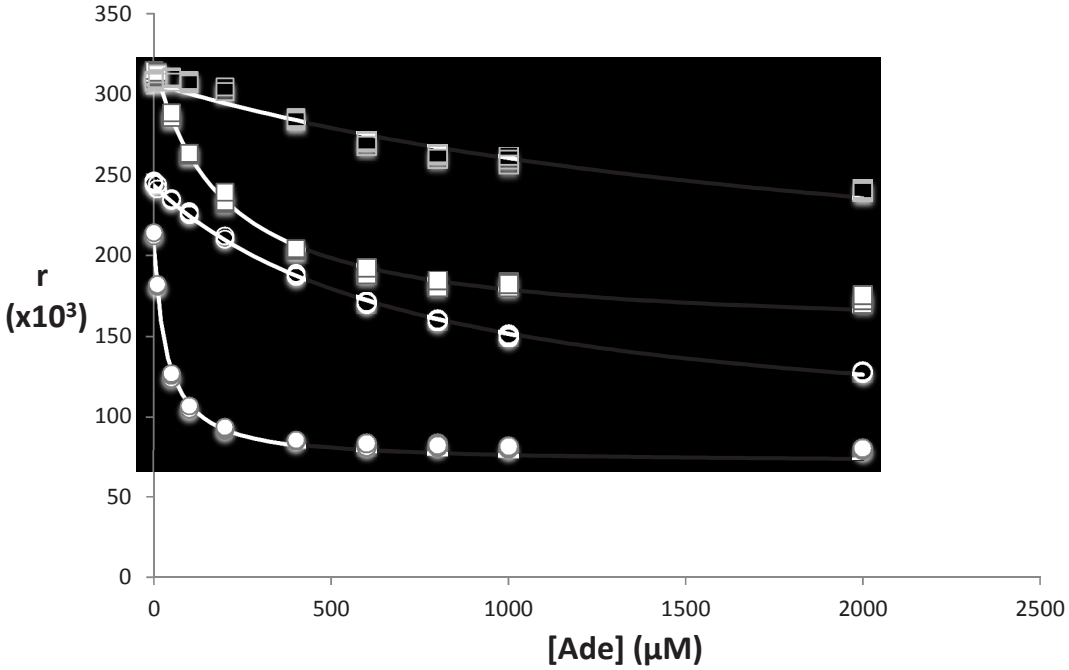

**Figure 5S.** Calibration curves for Ade using the T14-F-Apt-A probe under 50-fold (squares), 10-fold (triangles) and 5-fold (diamonds) diluted human serum conditions. Probe concentration = 10 nM. SSB concentration = 0.25 μM. $\Delta r = r - r_0$ where $r_0$ is the fluorescence anisotropy in absence of analyte.

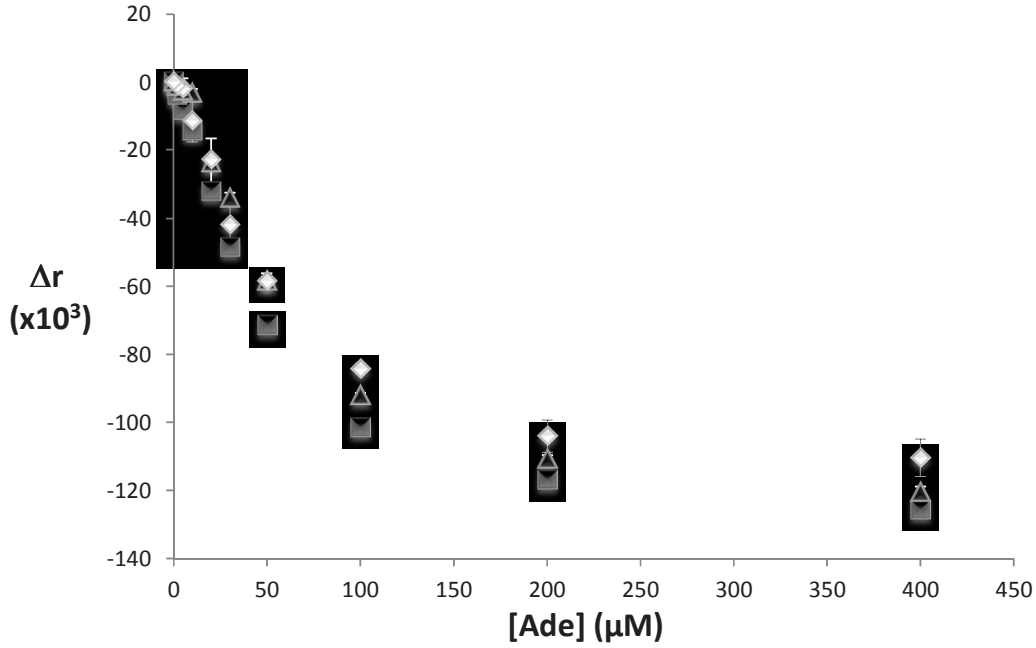

**Figure 6S. (a)** Predicted secondary structure for the Apt-R probe (adapted from ref 51). **(b)** Titration curves of 5'-F-Apt-R with increasing Rm concentration under SSB-assisted (black symbols) and direct (white symbols) FPAA modes. Grey symbols for SSB-assisted FPAA using the scramble 5'-F-Apt-R. Probe concentration = 10 nM. SSB concentration = 0.33 μM. Binding buffer conditions: 10 mM Tris-HCl, pH = 7.5, 100 mM NaCl. $\Delta r = r - r_0$ where $r_0$ is the fluorescence anisotropy in absence of analyte.

**(a)**

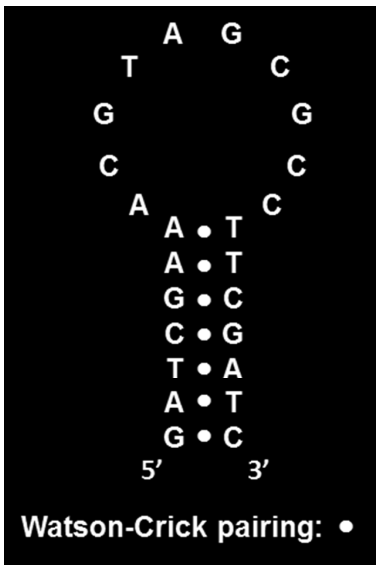


**(b)**

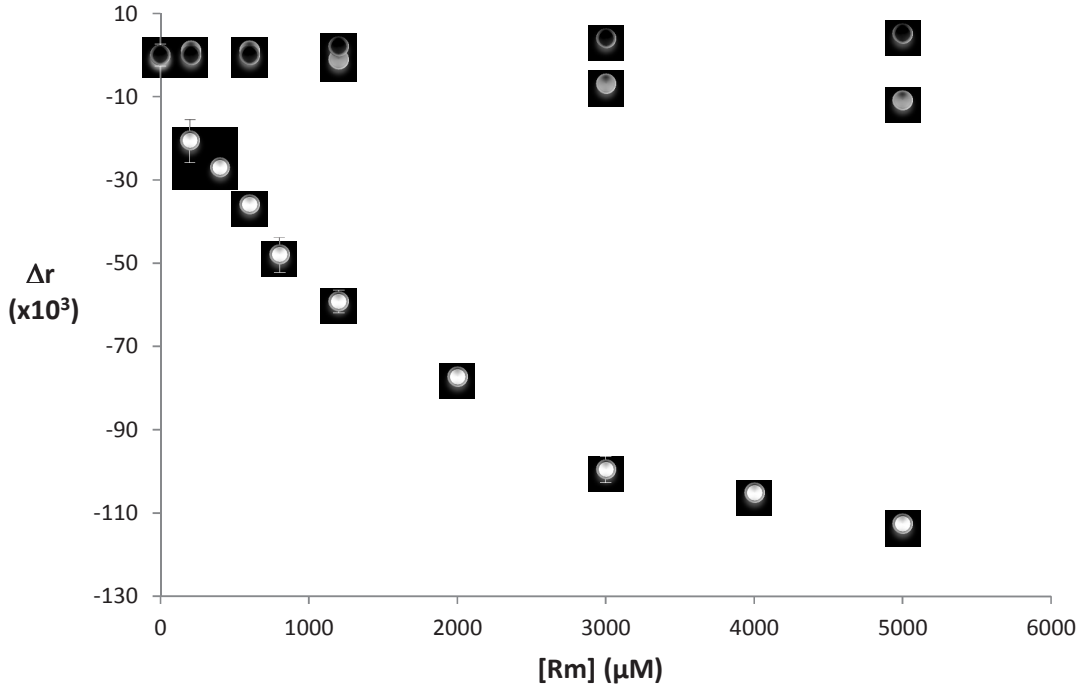

**Figure 7S. (a)** Schematic representation of the sandwich-like FPAA design with the SSB-assisted format. **(b)** Titration curves of split 5'-F-Apt-A (St1*:St2, 1:8 stoichiometry) with increasing Ade concentration in presence (circles) and absence (diamonds) of SSB protein. St1* concentration = 10 nM. SSB concentration = 1.67 µM. Binding buffer conditions: 50 mM Tris-HCl, pH = 7.5, 5 mM NaCl, 20 mM $MgCl_2$. $\Delta r = r - r_0$ where $r_0$ is the fluorescence anisotropy in absence of analyte.

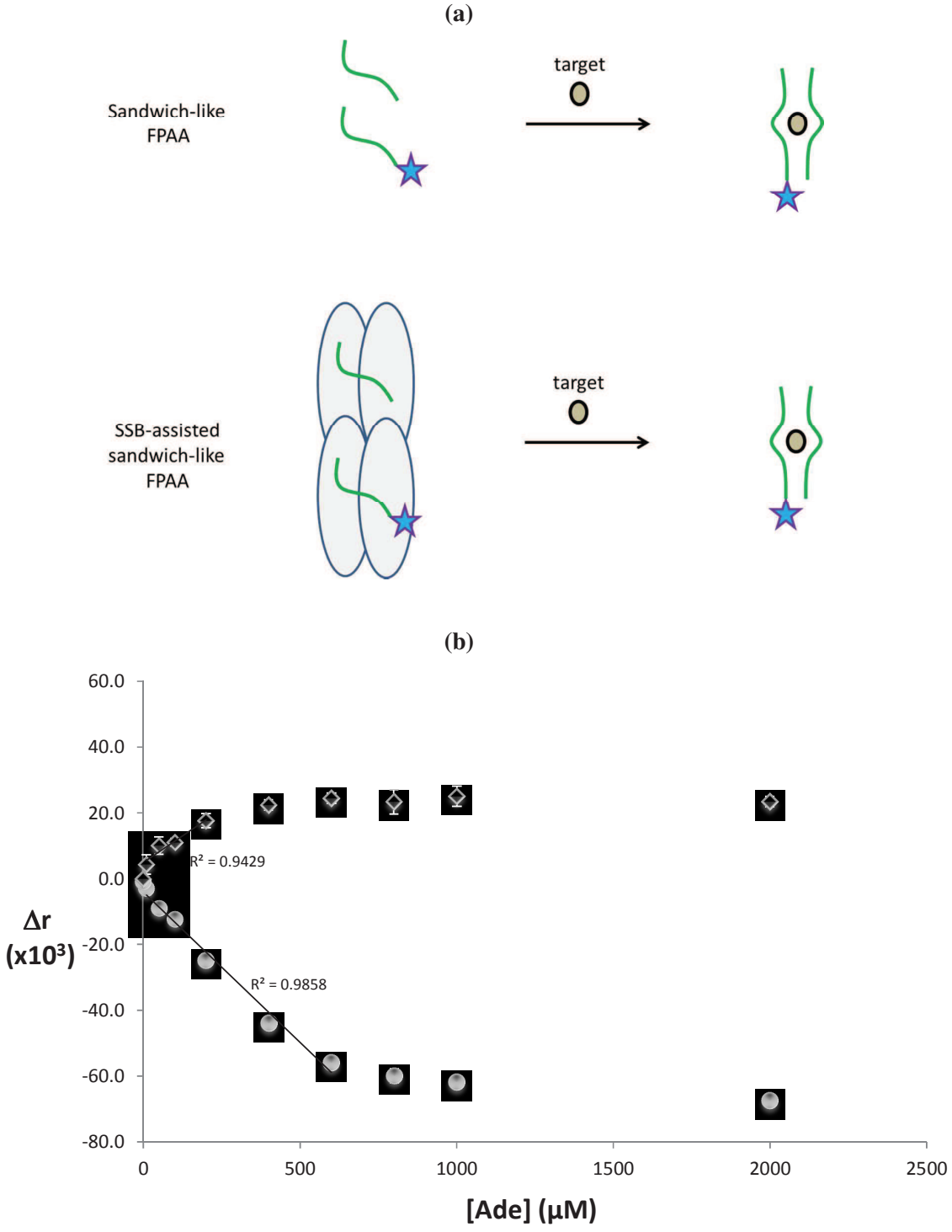

## II.4.3 Conclusions

In summary, aptamer-based fluorescence polarization/anisotropy offers significant advantages for some applications in clinical chemistry and bioassays and its use in biotechnology and drug discovery will no doubt continue to expand. First, polarization assays are homogeneous; that is, there is no necessity for separation of free and bound ligands. Second, polarization assays are reproducible and facilely automated. More importantly, because FP is less affected by environmental interferences, aptamer-based SSB assisted strategy can be successfully applied under realistic conditions, i. e. in diluted human serum, which made a big progress toward clinical diagnosis compare to the former aptamer-based methodologies.

However, several challenges still exist. For CS displacement strategy, FA signal generation is highly dependent on the length of the CS and the nature of the dye. Although SSB assisted strategy has greatly improved the assay response relatively to the previously reported small target assays, this method also has limitations since the affinity of SSB is too high for long aptamers. By careful consideration of experimental design, these limitations will be overcome and fluorescence polarization methods will become firmly entrenched, particularly for bioanalytical applications in the near future.

## References


264. Frazier R. A., Papadopoulou A., *Recent advances in the application of capillary electrophoresis for food analysis,* Electrophoresis, **2003**. 24: p. 4095-4105

265. Wang A. B., Fang Y. Z., *Applications of capillary electrophoresis with electrochemical detection in pharmaceutical and biomedical analyses,* Electrophoresis, **2000**. 21: p. 1281-1290

266. Thormann W., Lurie I. S., Mccord B., Malik N., *Advances of capillary electrophoresis in clinical and forensic analysis (1999-2000),* Electrophoresis, **2001**. 22: p. 4216-4243

267. Fukushi K., Takeda S., Chayama K., Wakida S. I., *Application of capillary electrophoresis to the analysis of inorganic ions in environmental samples,* Journal of Chromatography A, **1999**. 834: p. 349-362

268. Lagu A. L., *Applications of capillary electrophoresis in biotechnology,* Electrophoresis, **1999**. 20: p. 3145-3155

269. Cordova E., Gao J., Whitesides G. M., *Noncovalent Polycationic Coatings for Capillaries in Capillary Electrophoresis of Proteins,* Analytical Chemistry, **1997**. 69: p. 1370-1379

270. Kirby B. J., Hasselbrink Jr E. F., *Zeta potential of microfluidic substrates: 1. Theory, experimental techniques, and effects on separations* Electrophoresis, **2004**. 25: p. 187-202

271. Attard P., Antelmi D., Larson I., *Comparison of the zeta potential with the diffuse layer potential from charge titration,* Langmuir, **2000**. 16: p. 1542-1552

272. Cross R. F., Cao J., *Salt effects in capillary zone electrophoresis. I. Dependence of electrophoretic mobilities upon the hydrodynamic radius,* Journal of Chromatography A, **1997**. 786: p. 171-180

273. Terabe S., Otsuka K., Ichikawa K., Ando T., *Electrokinetic separations with micellar solutions and open-tubular capillaries,* Analytical Chemistry, **1984**. 56: p. 111-113

274. Terabe S., Otsuka K., Ando T., *Electrokinetic chromatography with micellar solution and open-tubular capillary,* Analytical Chemistry, **1985**. 57: p. 834-841

275. Acedo-Valenzuela M. I., Galeano-Diaz T., Mora-Diez, N., Silva-Rodriguez A., *Determination of neutral and cationic herbicides in water by micellar electrokinetic capillary chromatography,* Analytica Chimica Acta, **2004**. 519: p. 65-71

276. Pappas T. J., Gayton-Ely M., Holland L. A., *Recent advances in micellar electrokinetic chromatography,* Electrophoresis, **2005**. 26: p. 719-734

277. Molina M., Silva M., *Micellar electrokinetic chromatography: current developments and future* Electrophoresis, **2002**. 23: p. 3907-3921

278. Lieber C. M., *Nanoscale Science and Technology: Building a Big Future from Small Things,* MRS Bulletin, **2003**. 28: p. 486-491

279. Daniel M. C., Astruc D., *Gold nanoparticles: assembly, supramolecular chemistry, quantum-size-related properties, and applications toward biology, catalysis, and nanotechnology,* Chemical Reviews, **2004**. 104: p. 293-346

280. Nagarajan R., Hatton T. A., *Nanoparticles: Synthesis, Stabilization, Passivation, and Functionalization,* ACS Symposium Series, **2008**. 996

281. Corain B., Schmid G., Toshima N., *Metal Nanoclusters in Catalysis and Materials Sciences: The Issue of Size Control,* Elsevier, **2008**

282. Thomas K. G., Kamat P. V., *Chromophore-Functionalized Gold Nanoparticles,* Accounts of Chemical Research, **2003**. 36: p. 889-898

283. Andres R. P., Bein T., Dorogi M., Reifenberger R., *"Coulomb staircase" at room temperature in a self-assembled molecular nanostructure,* Science, **1996**. 272: p. 1323-1325

284. Jin R. C., Cao Y. W., Mirkin C. A., Zheng J. G., *Photoinduced conversion of silver nanospheres to nanoprisms,* Science, **2001**. 294: p. 1901-1903

285. Hutter E., Fendler J. H., *Exploitation of localized surface plasmon resonance,* Advanced Materials, **2004**. 16: p. 1685-1706

286. Underwood S., Mulvaney P., *Effect of the Solution Refractive Index on the Color of Gold Colloids,* Langmuir, **1994**. 10: p. 3427-3430

287. Mulvaney P., *Surface Plasmon Spectroscopy of Nanosized Metal Particles,* Langmuir, **1996**. 12: p. 788-800

288. Alivisatos A. P., Johnsson K. P., Peng X. G., Schultz, P. G. , *Organization of 'nanocrystal molecules' using DNA,* Nature, **1996**. 1996: p. 609-611

289. Brockman J. M., Nelson B. P., Corn R. M., *Surface plasmon resonance imaging measurements of ultrathin organic films,* Annual Review of Physical Chemistry, **2000**. 51: p. 41-63

290. Xu C. J., Wang B. D., Sun S. H., *Dumbbell-like Au-$Fe_3O_4$ Nanoparticles for Target-Specific Platin Delivery,* Journal of the American Chemical Society, **2009**. 131: p. 4216-4217

291. Faraday M., *Experimental Relations of Gold (and Other Metals) to Light,* Philosophical Transactions of the Royal Society, **1857**. 147: p. 145-181

292. Turkevich J., Stevenson P. C., Hillier J., *A study of the nucleation and growth processes in the synthesis of colloidal gold,* Discussions of the Faraday Society, **1951**. 11: p. 55-75

293. Frens G., *Controlled nucleation for the regulation of the particle size in monodisperse gold suspensions,* Nature, Physical Science, **1973**. 241: p. 20-22

294. Giersig M., Mulvaney P., *Preparation of ordered colloid monolayers by electrophoretic deposition,* Langmuir, **1993**. 9: p. 3408-3413

295. Brust M., Walker M., Bethell D., Whyman R., *Synthesis of thiol-derivatized gold nanoparticles in a two-phase liquid-liquid system,* Journal of the Chemical Society, Chemical Communications, **1994**. 7: p. 801-802

296. Hostetler M. J., Wingate J. E., Zhong C. J., Harris J. E., *Alkanethiolate Gold Cluster Molecules with Core Diameters from 1.4 to 5.2 Nanometers: Core and Monolayer Properties as a Function of Core Size,* Langmuir, **1998**. 14: p. 17-30

297. Guieu V., Ravelet C., Perrier S., Zhu Z. Y., Peyrin E., *Aptamer enzymatic cleavage protection assay for the gold nanoparticle-based colorimetric sensing of small molecules,* Analytica Chimica Acta, **2011**. 706: p. 349-353

298. Perrin F., *Polarization of light of fluorescence, average life of molecules,* Journal de Physique et le Radium, **1926**. 7: p. 290-401

299. Maragos C., *Fluorescence Polarization Immunoassay of Mycotoxins: A Review,* Toxins, **2009**. 1: p. 196-207

300. Lakowicz J. R., *Principles of fluorescence spectroscopy,* Kluwer Academic/Plenum, New York, **1999**

301. Owicki J. C., *Fluorescence polarization and anisotropy in high throughput screening: perspectives and primer,* Journal of Biomolecular Screening, **2000**. 5: p. 297-306

302. Dandliker W. B., Hsu M. L., Levin J., Rao B. R., *Equilibrium and kinetic inhibition assays based upon fluorescence polarization,* Methods in Enzymology, **1981**. 74: p. 3-28

303. Lundblad J. R., Laurance M., Goodman R. H., *Fluorescence polarization analysis of protein-DNA and protein-protein interactions,* Molecular Endocrinology, **1996**. 10: p. 607-612

304. Jameson D. M., Ross J. A. , *Fluorescence polarization/anisotropy in diagnostics and imaging,* Chemical Reviews, **2010**. 110: p. 2685-2708

305. Moerke N. J., *Fluorescence polarization (FP) assays for monitoring peptide-protein or nucleic,* Current Protocols in Chemical Biology, **2009**. 1: p. 1-15

306. David M. J., Justin A. R., *Fluorescence Polarization/Anisotropy in Diagnostics and Imaging,* Chemical Reviews, **2010**. 110: p. 2685-2708

307. Huwiler K. G., De Rosier T., Hanson B., Vogel K. W., *A fluorescence anisotropy assay for the muscarinic M1 G-protein-coupled receptor,* ASSAY and Drug Development Technologies, **2010**. 8: p. 356-366

308. Cleemann F., Karuso P., *Fluorescence anisotropy assay for the traceless kinetic analysis of protein digestion,* Analytical Chemistry, **2008**. 80: p. 4170-4174

309. Zaman G. J., Garritsen A., De Boer T., Van Boeckel C. A., *Fluorescence Assays for High-Throughput Screening of Protein Kinases,* Combinatorial Chemistry and High Throughput Screening, **2003**. 6: p. 313-320

310. Staeben M., Kleman-Leyer K. M., Kopp A. L., Robert G. L., *Development and validation of a transcreener assay for detection of AMP- and GMP-producing enzymes,* ASSAY and Drug Development Technologies, **2010**. 8: p. 344-355

311. Nutiu R., Li Y. F. , *Structure-Switching Signaling Aptamers,* Journal of the American Chemical Society, **2003**. 125: p. 4771-4778

312. Zhu Z. Y., Schmidt T., Mahrous M., Guieu V., Perrier S., Ravelet C., Peyrin E., *Optimization of the structure-switching aptamer-based fluorescence polarization assay for the sensitive tyrosinamide sensing,* Analytica Chimica Acta, **2011**. 707: p. 191-196

313. Kumke M. U., Li G., Mcgown L. B., Linn C. P., *Hybridization of fluorescein-labeled DNA oligomers detected by fluorescence anisotropy with protein binding enhancement,* Analytical Chemistry, **1995**. 67: p. 3945-3951

314. Walker T. G., Linn C. P., Nadeau J. G., *DNA detection by strand displacement amplification and fluorescence polarization with signal enhancement using a DNA binding protein,* Nucleic Acids Research, **1996**. 24: p. 348-353

315. Krauss G., Sindermann H., Schomburg U., Maass G. , *Mechanism of Interaction between Single-Stranded DNA Binding Protein and DNA,* Biochemistry, **2010**. 49: p. 843-852

# Chapter III
# Conclusions and Perspectives

Since the discovery of the aptamers in 1990, the field of aptamer research is continuing to progress at a rapid rate. In vitro selection has undoubtedly bought this field to flourish; we have seen the creation of hundreds of aptamers, each with a unique target specificity. These aptamers can bind substances ranging from small molecule to proteins to cells. Exploring in this avenue of aptamer research will not only emphasize the specific ability of aptamers to fold into distinct three-dimensional structures and interact with selected targets, they will also focus on the utility and practicality of aptamer research.

We have already witnessed the potential of using aptamers for various applications in medical diagnostics and therapeutics. On the therapeutic front, aptamers have been successfully used to sequester viral or defective proteins in cells as decoys. One example of this kind of molecule is "Macugen" (Pegaptanib), developed by EyTech Pharmaceuticals, USA, for the treatment of age-related macular degeneration. Archemix, a company specializing in the development of aptamer-based therapeutics, has developed anti-cancer aptamers that have been shown to be active in patients with renal carcinoma and acute myeloid leukemia in phase one and phase two clinical trials, respectively (www.archemix.com). On the diagnostic front, aptamers are now widely accepted as substitutes for antibodies in immunodiagnostics. In contrast to antibodies, aptamers are smaller and less complex and consequently are easier to manufacture and modify. The commercialization of some of these aptamer-based technologies was also achieved. For example, SomaLogic manufactures platforms containing aptamer arrays that enables for simultaneous detection of multiple biomarkers (www.somalogic.com). The affinities displayed by the aptamers are comparable to the affinities of antibodies for antigens; therefore, their utility as a fundamental molecular recognition element in biosensors has been realized.

In the past few years, more and more aptamer-based biosensors have been reported via elegant design. The principle of these biosensors is quite simple, they may be created by joining an existing aptamer, which serves as the molecular recognition element, to a signal transducer. This modular design is used to create different type of aptamer biosensors, whether they signal by optical, acoustic, mechanical, or electrical means. For certain targets, we can select sensors with signaling motifs that best suit our needs and convenience. However, one major challenge for the current aptamer-base biosensors is that most of the assays are confined to macromolecules such as proteins since the binding event leads to a significant structure change which can be easily converted into a detectable signal. Aptamer-based small molecule detections are not widely investigated.

In our studies, small biomolecule detection has been successfully achieved through various aptamer-based approaches. The first work of structure-switching aptamer-based CE makes it possible for multiple small molecule detection in a single run, which expands significantly the potential of small molecule analysis in terms of simplicity, adaptability, generalizability, and high-throughput analysis capability. The second aptamer-based gold nanoparticle colorimetric sensing allows a rapid, homogeneous, sensitive analysis which can be observed by naked eyes. Aptamer-based FP assay is a versatile and powerful method for the study of biomolecular binding interactions. The results described above greatly improve the response relatively to the previously reported small target assays, and as a significant progress, the SSB-assisted FP strategy can operate also under realistic (diluted human serum) conditions, which leads to a bright future for the aptamer-base clinical application.

Several problems related to the practical application of aptamers are still under study. When considering the role of aptamer arrays for the analysis of complex biological samples, any problems arising from cross-reactivity between targets and aptamers have to be scaled against the limitations of current analytical technologies. For example, aptamers configuration is sensitive to the salt composition; therefore, medium composition may affect the aptasensor properties. Several proteins may interact with DNA aptamers nonspecifically. They could bind to the sugar-phosphate backbone of DNA, and thus hinder the specific binding of analyte. The presence of nucleic acid in the biological liquids may cause hybridization with aptamers, and thus affect the aptamers conformation and maintaining the proper binding site. Furthermore, currently only approx. 250 aptamers are available to apply, while the number of various antibodies is much larger. Thus, despite the advantages of aptamers over antibodies, further effort is required for wide spreading aptamers-based technology in practical applications. It should be also noted that SELEX is still a highly specialized process and is not as popular amongst the wider scientific community as would be expected.

Future direction of the aptamer-based assay will probably see growth of microchips and nanochips. In the past two decades, there is strong interest in developing miniaturized bioanalytical systems that integrate various biochemical analysis components on a single chip. The development of microarrays based on aptamers used as receptors can be seen as a logical continuation of the DNA-chip technology. In the near future, aptamer microarrays are expected to play a dominant role in proteomics, thus extending the use of aptamer-based microarrays. Meanwhile, improved detection technique is another key in the future aptamer-based assay. The advantages of development for large-scale multiplexed aptamer arrays and the label-free target quantification methods are obvious. Given the commercial

opportunities and recent innovations in surface based analysis techniques, large scale molecular diagnostic arrays may not be too far away.

Overall, with the continuous improvement of the stability and reliability, more and more aptamer-based biosensors with excellent performances will be manufactured via smart designing strategies, which will endow them great opportunity to be applied in the fields of bioassay, biomedical diagnostic or environmental monitoring in the near future.

*Développement de nouveaux outils analytiques à base d'acides nucléiques aptamères pour la détection de petites molécules*

**Résumé :** La détection de petites molécules est d'un grand intérêt dans les domaines pharmaceutique, environnemental, alimentaire et de la biologie clinique. Les aptamères, sélectionnés par la méthode SELEX (pour *Systematic Evolution of Ligands by Exponential Enrichment*), sont des oligonucléotides qui se lient à une cible donnée avec une affinité et une spécificité importantes. L'objectif de ce travail est d'établir de nouvelles méthodologies analytiques basées sur l'utilisation des aptamères pour la détection de petites molécules. Dans un premier temps, une méthodologie par électrophorèse capillaire, dérivée du concept de déplacement du brin complémentaire de l'aptamère, est décrite pour la détection simultanée de plusieurs analytes dans un seul capillaire. La deuxième étude se focalise sur le développement d'un aptacapteur colorimétrique simple, rapide et peu coûteux, qui utilise le concept général de protection enzymatique de l'aptamère et les nanoparticules d'or en tant que système de transduction. Enfin, deux méthodes par polarisation de fluorescence, basées sur le concept de déplacement (du brin complémentaire ou de l'aptamère lui-même), sont présentées afin d'accroitre les potentialités des aptacapteurs dédiés à la détection des petites molécules.

**Mots clés:** Acide nucléique aptamères, SELEX, petites molécules, électrophorèse capillaire, nanoparticules d'or, polarisation de fluorescence, aptacapteurs.

*Development of novel analytical tools based on nucleic acid aptamers for the detection of small molecules*

**Abstract:** Small biomolecule detection is of great interest and importance in the pharmaceutical, environmental, food and clinical fields. Aptamers, selected by SELEX (*Systematic Evolution of Ligands by Exponential Enrichment*), are oligonucleotides that bind to a target with high affinity and specificity. The objective of the work is to establish novel methodologies of aptamer-based assays for the small biomolecule detection. In the first work, a rationalized capillary electrophoresis strategy, derived from the structure-switching aptamer concept, is described for the design of simultaneous detection of multiple analytes. The second work based on a gold nanoparticle colorimetric sensing strategy allows a rapid, label-free, homogeneous assay for small molecule using an aptamer enzymatic cleavage protection strategy. In the third work, two aptamer-based fluorescence polarization approaches, using the displacement concept, are described to improve the potentialities of the small molecule-dedicated aptasensors.

**Key words:** Nucleic acid aptamers, SELEX, small molecules, capillary electrophoresis, gold nanoparticles, fluorescence polarization, aptasensors.